ÉCOLE DE TECHNOLOGIE SUPÉRIEURE
UNIVERSITÉ DU QUÉBEC

MANUSCRIPT-BASED THESIS PRESENTED TO
ÉCOLE DE TECHNOLOGIE SUPÉRIEURE

IN PARTIAL FULFILLMENT OF THE REQUIREMENTS
FOR THE DEGREE OF DOCTOR OF PHILOSOPHY
Ph. D.

BY
Walid JOMAA

CONTRIBUTIONS TO UNDERSTANDING THE HIGH SPEED MACHINING EFFECTS ON AERONAUTIC PART SURFACE INTEGRITY

MONTREAL, JANUARY 22nd, 2015

BOARD OF EXAMINERS

THIS THESIS HAS BEEN EVALUATED

BY THE FOLLOWING BOARD OF EXAMINERS

Mr. Victor Songmene, Thesis Supervisor
Department of Mechanical Engineering at École de technologie supérieure

Mr. Philippe Bocher, Thesis Co-Supervisor
Department of Mechanical Engineering at École de technologie supérieure

Mr. Ilian Bonev, President of the Board of Examiners
Department of Automated Manufacturing Engineering at École de technologie supérieure

Mr. Mohamad Jahazi, Member of the jury
Department of Mechanical Engineering at École de technologie supérieure

Mr. Marek Balazinski, External Evaluator
Department of Mechanical Engineering at École polytechnique Montreal

Mr. Eric Feulvarch, External Evaluator
Department of Mechanical Engineering at Université de Lyon, ENISE (France)

THIS THESIS WAS PRESENTED AND DEFENDED

IN THE PRESENCE OF A BOARD OF EXAMINERS AND THE PUBLIC

ON JANUARY 14th, 2015

AT ÉCOLE DE TECHNOLOGIE SUPÉRIEURE

ACKNOWLEDGMENTS

I would like to thank my supervisor Prof. Victor Songmene and Co-supervisor Prof. Philippe Bocher. Their suggestions and guidance were very important to the development of this thesis. I also would like to thank the members of my dissertation committee, Prof. Ilian Bonev, Prof. Mohamad Jahazi, Prof. Marek Balazinski, and Prof. Eric Feulvarch for their insight and comments.

The author appreciates the financial support from National Sciences and Engineering Research Council of Canada (NSERC). Partial financial support by Fonds Québécois de la Recherche sur la Nature et les Technologies (FQRNT) by the intermediary of the Aluminium Research Centre, REGAL, is also gratefully acknowledged.

Special thanks to all my friends and labmates at laboratoire d'ingenierie, des produits, procedés, et systemes (LIPPS) and Laboratoire d'Optimisation des Procédés de Fabrication en Aérospatiale (LOPFA) for their help and support.

Thanks to all the stuff at the machine shop and to all people at École de technologie superieure who have helped me through this work.

I'm particularly grateful to my friend, Dr. Imed Zaghbani, for his encouragements and supports throughout my study's stay in Montreal.

Finally, I would like to express my deepest gratitude to my mother, my father, my sister, my two brothers, and my dear fiancée for their unlimited supports and encouragements.

CONTRIBUTION À LA COMPRÉHENSION DES EFFETS DE L'USINAGE À HAUTE VITESSE SUR L'INTÉGRITÉ DE SURFACE DES PIÈCES AÉRONAUTIQUES

Walid JOMAA

RÉSUMÉ

Pour assurer sa compétitivité, l'industrie aéronautique a de plus en plus besoin de composants et pièces mécaniques de haute performance fonctionnelle et de durée de vie en service plus longue. L'amélioration de la durée de vie en service des pièces usinées passe essentiellement par la maitrise et le contrôle de l'intégrité de surface. Ainsi, la présente étude a pour objectif d'investiguer, expérimentalement et théoriquement, les interactions outil/matière et leurs effets sur l'intégrité de surface lors de la coupe orthogonale à grande vitesse des alliages d'aluminium et des aciers durs utilisés dans la fabrication des pièces structurales en industrie aéronautique. Les matériaux d'étude sont deux alliages d'aluminium (6061-T6 et 7075-T651) et un acier faiblement allié (AISI 4340). L'acier AISI 4340 a été usiné à l'état traité par induction (58-60 HRC) (usinage dur). Ces matériaux ont été choisis dans le but de développer une approche globale pour prédire le comportement, en usinage à grande vitesse, de deux classes de métaux de caractéristiques mécaniques différentes (ductile et dur).

L'approche proposée se base sur trois étapes. Premièrement, nous avons établi un plan d'expérience afin de mener une investigation expérimentale sur les effets des conditions de coupe sur l'intégrité de surface et la formation de copeaux en usinage grande vitesse à sec. La configuration de la coupe orthogonale adoptée dans cette étude nous a permis d'explorer, théoriquement, les effets des paramètres technologiques (vitesse de coupe et avance) et physiques (efforts de coupe, température, angle de cisaillement, angle de frottement, et longueur de contact outil/copeau) sur les mécanismes de formation de copeaux et les caractéristiques de l'intégrité de surfaces usinées (contraintes résiduelles, déformation plastique, transformation de phase, etc.). Les conditions de coupe ont été choisies tout en respectant un plan d'expérience composite central (CCD) à deux facteurs (vitesse de coupe et avance par tour).

Dans le cas de l'usinage de l'aluminium 7075-T651, les résultats ont montré que la formation de l'arête rapportée (BUE) et l'interaction entre l'arête de coupe et les particules intermétalliques riches en fer sont les principales causes de la dégradation de la qualité de surfaces usinées. La formation de l'arête rapportée s'est intensifiée pour les avances élevées. Cependant, l'augmentation de la vitesse de coupe l'a réduit et a intensifié le collage de l'aluminium sur la face de coupe. L'étude a montré, également, qu'avec un choix judicieux de la vitesse de coupe et l'avance, il est possible de générer un état de contrainte de compression favorable à une meilleure durée de vie en fatigue des pièces en aluminium 7075-T651. Dans cette analyse, des corrélations ont été établi entre l'état de contrainte et les paramètres de coupe, tels que les efforts de coupe, angle de cisaillement, et angle de frottement.

D'autre part, nous avons étudié l'effet des conditions de coupe sur l'intégrité de surface en usinage dur de l'acier AISI 4340 durcis superficiellement par induction (58-60 HRC). Cette investigation a été motivée par le fait qu'une trempe par induction excessive a souvent engendré une couche durcie épaisse (2 mm) avec des contraintes résiduelles de compression faibles. Alors, notre objectif était de savoir si la finition par usinage dur, post-traitement d'induction, pourrait remédier à ce défaut. Les résultats ont montré que l'usinage dur à sec a permis d'améliorer l'état de contrainte résiduelle initial (après trempe par induction) en introduisant d'avantage des contraintes résiduelles de compression. Cependant, l'augmentation de la vitesse de coupe a induit des contraintes résiduelles de traction en surface. D'autre part, l'augmentation de l'avance a engendrée des contraintes résiduelles de compression et a accentuée l'endommagement de la surface usinée. L'analyse microstructurale au microscope électronique à balayage a révélé la formation de la couche blanche (épaisseur inférieur à 2 μm) en surface et des déformations plastiques sévères en sous-couches. Ces résultats ont démontré que l'usinage dur à sec avec un outil céramique est capable de produire des surfaces intègres qui peuvent concurrencer celles obtenues par rectification souvent jugée lente et très couteuse comparée à l'usinage dur.

L'étude expérimentale décrite ci-dessus et qui constitue la première étape de la présente thèse, nous a révélé que l'intégrité de surface est intimement liée aux mécanismes de formation de copeaux. Ces mécanismes, qui sont à l'origine des chargements thermomécaniques, peuvent être quantifiés par deux principaux paramètres : les efforts de coupe et la température générés lors de l'usinage. La quantification des efforts de coupe et température est indispensable dans la prédiction des caractéristiques de l'intégrité de surface (contraintes résiduelles, transformation de phase, etc.). D'où l'importance des modèles de prédiction des efforts de coupe et température. Dans la présente étude, nous avons choisi de développer un modèle de prédiction des efforts de coupe se basant sur une loi constitutive de comportement du matériau qui tient compte de l'effet de la déformation, vitesse de déformation, et la température. Par conséquent, la deuxième étape de cette étude a portée sur l'identification des coefficients de la loi de comportement de Marusich afin de simuler le comportement des matériaux étudiés en usinage à grande vitesse. Pour ce faire, nous avons proposé une méthode originale pour identifier les coefficients de la loi constitutive. Cette nouvelle approche, qui consiste à utiliser des tests dynamiques combinés à la méthode analytique inverse, a été appliquée aux alliages AA6061-T6, AA7075-T651, et AISI4340 (60 HRC). La méthode analytique consiste à déterminer, inversement, les coefficients matériaux à partir des essais d'usinages combinés aux modèles de surface de réponse établis dans la première partie de cette étude. Dans cette étape, nous avons étudié la sensibilité des coefficients matériaux aux modèles de températures utilisés dans la méthode inverse. Deux modèles matériau, pour chaque matériau testé, ont été déterminés à l'aide de deux différents modèles de température (model d'Oxley et de Loewen-Shaw). Les équations constitutives ainsi obtenues ont été validés à l'aide de résultats de tests dynamiques et aussi par un modèle éléments finis (EF) de l'usinage à grande vitesse. Une analyse de sensibilité a révélé que le choix du modèle de température influence significativement les coefficients matériaux et par la suite la prédiction de la contrainte d'écoulement et les paramètres de coupe (températures, forces, etc.). En général, les coefficients matériaux issues du modèle de température d'Oxley ont donné des résultats satisfaisants dans la prédiction du comportement dynamiques et aussi

dans la prédiction des efforts dans le cas de la modélisation par éléments finis de l'usinage à haute vitesse des matériaux testés.

Finalement, les modèles matériaux ainsi établies dans la deuxième étape, ont été, par la suite, implémenté dans le modèle analytique prédictive des efforts de coupe et de la température (troisième étape de l'approche). Nous avons testé seulement les coefficients obtenues par le modèle de température d'Oxley, vu leur meilleure performance comparée à ceux obtenus par le modèle de température de Loewen et Shaw. Cette partie de l'étude a pour objectifs de vérifier les coefficients matériaux déterminé et aussi de généraliser le modèle prédictive d'Oxley pour l'usinage à grande vitesse des alliages d'aluminium et aciers durs avec outils de coupe à arête semi-vif et ronde. Les résultats prédits (efforts de coupe, épaisseur du copeau, longueur de contact outil/copeau) ont été comparé avec les données expérimentales obtenues dans la présente étude et de la littérature, couvrant un large éventail de conditions de coupe (vitesse de coupe, avance, et angle de coupe). Un bon accord a été observé entre les forces de coupe prédites et mesurées pour tous les matériaux testés. Les constantes de vitesse de déformation dans la zone de cisaillement primaire et secondaire se sont révélées être sensibles aux conditions de coupe et leurs effets sur les données prédites ont été examinés en détail. Grace à la loi de comportement de Marusich, le modèle prédictif de coupe d'Oxley a été généralisé, a l'usinage à grande vitesse des alliages d'aluminium aéronautiques et acier durci par trempe à induction, avec succès. Le modèle de forces de coupe proposé pourrait être utilisé dans la prédiction analytique des contraintes résiduelles dont la prédiction par élément finis est souvent jugée délicate et lente.

A travers cette étude expérimentale et théorique, nous avons pu mettre en évidence les différents mécanismes physiques qui gouvernent la formation de copeaux et leurs effets sur l'intégrité de surface finie de deux classes de métaux (ductiles et durs). Cette approche permettra d'optimiser le choix des conditions de coupe afin de mieux maîtriser l'intégrité de surface. D'autre part, les résultats de cette étude ont été validés pour des faibles avances (10-30μm), comparables au rayon de l'arête de coupe utilisé (25 μm). Ainsi, les modèles de la coupe orthogonale développés dans cette étude (analytique et par éléments finies) peuvent être généralisés pour la prédiction et modélisation des procédés conventionnels (tournage, fraisage, et perçage) et non-conventionnels comme le micro-usinage.

Mots-clés : usinage à grande vitesses, intégrité de surface, modélisation, équation constitutive, alliages d'aluminium, acier dur.

CONTRIBUTIONS TO UNDERSTANDING THE HIGH SPEED MACHINING EFFECTS ON AERONAUTIC PART SURFACE INTEGRITY

Walid JOMAA

ABSTRACT

To remain competitive, the aeronautic industry has increasing requirements for mechanical components and parts with high functional performance and longer in-service life. The improvement of the in-service life of components can be achieved by mastering and optimizing the surface integrity of the manufactured parts. Thus, the present study attempted to investigate, experimentally and theoretically, the tool/work material interactions on part surface integrity during the machining of aluminium alloys and hardened materials (low alloy steels) using orthogonal machining tests data. The studied materials are two aluminum alloys (6061-T6 and 7075-T651) and AISI 4340 steel. The AISI 4340 steel was machined after been induction heat treated to 58-60 HRC. These materials were selected in an attempt to provide a comprehensive study for the machining of metals with different behaviours (ductile and hard material).

The proposed approach is built on three steps. First, we proposed a design of experiment (DOE) to analyse, experimentally, the chip formation and the resulting surface integrity during the high speed machining under dry condition. The orthogonal cutting mode, adopted in these experiments, allowed to explore, theoretically, the effects of technological (cutting speed and feed) and physical (cutting forces, temperature, shear angle, friction angle, and length Contact tool/chip) parameters on the chip formation mechanisms and the machined surface characteristics (residual stress, plastic deformation, phase transformation, etc.). The cutting conditions were chosen while maintaining a central composite design (CCD) with two factors (cutting speed and feed per revolution).

For the aluminum 7075-T651, the results showed that the formation of BUE and the interaction between the tool edge and the iron-rich intermetallic particles are the main causes of the machined surface damage. The BUE formation increases with the cutting feed while the increase of the cutting speed reduces it and promotes the BUL formation on the rake face of the cutting tool. We demonstrated also that by controlling the cutting speed and feed, it is possible to generate a benchmark residual stress state and good surface finish which can improve the in-service life of structural parts made of AA7075-T651aluminum alloys. In this context, correlations have been established between the stress state and the cutting parameters such as cutting forces, shear angle and friction angle.

We also investigated the effects of cutting conditions on surface integrity of induction hardened AISI 4340 steel (58-60 HRC) using mixed ceramic inserts. This investigation was motivated by the fact that excessive induction hardening treatment resulted in deep hardened layers (2 mm) with related low compressive residual stresses which may affect the performance of the induction heat treated parts. A judicious selection of the finishing process that eventually follows the surface treatment may overcome this inconvenient. The results

showed that the machining process induces significant compressive residual stresses at and below the machined surface. The residual stress distribution is affected by the cutting feed and the cutting speed. On one hand, surface residual stress tends to become tensile when the cutting speed is increased. On the other hand, an increase in cutting feed accentuates surface damage whilst it increases compressive surface residual stress. Microstructural analysis shows the formation of a thin white layer less than 2 μm and severe plastic deformations beneath the machined surface. These results attest that the dry hard machining using ceramic tools may be an alternative to grinding, considered expensive and time consuming, since an enhanced surface integrity in terms of residual stresses and microstructure conditions can be achieved.

The first step of this study (experimental study) showed that the surface integrity is closely related to the mechanisms of chip formation. These mechanisms, which are the origin of thermo-mechanical loads, can be quantified by two main parameters: the cutting forces and temperatures generated during machining. Therefore, any attempt to predict the characteristics of the machined surface integrity (residual stresses, transformation phase, etc.), should be, necessarily, involve the prediction of cutting forces and temperature generated during the machining. In this study, we opt out to develop a model for predicting cutting forces and temperatures based on a constitutive equation of the work material that takes into account the effect of strain, strain rate, and temperature. Therefore, the second step of this approach has focused on the identification of the Marusich constitutive equation in order to model the behavior of the materials in high-speed machining. To do so, we proposed an original methodology for identifying the coefficients of Marusich's constitutive equation (MCE) which demonstrated a good capability for the simulation of the material behaviour in high speed machining. The proposed approach, which is based on an analytical inverse method together with dynamic tests, was applied to aluminums 6061-T6 and 7075-T651, and induction hardened AISI 4340 steel (60HRC). The analytical method consists of determining the material constants inversely using machining tests combined with the response surface models established in the part one of the present thesis. In this section, we investigated the sensitivity of the material constants to the selected temperature models used in the inverse method. Two sets of material coefficients, for each work material, were determined using two different temperature models (Oxley and Loewen-Shaw). The obtained constitutive equations were validated using dynamic tests and finite element (FE) simulation of high speed machining. A sensitivity analysis revealed that the selected temperature model used in the analytical inverse method affected significantly the identified material constants and thereafter predicted dynamic response and machining modeling. In general, material constants obtained using Oxley temperature model gave satisfactory results, compared to Loewen and Shaw model, in predicting the dynamic behaviour and also in predicting the cutting forces during the finite element simulation of the high speed machining of the tested materials.

Finally, the material models which were identified in the previous step were thereafter implemented in a developed analytical model for predicting cutting forces and temperatures (the third step of the approach). We tested only the coefficients obtained by the Oxley temperature model, due to their better performance in predicting the cutting forces in FEM

compared to those obtained by model Loewen and Shaw ones. This part of the study aimed to verify the coefficients determined for materials and also to generalize the Oxley machining theory for high speed machining of aluminum and hard steel alloy using semi-sharp and honed cutting tool edges. The predicted results were compared with experimental data from the present study and from the literature, covering a large range of cutting conditions (speed, feed, and rake angle). An encouraging good agreement has been found between predicted and measured cutting forces for all tested materials. The strain rate constants in the primary and secondary shear zone were found to be sensitive to the cutting conditions and their effects on the predicted data were discussed in detail. Thanks to the Marusich's constitutive equation, the Oxley's machining theory was extended to the high speed machining of aeronautic aluminum alloys and induction hardened steels. The proposed predictive model can be extended also to the prediction of the residual stresses whose their prediction using finite element method is complex and time consuming.

Through this experimental and theoretical study, we were able to emphasize the physical mechanisms that govern the chip formation and their effects on the machined surface integrity of two classes of metals (ductile and hard). The proposed approaches can be used in the optimization of the cutting conditions in order to control the surface integrity on the machined parts. Furthermore, the results of this study have been validated for feed rates (10 to 50 μm) comparable to the cutting edge radius (5 and 25 μm) used in the experiments. Thus, the developed models (analytical and finite element) can be extended for studying and modeling the conventional machining processes (turning, milling, and drilling) and non-conventional ones such as the micro-machining process.

Keywords: High speed machining, Surface integrity, Modeling, Constitutive equation, aluminum alloys, induction hardened steels

TABLE OF CONTENTS

Page

LIST OF TABLES

Page

LIST OF FIGURES

Page

LIST OF ABREVIATIONS

BUE	Built-up edge
BUL	Built-up layer
CCD	Central composite design
FEM	Finite element modeling
JC	Johnson-Cook
MCE	Marusich's constitutive equation
MRR	Material removal rate
PSZ	Primary shear zone
RSM	Response surface methodology
SSZ	Secondary shear zone
TSZ	Tertiary shear zone
XRD	X-ray diffraction
WL	White layer

LIST OF SYMBOLS AND UNITS OF MEASUREMENTS

a_{th}	Thermal softening coefficient [MPa /°C]
C_t	Specific heat of the cutting tool material [J/kg.°C]
C_w	Specific heat of the workpiece material [J/kg.°C]
C_0	Strain rate constant on the primary shear zone
D_w	Thermal diffusivity of the work material [m^2/sec]
f	Cutting feed [mm/rev]
F	Friction force [N]
F_c	Cutting force [N]
F_t	Feed (thrust) force [N]
k_{prim}	Shear flow stress at the primary shear zone [MPa]
k_{int}	Shear flow stress at the secondary shear zone [MPa]
k_{tert}	Shear flow stress at the tertiary shear zone [MPa]
K_t	Thermal conductivity of the cutting tool material [W/m.°C]
K_w	Thermal conductivity of the work material [W/m.°C]
l_c	Chip/tool contact length [mm]
m_1	Low strain rate sensitivity exponents
m_2	High strain rate sensitivity exponents
n_{NL}	Strain hardening exponent
r	Chip thickness ratio
r_c	Chip compression ratio
r_n	Tool edge radii [mm]
t_{au}	Actual undeformed chip thickness [mm]
t_c	Chip thickness [mm]
T_{prim}	Average temperature at the primary shear zone [°C]
T_{int}	Average temperature on the secondary shear zone [°C]
T_0	Room temperature [°C]
V	Speed [m/min]

w	Cutting thickness [mm]
α	Normal rake angle [deg.]
α_{NL}	Thermal softening coefficient
γ_{prim}	Average shear strain at the primary shear zone
$\dot{\gamma}_{prim}$	Average shear strain rate at the primary shear zone [s^{-1}]
γ_{int}	Average strain on the secondary shear zone
$\dot{\gamma}_{int}$	Average strain rate on the on the secondary shear zone [s^{-1}]
ε_p	Equivalent plastic stress
$\dot{\varepsilon}_p$	Equivalent plastic strain rate [s^{-1}]
$\dot{\varepsilon}_t$	Transition strain rate [s^{-1}]
ε_0	Reference strain
$\dot{\varepsilon}_0$	Reference strain rate [s^{-1}]
ρ_t	Mass density of the cutting tool material [kg/m^3]
ρ_w	Mass density of the work material [kg/m^3]
σ	Flow stress [MPa]
σ_{prim}	Flow stress at the primary shear zone [MPa]
σ_0	Yield stress [MPa]
$\emptyset$	Shear angle [deg.]

INTRODUCTION

Background

Nowadays, most manufacturing industries, including aerospace industries, and particularly the machining sector is looking for producing parts with improved functional performance using environmentally friendly processes. The functional performance and in-service life of mechanical components are known to be significantly influenced by the machined surface integrity. Thus, it is worth studying the effects of tool/workpiece interaction and machining system parameters on the produced surface integrity.

To increase part performance in structural applications, new advanced material with high-strength and light-weight materials are, continuously, produced and precipitations treatable aluminum alloys such as AA6061-T6 and AA7075-T6 were ones of the most used light-weight alloys. However, the machining of such alloys is always accompanied by built-up edge formation and tangled chips which can affect the stability of the machining system and thereafter the surface quality of the machined parts. These shortcomings induce many technical issues in automatic control of the process during CNC machining. Moreover, to reduce the tool wear and improve the productivity, cutting fluid has traditionally been used. On the other hand, the use of dry high cutting speed which increases metal removal rate (MRR), reduces the formation of built up edges (BUE) and burrs (Rao et Shin, 2001) have been looked as an alternative, but it affects the surface integrity of the machined parts (Pawade, Joshi et Brahmankar, 2008). Traditionally the machining of aluminum alloys was performed using positive rake angle. However, it was found that negative rake angle with coated KC910 grade inserts gave the best performance in machining aluminium based metal matrix composite (MMC) (Abdullah, 1996). Vernaza-Peña *et al.* (Vernaza-Peña, Mason et Ovaert, 2003) reported that as the rake angle decreases, the cutting temperature is mainly generated by shearing in the primary shear zone rather than the friction at the tool/chip interface, in orthogonal machining of 6061-T6 aluminum alloy, which allow reducing the tool wear. Moreover, ultra-precision machining of 6061-T6 alloy was carried out using high

negative rake angle (-25°) and encouraging results in terms of surface quality were achieved as documented in (Abou-El-Hossein, Neethling et Olufayo, 2013).

Mechanical parts presenting high in-service performance in terms of fatigue life, such as gears and crankshafts, are also a concern in aerospace and automotive industries. The surface and subsurface characteristics of such components play a key role in controlling their service life (Novovic et al., 2004). To compete with price and lead time, gears and crankshafts are increasingly machined in the hardened state, however, the machining of hardened steels results to higher cutting temperatures and consequently high cutting tool wear rates. To overcome these problems, manufacturers used most of the times, wet machining to reduce cutting temperature and improve the tool life and surface quality (Dhar, Kamruzzaman et Ahmed, 2006). The use of lubricants has been widely criticized because their usage poses threat to ecology and health of workers (Sutherland et al., 2000; Vamsi Krishna, Srikant et Nageswara Rao, 2010).

Thanks to the development of new cutting tool materials and advanced techniques in metal processing (Chandrasekaran, 2006), dry machining of hardened steels has become possible. Hard machining is a metal cutting process for hardened ferrous metal that are often hardened above 40 HRC and up to 62 HRC. The hard machining process differs from conventional machining because of the workpiece hardness, the cutting tool required, and the chip formation mechanisms. By directly machining the parts after they have been hardened, hard machining using a single edge tools offers a number of potential benefits over traditional grinding; including lower equipment costs, shorter setup time, fewer process steps, greater geometric flexibility, and the elimination of the cutting fluid (Huang, Chou et Liang, 2007). If hard machining could be applied to the manufacture of complex parts, manufacturing costs could be reduced by up to 30% (Huang, Chou et Liang, 2007). Actually, research activities in hard machining sector are primarily focused on CBN tool wear (the predominantly used cutting tool material) (Grzesik, 2009). Some works (Çiçek et al., 2013; Gaitonde et al., 2009) stated that ceramic cutting tools, used in the metal cutting sector because of high hot hardness up to 1300–1500°C, and abrasive resistance and chemical stability (Grzesik, 2009), have

excellent performance in terms of tool life and surface quality during machining of hardened steels such as AISI D2 and AISI 4340. These alumina-based ceramic tools are up to 5 times less expensive than CBN tools and it is worth exploring their potential use.

The modeling and simulation of machining processes are need for both the comprehension the physical mechanism governing the surface integrity effects and the optimization of the cutting conditions. Predictive models and the simulation of machining process are also of great importance in modern manufacturing sector as they allow to improve products reliability and to save manufacturing time. The development of predictive models using analytical, empirical, and finite elements (FEM) is an alternative to expensive experimental tests. Although they provide precise results, FEM techniques are still time consuming and difficult to establish as the large plastic deformations achieved during the machining process not only bring complications from the mathematical point of view, but can also cause rapid solution divergence due to excessive element distortion (Vaz Jr et al., 2007). Empirical modeling needs extensive experimental works and therefore is expensive and the applicability of the obtained results is limited to the tested conditions domain. Finally, analytical modeling seems to be a reliable solution for machining modeling since it can relate physical phenomena to technological process parameters with low computation time and only few experimental data inputs. Oxley's machining theory (OMT) is considered as the most fundamental approach in analytical modeling of the machining process as it is based on the slip-line field theory (Kopalinsky et Oxley, 1984; Oxley et Hastings, 1977). In this theory, only material properties, tool geometry, and cutting conditions are needed to predict the cutting forces, chip thickness, average temperatures, and stresses in the deformation zones. However, its applicability has been limited to the machining of plain carbon steels, as the material constants of the used power-law are only available for these steels. In the last decade, several studies (Huang et Liang, 2003b; Karpat et Özel, 2006; Lalwani, Mehta et Jain, 2009; Lee, 2011; Long et Huang, 2005; Özel et Zeren, 2004; 2006) were carried out to extend the Oxley's theory to the machining of other materials by implementing Johnson-Cooke (JC) material model. In other context, Marusich's constitutive equation (MCE) has shown encouraging results for modeling and simulating high speed machining processes

(Huang et Liang, 2003b; Ren et Altintas, 2000). However, its use was very limited since only few material data were published in the open literature.

Both analytical and finite element modeling (FEM) of machining require accurate material constitutive equations in order to simulate the actual material behavior during processing. Studies performed by Fang (2005) and Jaspers *et* al. (2002) showed that the behavior differs significantly from one material to the other and it cannot be described by one set of general constitutive equations. Accordingly, to succeed any process modeling, two critical issues should be solved: first, the selection of the proper constitutive equations for the material to be studied and, second, the identification of the suitable coefficients.

Research objectives

Currently, fundamental understanding of the chip formation (chip morphology, cutting forces, cutting temperature, etc.) and its effect on surface integrity during the machining of ductile alloys and induction hardened steels is still lacking. To do so, the Oxley's machining theory should be extended to both classes of materials (ductile and hardened) by mean of a selected constitutive equation. In this context, the present study will investigate experimentally and theoretically the chip formation and surface integrity characteristics during the machining of two aluminum alloys (AA6061-T6, AA7075-T651) commonly used for structural applications and an induction hardened steel (AISI 4340) which is typical for mechanical applications. Hence, the main objectives of the present study are:

i) Investigate experimentally the chip formation process and its effect on the surface integrity of AA6061-T6, AA7075-T651, and induction hardened AISI 4340 (58-60 HRC) under high speed dry orthogonal machining conditions.

ii) Develop a methodology to identify the proper material constants of a selected constitutive equation (Marusich's constitutive equation) to simulate the high speed machining of the aluminums AA6061-T6, AA7075-T651, and the induction hardened AISI 4340 (58-60 HRC).

iii) Finally, extend Oxley's machining theory to analytically predict the cutting forces in high speed machining of the aluminums AA6061-T6, AA7075-T651, and the induction hardened AISI 4340 (58-60 HRC) steels using the Marusich's constitutive equation.

Thesis outline

Machining issues and objectives presented above are discussed and detailed throughout four chapters in the thesis.

Chapter 1 covers a literature review on machining aluminum alloys and hardened steels. A focus on the chip formation mechanisms and surface integrity characteristic is provided.

The experimental investigation has an objective to highlights the characteristics and particularities of the surface integrity in machining light alloys (aluminums) and induction hardened steels. Thus, in Chapter 2, we focus on the effects of cutting conditions on the surface finish and residual stresses induced by orthogonal dry machining of AA7075-T651 alloy. Specifically, the effects of cutting speed and cutting feed were discussed.

Chapter 3 discusses the effects of cutting conditions on the surface integrity characteristics in orthogonal dry machining of induction hardened AISI 4340 steel using PVD TiN coated mixed ceramic inserts. The effect of induction hardening on residual stress and microhardness distribution were also addressed. A modified analytical temperature model was proposed to assess the temperature on both the workpiece and chip/tool interface based on Loewen and Shaw model (1954). Measured cutting forces and chip thickness were also documented in this investigation.

From the experimental results of Chapters 2 and 3, we conclude that cutting forces and temperatures have significant effects on both chip formation mechanisms and surface integrity characteristics. Thus, in the theoretical part of this study, we proposed a predictive analytical cutting model, based on a material constitutive equation, for high speed machining

of the studied alloys. Firstly, in Chapter 4 we propose a methodology for the identification of the Marusich's constitutive equation for the aluminum alloys (AA7075-T6 AA7075-T6) and the induction hardened steel (AISI 4340- 60 HRC). This approach is based on a hybrid inverse method including orthogonal machining tests performed in Chapter 2 and 3 and dynamic tests from the literature. The response surface methodology was implemented to improve the accuracy of the inverse method by generating large sets of machining data. Two sets of material constants were determined, for each material, using two different analytical temperature models ((Oxley et Young, 1989) and (Loewen et Shaw, 1954)). The proposed constitutive equations were validated using dynamic tests and finite element model for high speed machining using Deform 2D® software. Secondly, in chapter 5, Oxley's predictive theory was extended to the high speed machining of aluminum alloys (AA6061-T6 and AA7075-T651) and the induction hardened steel (AISI 4340) using the Marusich's constitutive equations identified in Chapter 4. The proposed predictive cutting forces model was validated for the three tested alloys using experimental results from Chapters 2 and 3 and with machining data from the literature.

The thesis conclusions and suggestions for future work and recommendations are also addressed as additional sections

CHAPTER 1

LITERATURE REVIEW

1.1 Introduction

In the present study, we investigate, experimentally and theoretically, the tool/work material interactions during the machining of ductile (light alloys) and hardened materials (low alloy steels) used in the aircraft industry. The studied materials are two aluminum alloys (AA6061-T6 and AA7075-T651) and AISI 4340 steel. The aluminums AA6061-T6 and AA7075-T651 are a precipitation treatable aluminum alloys which are some of the most promising candidates for fabricating thermally stable, high strength and light-weight mechanical components. The AISI 4340 steel was machined after having been induction heat treated to 58-60 HRC. It is low alloy steel characterized by high tensile strength and toughness and used in several structural components (gears, crankshaft, etc.) for automotive and aircraft industries. We selected these materials in an attempt to provide a comprehensive study of the machining of large range of metals (from ductile to hardened one). The proposed approach is built on four steps. First, we analyzed the chip formation and the resulting cutting forces under high speed orthogonal machining conditions. Second, we developed relationships amongst these aspects and the alterations of the surface and subsurface of the machined samples (surface integrity). Third, we proposed an approach to identify a selected constitutive equation in order to predict the material behavior at high speed machining. Finally, the obtained constitutive equations were implemented, thereafter, in a predictive analytical model for high speed machining of the tested materials.

Therefore, this chapter reviews previous research works in areas relevant to the machinability and surface integrity characteristics of machined parts made of aluminum alloys and hardened steels. The machinability of materials is usually evaluated using indicators such as chip formation, tool life, cutting forces but the tool wear is the most used criteria. Since the

tool wear is not considered in the present work, only chip formation and cutting forces results were documented. Previous research works on the surface integrity of machined aluminum alloys and hardened steels were reported in this chapter. Finally, basics of the machining theory and modeling were also documented.

1.2 Generalities about the machining process

The earliest machining or cutting of material experiments has been carried out from the latter part of the eighteenth century (Boothroyd, 1988). The term *machining* deals with any process in which material is removed gradually from a workpiece. The narrower term *cutting* is intended to include operations in which a thin layer of material, the *chip*, is removed by a wedge-shaped tool (Grzesik, 2008). Generally, the machined surface is generated by a relative motion between the cutting tool and the workpiece (Figure 1.1). Since the present work deals with the turning process, we will only focus on the lathe machine and cutting tools used in turning. Two kinds of relative motion must be provided by a lathe machine-tool: The primary motion (rotational or linear) is the main motion, known also as the cutting speed (Astakhov, 2006). The feed motion (feed rate/cutting feed) is a linear motion that is additionally provided to the tool or workpiece.

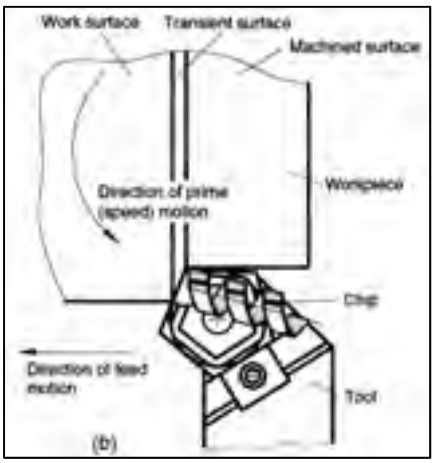

Figure 1-1 Illustration of the turning operation (Astakhov, 2006)

1.2.1 Cutting tool angles

In addition to the cutting speed and feed rate, the cutting tool angles are of great importance in machining and should be carefully selected. Figure 1-2 shows the rake, wedge, and flank angles (γ, β and α, respectively). They are defined in a series of reference planes (Po, Pf, Pp, Pn, and Pr) in tool in-hand system. The general rule of thumb is to select a positive rake angle (Figure 1-3a) for machining ductile materials such as aluminum alloys and negative one for machining hardened steels (hard machining) (Figure 1-3c). On the other hand, depending on the machining operations and materials, low wedge angles, β, of 35° or 55° are usually selected for semi-finishing and/or finishing operations. The cutting edge inclination angle, λs, (Figure 1-4) is the angle between the cutting edge and the reference plane Pr. The sign of the inclination angle defines the chip-flow direction (Astakhov, 2006). When λs is positive, the chip flows to the right and when λs is negative, the chip flows to the left.

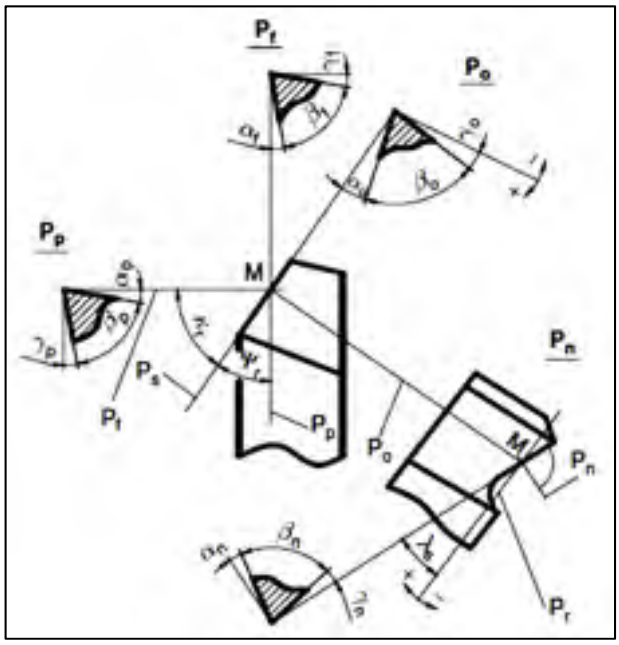

Figure 1-2 Tool angles in the tool-in-hand system (Grzesik, 2008)

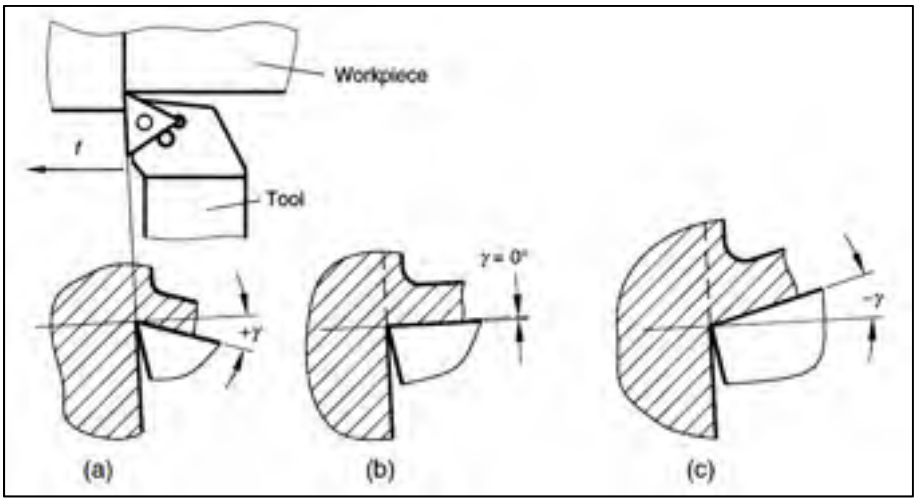

Figure 1-3 (a) Positive, (b) zero and (c) negative rake angles (Astakhov, 2006)

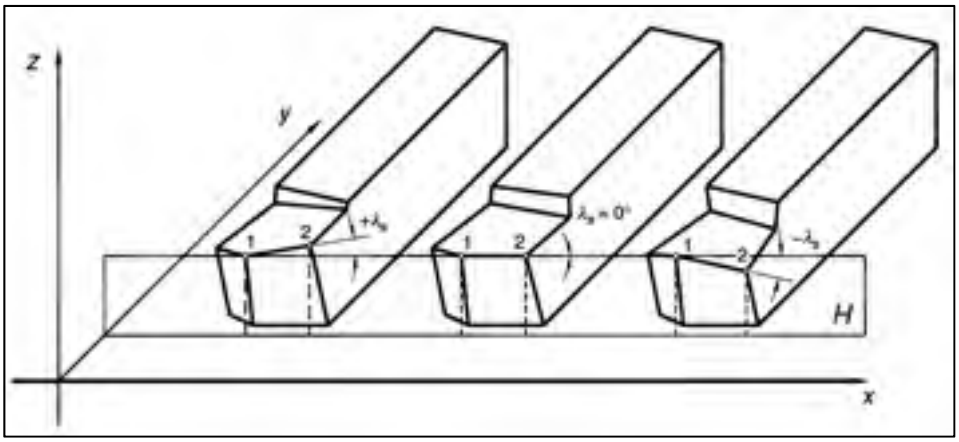

Figure 1-4 Sense of the sign of the inclination angle (Astakhov, 2006)

1.2.2 Chip formation in machining

In metal cutting, the term "chip formation" has been used since the nineteenth century (Astakhov, 2006). Its initial meaning is the formation of the chip in the primary and secondary deformation (shear) zones (Figure 1-5). The primary shear zone PSZ is a region on which the plastic deformation begins and ends with the chip is entirely work harden. The secondary shear zone is the result of intensive interfacial friction adjacent to the tool/chip

interface. The tertiary shear zone, TSZ, is localized below the tool edge and is the results of the friction between the tool and the new machined surface.

The tool/work material/environment interactions during machining influences the thermo-mechanical loads at the shear zones leading to different chip forms and types. The chip forms produced in metal machining process are classified based on their sizes and shapes according to ISO 3685-1977 (Table 1-1). The chips can also be classified based on the mechanisms of deformation and fracture resulting from the properties of work material and process conditions (Grzesik, 2008). Figure 1-6 illustrates four types of chips that can be form during the machining of materials with different mechanical properties: 1) continuous chip, 2) segmented chip, 3) elemental chip, and 4) discontinuous chip. More details about the chip formation characteristics in machining aluminum alloys and hardened steels will be discussed later in this chapter.

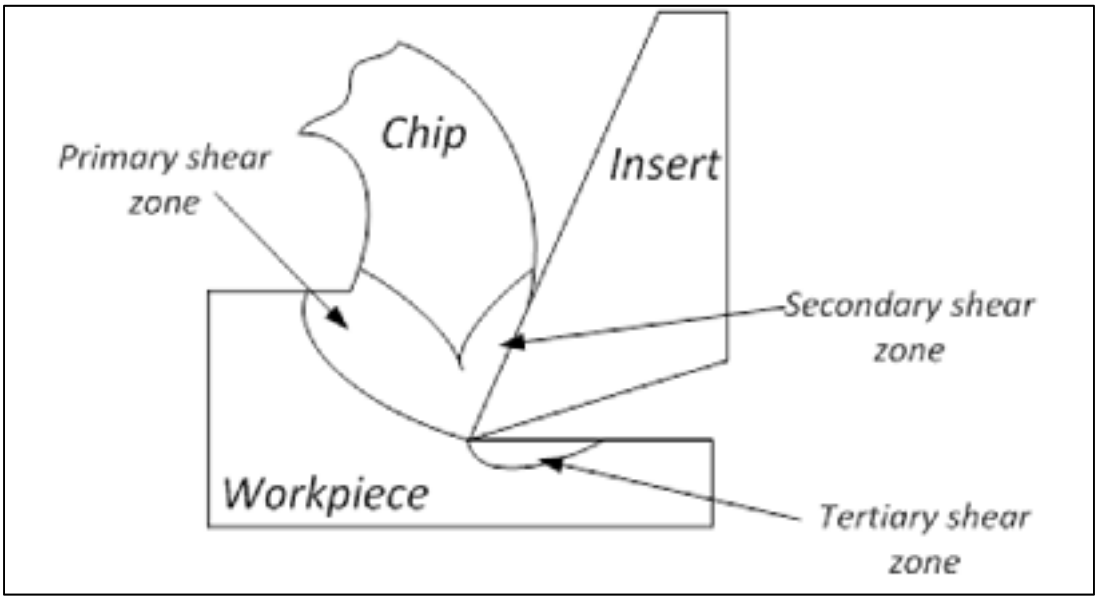

Figure 1-5 Illustration of the deformation zones in metal cutting process

Table 1-1 Classification of chip forms according to ISO 3685-1977

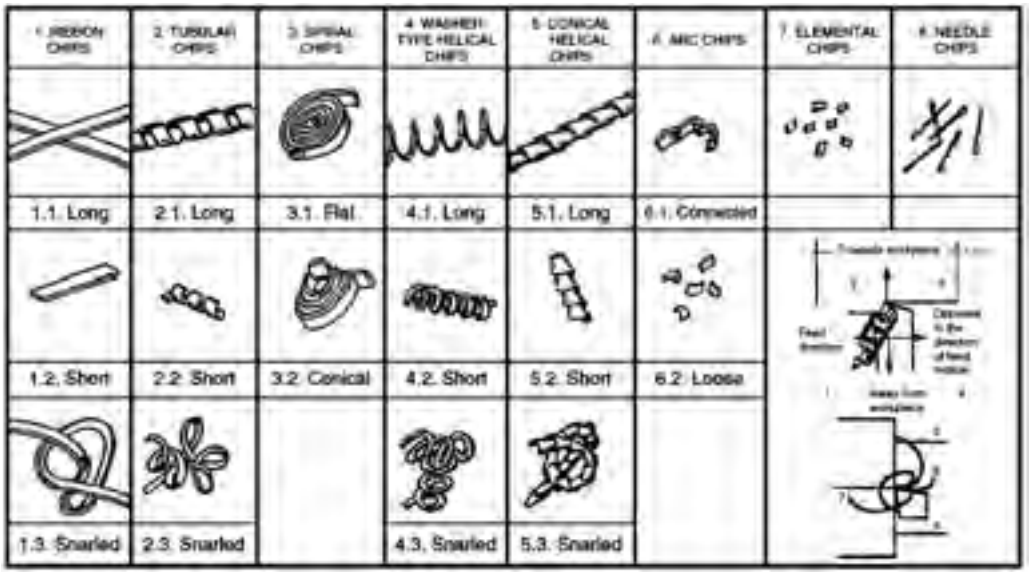

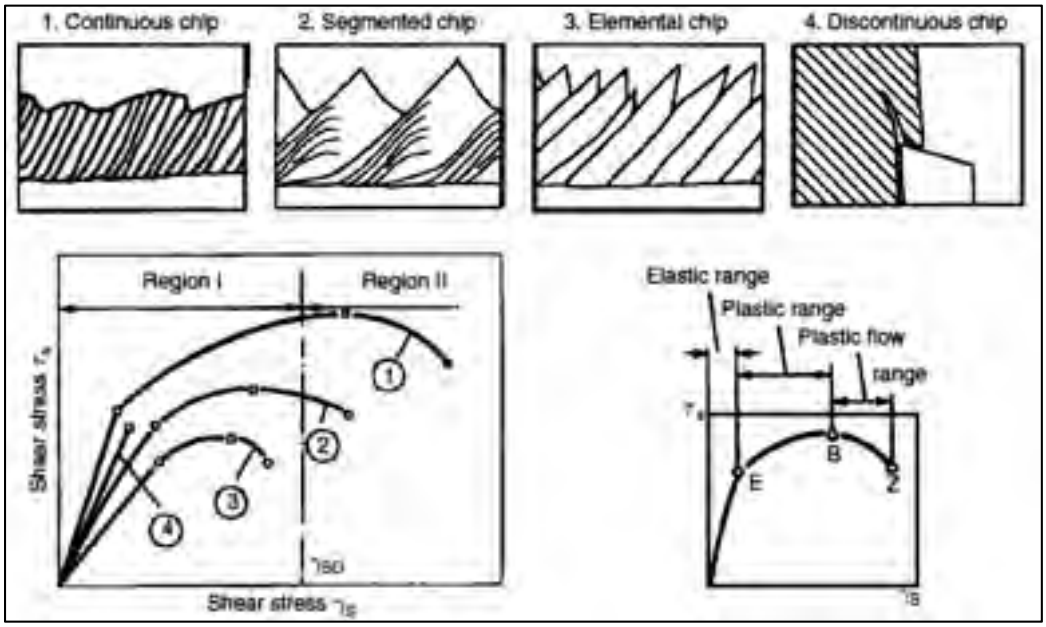

Figure 1-6 Chip formation in terms of stress/strain curves (Grzesik, 2008)

As we mentioned above, the chip forms under a thermo-mechanical load. The mechanical load is the result of the cutting forces applied by the cutting tool during the chip formation. The cutting forces system depends on the cutting configurations including 3D machining (turning, milling, drilling), oblique machining, and orthogonal machining.

1.2.2.1 Cutting forces system in turning

The turning process is considered as 3D machining operation since the tool nose is engaged, partially or entirely, in the work material. In this case, both the primary and the secondary (trailing) cutting edges participate in the cutting process. Indeed, the cutting force system is composed of three components: the cutting force Fz, the feed force Fx, and the thrust (penetration) force Fy as shown in Figure 1-7

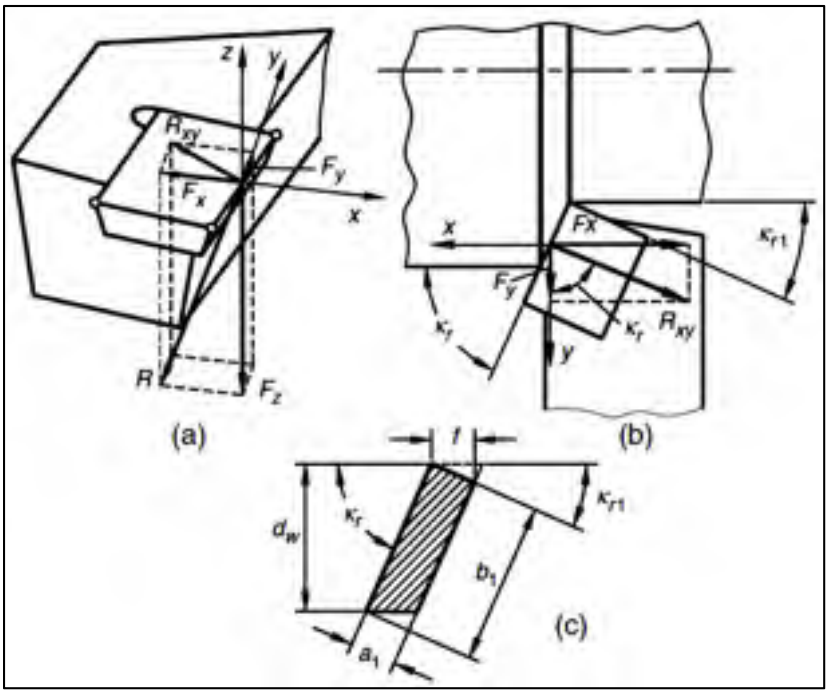

Figure 1-7 Cutting forces system and uncut chip thickness for a single-point cutting tool (Astakhov, 2006)

1.2.2.2 Cutting forces system in orthogonal machining

The orthogonal machining (Figure 1-8) is a cutting configuration in which specific dimensional and geometrical considerations between the tool and the machined workpiece should be respected in order to ensure plane-strain conditions in the cutting zone.

The following are the main considerations:

- Free machining: the tool nose does not participate in the cutting process;
- The cutting is ensured by a straight sharp cutting edge;
- The cutting edge is wider than the width of the workpiece;
- The undeformed (uncut) chip thickness should be at least 10 times smaller than the width of cut;
- The cutting speed direction is perpendicular to the cutting edge which meaning that the inclination angle λ should be equal to zero.

The 3D system of the cutting forces is therefore reduced to 2D system with Fc is the main cutting force and Ft is the feed (thrust) force as shown in Figures 1-9 and 1-10. It is worth noticing that the orthogonal cutting mode has attracted a great attention in the modeling and simulation of machining process studies using both analytical and finite element methods. In practice, two setups can be used to simulate the orthogonal machining: the first uses a disc-shaped workpiece (Figure 1-9) while the second uses a tube end turning (Figure 1-10). These two configurations have two major drawbacks when machined surface integrity is considered: firstly, the determination of the representative zone due to the tool retraction and, secondly, the effect of subsequent passes during machining. In the present study, attention has been given to determine accurately the representative zone for surface integrity analysis.

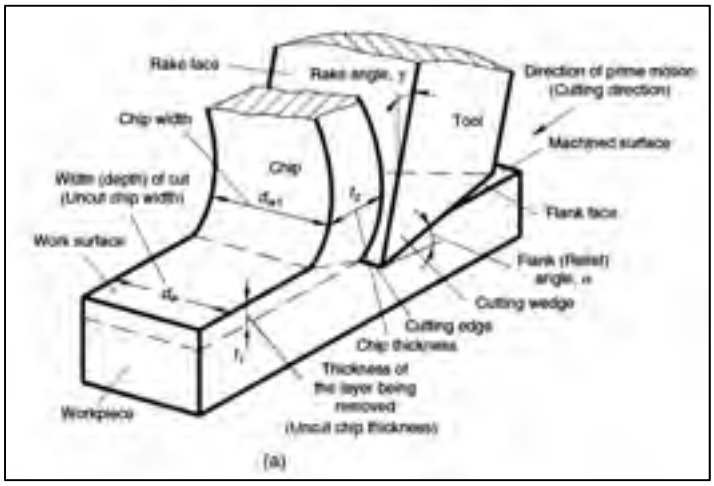

Figure 1-8 Illustration of the orthogonal machining (Astakhov, 2006)

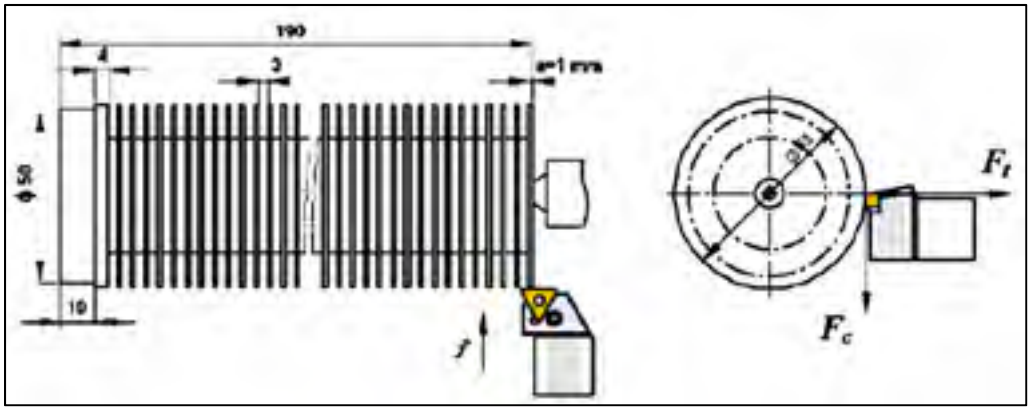

Figure 1-9 Cutting force system in orthogonal cutting set-up on disc-shaped workpiece (all units are in mm) (Ucun et Aslantas, 2011)

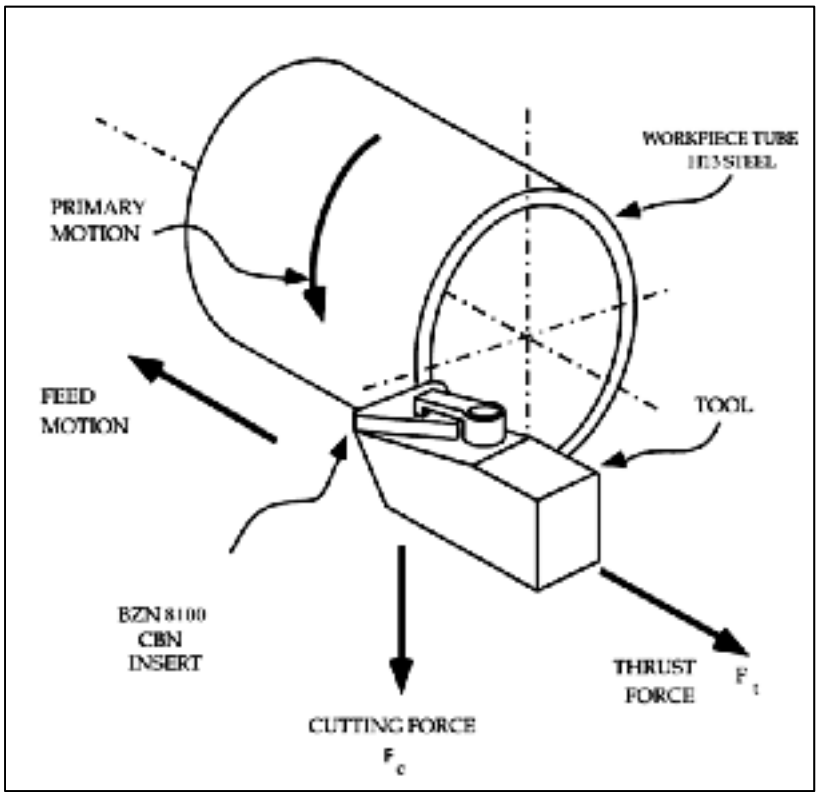

Figure 1-10 Illustration of orthogonal cutting experimental set-up on tube-shaped workpiece (Özel, 2003)

1.2.3 Surface integrity characteristics in machining

Field and Kahles (1964) were the first to introduce the concept of ''surface integrity" by means of defining « *the inherent or enhanced condition of surface produced in machining or other surface generation operation »* (M'Saoubi et al., 2008). Their pioneer work led to the subsequent establishment of an American National Standard on surface integrity (ANSI B211.1, 1986). The machining affected surface layer was defined as the layer from the geometrical surface inward that shows changed physical and sometimes chemical properties, as compared with the material before machining (Youssef et El-Hofy, 2008a). These modifications include topographical features (surface finish), mechanical, and metallurgical alterations of the machined surface (Figure 1-11) and their relationship to functional performance (Griffiths, 2001).

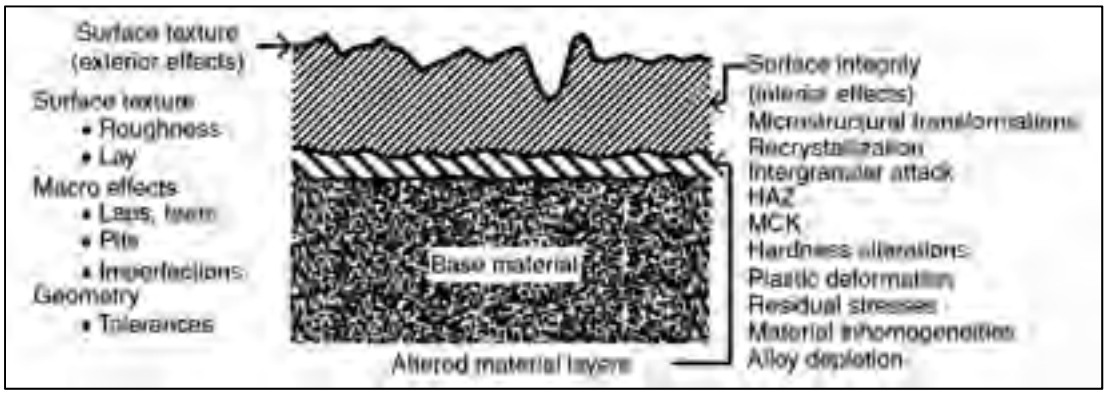

Figure 1-11 Typical machining affected layers (Youssef, Helmi A., and Hassan El-Hofy, 2008a)

1.2.3.1 Surface topography of the machined parts

Surface topography or texture (Figure 1-12) is concerned with the geometrical irregularities of the machined surface, which is defined in terms of surface roughness, waviness, lay, and flaws (Youssef et El-Hofy, 2008a).

According to ISO 13565-2:1997 standard, the roughness parameters can be classified in four categories as follow:

- Amplitude or height parameters (Ra, Rt, Rz);
- Spacing parameters (RSm, Rλq);
- Hybrid parameters (RΔa , RΔq);
- Surface waviness parameters (Wa, Wt).

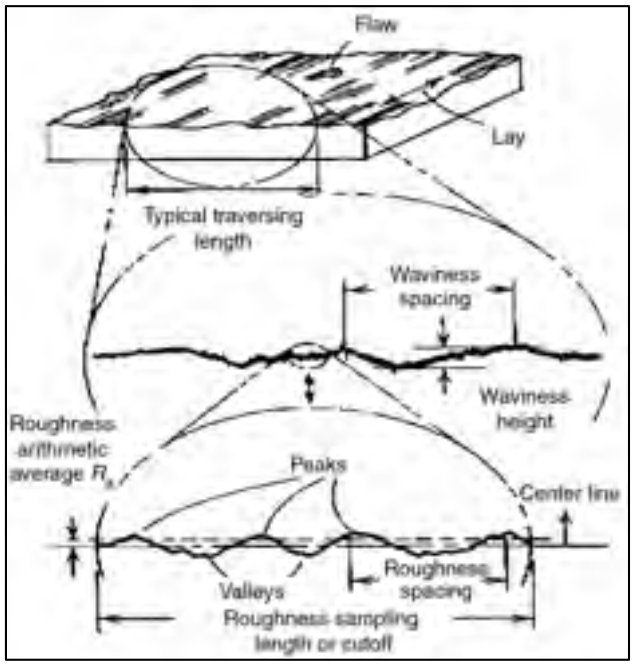

Figure 1-12 Surface texture features
(Youssef et El-Hofy, 2008a)

1.2.3.2 Mechanical alterations

The machining process induces several changes on the initial surface and sub-surface mechanical state of the machined parts. The main changes include the generation and/or modification of the residual stress state, plastic deformation, and hardness alteration (work hardening/material softening).

The residual stresses are defined as those stresses that would exist in an elastic body if all external loads were removed. Hence, they are related to the incompatibility between a surface layer and the bulk material (Capello, 2005). Three mechanisms can lead to the residual stress formation in machining:

- The mechanical effect due to inhomogeneous plastic flow caused by the cutting forces;
- The thermal effect due to inhomogeneous plastic flow caused by thermal gradient;
- The metallurgical or physical effect due to specific volume variation caused by phase transformation.

The residual stress state can be the result of more than one phenomenon at the same time and the resulting residual stress state is, therefore, a superposition of the residual stress generated by a single mechanism (Capello, 2005). The residual stress state can be either positive (tensile stress) or negative (compressive stress), depending of the leading mechanism, during the cutting process. It is well recognised that both mechanical and metallurgical effects induce compressive residual stress state while the thermal mechanism induces tensile residual stress state. The tensile residual stress state is detrimental for fatigue life since compressive stress acts to close crack formation, while tensile one applies additional stress to the crack as stated by Dogra et al. (2010).

The residual stresses may also be categorised by the scale over which they self-equilibrate, or according to the method by which they are measured. When the length scale is considered, three types of stresses (Figure 1-13) can be described as follow (Withers et Bhadeshia, 2001):

- The macrostresses (type I) vary continuously over large distances (some grains to mm);
- The intergranular stresses (type III) vary over the grain scale. Low level type II stresses nearly always exist in polycrystalline materials simply from the fact that the

elastic and thermal properties of differently oriented neighbouring grains are different;

- The stresses at atomic scale (type III) which typically includes stresses due to coherency at interfaces and dislocation stress fields.

In practice, residual stresses cannot be measured directly; instead the stress must be inferred from a measure of the elastic strain, displacement or secondary quantity, such as the speed of sound, or magnetic signature that can be related to the stress (Withers et Bhadeshia, 2001).

Many techniques are used to measure the residual stresses including non-destructive and destructive method for different length scales according to the spatial resolution needed and the depth at which the measurements can be taken as shown in (Figure 1-14). The X-ray diffraction method has received a growing attraction in measuring the residual stresses induced by the machining process. Unless applied in combination with destructive layer removal, conventional X-ray diffraction is limited to a depth of 5 μm or so from the surface for steels due to the poor levels of penetration of approximately Ångstrom wavelength X-ray beams (Figure 1-14).

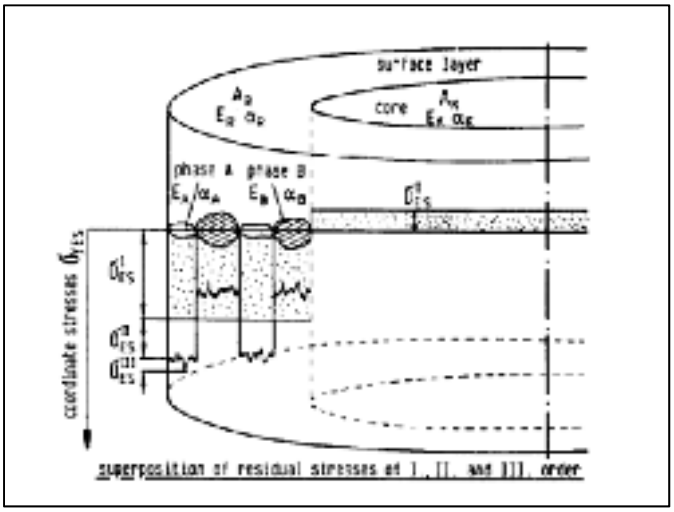

Figure 1-13 Analysis of residual stresses sources induced by material, manufacturing and operating conditions adapted from (Davim, 2010)

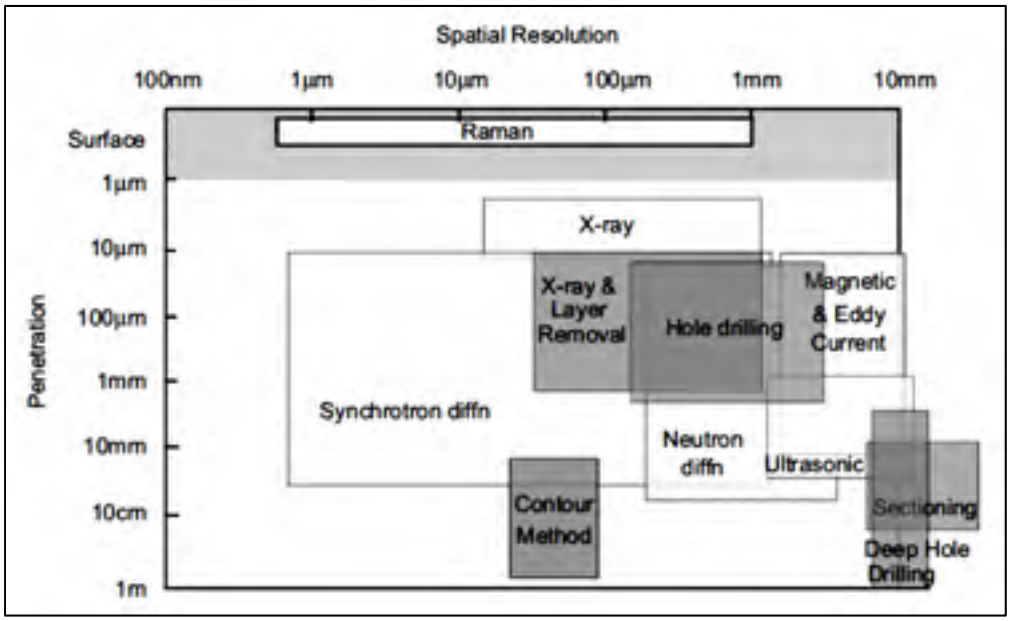

Figure 1-14 Approximate current capabilities of the various measurement techniques. The destructive techniques are shaded grey (Withers et al., 2008)

As mentioned above, the machining process may induce a severe plastic deformation at the machined surface under some specific cutting conditions. The plastic deformation is governed by the interaction between the microstructure of the work materials and the levels of thermal and mechanical loads generated during the cutting process. The deformation, slip in the grain boundaries, and elongation of grains indicate this severe plastic deformation. The tool wear was found the major reason for these deformations as stated by Ezugwu et al. (1999). It is hard to measure or observe because it mainly occurs at the sub-surface in a very short time and in a very narrow region of the machined surface (Ulutan et Ozel, 2011). Jin and Liu (2013) have used optical micrographs to assess the maximum plastic shear strain as shown in Figure 1-15. It was calculated using the following formula:

$$\gamma_{max} = \frac{\overline{AB}}{\overline{BC}} \tag{1.1}$$

The microgrids based techniques have been received wide attentions in assessing plastic strains below the machined surface. Bailey and Jeelani (1976) have used a technique based on embossing an orthogonal array of lines (grid) (Figure 1-16) on the workpiece to determine the plastic strain on the machined surface of copper.

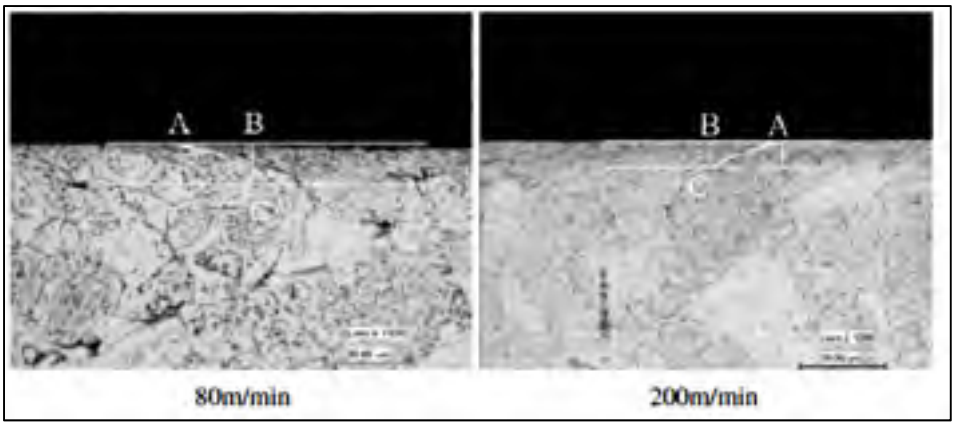

Figure 1-15 Measurements of plastic strain induced by machining (Jin et Liu, 2013)

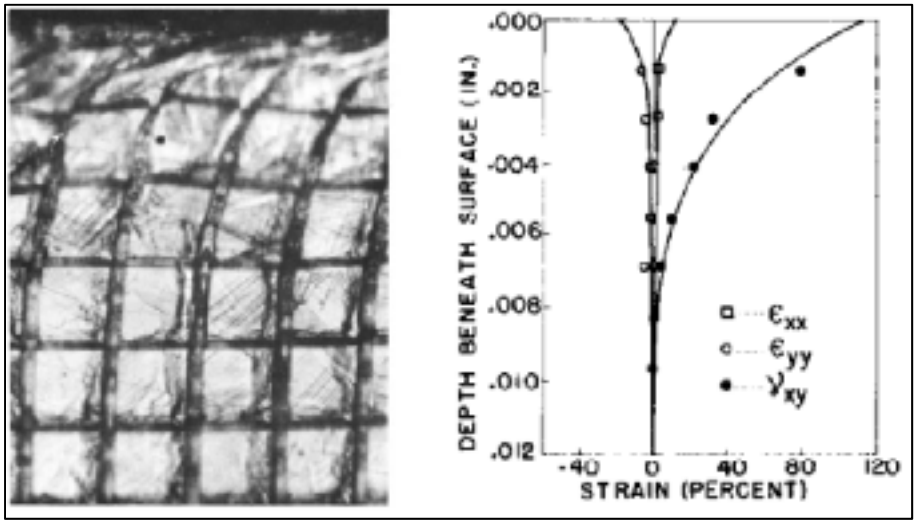

Figure 1-16 Measurement of plastic strain using micro-grid technique for machined copper workpiece (Bailey et Jeelani, 1976)

1.2.3.3 Metallurgical alterations

The machining process can induce different forms of metallurgical modifications on the work material. Depending on the microstructure and chemical composition of the work material and cutting conditions, these modifications may include phase transformation, recrystallization, twining, change in grain size and distribution, and change in precipitate size and distribution (Youssef et El-Hofy, 2008a). Moreover, the work materials are exposed to mechanical, thermal, and chemical energy that can lead to strain aging and recrystallization during the machining (Ulutan et Ozel, 2011). Due to this strain aging process, the material might become harder but less ductile, and recrystallization might cause the material less hard but more ductile. A layer that resist to etching, known as white layer, can form under severe cutting conditions of steels as can be seen in Figure 1-17. Although many investigations were carried out on white layer formation, the nature of this layer and mechanisms leading to its formation during machining are not yet clarified.

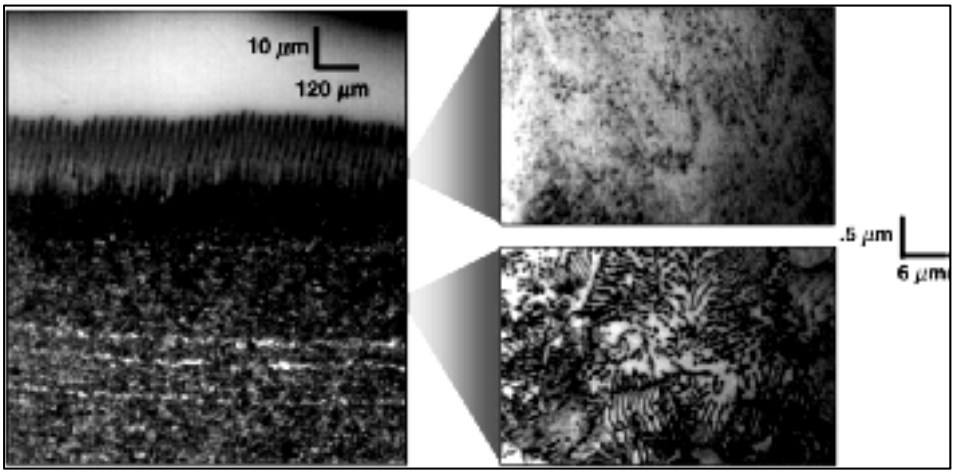

Figure 1-17 Phase transformed structure at a machined AISI 4340 steel (Chou, 2002)

Since the present study only deals with the machining of aluminum alloys and hardened steels, we will focus, in the next sections, on the chip formation and surface integrity, achieved during the machining of these two alloys family.

1.3 Machining of aeronautic aluminum alloys

The machining of aeronautical aluminum parts is characterized by the generation of complex shapes (Figure 1-18). The volume of metal to be removed during the machining of such parts is significantly high which increases the machining time. To be more efficient and competitive, most of machining workshops working in aeronautical industry have integrated the high speed machining HSM. The use of high cutting speed increases metal removal rate (Rao et Shin, 2001); however, it affects the chip formation mechanisms and surface integrity characteristics of the machined parts (Pawade, Joshi et Brahmankar, 2008).

Figure 1-18 Precision CNC Machining of 6061-T651 aluminum Brackets (courtesy of EMF Inc.)

1.3.1 Chip formation in machining aluminum alloys

The main difficulties encountered when machining aluminum alloys, which are considered as ductile materials, are their tendency to form long stringy chips and built-up layer BUL and built-up edge BUE during the machining. The BUL is a part of the work material that, due to the high pressure and temperature, sticks to the tool rake face. The BUE is a part of work material that sticks to the cutting edge under specific cutting conditions. The formation of

BUE is known to produce unstable cutting forces during the machining. To overcome these difficulties, many investigations were performed in order to optimize the machining of these alloys. The cemented carbide (WC-Co) tools are often used in machining aluminum alloys. However, the WC-Co tools promote the formation of the BUL on the tool rake face (Gangopadhyay et al., 2010). On the other hand, the BUL could be brought down significantly by using CVD diamond coated and PCD insert tools even at a low cutting speed of 200 m/min (Figure 1-19). The morphology and the mechanisms leading to the formation of BUE and BUL during machining has been the subject of several research studies (Bandyopadhyay, 1984b; Carrilero et al., 2002; Iwata et Ueda, 1980; Sánchez et al., 2005). Iwata and Ueda (1980) stated that there are two types of cracks associated with the BUE formation: one forms below the flank face of the tool, while the other subsequently forms ahead of the rake face of the tool. Recently, Gómez-Parra et al. (2013) indicated that severe cutting conditions can promote a faster formation of the primary BUL in machining aerospace aluminum alloys such as UNS A92024 (Al–Cu) and UNS A97050 (Al–Zn).

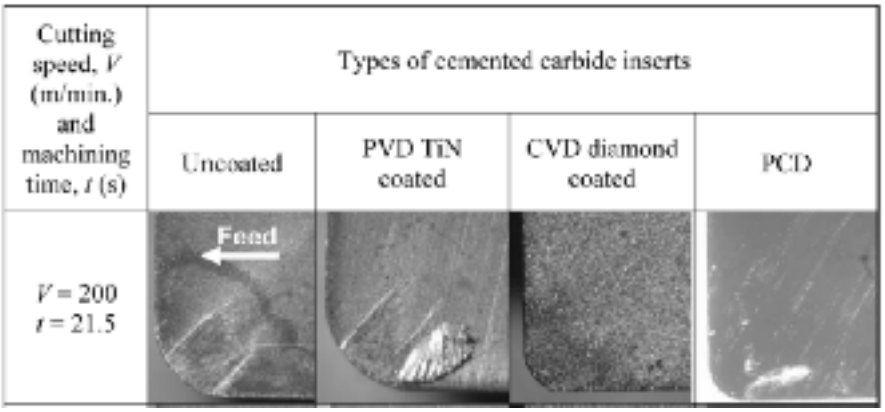

Figure 1-19 Optical micrographs of rake surfaces of different cutting tools after machining of AA6005 (Gangopadhyay et al., 2010)

The chip morphology was also investigated during the machining of aluminum alloys. Rao and Shin (2001), in studying the high-speed face milling of the 7075-T6 alloy, have observed that no significant variation in the morphology of the chips with changes in cutting speed and depth of cut ranges used in their study. However, the chip morphology was more sensitive to the feed variation (Figure 1-20). Specifically, segmented chip with shear localization were

observed at the highest feed (Figure 1-21b). The segmented chip formation has been studied during the high speed machining of the Al-7075-T651 alloy (Campbell et al. 2006). The authors have used optical metallography with differential interference contrast (DIC) to identify the shear band region (Figure 1-22). It was found that, for the 0° rake angle cutting condition, the distance between shear bands does not change significantly with the cutting speed variation. However, the width of the shear band does increase with the cutting speed as shown in Figure 1-23. Conversely, for the +15° rake conditions, the distance between the shear bands increases with the cutting speed, but, no significant change in the width of the shear bands has been observed. Finally, Campbell et al. (2006) demonstrated that dynamic recrystallization occurs in the shear bands of the chips resulting in recrystallized grains. The localized shear strains present in the shear bands of the chips are more than twice that predicted by global estimates and the localized strain rates are predicted to be an order of magnitude higher ($\approx 10^{-6}$ s^{-1}) than the global strain rates in the chip. On the other hand, Mustafa and Tanju (2011) studied the machinability of the Al 7075 alloy using a diamond cutting tool. The authors have found that the effective parameters for the increase of cutting forces are depth of cut, cutting speed and feed and the heat generation during the chip removal is proportional with the cutting feed. The cutting forces (mechanical effect) and the heat generation (thermal effect) not only affect the chip formation but also influence the surface integrity characteristics, particularly the residual stress state, of the machined aluminum parts.

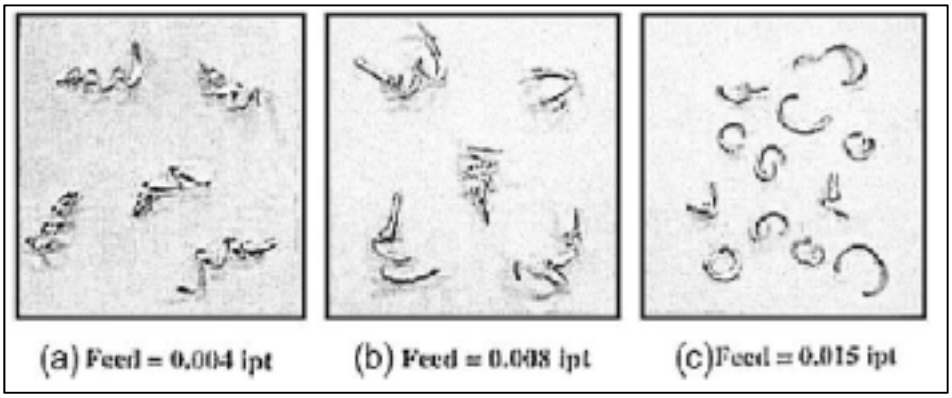

Figure 1-20 Chip morphology in face milling of AL7075-T6 for different feeds with carbide tool (speed=1250 m/min, depth of cut=1.27mm) (Rao et Shin, 2001)

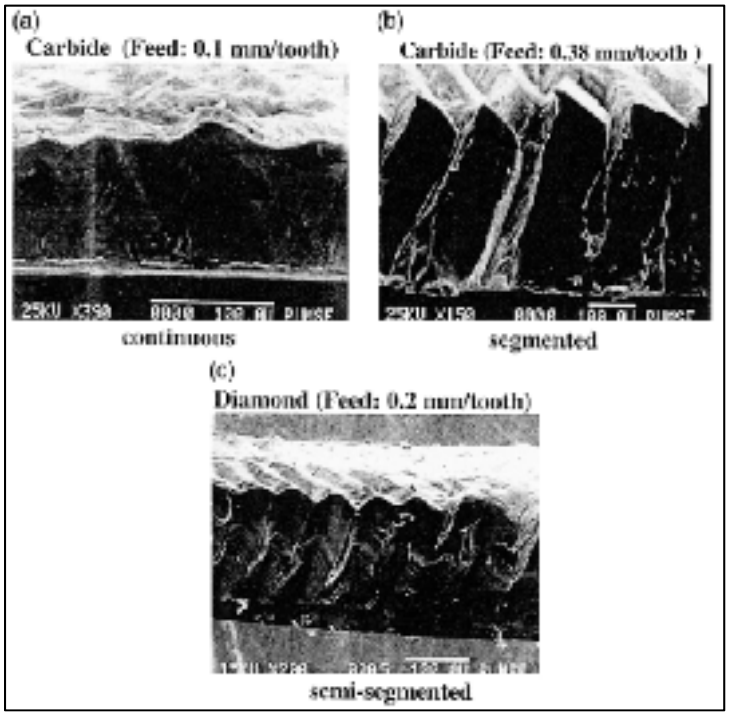

Figure 1-21 Continuous and segmented chips of AL7075-T6 (cutting speed=1250 m/min and depth of cut=1.27 mm) (Rao et Shin, 2001)

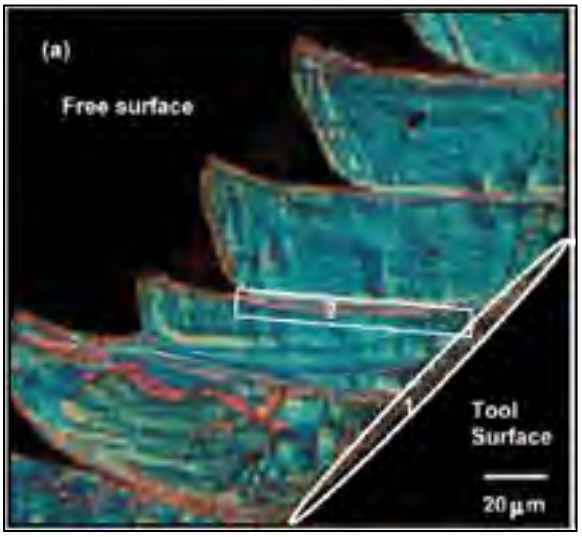

Figure 1-22 Optical metallography using differential interference contrast (DIC) of the chips from HSM at 540 m/min of Al-7075-T651. (Campbell et al., 2006)

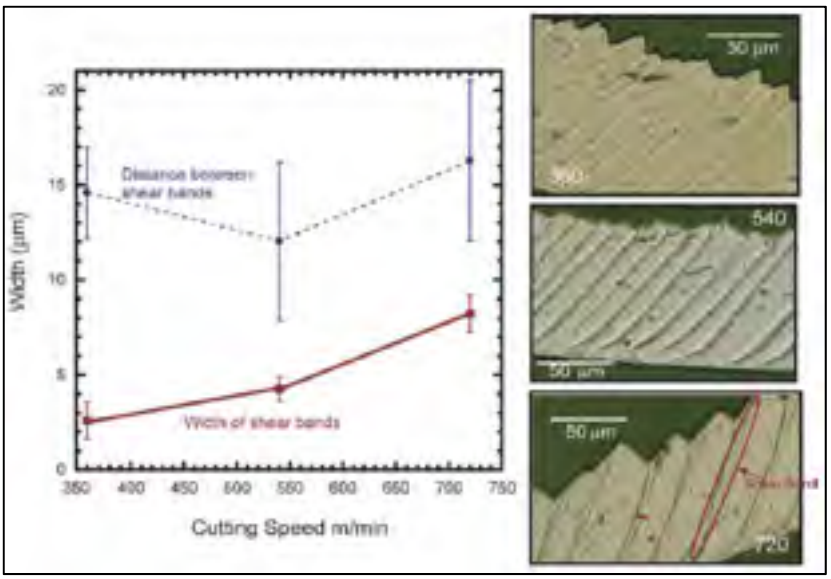

Figure 1-23 Effect of cutting speed on chip segmentation and shear band width for rake angle 0° rake angle machining of Al-7075-T651 (Campbell et al., 2006)

1.3.2 Surface integrity in machining aluminum alloys

The in-service life of the aluminum parts was found to be sensitive to the surface integrity after machining. Specifically, the fatigue resistance of precipitation-hardened aluminum alloys experienced a high sensitivity to the surface roughness and residual stress in research works performed by Suraratchai et al. (2008) and Chaussumier et al. (2013). Thus, it is worth to understand how surface integrity characteristics, especially, the surface finish and residual stress, were affected during the machining of aluminum alloys.

1.3.2.1 Surface finish in machining aluminum alloys

The surface finish, which includes the topography and defects of the machined surface after machining of aluminum alloys, has been investigated in several studies. The surface roughness parameters are good indicators for the machined surface quality. Previous work (Ammula et Guo, 2005) showed that the cutting speed has a dominant effect on the surface roughness compared to the feed and depth of cut in high speed milling 6061-T651 aluminum

alloy. The surface roughness trends were often associated to BUE formation during the machining of aluminum alloys. Gómez-Parra et al. (2013) showed that the BUE growth is responsible for a decrease in Ra roughness. In fact, the presence of the BUE increases the tool nose radius, therefore, improves the surface roughness. However, Iwata and Ueda (1980) stated that the rearward disappearance of the BUE leaves debris containing cracks on the machined surface. Such surface damage is undesirable because it increases the surface roughness and deteriorates the strength of the workpiece. Gangopadhyay (2010) evaluated the performance of different cutting tools in terms of BUE/BUL formation and surface roughness during the machining of AA6005 alloys. The authors found that the surface roughness decreases with an increase in cutting speed and related this trend to an increase in cutting temperature, which in turn might lead to slight reduction in material adhesion. Cai *et al*. (2012b) studied the effect of high speed end milling on the surface integrity of 7075 aluminum alloy. Their results showed that a high cutting speed has a positive effect on the surface finish. Furthermore, the residual stresses will be transformed from tensile values to compressive values when the cutting speed increases. Conversely, Ammula and Guo (Ammula et Guo, 2005) reported that an increase in the cutting speed increases the arithmetic mean (Ra) during the high speed milling of Al 7050-T7451 alloy. More recently, Mustafa et Tanju (2011) showed that the feed rate is most effective factor on controlling the surface roughness when machining Al 7075-T6 using diamond cutting insert.

On the other hand, Suraratchai et al. (2008) attested that surface roughness is considered as generating local stress concentration. Additionally, experimental observations showed that fatigue cracks were initiated on intermetallic inclusions located at the bottom of the machining grooves during the machining of precipitation-hardened aluminum alloys.

1.3.2.2 Residual stress in machining aluminum alloys

It is well recognized that the residual stress state is very sensitive to the machining process parameters such as cutting tool geometry and material, cutting speed, feed rate, and depth of cut. Rao and Shin (Rao et Shin, 2001) studied the effect of high speed face milling on the

surface integrity of 7075-T6 aluminum alloy. Their results showed that an increase in feed induced high compressive residual stresses in the workpiece, while higher cutting speed and depth of cut show an opposite effect. In addition, the surface roughness was improved with the cutting speed up to 1524 m/min, beyond which it showed degradation. On the other hand, it was found that the residual stress in the feed direction is tensile near the surface and quickly changes to compressive stresses at about 35 μm when high speed milling 6061-T651 aluminum alloy (Grum, 2001). Jeelani *et al.* (1986) investigated the effect of cutting speed and tool rake angle on residual stress distribution during the machining of 2024-T351 aluminum alloy. The results showed that the residual stresses are compressive at the machined surface and decrease with depth beneath the machined surface. The maximum (near-surface) residual stress and the depth of the severely stressed region increase with an increase in the cutting speed. In addition, a little change in the residual stress distribution due to a change in the rake angle was observed. Denkena *et al.* (2008) investigated the influence of the machining parameters as well as the cutting edge geometry on the residual stress changes in the machining of forged Al7449 T7651aluminum alloy. It has been shown that an increase in the feed per tooth, a decrease of the width of cut or the use of higher radii at the secondary cutting edge lead to more pronounced compressive residual stresses at deeper depths below the machined surface. Chaussumier et al. (2013), in studying the surface integrity of 7000 series aluminum alloys, have shown that the fatigue resistance is primarily influenced by the surface roughness; however, residual stresses play a second role.

In summary, previous research works on machining of aluminum alloys indicated that the BUE and/or BUL formation is the main parameter influencing the chip formation and surface quality of the machined parts. The use of high speed machining could improve the surface quality and integrity. However, tensile stresses could be achieved in high speed conditions. Although high strength aluminum alloys are used in several applications, a few studies were performed on the effect of the chip formation on the surface integrity characteristics and basic understanding of the tool/workpiece microstructure interactions still lacking. In the next section, we will focus on the chip formation and surface integrity alterations during the machining of hardened steels.

1.4 Machining of hardened steel (Hard machining)

The hard machining is a process based on the strengthening of the cutting tool, allowing the work material to be machined at its hardened state (45-68 HRC). The hard machining has become possible due to the development of advanced cutting tool materials such as Polycrystalline Cubic Boron Nitride (PCBN) (Zhou et al., 2003). TiN-coated cermets and AL_2O_3-TiC ceramic tool were also used for the machining of hardened steels (Poulachon, Moisan et Jawahir, 2001). In order to obtain sufficiently high production rates at minimum cost, and to withstand large tool stresses, specific cutting edge preparations are used in hard machining. The cutting tool edge should be protected from the chipping and premature failure by selecting some specific geometric designs for hard turning. As a result, various types of cutting tool edges preparation, such as sharp, hone, chamfer, and hone plus chamfer cutting edges, are used in machining hard-to-cut materials (Figure 1-24). In fact, chamfered cutting edges were usually selected due to their high wedge strength and chipping resistance, but they also experienced cutting forces higher than positive or zero rake angle tools (Zhou et al., 2003). The cutting edge geometries not only affect the surface integrity characteristics but also resist to the wear in different ways (Figure 1-25). In the next sections, we will focus on the effect of cutting tool geometry and material, cutting conditions, and work material on the chip formation and surface integrity in hard machining.

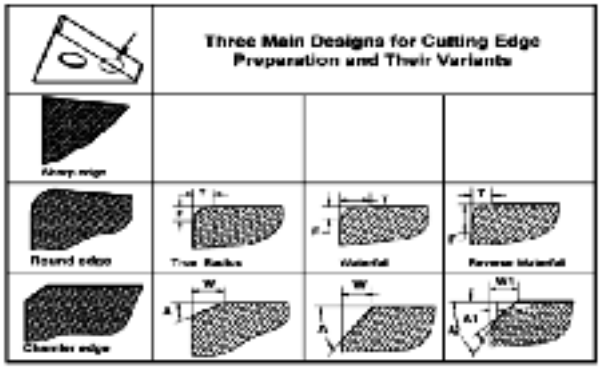

Figure 1-24 Typical cutting edge preparation designs and their variants for commercial inserts (Yen, Jain et Altan, 2004)

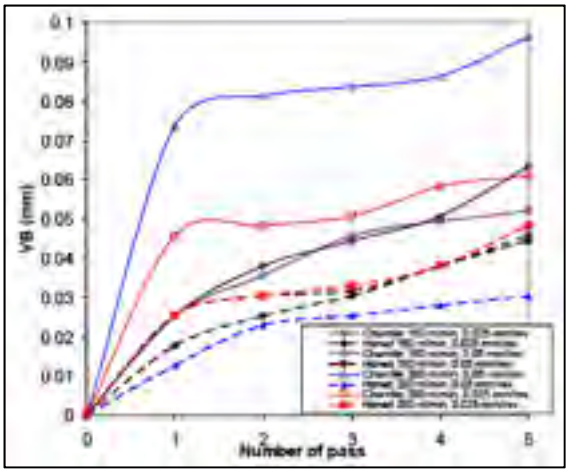

Figure 1-25 Flank wear for different
PCBN cutting edge geometries
(Karpat et Özel, 2007)

1.4.1 Chip formation and cutting forces in hard machining

The formation segmented chip (Figure 1-26), also well-known as saw-tooth or serrated chip, is a primary characteristic of the hard machining process. Different theories and models were developed in order to explain the formation mechanism of such chips. Previous studies (Barry et Byrne, 2002b; Komanduri et al., 1982; Liyao, Minjie et Chunzheng, 2013) suggested that that segmented chip generation in hard machining is essentially an adiabatic shear process. The adiabatic shear is often defined as a highly periodic instability within the primary shear zone (Figure 1-27). Astakhov (2006) stated that segmented chips are formed under a cyclic phenomenon due to the variation of the stress and the plastic deformation states and the resulted temperature on the cutting zone. Others (Vyas et Shaw, 1999) suggested that the fracture/crack propagation mechanism is at the root of the generation of such chips. The occurrence of the crack is also a point of contention. For some researchers, such as Poulachon et al. (2001), the crack initiates on the free surface of the work material and propagates to the tool tip. However, others (Astakhov, Shvets et Osman, 1997b; Barry et Byrne, 2002c) argued that the crack occurs at the tool tip, and propagates partway to the free workpiece surface. Jomaa et al. (Jomaa et al., 2011), in studying the turning of hardened AISI D2 steel (60-62 HRC) using PCBN tools, showed that segmented chips are formed in three

steps including, first, elastic loading, second, crack initiation at microstructure defects, and finally, ductile/brittle fracture (Figure 1-28). The authors claimed that the mechanical characteristics (high hardness and yield stress) of the work material, the micro-geometric defects of the workpiece surface and the edge preparation of the cutting tool are responsible of the segmented chip formation.

It is understood that the segmented chip formation is detrimental for the stability of the machining system although they break easily. In fact, high oscillated cutting forces were always obtained when segmented chips are formed which can induce dimensional and geometrical errors and poor surface finish of the machined parts.

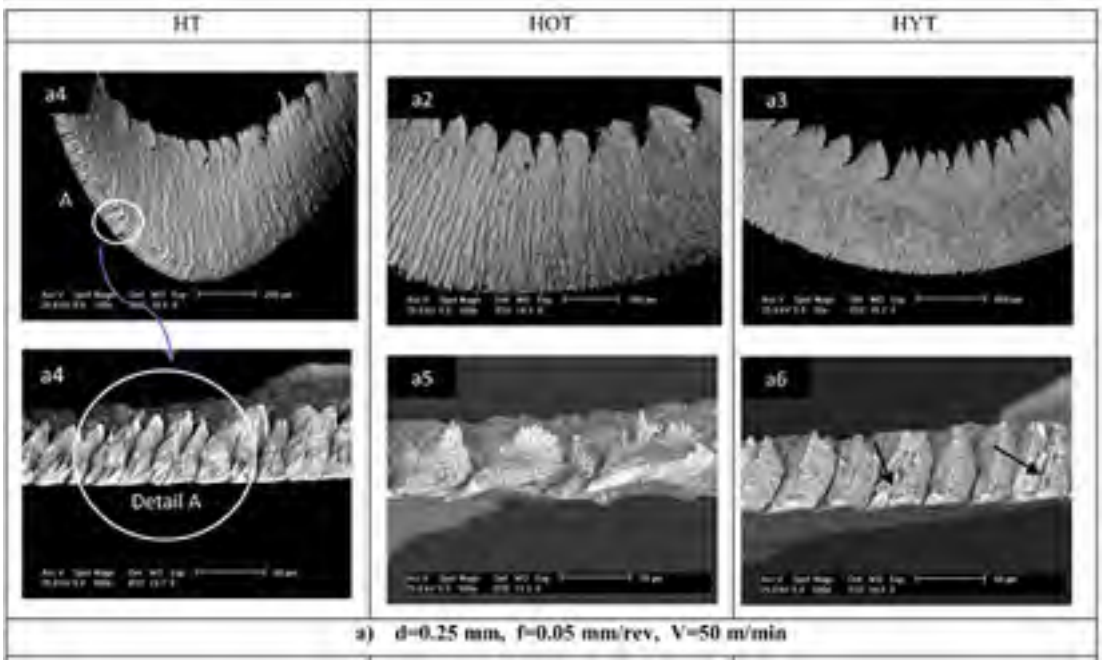

Figure 1-26 SEM micrograph of segmented chips generated by PCBN hard turning (HT) of AISI D2 steel (Jomaa et al., 2011)

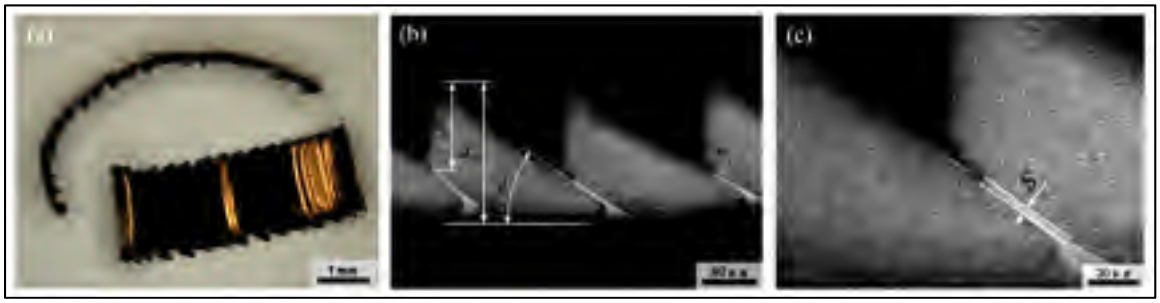

Figure 1-27 Macrograph and micrographs of discontinuous serrated chip of hardened AISI1045 steel at cutting speed of 1000 m/min (Liyao, Minjie et Chunzheng, 2013)

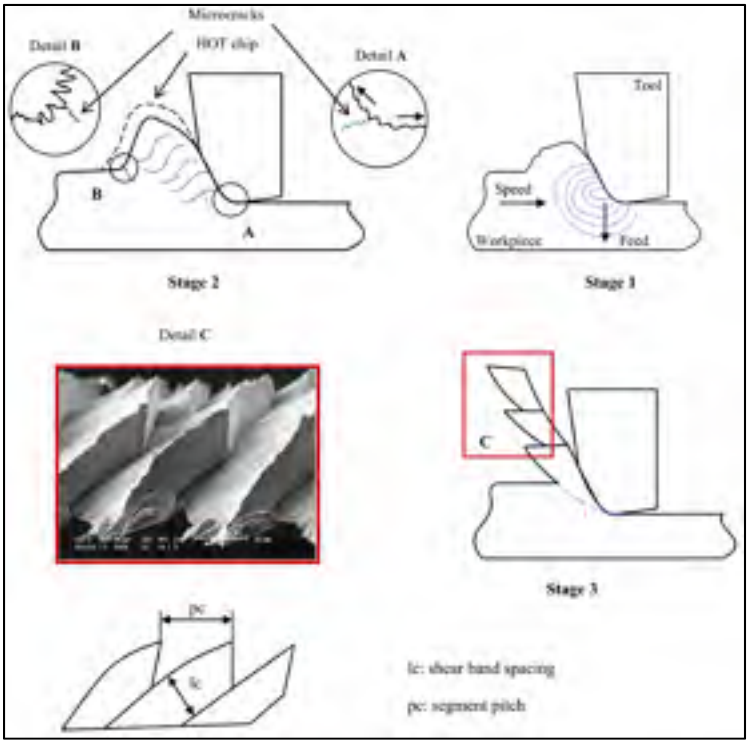

Figure 1-28 Segmented chip formation during turning of hardened AISI D2 steel (60-62 HRC) using PCBN tool (Jomaa et al., 2011)

The machining of difficult-to-cut materials using advanced cutting tools such as cermets and CBN is evidently different from the machining of soft materials using ordinary carbide cutting tools. In fact, the forces involved in hard turning are approximately 2 times higher than those for an equivalent annealed workpiece (Lalwani, Mehta et Jain, 2008). Unlike conventional machining, where the tangential force is the highest force component, the thrust

force is higher than the tangential (cutting) force in hard machining (Figure 1-29) (Jomaa et al., 2011). This trend is mainly governed by the geometric effect of the cutting tool with respect to the depth of cutting. Most of the cutting tools used in hard machining have a honed and/or chamfered cutting edge. In machining hardened steel, because of small depth of cut (smaller than the edge radius or the chamfer length), the chips were formed by the region of the edge chamfer or the radius of the cutting edge (Liu, Takagi et Tsukuda, 2004) leading to high negative effective rake angle. A large negative rake angle increases the cutting forces only a little, whereas increases the thrust forces significantly. Besides, as the cutting edge hone increases, the total machining force increases and the contribution of the ploughing component of force increases in magnitude (Thiele et N. Melkote, 1999). Because the ploughing forces in turning are resolved mainly in the axial and radial directions (the thrust direction in orthogonal cutting), these force components increase, significantly, whilst the tangential one increases only slightly. Jomaa et al. (Jomaa et al., 2011) investigated the effect of cutting speed, feed rate and depth of cut on the cutting forces in hard machining AISI D2 steel at 62 HRC using PCBN inserts. Their results showed that the cutting forces decrease with the increase in cutting speed and increase with the increase in feed rate and depth of cut. However, the cutting speed higher than 150 m/min has not been recommended because of increased tool wear rates and poor surface finish. Furthermore, Sahin (Sahin, 2009) has found that the tool life of the mixed ceramic cutting insert grade decreases significantly when machining hardened bearing steel (AISI 52100-659HV) at cutting speed above 140m/min. Some other works (Dogra et al., 2010; Poulachon, Moisan et Jawahir, 2001; Yallese et al., 2009) showed that the optimal cutting speed for both, tool life and chip formation, was in the 100-130 m/min range and that did not recommend further increase in cutting speed during hard machining.

The severe cutting conditions of the hard machining does not only affect the chip formation and tool wear, but also the surface integrity characteristics such as the residual stress, phase change, plastic deformations, and etc.

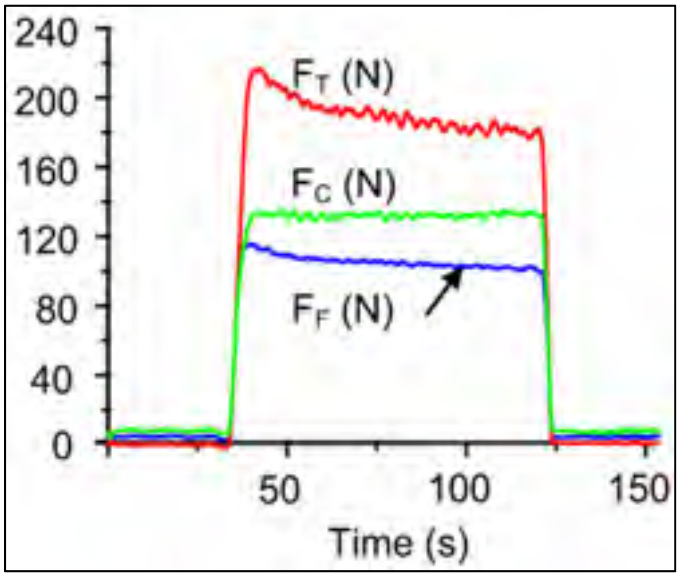

Figure 1-29 Temporal signals of cutting force components in hard turning of AISI D2 steel (60-62 HRC) at cutting speed=150 m/min (Jomaa et al., 2011)

1.4.2 Surface integrity effects in hard machining

Hard machined parts are exposed to different alterations including mechanical, metallurgical, thermal and chemical, during the machining (Youssef et El-Hofy, 2008b). the mechanical alterations are represented by the residual stresses, plastic deformations, and microhardness gradients (softening or hardening). The metallurgical alterations include phase changes (white layer, dark layer).

1.4.2.1 Surface finish in hard machining

Liu *et al.* (2002) investigated the effect of workpiece hardness on the surface quality during finish hard turning of through-hardened AISI 52100 steel. The results show that 50 HRC is critical workpiece hardness for the AISI 52100 material. When the hardness exceeded 50 HRC, the surface roughness was decreased as the hardness increased, and poor surface quality was generated around the critical hardness (50 HRC). Thiele and Melkote (1999)

examined the effects of tool cutting edge preparation and workpiece hardness on the surface finish in the finish hard turning of AISI 52100 steel. The study revealed that the cutting edge preparation has a significant effect on the surface generation during the hard turning: increasing the edge hone radius lead to the increase of the average surface roughness. It also showed that the two-factor interaction of the workpiece hardness and cutting edge preparation on the surface roughness is very significant. The effect of the cutting edge radius, on the surface roughness, depends on the workpiece hardness: as low is the hardness, as high is the effect of the cutting edge radius. On the other hand, Rech and Moison (2003) indicated that the feed rate is the main parameter influencing surface roughness in the machining of case-hardened 27MnCr5 steel. Furthermore, the average roughness parameter, Ra, was not very sensitive to the flank wear and, consequently, to the material side flow occurrence. Poulachon et al. (2005) investigated the effect of work material microstructure on the surface finish of hard machined parts using PCBN tools. The authors have established a correlation among the surface profile, grooves on the flank face, and carbides on the microstructure as shown in Figure 1-30. Moreover, the surface profile can be different due to the microstructure size for materials with a similar tool-wear rate. 35NiCrMo16 steel has nearly no surface roughness of the order of 4 whereas X38CrMoV5 has large variations in surface roughness as shown in Figure 1-31.

In order to improve the productivity without affecting the surface quality of hard machined parts, new generation of cutting tool inserts has been developed in the last decades. Tool inserts with wiper geometry are one of these cutting tools (Figure 1-32). Grzesk and Wanat (Grzesik et Wanat, 2006), in studying the hard turning of quenched alloy steel parts using conventional and wiper ceramic inserts, showed that keeping equivalent feed rates, i.e. 0.1 mm/rev for conventional and 0.2 mm/rev for wiper tools, the surfaces obtained have similar 3D height roughness parameters, and comparable values of skew and kurtosis. Furthermore, at defined cutting parameters, surfaces produced by wiper were recorded during peaks with distinctly smaller slopes resulting in better bearing properties (Figure 1-33).

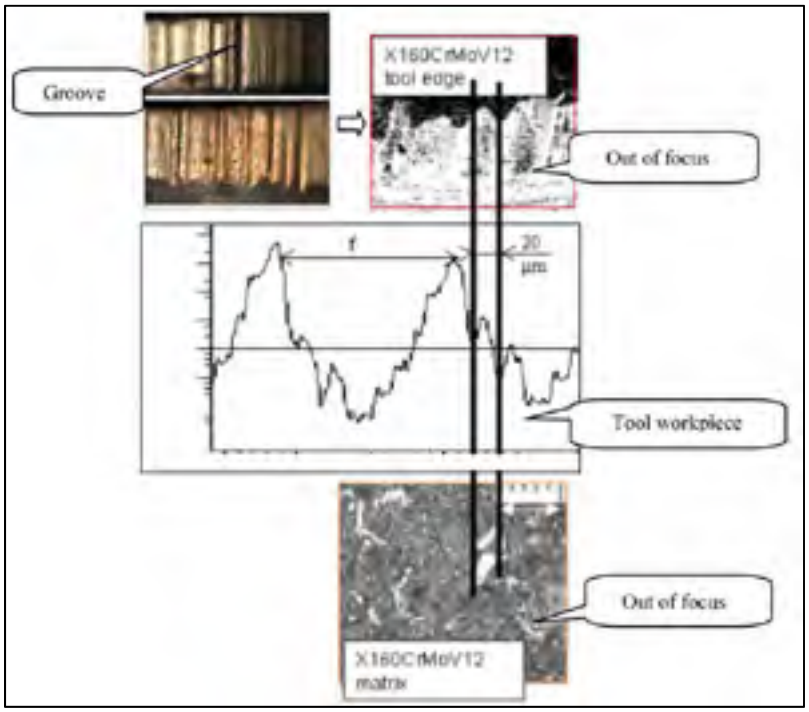

Figure 1-30 Correlation between roughness profile, tool edge and microstructure for X160CrMoV12 steel (Poulachon et al., 2005)

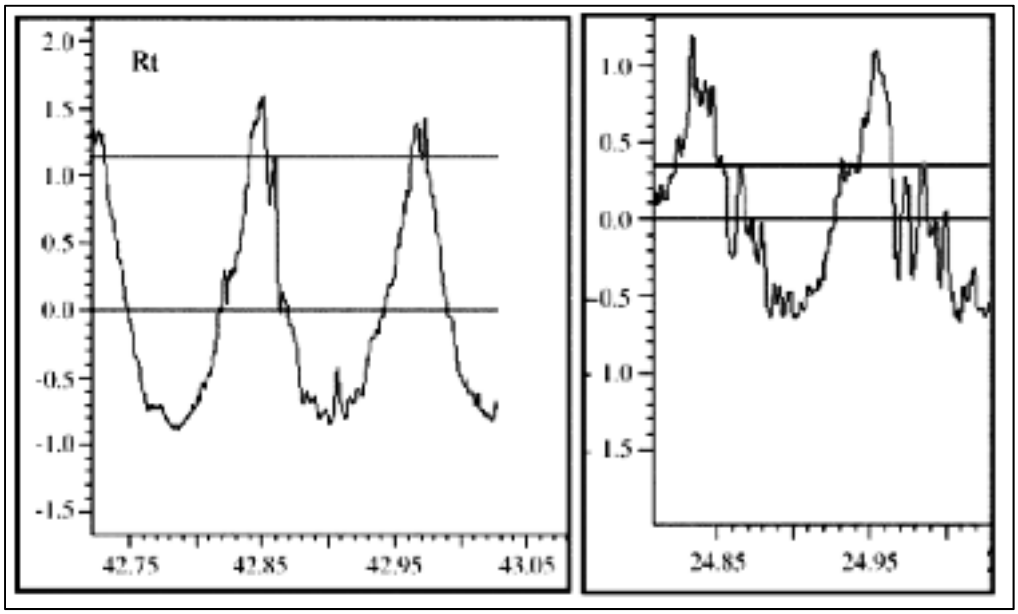

Figure 1-31 35NiCrMo16 (right) and X38CrMoV5 (left) surface profile at a time=5 min (Poulachon et al., 2005)

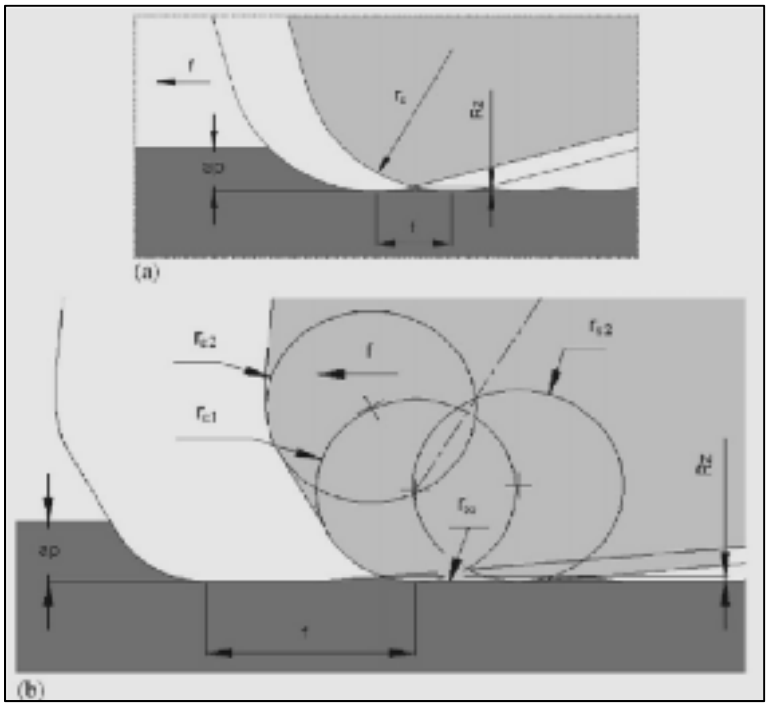

Figure 1-32 Comparison of inserts with conventional geometry (a) and wiper (b) (Grzesik et Wanat, 2006)

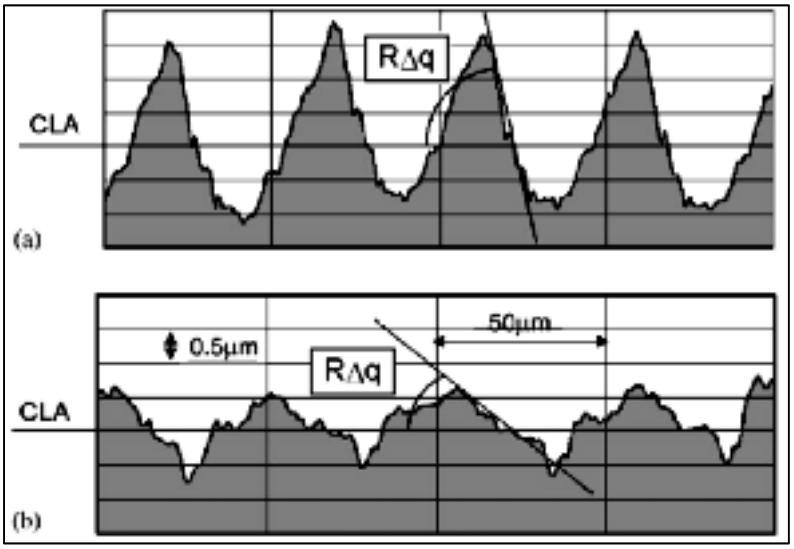

Figure 1-33 Characteristic shapes of the profiles generated in turning with (a) conventional and (b) wiper tools (Grzesik et Wanat, 2006)

1.4.2.2 Residual stress in hard machining

the residual stresses are one of the most relevant characteristics of surface integrity that affects significantly the structural components life and performance. It is generally agreed that tensile residual stress reduces the fatigue strength and compressive residual stress improves it (Hashimoto, Guo et Warren, 2006).

In the hard machining, the effect of cutting parameters on residual stresses have been extensively investigated. Dahlman et al. (2004) and Dogra et al. (2011) showed that the rake angle has the strongest influence on the residual stresses. Moreover, the use of high negative effective rake angle and chamfer plus hone radius inserts induced a large compressive residual stresses (Figure 1-34). The compressive stresses become greater with increased feed rate while no effect was observed for the cutting depth (Figure 1-35). Thiele et al. (2000) investigated the effects of cutting-edge geometry and workpiece hardness on the surface residual stresses in finish hard-turning of AISI52100 steel (HRC 59-61). Their results showed that large edge hone tools induced compressive surface residual stresses in the axial and circumferential directions (Figure 1-36). Similar results were obtained in the hard turning of bearing steel using chamfer+hone cutting edge geometry (Hua et al., 2005). The authors argued that, with the use of the chamfered tool, a very strong compressive deformation state on the cutting edge was obtained. Thus, the burnishing process becomes a dominant factor in the chip formation due to the squeezing of the material under the cutting edge. This has leading to larger compressive residual stresses due to severe elastic and plastic deformation resulting in the machined surface. It is worth noting here that for most of the previous investigations, the maximum compressive stresses were obtained below the machined surface while the surface residual stresses were most of the time a tensile one. This was explained by the fact that high temperature (thermal effect) was generated during machining hardened material (Figure 1-37) (Hua et al., 2005).

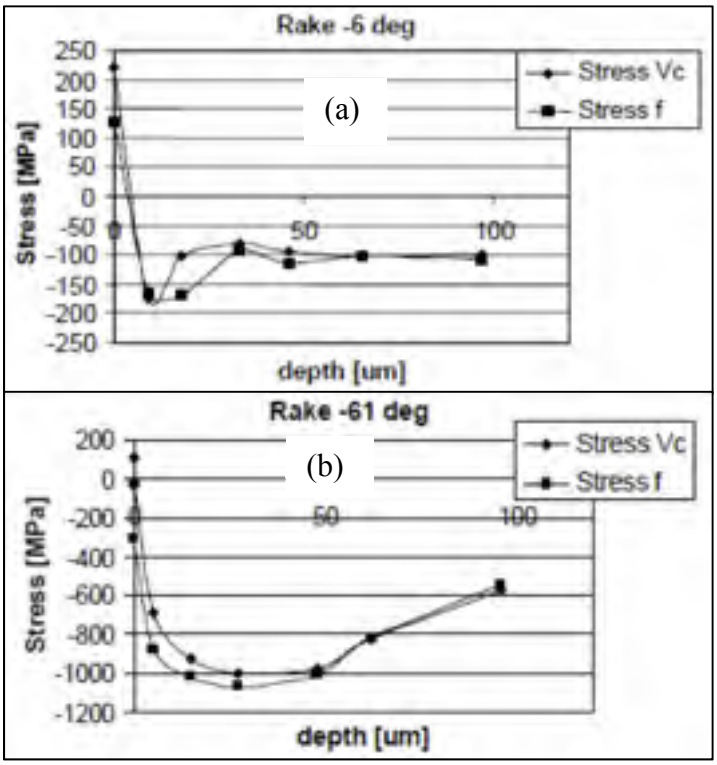

Figure 1-34 Residual stress distributions for a) -6 ° and b) -61° rake angles (Dahlman, Gunnberg et Jacobson, 2004).

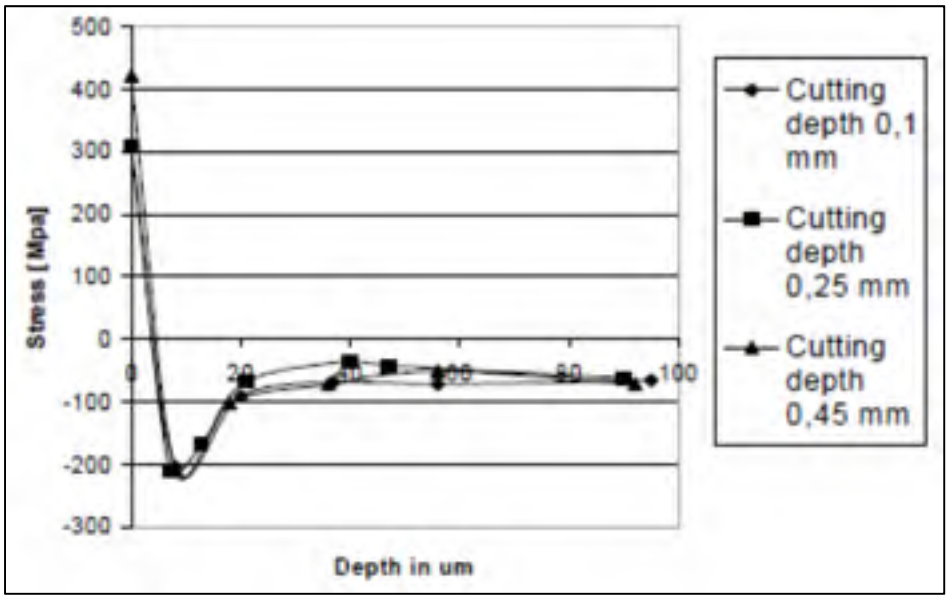

Figure 1-35 Effect of depth of cut on speed direction residual stresses for different cutting depths (Dahlman, Gunnberg et Jacobson, 2004).

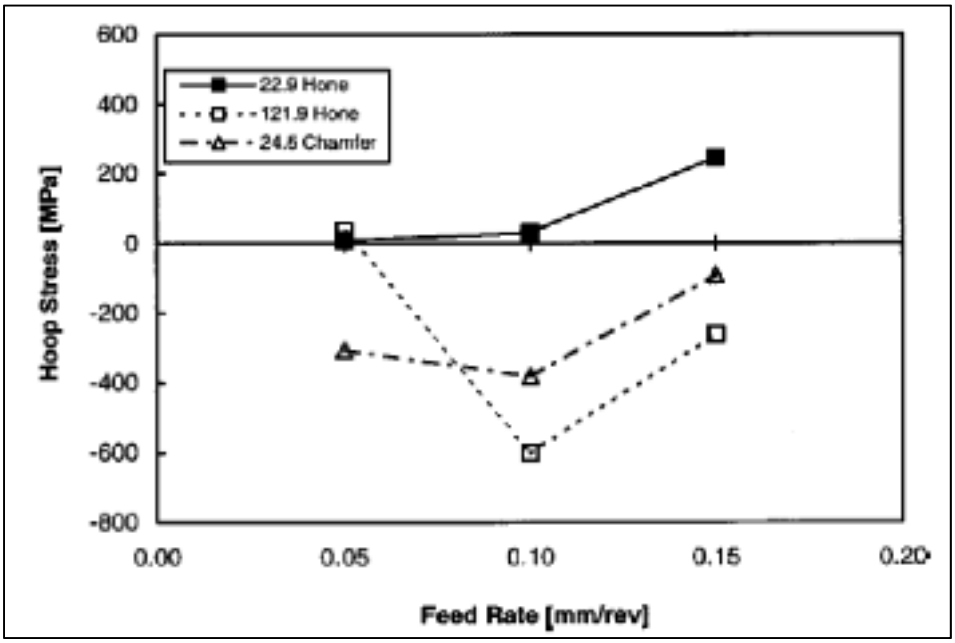

Figure 1-36 Effect of edge preparation and feed rate on hoop stress for 57 HRC workpiece

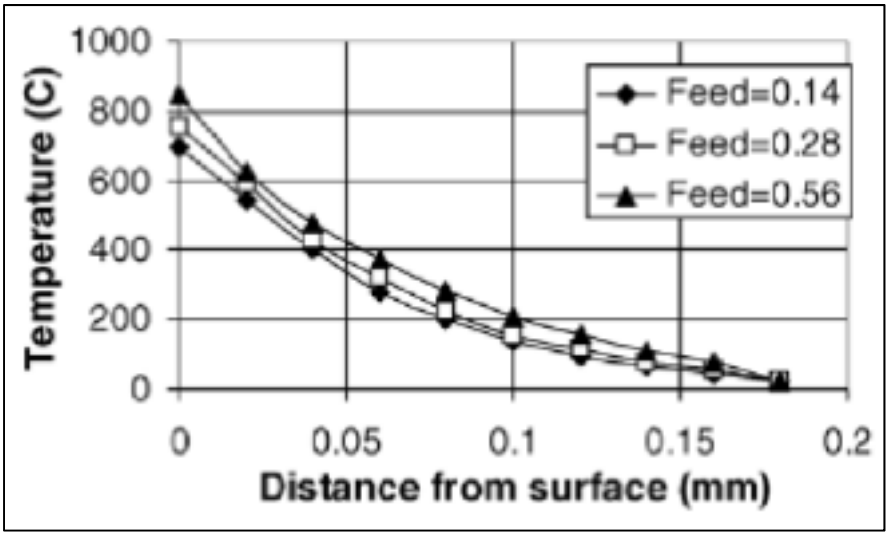

Figure 1-37 Distribution of temperature in the machined surface under the cutting edge at cutting speed=120 m/min and 62 HRC (Hua et al., 2005)

1.4.2.3 Plastic deformation and work hardening in hard machining

The plastic deformation is a critical factor in determining the residual stress state of the machined parts (Ramesh, Thiele et Melkote, 1999). Thiele and Melkote (2000) showed that PCBN inserts with a large cutting edge radius (121.9 microns) induce a plastic flow in the circumferential direction when machining AISI 52100 steel with a hardness of 41 and 57 HRC. However, the plastic flow was not observed for honed (22.9μm) and chamfered cutting edge inserts. On the other hand, Ramesh et al. (1999) heve compared the machine microstructures of two hard materials (AISI4340 and AISI 52100) with the same hardness (HRC 57). The results showed that the plastic deformation was observed for all tested feed (0.05, 0.1, 0.15 mm / rev) and tool geometries during the machining of the AISI4340 steel. The authors related this trend to the high amount of the residual austenite in the martensitic microstructure of the AISI4340 steel compared to the AISI52100 steel.

The microhardness profile is very useful for the identification of the metallurgical transformations such as the dark layer (tempered martensite) and white layer (untempered martensite) and their consecutive depth beneath the machined surface (Guo et Sahni, 2004). However, in many cases, the profile of microhardness was misinterpreted due to the small thickness of the white layer. Unexpected changes in the microhardness were often reported in the literature. Liu et al. (2002) showed that the depth of the work hardened layer increases with the hardness of the material and achieved its maximum levels at 50 HRC. Beyond the hardness of 50HRC, the depth of the work hardened layer remains unchanged.

1.4.2.4 White layer formation in hard machining

The machining process can induces microstructural changes of the work material at and below the machined surface. A white layer has been frequently observed in the hard machining with specific cutting tool geometries (Barry et Byrne, 2002b). Guo et Sahni (2004) stated that the austenitizing temperature is generally exceeded during the machining. Barry et Byrne (2002b) argued that the white layer can form by the rapid self-cooling of the

workpiece during the machining (Figure 1-38). Several theories have been developed to describe the nature of the microstructure of the white layer. Barry and Byrne (2002b) and Poulachon et al. (2005) assumed that the white layer is a kind of martensite composed of nanocrystals and characterized by a high density of dislocation. The surface obtained by hard turning often consisted of three layers: white layer (untempered martensite), dark layer (tempered martensite) and the bulk material. Several studies have shown that the white layer is the hardest one while the dark layer has an intermediate hardeness, between the hardness of bulk material and that of the white layer layer (Guo et Sahni, 2004). Jacobson et al. (2002) performed machining tests on AISI4340 with a hardness of 58HRC and they noticed that only 5% of workpieces having white layer of about 1μm thickness at a cutting speed of 50m/min. Ramesh et al. (1999) studied the influence of the tool geometry and the feed rate on the white layer formation during the hard machining of AISI 4340 and AISI 52100 steels. Their analysis of the micrographs reveals the absence of the white layer when machining AISI 4340 steel using a chamfered tool inserts and cutting feed of 0.05 mm/rev while a thin white layer was appeared at a cutting feed of 0.15 mm/rev. However, a continuous white layer was observed for all tested cutting feed when machining using 121.9 μm cutting edge radii.

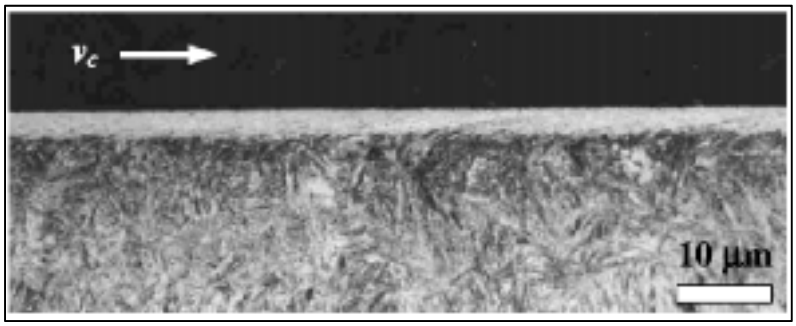

Figure 1-38 White layer of BS 817M40 steel at 52 HRC,
machined with a severely worn cutting tool
(*VB*C ≈400 μm) (Barry et Byrne, 2002a)

1.4.3 Comparison between hard machining and grinding

The hard machining process was developed in order to replace the grinding operations during the manufacturing of hard materials. Compared to grinding, hard machining enables relatively high material removal rates, great flexibility, the manufacture of complex shapes in a single setup, and hence, substantial cost reduction. Additionally, since hard turning is a single-point cutting tool process, it is possible to precisely modify the rake angle to control tool wear and surface integrity and to adapt hard turning to both roughing and finishing operations. This is not possible for grinding, due to multiple edges which are randomly scattered on the grinding wheel, and the effective rake angles vary over a large range (Dahlman, Gunnberg et Jacobson, 2004). Therefore, hard machining, particularly hard turning is increasingly accepted as a competitive process and as an effective alternative for grinding operations.

In order to ensure suitable dimensions and surface roughness, induction hardening is, most of the time, followed by grinding (Grum, 2001). However, additional grinding of the induction hardened surface has an inverse effect on the stress state, since grinding always induces tensile residual stresses (Boothroyd, 1988). In addition, a thick white layer can be formed in grinding under certain conditions (Guo et Sahni, 2004). Abràо et al. (1996) showed that the assessment of the fatigue life of turned and ground hardened bearing steel indicated that superior fatigue strength was obtained with turned specimens. Konig et al. (1993) compared the properties of ground and hard turned workpiece surface zones and the results showed that the formation of a so-called 'soft skin' is largely suppressed in hard turning operations due to the stress-induced hardening of the workpiece material. Such hard turned surfaces can consequently demonstrate high levels of rolling strength even with a 'white layer', similar to grinding burn (König, Berktold et Koch, 1993). Residual stresses are widely studied in the case of grinding of induction surface hardened materials (Grum, 2007; Grum, 2000; 2001; Savaria, Bridier et Bocher, 2012), on the contrary to machining processes, using a single point tool, as well as turning and milling.

To summarize, the machining of hardened materials lead to the formation of segmented chip and high cutting forces compared to the machining of non-heat treated ones. Compressive residual stresses can be achieved. In addition, a white and dark layer can form in specific cutting conditions. The driven mechanisms of the white layer formation still unresolved. Furthermore, the effect of the chip formation mechanisms and cutting forces on the residual stresses and microstructure alterations during the machining of induction heat treated steels is still lacking. Cutting forces modeling is the basis to understand the cutting process and its effect on the machined surface integrity. In the next section, we will briefly present the most used modeling techniques and will focus on the Oxley's machining theory.

1.5 Modeling of the machining process

In today's highly competitive machining industry, research's studies are focusing on the development of predictive models using analytical, empirical, and finite elements (FEM). The development of reliable models helps to optimize and to control the machining process by avoiding time consuming and expensive experimental works leading to reduced parts cost. Although it can provide precise results, FEM techniques are still time consuming and difficult to establish as large plastic deformations not only bring complications from the mathematical point of view, but can also cause rapid solution degradation due to element distortion (Vaz Jr et al., 2007). Empirical modeling needs extensive experimental works and therefore it is expensive and the applicability of the obtained results is limited to the tested conditions domain. Finally, analytical modeling seems to be the optimal solution for machining predictions since it can relate physical phenomena to technological process parameters with low computation time and few experimental data inputs. Oxley's machining theory (OMT) is considered as the most fundamental approach in the analytical modeling of the machining process based on the slip-line field theory (Kopalinsky et Oxley, 1984; Oxley et Hastings, 1977).

1.5.1 Basics of Oxley's machining theory (Hastings, Mathew et Oxley, 1980; Kopalinsky et Oxley, 1984; Oxley et Hastings, 1977)

The main contribution of Oxley and co-workers was the development of a predictive machining theory by considering the effects of strain, strain-rate, and temperature on the flow stress of the work material. Only material properties, tool geometry and cutting conditions are needed to predict the cutting forces, chip thickness, average temperatures, and stresses in the deformation zones.

In the model of chip formation (Figure 1-39), on which the theory is based, it was assumed that:

- Plane strain and steady-state conditions;
- The tool is perfectly sharp;
- The shear plan AB and the tool/chip interface are both direction of maximum shear stress and maximum shear strain rate;
- In the chip adjacent to the tool cutting face, a boundary layer exists of thickness δt_c across which the velocity changes linearly from zero at the tool surface to the chip velocity *Vc;*
- The effect of temperature gradient is neglected;

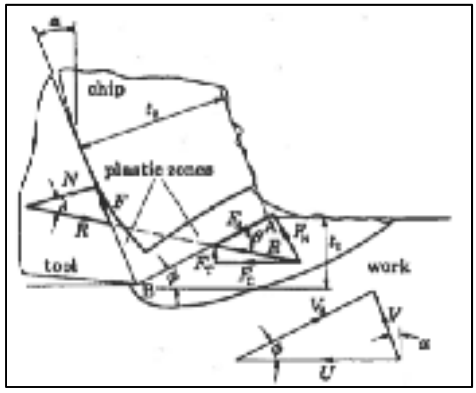

Figure 1-39 Chip formation model in Oxley's theory (Hastings, Mathew et Oxley, 1980)

Oxley has used the quick-stop method to measure the flow field and proposed a slip line field as shown in Figure 1-39. The slip-line field and the corresponding hodograph indicated that the strain rate in the primary shear zone increases with cutting speed and has a maximum value at the plane AB. Based on these experimental observations, he proposed the empirical relation in Eq (1-2) for the shear strain rate average value along AB:

$$\dot{\gamma}_{prim} = C_0 \frac{V cos\alpha \sin \emptyset}{t_u cos(\emptyset - \alpha)} \tag{1.2}$$

The basis of the theory is to analyse the stresses along the plane AB and at the tool/chip interface in terms of the shear angle ($\emptyset$) and the cutting conditions, then, to select as the solution for $\emptyset$ the value for which the shear stress τ_{int}, calculated from the resultant force (R) across AB, equals the shear flow stress k_{chip} in the chip material at the interface. The strain rate constant C_0 is determined with the machining theory as part of the solution by imposing the normal stress σ_N at the tool/chip interface to be equal to the normal stress σ_N' calculated at point B (Figure 1-39). The strain rate constant at the secondary shear zone δ is therefore selected so as to minimize the main cutting force (F_c).

Once $\emptyset$ is known, then the chip thickness t_c and the various components of the machining force can be determined from the following geometrical relations:

$$F_c = R\cos(\lambda - \alpha), F_t = R\sin(\lambda - \alpha) \tag{1.3}$$

$$F = R\sin\lambda, N = R\cos\lambda \tag{1.4}$$

$$R = \frac{F_s}{\cos\theta} = \frac{k_{AB} t_u w}{\sin\emptyset\cos\theta} \tag{1.5}$$

$$\lambda = \alpha + \theta - \emptyset \tag{1.6}$$

where the symbols used in the Figure 12-39 and above equations are defined in the nomenclature.

1.5.2 Generalization of the Oxley's machining theory

Oxley's theory requires the inputs for flow stress data of the work material that depends on strain, strain rate, and temperature. Thus, a power law (Equation (1-7)) equation for material flow stress was used. In this equation, the constants σ_1 and n of the flow stress depend on velocity-modified temperature (T_{mod} (Equation (1-8)) concept given by Macgregor and Fisher (MacGregor et Fisher, 1946). It is worth recalling that the velocity-modified temperature depends on the strain rate.

$$\sigma = \sigma_1(T_{mod})\varepsilon^{n(T_{mod})} \tag{1.7}$$

$$T_{mod} = T\left[1 - \vartheta \log\left(\frac{\dot{\varepsilon}}{\dot{\varepsilon}_0}\right)\right] \tag{1.8}$$

where T is the temperature, $\dot{\varepsilon}$ is the strain rate and ϑ and $\dot{\varepsilon}_0$ are constants. The constants σ_1 and n are expressed by a different order polynomial equation in the different ranges of T_{mod} and high order polynomials were used in some range of T_{mod} for required accuracy (Figure 1-40).

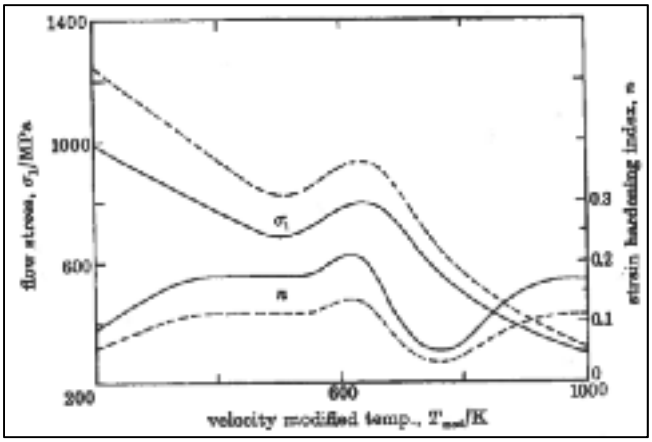

Figure 1-40 Flow stress results plotted against velocity modified temperature for 0.2% and 0.38 % Carbon steel (Hastings, Mathew et Oxley, 1980)

However, such relations are only available in the literature for the low carbon steels (Kopalinsky et Oxley, 1984; Oxley et Hastings, 1977). It was found that this approach (velocity-modified temperature) is not suitable for hardened materials due to heat-treated processing as stated by Lee (2011). Kristyanto *et al* (2002) applied the Oxley's theory to the machining of two aluminum alloys. Their result showed some discrepancies between predictions and experiments, particularly, at lower cutting speeds and /or feed rates.

Hence, to overcome these shortcomings, research studies (Adibi-Sedeh, Madhavan et Bahr, 2003; Huang et Liang, 2003b; Karpat et Özel, 2006; Lalwani, Mehta et Jain, 2009; Lee, 2011; Long et Huang, 2005; Özel et Zeren, 2004; 2006; Ren et Altintas, 2000) were carried out during the last decade to extend the applicability of the Oxley's machining theory to a broader class of materials. Huang and Liang (2003b) generalized Oxley's predictive theory to the hard machining of H13 steel using the Johnson-Cook equation. Their model considers the effect of the tool thermal properties thanks to the applied moving heat source method in modeling the cutting temperature rather than the empirical model used by Oxley. The results showed that the modified Oxley's approach predicts higher thrust force compared to the original Oxley's approach. This result was explained by the high softening effect due to the higher temperature estimated by the original Oxley's approach (Huang et Liang, 2003b). Long and Huang (2005) studied the cutting force modeling under dead metal zone effect in orthogonal cutting with chamfered tools using the J-C constitutive equation. It was found that the proposed approach underestimated the cutting forces in orthogonal cutting of the P20 mould steel. Karpat and Özel (2006) combined oblique moving band heat source theory with non-uniform heat intensity at the tool/chip interface and modified Oxley's parallel shear zone theory to predict cutting forces, stress, and temperature distributions. The proposed methodology has been successfully applied to the AISI 1045 steel, Al-6082-T6, and Al 6061-T6 aluminum alloys. Lalwani *et al* (Lalwani, Mehta et Jain, 2009) extended the Oxley's predictive theory using J-C flow stress model. The mean contribution is the introduction of a new expression for the strain hardening exponent n. Recently, Lee (Lee, 2011) developed a model to predict cutting forces for hard turning based on Oxley's theory and the J-C material model. The tool geometric parameter, the nose radius, was considered in the proposed model.

The various modifications of the Oxley's theory cited above were mostly performed using the Johnson-Cooke (J-C) material model (Huang et Liang, 2003b; Karpat et Özel, 2006; Lalwani, Mehta et Jain, 2009; Lee, 2011; Long et Huang, 2005; Özel et Zeren, 2004; 2006). However, the J-C equation could perform better for some materials and couldn't for others as stated by Jaspers and Dautzenberg (Jaspers et Dautzenberg, 2002). Fang (Fang, 2005) studied the sensitivity of the flow stress of 18 materials in machining and showed that the behavior differs significantly from material to other and they cannot be described by one equation. Even for the same type of material, chemical compositions and heat treatment conditions also affect the constitutive behavior.

The Marusich's constitutive equation (MCE) has shown encouraging results for the modeling and the simulation of the machining processes (Huang et Liang, 2003b; Ren et Altintas, 2000). However, its use was very limited since only a few material data were published in the open literature (AISI4340 in (Marusich et Ortiz, 1995), AA6061-T6 and AA7075-T6 in (Zaghbani et Songmene, 2009)). In the reference (Zaghbani et Songmene, 2009), the material constants were determined using an inverse optimization technique based on the J-C material model published in the open literature for the two studied materials. Moreover, many studies were performed on the FEM of the machining, based on the MCL, using the commercial software Advantage®. However, due to data confidentiality, the material constants were not published and Marusich's equation has not been used or tested with other FEM packages (Sartkulvanich, Altan et Soehner, 2005).

1.5.3 Material's constitutive equations applied to the machining modeling

Both the analytical and finite element modeling (FEM) of the machining process require accurate material constitutive equations in order to simulate the actual material behavior during the processing. To succeed any process modeling, two critical issues should be solved: first, the selection of a proper constitutive equation for the studied work material, and second, find its suitable constants. In the last decade, many techniques have been used for the identification of the constitutive equations applied to the finite element modeling (FEM) of

machining. These techniques include split Hopkinson pressure bar (SHPB) test (Lesuer, Kay et LeBlanc), Taylor tests (Rule, 1997), machining tests (Özel et Zeren, 2006; Tounsi et al., 2002). The former, also known as the "inverse method", can provide material constants representing the actual material behavior during machining. The material constants are obtained using a nonlinear regression solution. The disadvantage of this technique is its circular nature where machining tests are used for obtaining the flow stress data that are used for making machining prediction (Kristyanto, Mathew et Arsecularatne, 2002). In this method, the measured cutting forces and chip thickness are used to calculate, analytically, the flow stress, strain, strain rates and temperatures in the primary shear zones. Different analytical models have been used for estimating the cutting temperature in the primary shear zone. However, large discrepancies have been observed in the published results. As an illustration, the difference between analytically predicted primary shear zone temperatures in the machining of the AISI 1045 steel has achieved 600°C as documented in (Özel et Zeren, 2006). Although the sensitivity of the flow stress and the FEM to the material constant was extensively studied (Fang, 2005; Umbrello, M'Saoubi et Outeiro, 2007), the sensitivity of the material constants to the different applied temperature models is still lacking.

1.6 Concluding remarks

In this chapter, a literature review on the machining of aluminum alloys and hardened steels has been presented. We have focused on the published results including the chip formation mechanisms and the surface integrity. Moreover, the basics of Oxley's predictive theory, its limitations, and research works on its generalization to other materials were discussed and criticized. Methods and approaches developed for the identification of constitutive equations applied to the machining modeling were also reviewed. The following are the significant findings of this review:

- The machining of the aluminum alloys that have been studied, the most involved 3D setups (end milling, face milling, and turning). In these machining processes, the surface profile was strongly influenced by the cutting feed and the shape of the tool

nose. When examining the surface quality during the machining of aluminums, most of the work that has been done takes into account only of the height parameters, such as the arithmetic mean (Ra), which may not fully describe the machined surface texture. Although several studies have been performed on the effect of the surface integrity during orthogonal machining, the effect of the surface finish and residual stress induced by the orthogonal and dry machining of AA7075-T651 using negative rake angle was not addressed yet.

- The machining of hardened steel induces compressive residual stresses and white layer on the machined surface. The driven mechanisms of the white layer formation still unresolved. Furthermore, the effect of the chip formation mechanisms and cutting forces on the residual stresses and microstructure alterations during the machining of induction heat treated steels is still lacking. The hard machining was found to perform better than grinding in terms of surface integrity characteristics.

- For a given cutting tool geometry and material, the feed rate and the cutting speed still have a significant effect on the chip formation and surface integrity characteristics.

- The Oxley's predictive theory is a fundamental approach in understanding the cutting process, but its application was limited to the plain carbon steels. Oxley's machining theory was successfully extended to materials other than plain carbon steels, but most of the time using the Johnson-Cooke constitutive equations

- Johnson-Cooke constitutive equation could not simulate all actual machined materials. The material constants can be affected by the selected temperature models when using the inverse method for the identification of the constitutive equations applied to machining modeling.

CHAPTER 2

SURFACE FINISH AND RESIDUAL STRESSES INDUCED BY ORTHOGONAL DRY MACHINING OF AA7075-T651

Walid Jomaa, Victor Songmene, and Philippe Bocher

Article in *Materials* 2014, 7, 1603-1624; doi:10.3390/ma7031603

Abstract: the surface finish was extensively studied in conventional machining processes (turning, milling, and drilling). For these processes, the surface finish is strongly influenced by the cutting feed and the tool nose radius. However, a basic understanding of tool/surface finish interaction and residual stress generation has been lacking. This paper aims to investigate the surface finish and residual stresses under the orthogonal cutting since it can provide this information by avoiding the effect of the tool nose radius. The orthogonal machining of AA7075-T651 alloy through a series of cutting experiments was performed under dry conditions. Surface finish was studied using height and amplitude distribution roughness parameters. SEM and EDS were used to analyze surface damage and built-up edge (BUE) formation. An analysis of the surface topography showed that the surface roughness was sensitive to changes in cutting parameters. It was found that the formation of BUE and the interaction between the tool edge and the iron-rich intermetallic particles play a determinant role in controlling the surface finish during dry orthogonal machining of the AA7075-T651 alloy. Hoop stress was predominantly compressive on the surface and tended to be tensile with increased cutting speed. The reverse occurred for the surface axial stress. The smaller the cutting feed, the greater is the effect of cutting speed on both axial and hoop stresses. By controlling the cutting speed and feed, it is possible to generate a benchmark residual stress state and good surface finish using dry machining.

keywords: Machining; Aluminum; Surface finish; Residual stress; Carbide tool

2.1 Introduction

Structural aeronautic and automotive components are expected to demonstrate superior quality and enhanced functional performance. Nevertheless, the latter is strongly influenced by the surface conditions of the components. It has long been recognized that fatigue cracks generally initiate from free surfaces and that performance is therefore reliant on the surface topography/integrity produced by machining (Novovic et al., 2004). As high speed machining (HSM) is widely used in the aircraft industry due to several advantages it boasts over conventional machining, it is worth studying the integrity of dry machined surfaces. In the case of aluminum alloys, the use of high cutting speed increases metal removal rate (MRR), reduces the formation of built up edges (BUE) and burrs (Rao et Shin, 2001); however, it affects the surface integrity of the machined parts (Pawade, Joshi et Brahmankar, 2008). It has previously (Chaussumier et al., 2013) been shown that in the case of 7000 series aluminum alloys, fatigue resistance is primarily influenced by machining surface roughness; however, residual stresses play a second role. For machined parts made of precipitation-hardened aluminum alloys, surface roughness is considered as generating local stress concentration, and fatigue cracks were initiated on intermetallic inclusions located at the bottom of the machining grooves (Suraratchai et al., 2008). Thus, it is very important to understand how surface finish and residual stress state are influenced by machining of aluminum alloys.

The main difficulty in machining aluminum alloys with uncoated cemented carbide insert lies in the formation of build-up layer (BUL) on the rake surface, according to Gangopadhyay *et al*. (2010). The morphology and the mechanisms leading to the formation of BUE and BUL during machining has been the subject of several research studies (Bandyopadhyay, 1984a; Carrilero et al., 2002; Iwata et Ueda, 1980; Sánchez et al., 2005). Iwata and Ueda (1980) stated that there are two types of cracks associated with BUE formation: one forms below the flank face of the tool, while the other subsequently forms ahead of the rake face of the tool. Recently, Gómez-Parra *et al*. (2013) indicated that higher cutting parameter values can promote a faster formation of primary BUL in machining aerospace aluminum alloys such as

UNS A92024 (Al–Cu) and UNS A97050 (Al–Zn). Moreover, the results they obtained confirmed that BUE growth is responsible for a decrease in Ra roughness (Gómez-Parra et al., 2013). Nevertheless, Iwata and Ueda (1980) stated that the rearward disappearance of a BUE leaves debris containing cracks on the machined surface, and that such surface damage is undesirable because it increases the surface roughness and deteriorates the strength of the workpiece. In previous work, Gangopadhyay *et al*. (2010) evaluated the performance of different cutting tools in terms of BUE/BUL formation and surface roughness during machining of AA6005 alloys. They found that the surface roughness decreases with an increase in cutting speed. The authors (Gangopadhyay et al., 2010) related this decrease in surface roughness to an increase in cutting temperature, which in turn might lead to slight reduction in material adhesion.

Cai *et al*. (2012a) studied the effect of high speed end milling on the surface integrity of 7075 aluminum alloy. Their results showed that a high cutting speed has a positive effect on the surface finish, and that residual stresses will be transformed from tensile values to compressive values when the cutting speed increases. Conversely, Ammula and Guo (2005) reported that the cutting speed has a dominant effect on surface roughness, and that an increase in the cutting speed increases the arithmetic mean (Ra) during high speed milling of Al 7050-T7451 alloy. Furthermore, they found that the residual stress in the feed direction is tensile near the surface and quickly changes to compressive stresses at about 35 μm. Balkrishna and Yung (2001) studied the surface integrity during the high speed face milling of 7075-T6 aluminum alloy. They reported that an increase in feed is shown to leave higher compressive residual stresses in the workpiece, while higher cutting speed and depth of cut show an opposite effect. In addition, the surface roughness improved with the cutting speed up to 1524 m/min, beyond which it showed degradation.

Based on the literature results, the machining processes that have been studied the most involved 3D setups (end milling, face milling, and turning). In these machining processes, the surface profile is strongly influenced by the cutting feed and the shape of the tool nose. Moreover, when examining the surface quality, most of the work that has been done takes

into account only of the height parameters, such as the arithmetic mean (Ra), which may not fully describe the machined surface texture. Conversely, in orthogonal machining, the surface profile and roughness are influenced by the cutting conditions, the thermo-mechanical behavior of the work materials, and the possible vibration of the machining system, rather than the geometry of the tool nose. Thus, orthogonal machining seems to provide a good indication of the inherent capability of the material to produce an enhanced/poor surface finish, regardless of the cutting tool geometry. Although several studies have been performed on the effect of surface integrity during orthogonal machining (Elkhabeery et Bailey, 1984; Jin et Liu, 2013; M'saoubi et al., 1999; Ojolo, Damisa et Iyekolo, 2011), the effect of surface finish and residual stress induced by the orthogonal and dry machining of AA7075-T651 was not addressed yet. This has therefore meant that a basic understanding of tool/surface finish interaction and residual stress generation have been lacking.

This chapter presents an experimental study on the surface finish and residual stresses generated by the orthogonal dry machining of AA7075-T651 alloys. The effect of cutting conditions will be discussed. The surface topography will be analyzed using two groups of surface roughness parameters: height and distribution parameters. Surface damage mechanisms were investigated in detail.

2.2 Experimental Procedure

Workpieces made of AA7075-T651 alloy were used. This precipitation hardenable aluminum alloy is widely used for the manufacture of aerospace and automotive structural components. The microstructure of the AA7075-T651 alloy is presented in Figure 2.1. The tested workpieces were disc-shaped, with a 70 mm external diameter, a 19 mm internal diameter, and a 4 mm thickness. Orthogonal tests were conducted on a NEXUS 410A 3-axis CNC machine (MAZAK, US) under dry cutting conditions (Figure 2.2). All cutting tests were performed with uncoated carbide inserts which referenced as TNMA120408 (K68 tool, Kennametal, US). The inserts were mounted on a right hand tool holder, DTFNR2525M16KC04 (Kennametal, US), with a back rake angle of −5°. A newer cutting

tool edge was used for each cutting condition in order to eliminate the effect of possible tool wear on the residual stresses. The specimens were machined at different cutting speeds and feeds, as shown in Table 2.1. The roughness parameters were measured using a Mitutoyo SJ-400 instrument (Mitutoyo, Japan) with a diamond stylus contact profilometer (Figure 2.3). The cut-off was set to 0.8 mm and a Gaussian filter was used during the measurements.

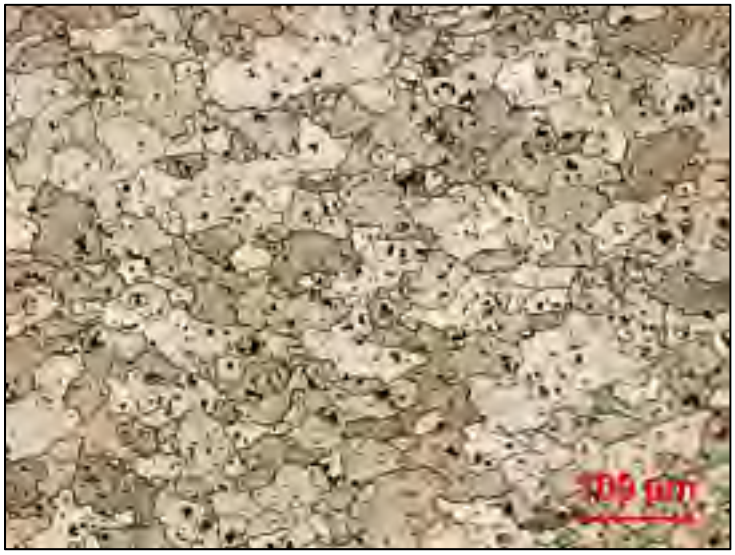

Figure 2-1 Optical microstructure of the aluminum AA7075-T651 alloy.

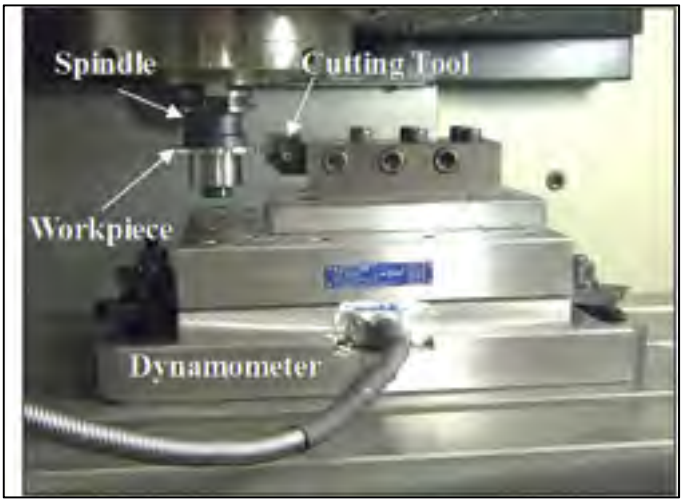

Figure 2-2 Orthogonal machining setup

Table 2-1 Cutting conditions.

Trial #	width of cut, DOC (mm)	Cutting feed, f (mm/rev)	Cutting speed, V (m/min)
1	2	0.05	300
2		0.25	300
3		0.05	1000
4		0.25	1000

During the retraction of the cutting tool, a part of the workpiece is machined with a cutting feed different from that programmed for a given cutting test. This change in the cutting feed is due to the deceleration of the cutting tool before the movement direction is changed during the retraction. Thus, in order to analyze the surface integrity of the machined workpiece, it was necessary to choose part of it to be representative of the cutting test. The representative zone was identified via the measurement of the circularity profile (Figure 2.4) using a coordinate measuring machine, BRIGHT STRATO 7106 (Mitutoyo, US). The X-ray diffraction technique and classical $\sin^2\Psi$ method were used for the residual stress measurements using a Proto iXRD® system (Proto Manufacturing, US) (Figure 2.5), with a chromium tube. In-depth measurements were performed after the removal of the layer using electrochemical polishing. The residual stresses were measured in the circumferential direction (parallel to the cutting direction) and in the axial direction. Residual stress measurement provides the average stress in a diffracting volume defined by the size of the irradiated area and the depth of penetration of the X-ray beam (about 10 μm for 311 lattice plane in aluminum with Cr tube) (SAE International , Residual Stress Measurement by X-ray Diffraction, HS-784). The residual stress distributions produced by machining may vary significantly over depths of the same order of the X-ray's penetration depth (Brinksmeier et al., 1982). In the present work, the measured residual stresses were corrected using a commercial PROTO GRADIENT code. The cutting forces *Fc* and feed force *Ft* were measured using a Quartz 3-component dynamometer (Kistler, USA) (type 9255B) with the help of a Kistler charge amplifier.

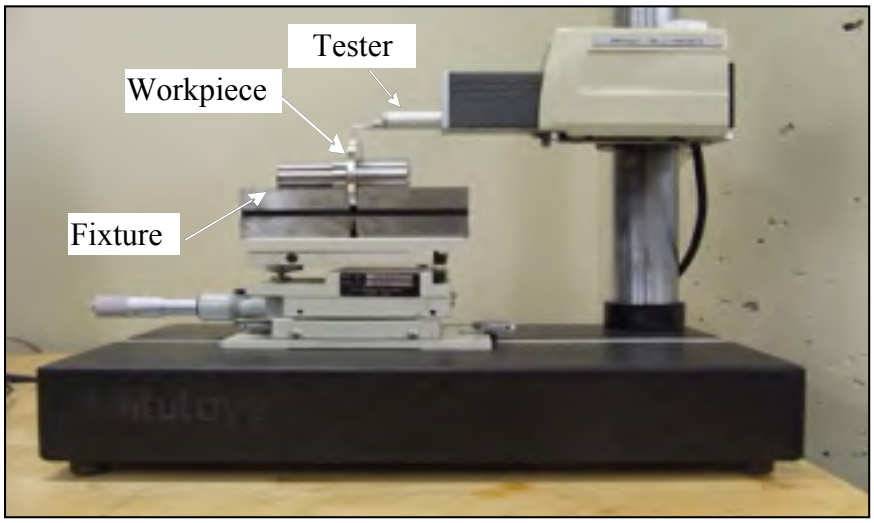

Figure 2-3 Surface roughness measurements using Mitutoyo SJ-400 instrument

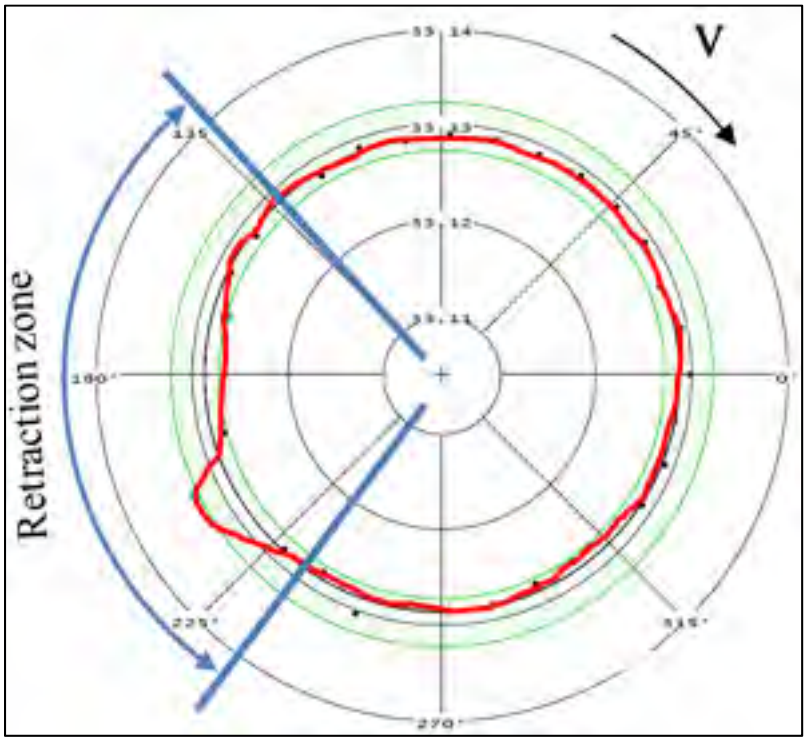

Figure 2-4 Circularity deviation of the machined workpiece for Trial #2

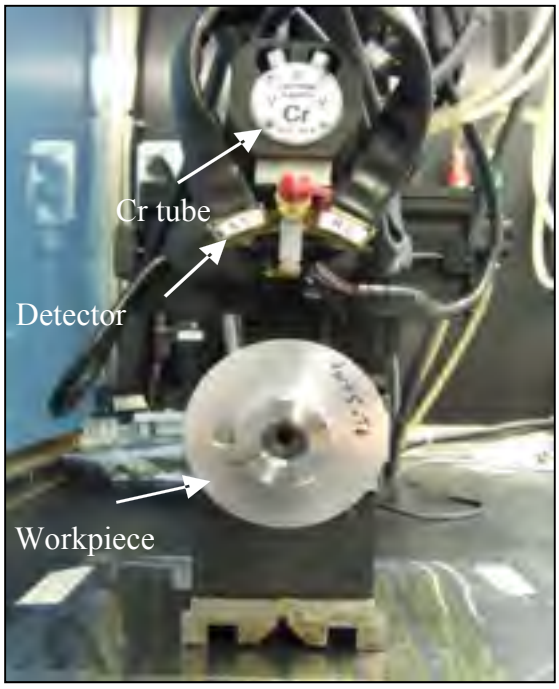

Figure 2-5 Setup for residual stress using Proto iXRD® machine

2.3 Results and Discussion

2.3.1 Surface Finish

The surface roughness measurements and surface damage analysis were carried out in the representative zone. In the axial direction, 2D profiles (Figure 2.6) revealed grooves parallel to the tool motion. A quantitative analysis was developed in order to quantify the effect of cutting conditions on surface topography. The height and amplitude distributions of 2D surface roughness parameters were described by the parameters given in Table 2.2.

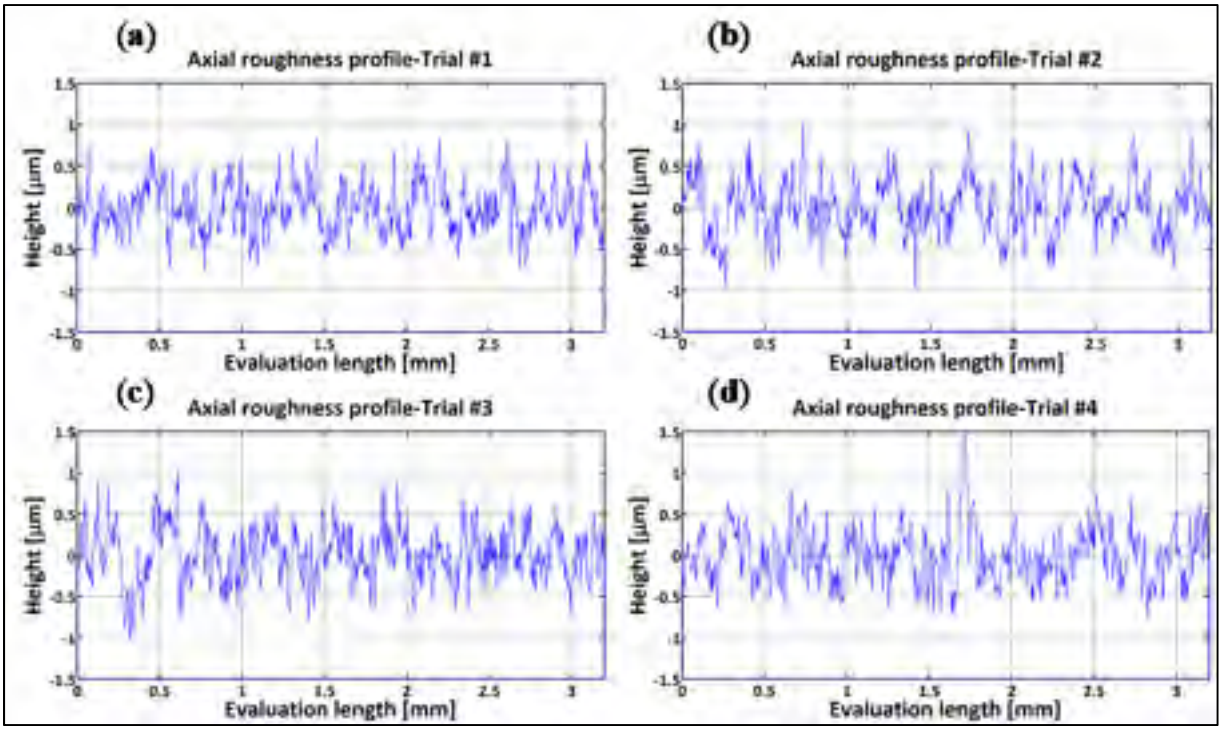

Figure 2-6 Examples of surface roughness profiles obtained in axial direction for (a) Trial #1, (**b**) Trial #2, (**c**) Trial #3, and (**d**) Trial #4

Table 2-2 2D roughness parameters.

Height (µm)	Amplitude distribution	
	Dimensional parameters(µm)	Dimensionless parameters
Ra, Rq, Rpm, Rz, Rt	Rk, Rpk, Rvk	Rsk, Rku

Each of these roughness parameters describes one or more of the machined surface characteristics. For example, the peak-to-valley height (Rt), the mean peak to valley height (Rz), and the mean height of peak height (Rpm) parameters are sensitive to the presence of high peaks and deep scratches. The skewness (Rsk) describes the symmetry of the height distribution in relation to the mean line. On the other hand, Kurtosis (Rku) is the measure of the sharpness of the height distribution, and for a Gaussian profile, its value is equal to 3 (Grzesik et Wanat, 2006).

In the axial direction, the observed grooves on the machined surfaces are attributed to the ploughing effect of micro-built-up edge BUE and the micro-chipping of the cutting edge. On the other hand, it can be observed that roughness parameters are influenced by the cutting

feed and the cutting speed, as shown in Figures 2.7 and 2.8. The surface roughness values are the average of three measurements conducted in both the axial and hoop directions. Figure 2.7 show that Rt, Rz, and Rpm parameters are more sensitive and increase with the cutting feed and cutting speed, unlike the arithmetic average (Ra) and the root mean square (Rq) parameters, which change only slightly over the tested cutting conditions. Figure 2.8 illustrates the effect of the cutting conditions on amplitude distribution parameters. The skewness was positive and ranged between 0.078 and 0.5 (Figure 2.8a) indicating that the heights are symmetrically distributed about the mean line, and hence, the surface profiles were random in the axial direction (Grzesik et Wanat, 2005). The kurtosis Rku increases with the cutting feed and the recorded values were lower than 3, except for Trial #4 (Figure 2.8a) indicating that the distribution curve has relatively few high peaks and low valleys. Moreover, the core roughness depth Rk, which assesses the effective roughness depth after the running-in process (Grzesik et Wanat, 2005; Sugimura, Watanabe et Yamamoto, 1994), is slightly affected by the cutting conditions (Figure 2.8b). On the other hand, the reduced valley depth Rvk and the reduced peak height Rpk increases with the cutting feed when machining at lower cutting speeds (Trials #1 and #2). However, when machining at higher cutting speeds (Trials #3 and #4), the Rpk decreases and the Rvk increases with the cutting feed (Figure 2.8b).

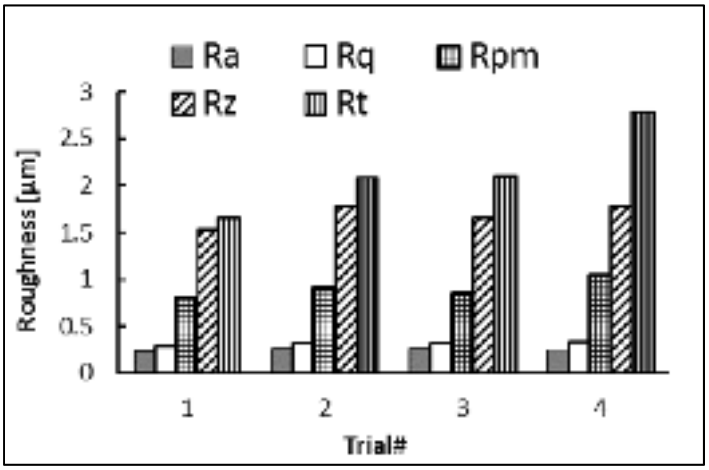

Figure 2-7 Effect of cutting conditions on the height parameters in axial direction.

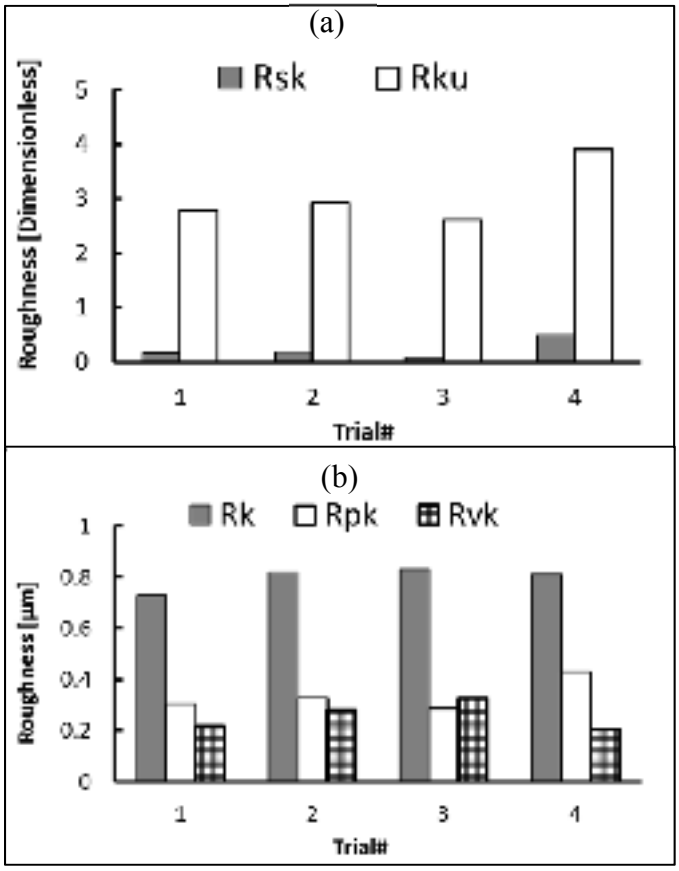

Figure 2-8 Effect of cutting conditions on amplitude distribution parameters in axial direction. (a) Dimensionless parameters and (b) dimensional parameters

Distinguishing features can be identified in the hoop direction as cutting conditions change (Figure 2.9). Sharp peaks and deep valleys are produced at lower cutting speeds (Figure 2.9a and b) and blunt irregular peaks are seen when machining at higher cutting speeds (Figure 2.9c, d). Figures 2.10 and 2.11 present the effect of cutting conditions (cutting speed and cutting feed) on surface roughness parameters measured in the hoop direction. The highest surface roughness values were obtained in Trial #2 where a cutting feed of 0.25 mm/rev and cutting speed of 300 m/min were used. Furthermore, for both groups of roughness parameters analyzed here, the values increase with the cutting feed and decrease with the cutting speed. This result is in agreement with those obtained when machining using standard cutting

operations such as turning and milling (Kuttolamadom, Hamzehlouia et Mears, 2010; Sasimurugan et Palanikumar, 2011).

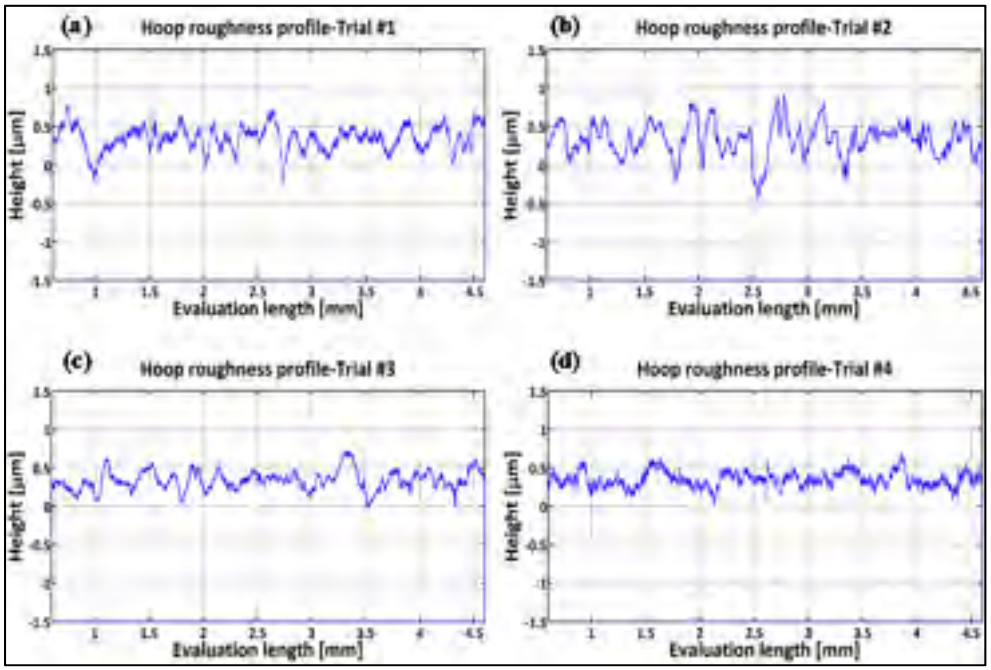

Figure 2-9 Surface profiles in hoop direction for (a) Trial #1, (b) Trial #2, (c) Trial #3, and (c) Trial #4

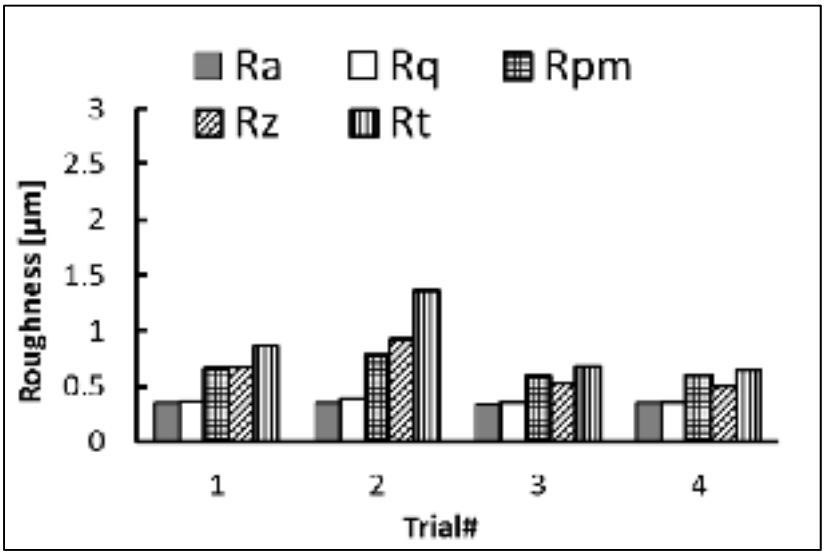

Figure 2-10 Effect of cutting conditions on the height roughness parameters in hoop direction

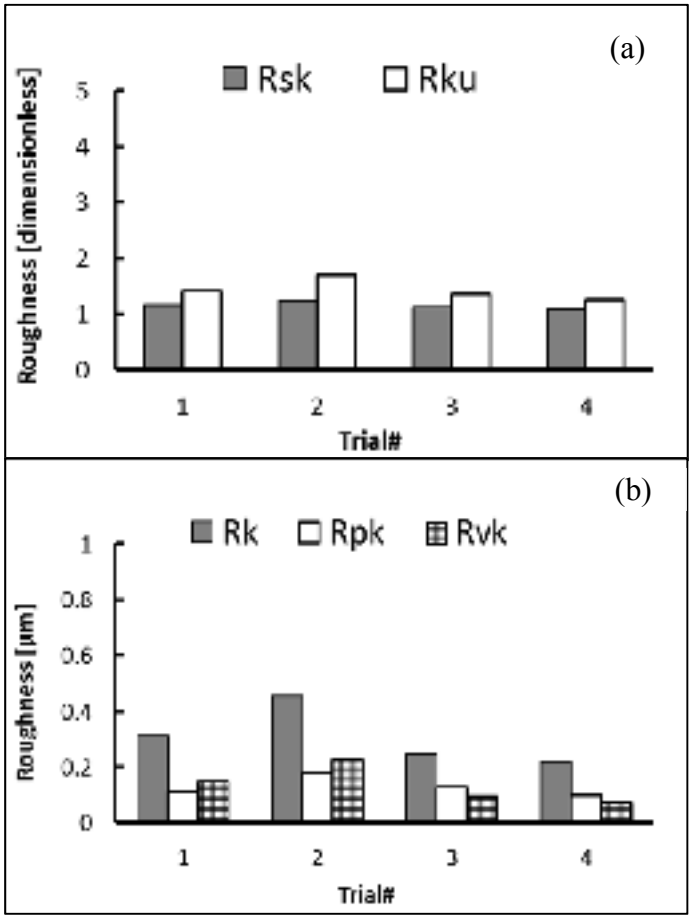

Figure 2-11 Effect of cutting conditions on amplitude distribution parameters in hoop direction: (a) dimensionless parameters and (b) dimensional parameters

In the hoop direction, the skewness ranged between 1.089 and 1.236, which once again indicates the non-random aspect of the surface profile. In addition, the Rku values were lower than 3 for all tested conditions indicating that only relatively few high peaks and low valleys were found (Gadelmawla et al., 2002).

To investigate the tool/work material interaction during machining and its effect on the surface quality, SEM analyses were performed on both the cutting tool and the machined surface. Figures 2.12 and 2.13 illustrate the formation of the BUE and BUL on the cutting tool. The formation of BUE was intensified by increasing the cutting feed (Figure 2.13). The presence of microgrooves on the BUL that formed on the flank face could be related to the

hard intermetallic phase present in the T6 condition of the alloy (Handbook, 2005). However, an increase of the cutting speed reduces this phenomenon and promotes the formation of the BUL on the rake face, as can be seen in Figure 2-14. Figure 2-14a shows a thin layer, which is considered as the primary BUL, on the rake face. Moreover, depending on the cutting conditions, the tool-chip contact area can be divided into three regions: (a) first sticking zone, close to the edge; (b) a sliding zone and (c) second sticking zone at the rear end of the contact as shown in Figure 2-14a (Oishi, 1996). The sticking area starts to develop and enlarge as the cutting speed increases, and results in a secondary BUL (Figure 2-14b). In fact, when dry machining aluminum alloys, the temperatures in the chip-tool interface is high enough to soften the aluminum matrix and it can thus provoke the adhesion of quasi-pure aluminum to the tool rake face (Gómez-Parra et al., 2013; Sánchez et al., 2005). Increasing the feed and speed involves increasing in the intensity of the adhesion effects (Roy et al., 2009). These results agree with those obtained by Gangopadhyay *et al*. (2010) in the case of dry machining of AA6005 in a cutting speed range of 200–1000 m/min. The high degree of chemical affinity of aluminum alloy towards cemented carbide (composite of WC and Co) is thought to be the primary reason for this phenomenon (Kirman, 1971).

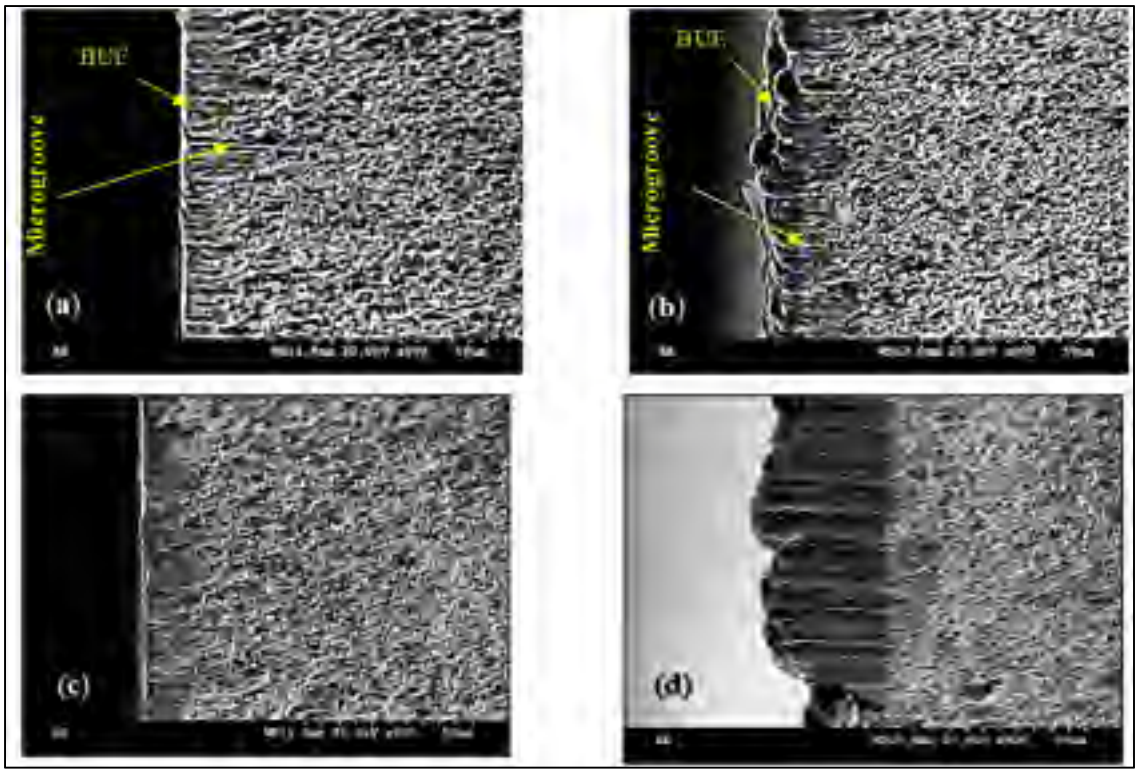

Figure 2-12 Flank face of the cutting tool after machining at (a) Trail #1, (b) Trial #2, (**c**) Trial #3, and (**d**) Trial #4

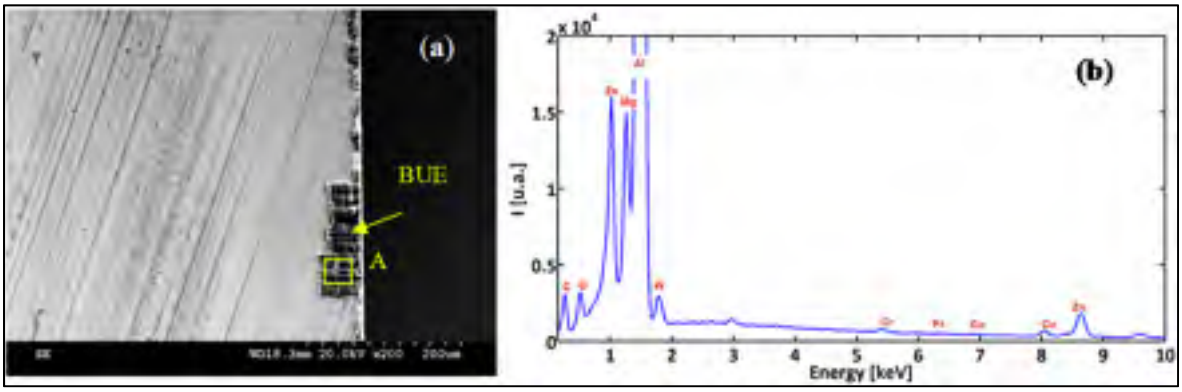

Figure 2-13 (a) Rake face of the cutting insert for Trial #2 and (b) EDS spectra acquired on BUE-Detail A

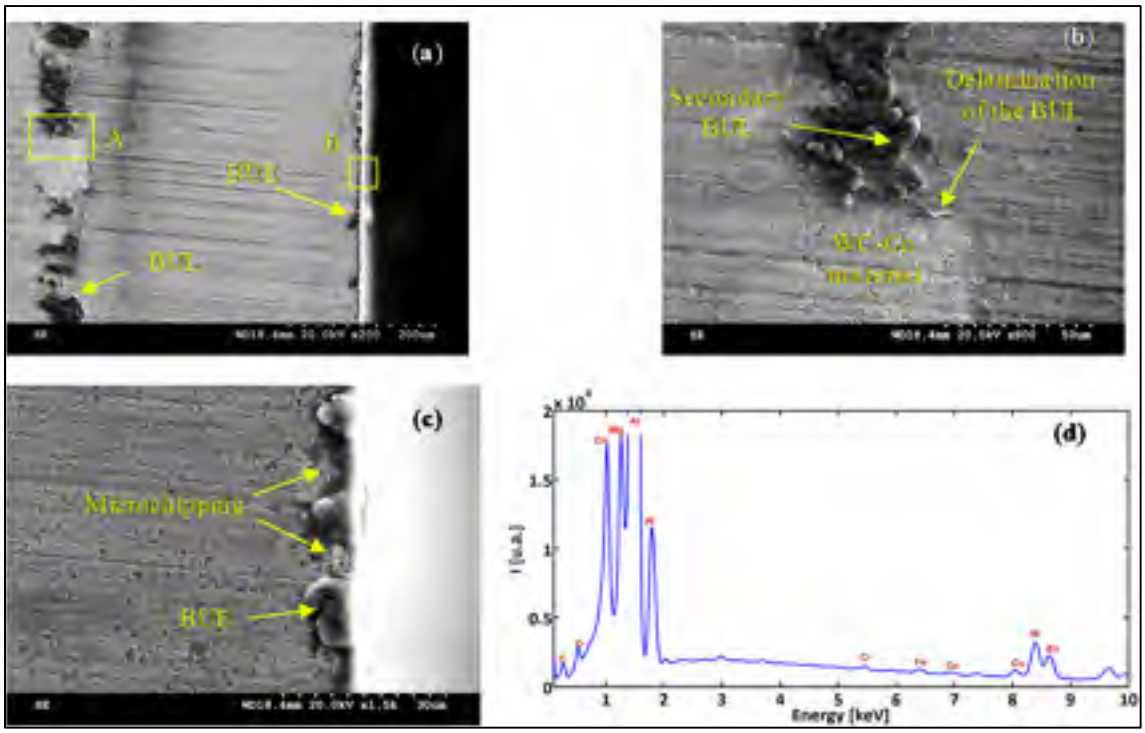

Figure 2-14 (a) Rake face of the cutting insert for Trial #4, (b) BUL-Detail A, (c) micro-chipping of the tool edge Detail B, and (d) EDS spectra acquired on secondary BUL

In order to characterize and distinguish the morphology differences between BUL and BUE, EDS analysis of both zones was carried out. Figures 2.13b and 2.14d display the EDS spectra acquired on zones corresponding to BUE (A) and BUL (B), respectively. As a reference, an EDS spectrum acquired on a machined AA7075-T651 alloy is also reported (Figure 2.15). The EDS spectra are quite different in particular for the intensities of the Mg, Fe, and W peaks. They are lower in the BUE than those in the BUL. This could point out the dissimilar nature of the BUE and BUL regions (Sánchez et al., 2005). In fact, the high temperatures reached in the initial stages of the cutting process cause the incipient melting of the Al matrix in the alloy, which flows on the rake face of the tool (Carrilero et al., 2002). Under these conditions, the metallic chips would drag off the hard intermetallic particles and a part of these particles will attach to the second sticking zone, leading to high amounts of Fe and Mg elements on the secondary BUL. In addition, when the cutting speed increases, the BUE increases to a critical thickness, after which it is plastically extended over the BUL (Sánchez et al., 2005) and/or broken due to the action of mechanical forces. This cyclic phenomenon

induces the micro-chipping of the tool edge, and, therefore, W-riche particles will be dragged off by the chip and adhere to the secondary BUL leading to a higher percentage of W as compared to the BUE. The broken BUE is not only evacuated by the chip but, depending on the cutting conditions, it can be squeezed under the cutting edge, causing damage to the new machined surface. Moreover, the disappearance of the BUE results in debris adhered to the machined surface, which degrades its roughness (Iwata et Ueda, 1980). This can explain the enhancement of the surface finish as the cutting speed increases (Oishi, 1996), as stated above.

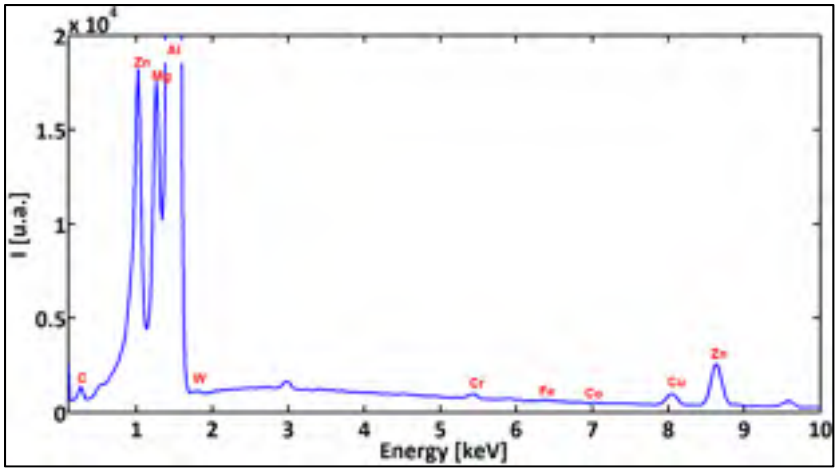

Figure 2-15 EDS spectra acquired on a machined surface

A close examination of the machined surface using SEM reveals a different type of surface damage. Figure 2.16 shows that surface damage was produced by the interaction between the cutting tool and hard particles present within the work material matrix. The different forms of damage documented here were cracks of the hard particles (Figure 2.16a), smearing (Figure 2.16b), dragging of hard particle (Figure 2.16c), and voids (Figure 2.16d). These particles are composed mainly of iron-rich intermetallic phase as shown by the EDS spectra (Figure 2.17) (Handbook, 2005).

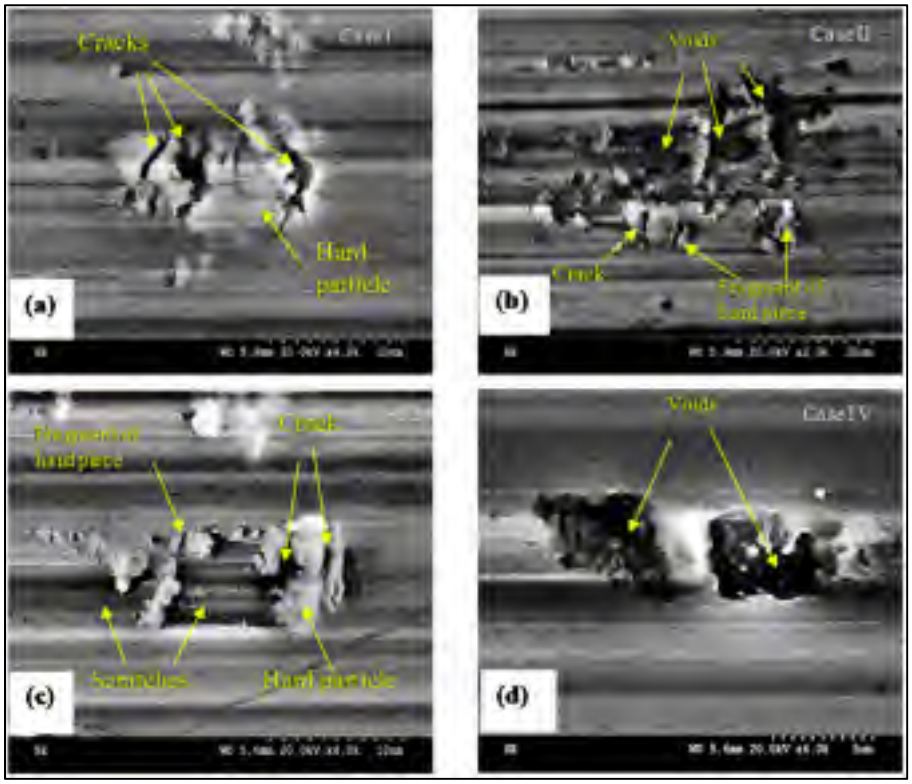

Figure 2-16 SEM micrographs of the machined surfaces showing (a) hard particle cracking, (b) smearing, (c) cracking and dragging of hard particles, and (d) voids. (a) and (b) for Trial #2 and (c) and (d) for Trial #4

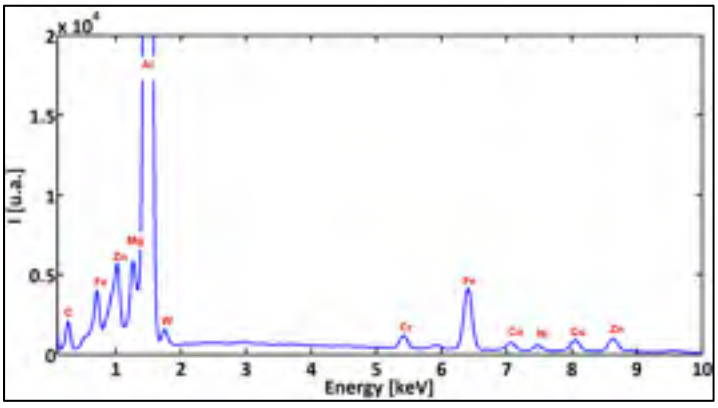

Figure 2-17 EDS analysis of the hard particle

Depending on the cutting conditions and the relative position of these particles with regard to the tool edge, four cases of surface defects can be distinguished (Figure 2.18). If the hard

particle is large enough and the volume embedded in the matrix is comparable to that located above the tool edge path (Figure 2.18, Case I), then the particle will crack and some of theme remain attached to the surface (Figure 2.16a). When the tool comes into contact with a large but thin hard particle (Figure 2.18, Case II), the latter breaks up into small parts, resulting in a smearing, as shown in Figure 2.16b. When the hard particle is long enough and the volume embedded in the matrix is higher than that located above the tool edge path (Figure 2.18, Case III), then the latter will crack and some of the cracked particles will be dragged, resulting in a grooved surface (Figure 2.16c). Finally, case IV is similar to case III, but the volume embedded in the matrix is lower than that located above the tool edge path (Figure 2.18-Case IV). In this case, the hard particle will break, and the fragments will be removed from the surface, leading to surface voids, as shown in Figure 2.16d.

It should be noted here that, based on the SEM images, no quantitative conclusion could be made about the effect of cutting parameters (feed and speed) on the generation of these damages. However, we can argue that hard particles together with the BUE formation are the primary sources of the micro-chipping of the cutting tool edge (Figure 2.19).

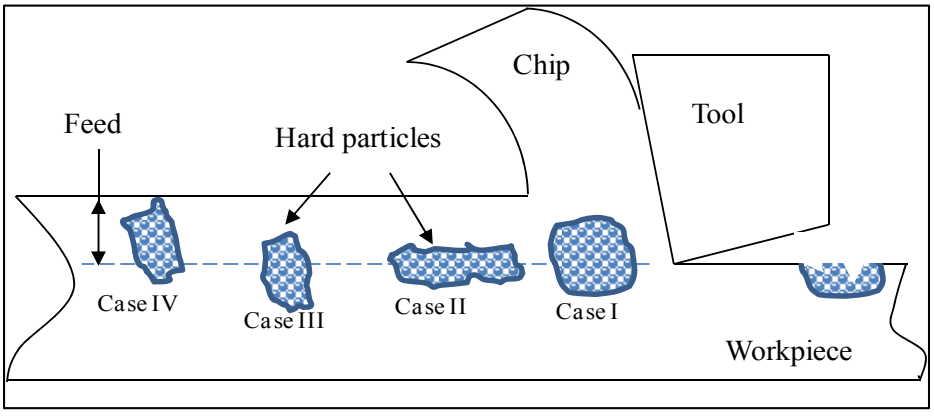

Figure 2-18 Illustration of mechanisms of surface damage induced by tool/hard particle interaction

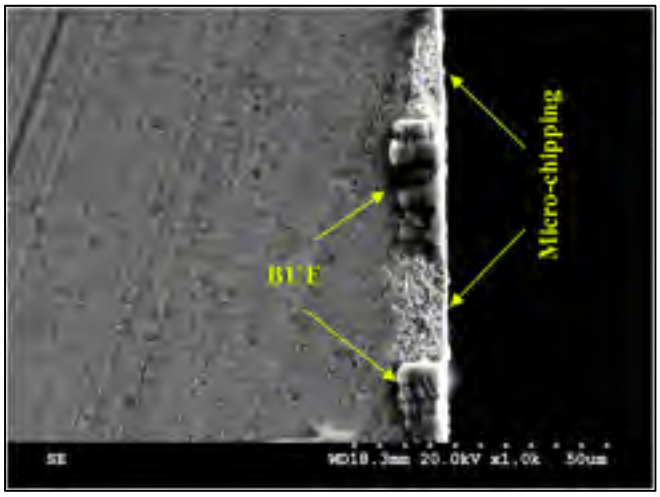

Figure 2-19 SEM image of the cutting insert
for f=0.25 mm/rev and V=300 m/min

In the present study, the analysis of the surface topography showed that the surface roughness values were not zero as theoretically expected, and in contrast, were sensitive to changes in cutting parameters (cutting feed and speed). Surface roughness was found to be influenced by the formation of BUE and the interaction between the tool edge and the iron-rich intermetallic particles. Moreover, the effect of cutting speed and cutting feed on height roughness parameters (such as Rt and Rz) depend on the measurement direction (Axial or hoop). Both cutting speed and feed increases the height roughness measured in the axial direction. This suggests that the micro-chipping of the cutting tool edge is intensified when the cutting feed and cutting speed were increases. On the other hand, the appearance of surface damages, such as cracks, voids and smearing is governed by a complex phenomenon including the degree of material softening, cutting forces and cutting temperature. These defects could be sites of failure initiation (Barter et al., 2002) and that surface roughness measurements are not sufficient to determine the surface conditions (Bailey, 1977). In addition, adjusting cutting parameters according to these defects is very hard, and even then, a complete elimination is not possible (Ulutan et Ozel, 2011).

2.3.2 Residual Stress

The machining induced residual stresses are very important parameters that should be considered in the design of mechanical parts. This section focuses on the effect of cutting conditions on the residual stress distribution. The residual stress distribution in both the hoop and axial directions were measured and are shown in Figures 2.20 and 2.21. The residual stress values increases or decreases from an extreme level at the surface, and fluctuates along the measured depth. These results are in agreement with previous work (Cai, Ming et Chen, 2012a) and these deviations could be related to the coarse grain microstructure of the aluminum alloy. Surface hoop stress was predominantly compressive for low cutting speed (Figure 2.22a). However, axial stresses tends to be tensile when cutting speed increases (Figure 2.22b). In addition, the smaller the cutting feed, the greater the effect of cutting speed on both axial and hoop stresses.

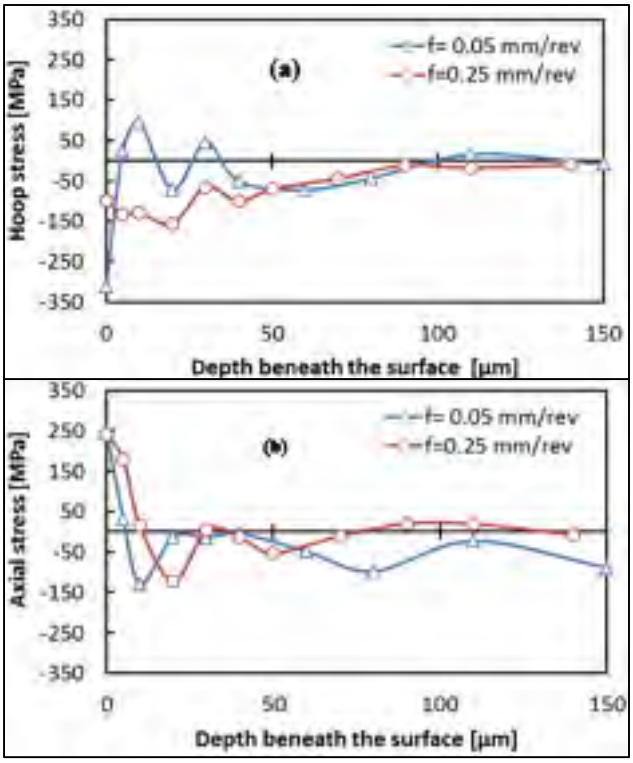

Figure 2-20 Effect of cutting feed on (a) hoop and (b) axial residual stress distribution for cutting speed of 300 m/min

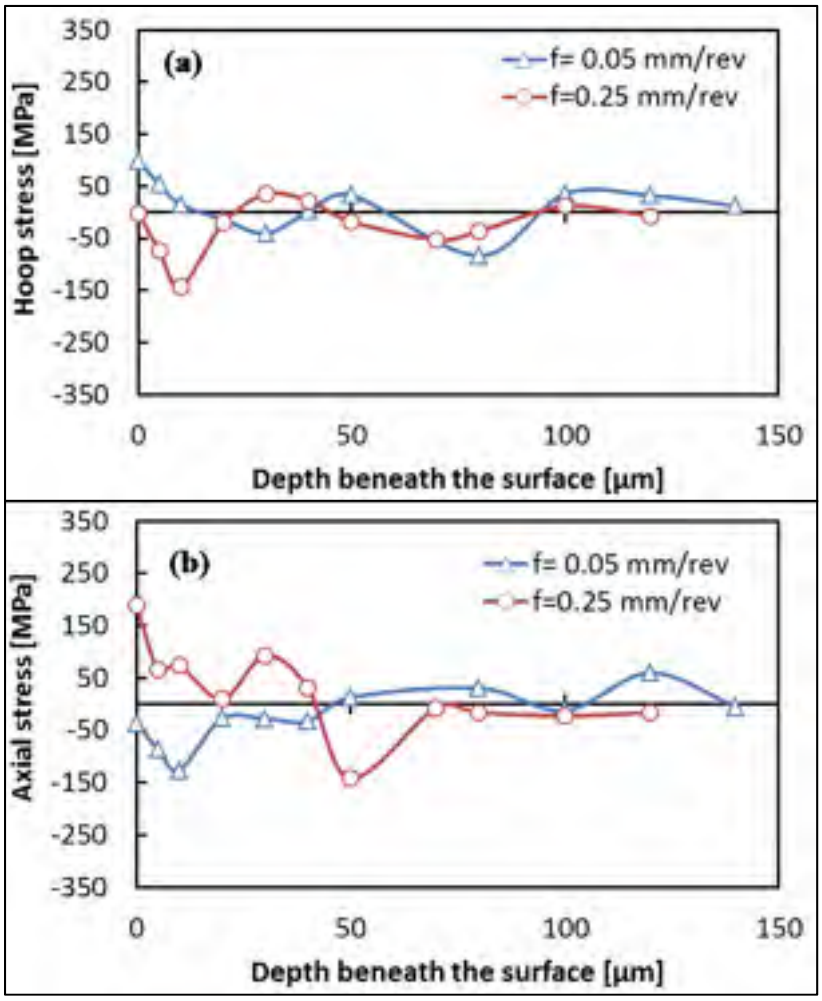

Figure 2-21 Effect of cutting speed on hoop (a) and axial (b) residual stress distribution for cutting speed of 1000 m/min

The residual stresses could be interpreted using geometrical parameters of the cutting zone as proposed by Liu and Barash (1976). The shear plane length is the fundamental parameter that governs the mechanical state of the surface (for both residual stresses and plastic deformation) since it is related to the frictional and shearing processes of the chip removal. According to the cutting mechanic, the shear plane length l_s is inversely proportional to the shear angle Ø (Figure 2.23a). The shear Ø and friction angles β were calculated, based on the measured cutting F_c and feed F_t forces, chip/tool contact length l_c, and chip thickness t_c (Figure 2.23b), and using the well-known Merchant's cutting theory. The measured and calculated machining data were presented in Table 2.3.

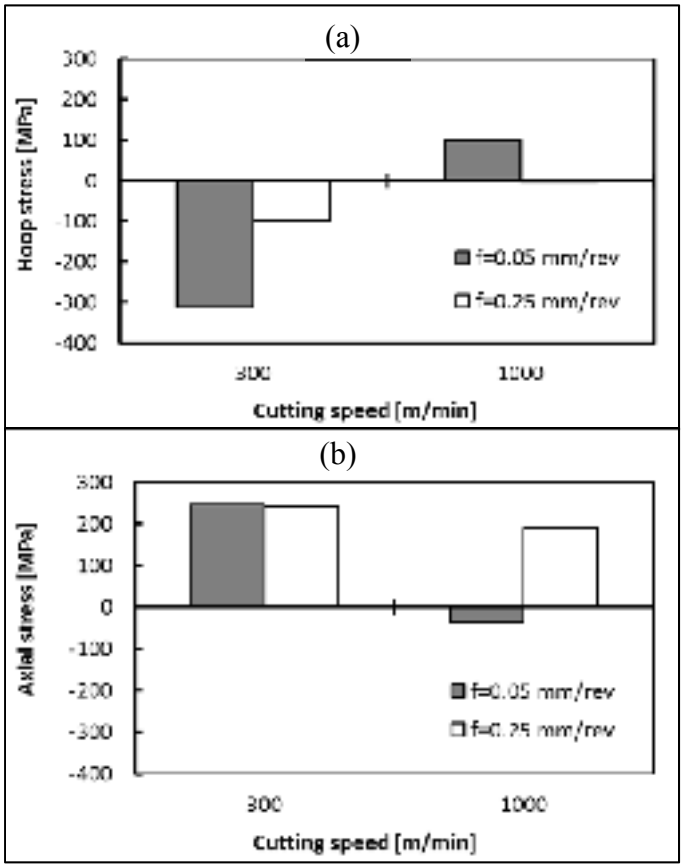

Figure 2-22 Effect of cutting speed on (a) hoop and (b) axial surface residual stresses

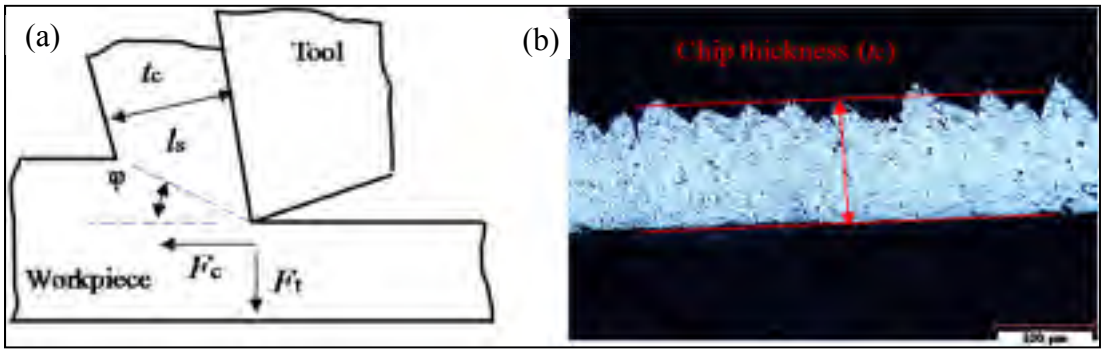

Figure 2-23 (a) An illustration of the chip formation in orthogonal machining and (b) Example of an optical image of the chip thickness measurement for Trial #1

Table 2-3 Experimental results of the orthogonal machining.

Trial#	Ft (N)	Fc (N)	lc (mm)	tc (mm)	Φ (Deg)	β (Deg)
1	168	271	0.428	0.130	21	45
2	323	901	0.426	0.217	46	15
3	108	234	0.113	0.105	25	20
4	171	707	0.312	0.196	63	11

Figure 2-24 presents the effect of cutting speed on shear and friction angles. The cutting feed strongly affects the shear angle irrespectively of the cutting speed used. On the other hand, the shear angle is slightly affected when machining at low cutting feed, but it is significantly affected when machining at high cutting feed (Figure 2-24a). The reverse occurs for the friction angle (Figure 2-24b). Liu and Barash (1982) stated that the larger the rake angle and/or the smaller the friction angle is, the larger the shear angle and consequently the better the surface quality. However, if one tries to describe the cutting phenomena with these geometric parameters, it is clear that as the shear angle increases (Figure 2-25); the surface stresses tend to be tensile in the hoop direction and compressive in the axial direction and this is true whatever the used cutting feed. This could be due to the triaxiality of the stress state during orthogonal machining. When one looks at the friction angle as a describing parameter (Figure 2-26), it appears that the tendency is reversed. Interestingly, the trend (the slope) seems similar for both tested cutting feeds. As a final comment, it seems that to guarantee a good surface quality and compressive residual stresses, an optimization, in terms of the shear angle and friction angle, of the cutting conditions should be done.

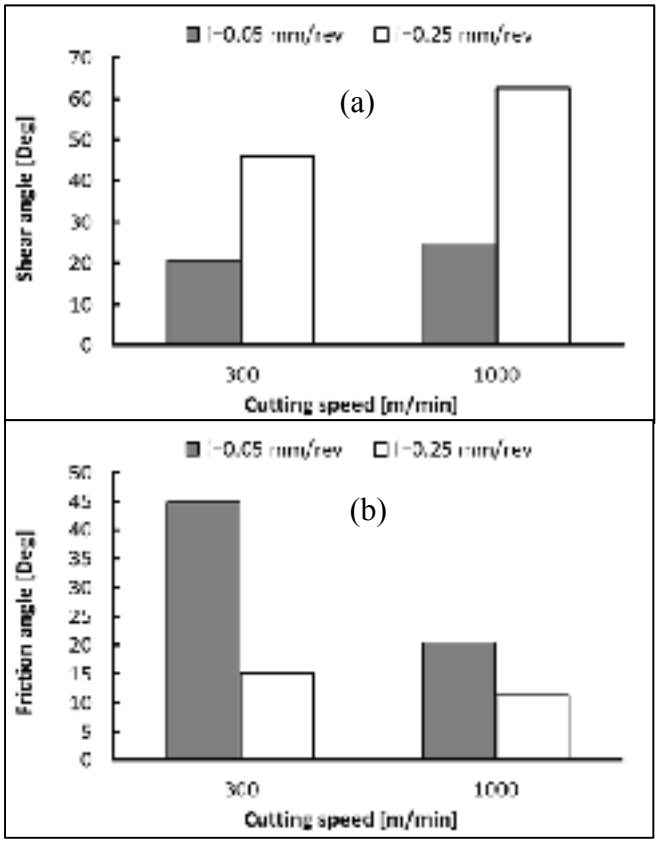

Figure 2-24 Effect of cutting speed on (a) shearing and (b) friction angle

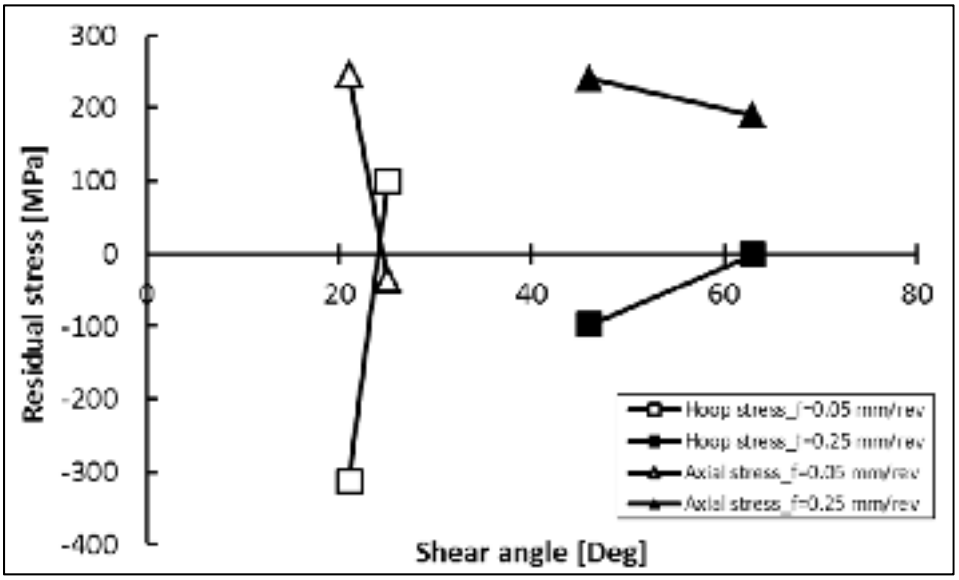

Figure 2-25 Effect of the shear angle on the surface residual stresses

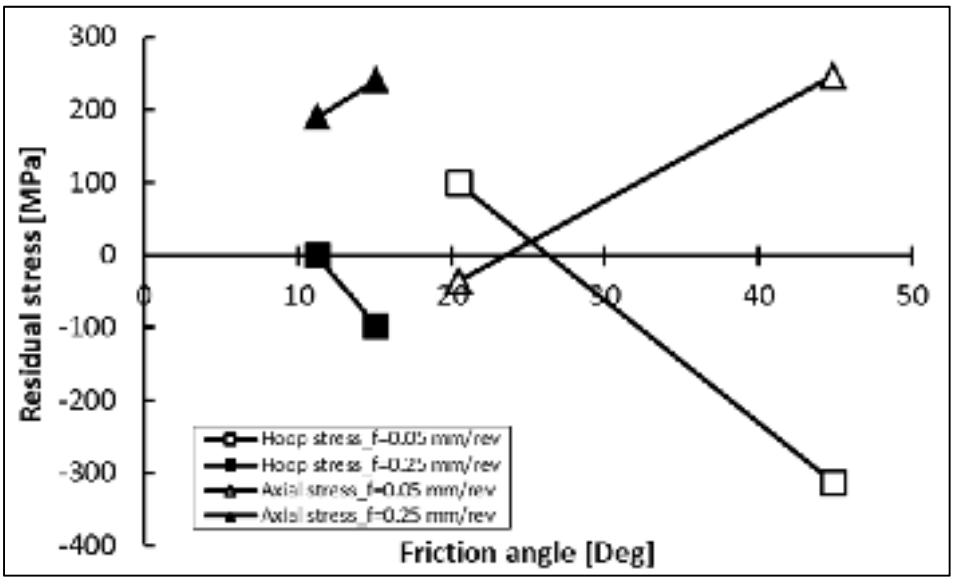

Figure 2-26 Effect of the friction angle on the surface residual stresses

2.4 Conclusions

This investigation showed the experimental results of the orthogonal dry machining of the AA7075-T651 alloy using an uncoated cemented carbide tool. The assessment of the surface finish shows that surface profiles displayed different features and are sensitive to cutting conditions in the axial as well as in the hoop direction. The formation of BUE was intensified by an increase in the cutting feed; however, an increase in the cutting speed reduced it and promoted the formation of the BUL on the rake face. The EDS analyses showed that the BUE and BUL have a dissimilar nature. SEM and EDS analyses showed that the primary origin of surface damage was the interaction between the tool edge and the iron-rich intermetallic phases present within the work material matrix. The hoop stress was predominantly compressive on the surface, and tended to be tensile as the cutting speed increased. The reverse occurred for the surface axial stress. The smaller the cutting feed, the greater the effect of the cutting speed on both axial and hoop stresses.

CHAPTER 3

EFFECTS OF DRY HARD MACHINING ON SURFACE INTEGRITY OF INDUCTION HARDENED AISI 4340 STEEL

Walid Jomaa, Victor Songmene, and Philippe Bocher

Article submitted, Journal of Materials and Manufacturing Processes, 21st January, 2015

Abstract: Excessive induction hardening treatment may result in deep hardened layers with related low compressive residual stress which may affect the performance of the mechanical parts. However, a judicious selection of the finishing process that eventually follows the surface treatment may overcome this inconvenient. To illustrate this, dry orthogonal machining of induction hardened AISI 4340 steel (58-60 HRC) using mixed ceramic inserts, was performed in this work. It was found that the machining process induces significant compressive residual stresses at and below the machined surface. The residual stress distribution is affected by the cutting feed and the cutting speed. On one hand, surface residual stress tends to become tensile when the cutting speed is increased. On the other hand, an increase in cutting feed accentuates surface damage whilst it increases compressive surface residual stress. Microstructural analysis shows the formation of a thin white layer less than 2µm and severe plastic deformations beneath the machined surface. These results attest that the hard machining process may be an alternative to grinding since an enhanced surface integrity in terms of residual stresses and microstructure conditions can be achieved.

keywords: Hard Machining; Residual Stresses; White Layer; Cutting Forces, Cutting Temperatures, Induction Hardening; 4340 Steel

3.1 Introduction

Many aerospace and automotive systems require structural parts presenting high in-service performance in terms of fatigue life and wear resistance. Gears and crankshafts are among these components, whose surface and subsurface characteristics play a key role in controlling their service life. Hence, additional surface treatments are used in order to enhance their mechanical behavior by introducing favorable compressive residual stress and high surface hardness. In fact, it is generally agreed that surface hardness improves wear resistance and residual stresses significantly affects the life and performance of structural components. Several studies have found that tensile residual stress reduces fatigue strength, while compressive residual stress increases it (Hashimoto, Guo et Warren, 2006). Such combination of high surface hardness and compressive residual stress can be achieved by induction surface hardening. This process offers a number of advantages over other heat treatments as it guarantees a good repeatability in terms of the hardened layer quality, is a short heat treatment process (seconds), and is easily incorporated into automated manufacturing processes (Grum, 2007). Furthermore, compressive residual stresses can be generated along with proper hardened depths (Grum, 2000). To ensure suitable dimensions and surface roughness, induction hardening is most often followed by grinding (Grum, 2001). However, additional grinding of the induction hardened surface has an inverse effect on the stress state at the surface layer, as grinding always induces tensile residual stresses (Kundrák et al., 2012). In addition, a thick white layer can be produced by grinding under certain conditions (Guo et Sahni, 2004). Abràо et al. (1996), assessing the fatigue life of turned and ground hardened bearing steel, indicated that superior fatigue strength was obtained with turned specimens. Konig et al. (1993) compared the properties of ground and hard-turned workpiece surface and found that parts manufactured by hard turning operations demonstrate high levels of rolling strength compared to grinding even a white layer was present (König, Berktold et Koch, 1993).

Unlike machining processes (turning and milling), residual stresses have been widely studied in the case of grinding of induction surface hardened materials (Grum, 2007; Grum, 2000;

2001; Savaria, Bridier et Bocher, 2012). On the other hand, previous works (Çiçek et al., 2013; Gaitonde et al., 2009) stated that ceramic cutting tools have excellent performance in terms of tool life and surface quality during machining of hardened steels such as AISI D2 and AISI 4340. In this chapter, the effect of orthogonal dry machining on the surface integrity of induction hardened AISI 4340 steel using mixed ceramic inserts is presented. Residual stress distributions and microstructures are investigated in terms of cutting parameters (cutting speed and cutting feed).

3.2 Material and methods

Orthogonal machining using PVD TiN coated mixed ceramic inserts was carried out on a MAZAK 3-axes CNC machine under dry cutting conditions (Figure 2-2-Chapter 2). The inserts' geometry was TNGA 120408-E (KY4400 grade Kennametal Inc.) and the inserts were mounted on a right hand tool holder, DTFNR2525M16KC04, with a back rake angle of -5°. A newer cutting tool edge was used for each cutting condition in order to eliminate the effect of possible tool wear on the surface integrity. The tested specimens were disc-shaped, with an external diameter 70 mm, an internal diameter of 19 mm, 4 mm thick (Figure 3-1).

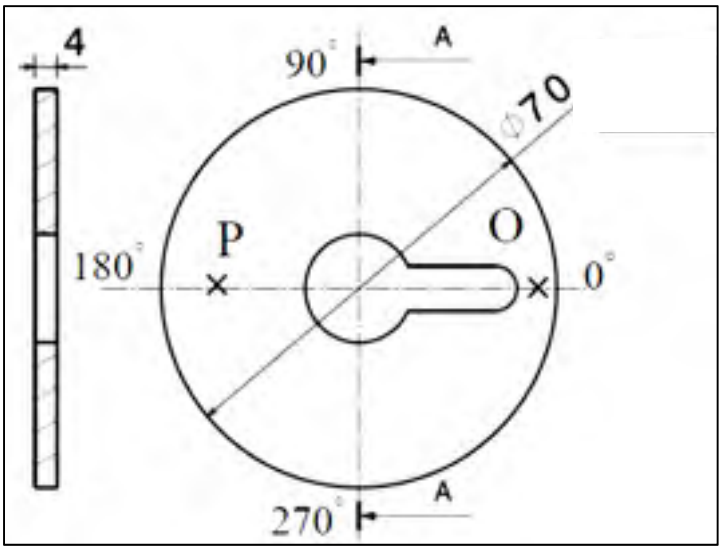

Figure 3-1 Geometry of the workpiece (all dimensions are in mm)

The material used in this study was AISI 4340 Vacuum Arc Remelting (VAR) steel (6414 grade for Aerospace Material Specification, AMS) and its chemical composition is presented in Table 3-1. It is a low-alloy steel with a good combination of strength, ductility, and toughness along with high hardenability. It is used for aircraft components, including landing gear, gears, and crankshafts. In the present work, the work material was first rough machined, induction surface hardened, and finally machined under different cutting conditions. The specimens were machined at cutting speeds (V) ranging from 54 to 202 m/min and cutting feed (f) ranging from 0.01 to 0.15 mm/rev. The depth of cut (DOC) was kept constant (0.5 mm) for all the experiments. The cutting forces (tangential force, *Fc*, and thrust force, *Ft*) were measured using a quartz three-component dynamometer (type 9255B) with the help of a Kistler charge amplifier. The raw force signals were numerically filtered and analyzed using a proper Matlab code.

Table 3-1 Chemical composition of the as-received 4340 VAR steel

Element	C	Mn	Cr	Ni	Mo	Cu	Si	P	S
wt (%)	0.4	0.7	0.76	1.76	0.24	0.1	0.27	0.004	0.001

The induction surface hardening treatment was conducted on an EFD machine (Figure 3-2) equipped with a medium and high frequency generator (power of 1.2 MW). The treated workpiece treated with a power of 80 kW, frequency of 10 kHz, and time of 1.2 sec to achieve a deep hardened layer of 2 mm (Figure 3-2a and 3.-2c). The part was rotated at 600 RPM during the heating stage. A mixture of water and polymer (12%) was used as a quenching medium. The quenching was applied immediately after the power had been turned off.

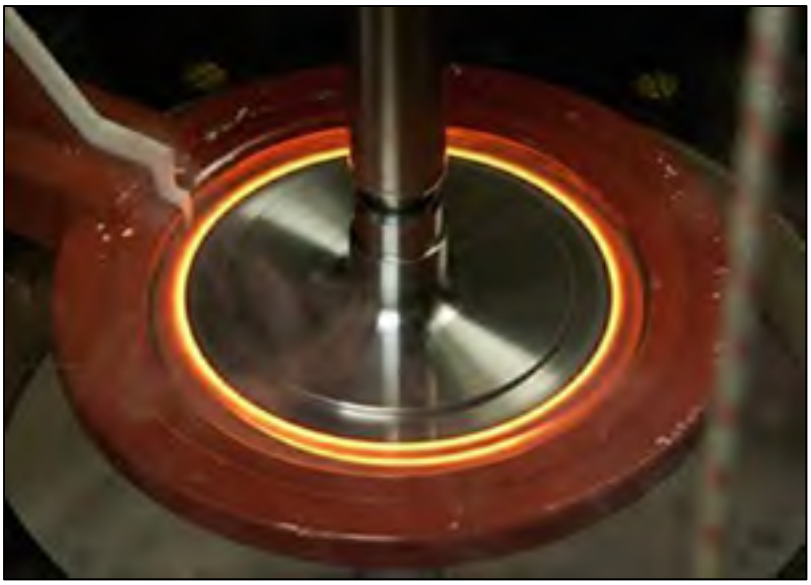

Figure3-2 Induction heating machine EFD™

The X-ray diffraction technique and the classical $\sin^2\Psi$ method were used for the residual stress measurements using a Proto iXRD® system with a chromium tube running. In-depth measurements were performed after removal layer using electrochemical polishing. The electropolished pocket was a rectangular-shape and had a size of 2x6mm. The residual stresses were measured in the circumferential direction (parallel to the cutting direction) and axial direction (perpendicular to the cutting direction). In the present work, the measured residual stresses were corrected regarding the penetration depth of the X-ray diffraction, using a commercial PROTO GRADIENT code. X-ray parameters used in the present work are given in Table 3-2.

Table 3-2 X-ray diffraction parameters

Parameters	Value
Radiation	Cr Kα (λ=2.291 Å at 20 kV, 4 mA)
Filter	Vanadium
Bragg angle (2θ)	156
Number of ψ angle	11
Ψ oscillation (deg)	1
Collimator spot size (mm)	2
X-ray elastic constant (MPa)	171

An optical microscope, model Olympus GX51, was used to study the microstructures of the samples before and after induction hardening treatments. The as-received, induction hardened and machined samples were polished and etched for about 3 minutes using 10% picric acid solution. The microstructure and texture changes induced by machining were also examined using a HITACHI S-3600N scanning microscope (SEM). The microhardness was measured below the surface using a Future Tech FM hardness tester (200HV 200 gf and 25 gf). The roughness parameters were measured using a Mitutoyo SJ-400 instrument with a diamond stylus contact profilometer. The cut-off was set to 0.8 mm according to the ISO 4288 standard and a Gaussian filter was used during the measurements.

3.3 Results

3.3.1 Induction hardening treatment

The as-received work material was a normalized and tempered 4340 VAR steel at 20-23 HRC (Figure 3-3d). After the induction hardening treatment, a finer martensitic microstructure was obtained along the case depth (Figures 3-3a and 3-3b)) with a typical hardness of 58-60HRC. Figure 4.4 presents the in-depth microhardness profiles measured on two different induction hardened samples and at the two locations O and P (Figure 3-1). The hardening depth is assumed as the depth for which the Vickers hardness is 500 HV200 gf. The results indicate that the microhardness profiles were similar, however, one can note that the hardness vary slightly from one location to the another due to the specific geometry around the position O. In fact, at this location less heat sink effect took place during the induction hardening treatment and a deeper case depth was found. Hence, the hardened layer depth was estimated to be between 2 and 2.35 mm. This difference can be considered negligible regarding the machining DOC (0.5 mm). The decreasing trend around 1.5 mm can be related to the difference in the cooling rate between surface and subsurface regions resulting in different microstructures (from fully martensitic to martensitic +bainite).

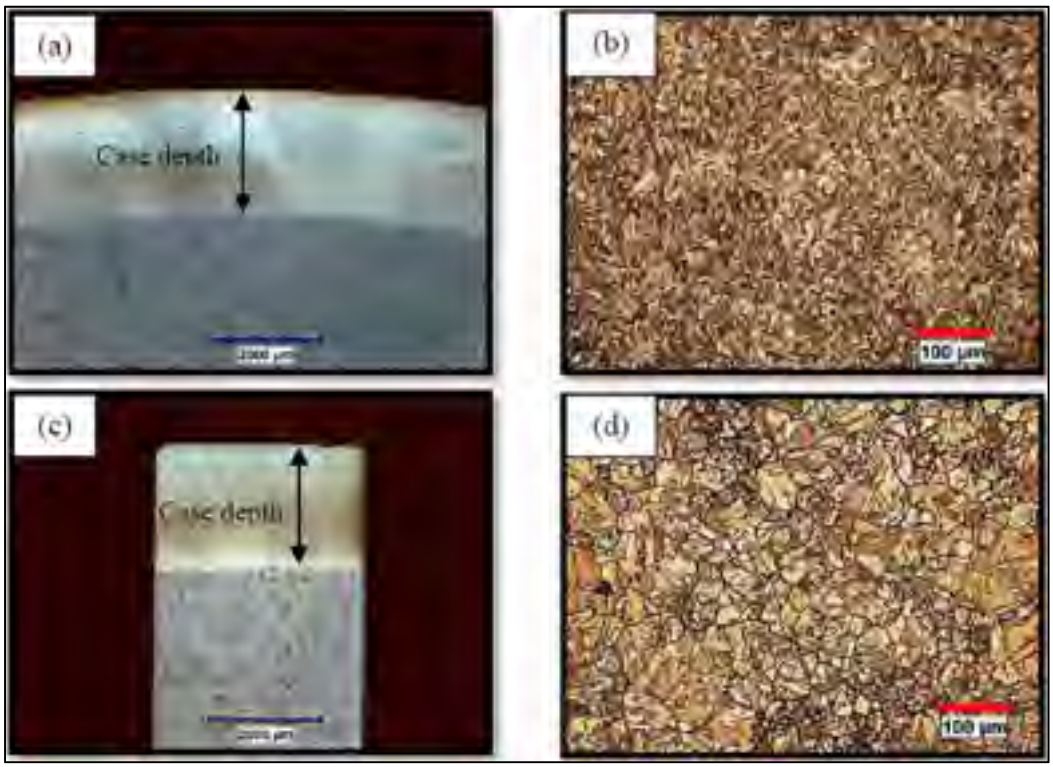

Figure 3-3 (a) Transversal cross section of the induction hardened layer, (b) microstructure of the hardened material, (c) longitudinal cross section of the induction hardened layer, and (d) microstructure of the bulk material

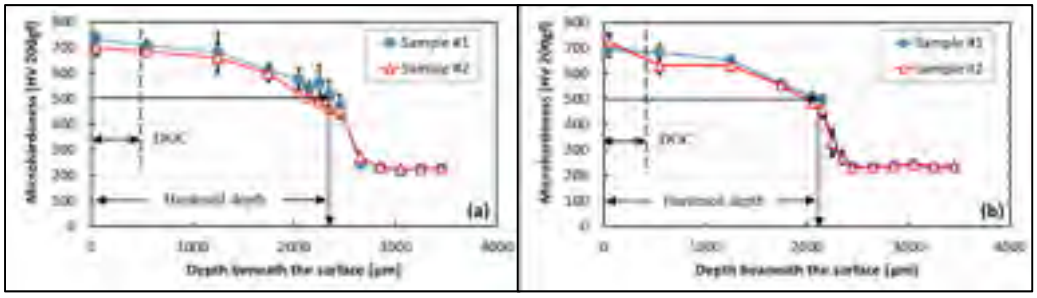

Figure 3-4 Microhardness distributions after induction hardening measured on a) Position O and b) Position P (see Figure 4-1)

The surface residual stress in the hoop and axial directions obtained after induction hardening treatment and successive electro-polishing are presented in Figure 3-5. The very high tensile stresses measured at the surface just after induction hardening were due to the oxidized layer formed during heating. As the hardened layer is rather deep, the resulting residual stresses are tensile, but they become progressively compressive after some depth. Compressive residual

stresses were found in the hoop direction but some tensile stress was found in the axial direction in the treated zone. More specifically, the stress state at a 0.5 mm below the surface, (which represents the depth of cut during machining) was around -20 MPa for the axial stress and -200 MPa for the hoop stress (Figure 3-5b). These residual stress states represent what will be consider as the reference "initial" stress levels for comparison with the residual stress levels obtained after machining.

The force signals (Figure 3-6) suggested that the selected DOC (0.5 mm) is sufficient to achieve the steady state during machining, although only three revolutions were machined for the highest cutting feed (0.15 mm/rev).

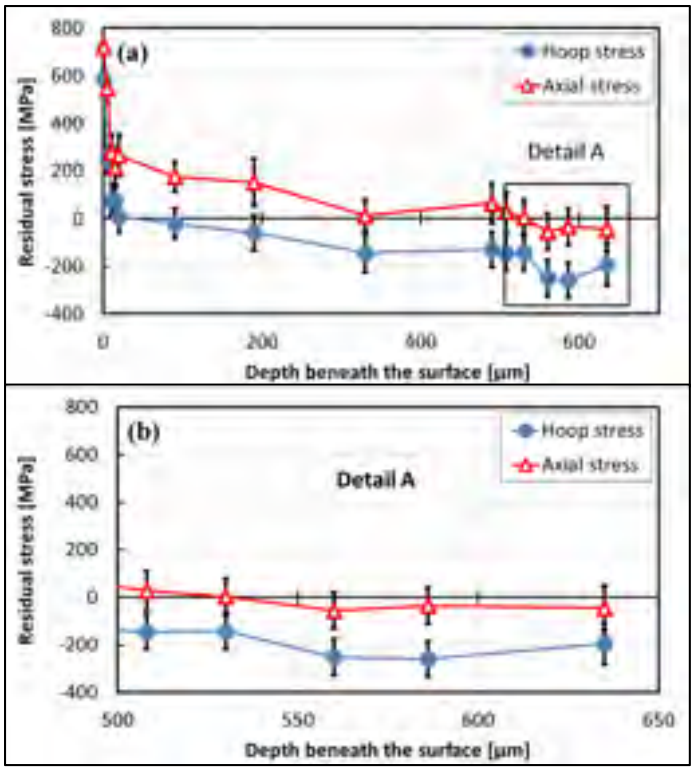

Figure 3-5 (a) Residual stress distribution after induction hardening treatment, (b) residual Stress state before machining measured on position P (see Figure 4-1)

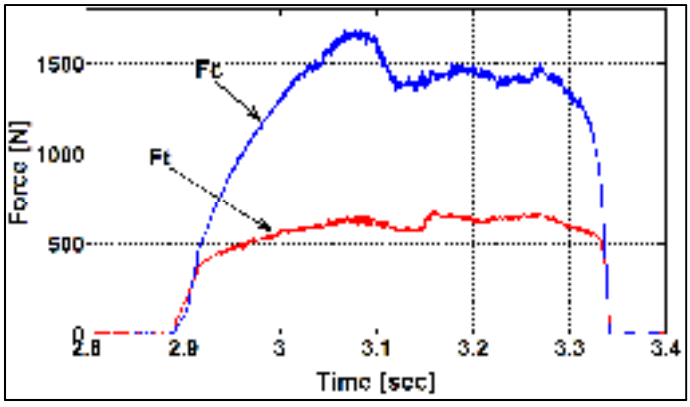

Figure 3-6 Signals of main cutting force Fc and thrust force Ft for V=128 m/min, f=0.15 mm/rev and DOC=0.5 mm

3.3.2 Influence of the tool retraction

When orthogonal machining is performed on a disc-shaped workpiece, a part of the workpiece is machined with a variable cutting feed due to the retraction movement of the tool at the end of the test. Hence, in order to analyze the surface integrity of the machined workpiece in the steady state condition, it was necessary to define a region that represents the cutting test. Several techniques can be used to document the effects of tool retraction on the produced machined surface due to the transient condition (M'saoubi et al., 1999; Outeiro, Umbrello et M'Saoubi, 2006; Umbrello, 2013). According to M'saoubi et al. (1999), it is possible to determine the tool retraction zone (TRZ) using the circularity deviations of the machined samples. Circularity profiles were consequently measured on each machined workpiece using a coordinate measuring machine (CMM) system. Figure 4-7 show the circularity deviation measurements for different cutting feed (0.08 and 0.15 mm/rev). Three stages can be observed at the end of the machining considering the relative tool/workpiece motion: first, the cutting tool advances from position A to B with the cutting feed decreases; second, at the end of the path (position B), the cutting tool stops for a short period of time (called dwell time); third, the cutting tool retracts from position B to C.

Surface residual stress measurements were also performed all around the workpiece in the axial and hoop direction. The results shows that the surface residual stress values vary from -

209 to -438 MPa for axial stress and -800 to -1008 MPa for hoop stress, as shown in Figure 4-8. In addition, One can observes that the hoop and axial residual stresses measured between 0° and 180° are lower than those measured between 180° and 360°, but no clear indication of the tool stop point can be detected from these measurements.

On the other hand, the surface roughness was measured and found to be strongly correlated to the circularity profile if the tool retraction zone is considered as the zone of minimum roughness values (Figure 3-9). In fact, the reduced cutting feed during tool retraction results in lower surface roughness values. Since measurements of residual stresses using the X-ray diffraction method are time-consuming and expensive, surface roughness measurements can constitute an accurate and reliable method for selecting the representative cutting condition zone during orthogonal machining.

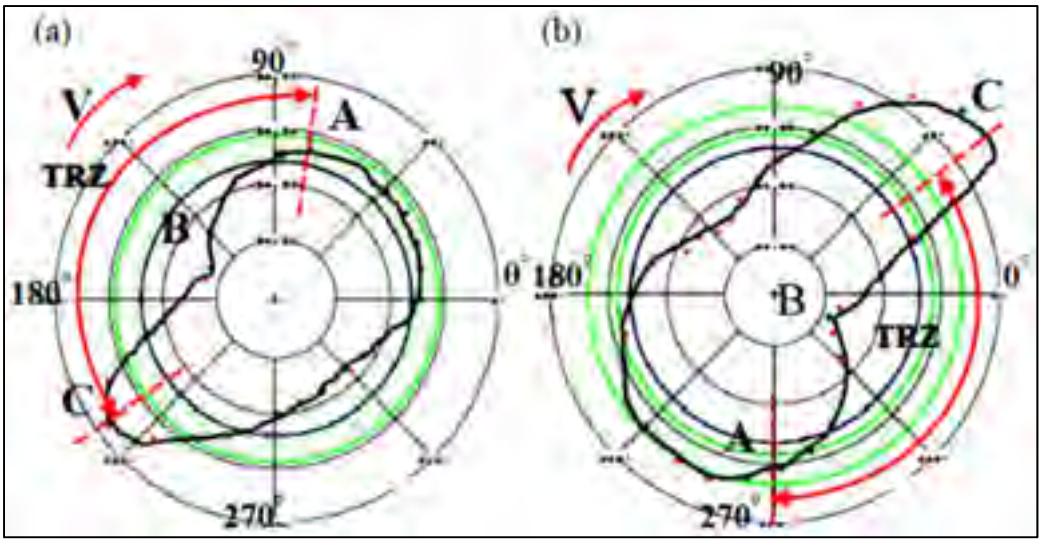

Figure 3-7 (a) Circularity deviation of the machined samples at cutting feed of (a) 0.08 mm/rev and (b) 0.15 mm/rev, V=128 m/min, TRZ: Tool Retraction Zone

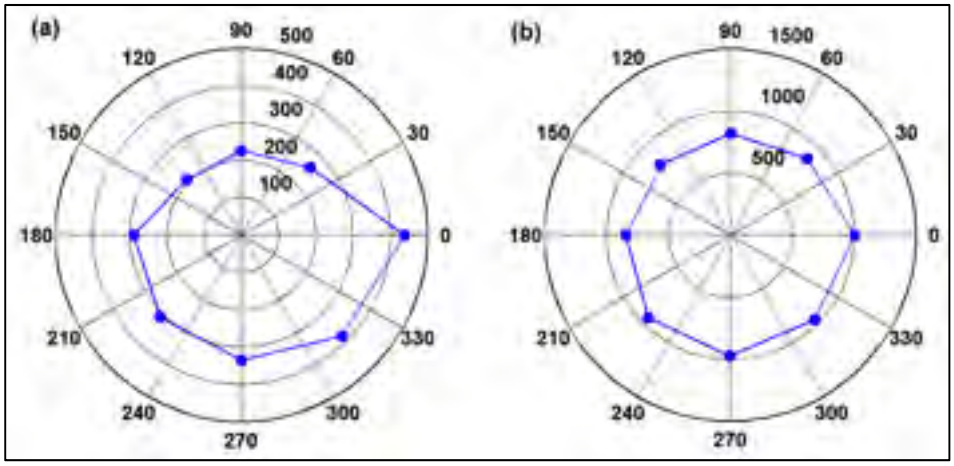

Figure 3-8 Surface residual stress measurements (in MPa) all around the workpiece in the (a) axial direction and (b) hoop direction for f=0.08 mm/rev, V=128 m/min and DOC=0.5 mm

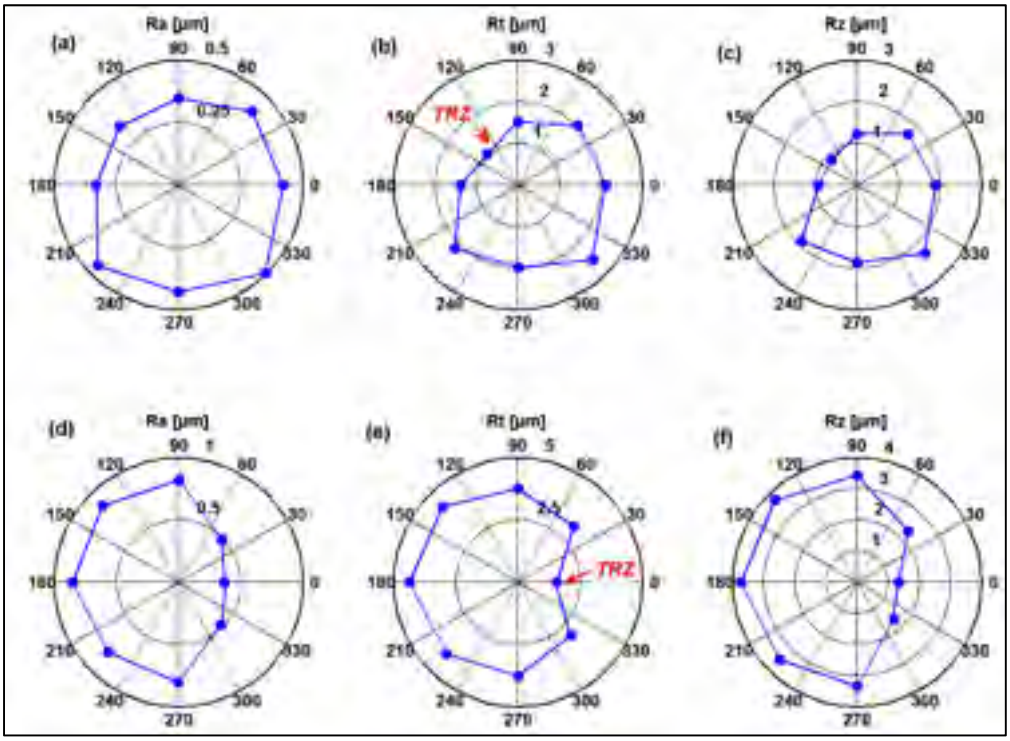

Figure 3-9 Surface roughness measurements (Ra, Rt, Rz) all around the workpiece for cutting feed of 0.08 mm/rev (a, b, and d) and 0.15 mm/rev (d, e, and f), V=128 m/min and DOC=0.5 mm

3.3.3 Surface finish

The close examination of the machined surfaces under a scanning microscope (SEM), revealed several distinguishing features. Long straight grooves, parallel to the relative work-tool motion, were found as shown in Figure 3-10 and 3-11. These grooves have been attributed to the effect of micro-asperities formed on the tool cutting edge and the ploughing of microbuilt-up edges (Elkhabeery et Bailey, 1984). An additional feature observed in the specimens was the presence of chatter marks perpendicular to the direction of relative work-tool motion. It was observed that when the cutting feed increases, these grooves and chatter marks increase and become deeper (Figure 3-10b and 3-10c). Furthermore, Figure 4-10c shows the presence of fractured areas accompanied by the formation of voids (Figure 3-10e) and material smearing and cavities (Figure 3-11d) at higher cutting feed (0.15 mm/rev). However, it was found that an increase in cutting speed led to the progressive reduction of chatter marks (Figure 3-11). The formation of these grooves indicates the existence of a material side flow due to the occurrence of sever plastic deformation during machining (Figure 3-11d).

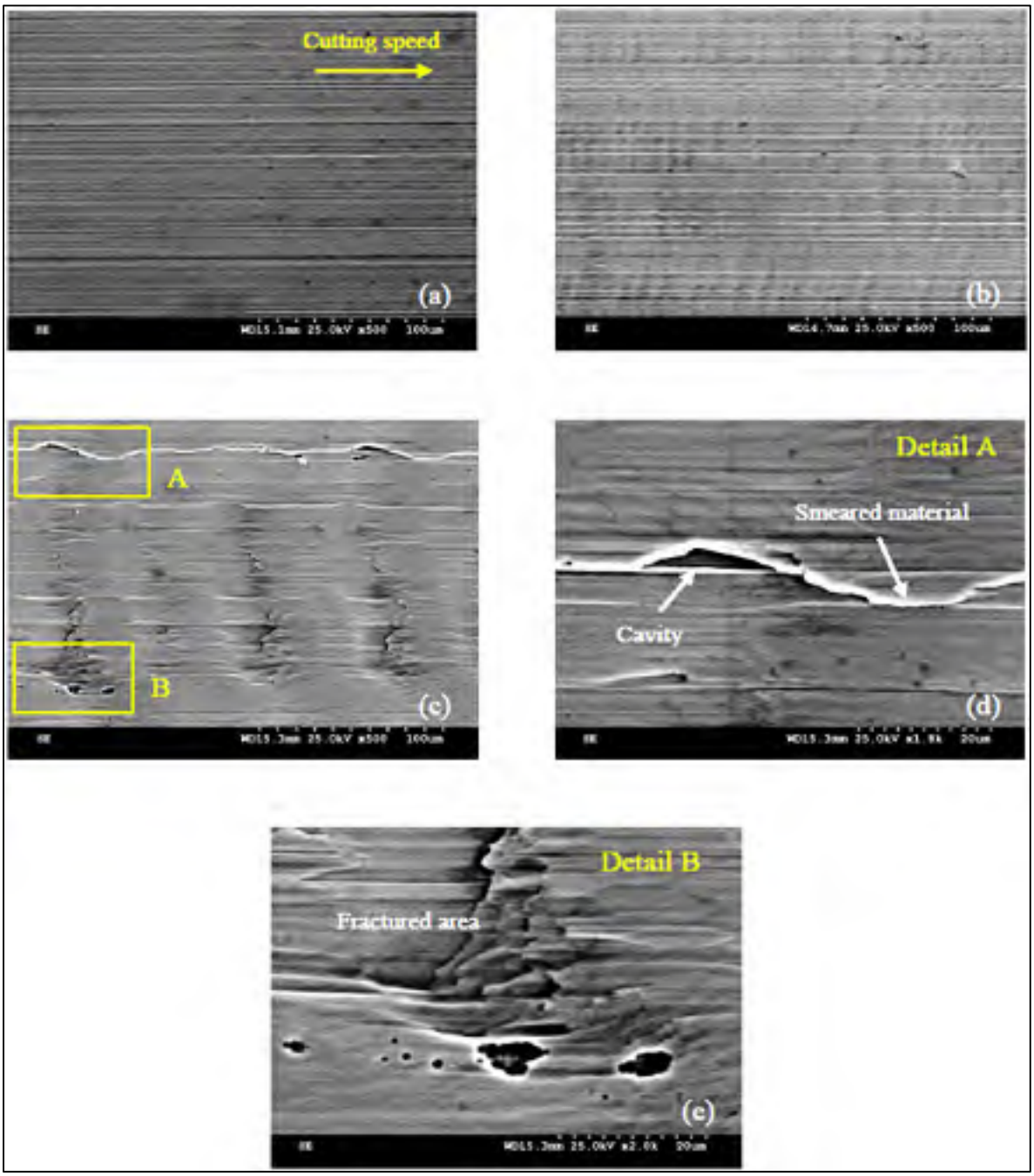

Figure 3-10 SEM images of the machined surface at cutting feed of a) 0.01 mm/rev, b) 0.08 mm/rev, c) 0.15 mm/rev, d) detail A of c), and e) detail B of c), V=128 m/min, DOC=0.5 mm

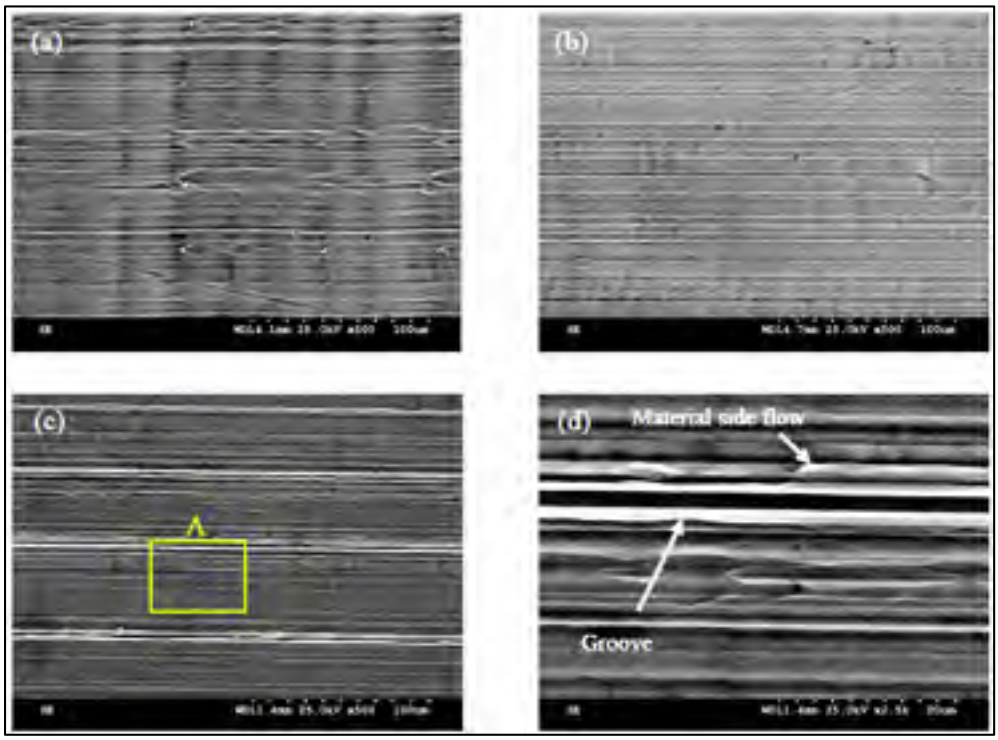

Figure 3-11 SEM images of the machined surfaces at cutting speed of a) 54 m/min, b) 128 m/min, c) 202 m/min, and d) detail A of c), f=0.08 mm/rev, DOC=0.5 mm

3.3.4 Residual stress

The machined induced residual stresses were analyzed in terms of surface residual stress (SRS), maximum compressive stress (MCS), and area of the compressive zone (ACZ) as shown in Figure 3-12. The maximum residual stress is compressive and located at about 10 to 20 µm below the machined surface for all measured residual stress profiles, in both the axial and hoop directions. In this work, a significant compressive residual stress state was obtained under all cutting conditions and the best way to discriminate the extent of the compressive stresses as a function of machining parameters was to use the concept of area of compressive zone (ACZ) induced by the cutting process. The measured residual stress results were fitted using a polynomial function of degree 5 and the ACZ was calculated as the integral of this function calculated over the region where the compressive residual stress have

increased compare to the initial stress state (-20 MPa for axial stress and -200 MPa for hoop stress).

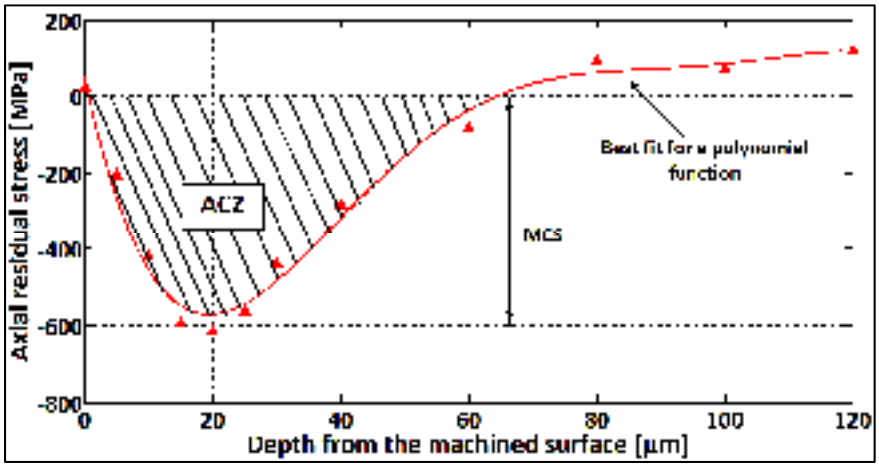

Figure 3-12 Axial residual stress profile measured by X-ray diffraction after machining for V=202 m/min, f=0.08 mm/min and DOC=0.5 mm

The effect of the cutting feed on the measured residual stress distributions and the ACZ is presented in Figures 3-13 and 3-14. The results show that the MCS and the ACZ increase with the cutting feed for both, the hoop and axial directions. The MCS was located deeper in the workpiece for higher values of the cutting feed. Moreover, the residual stress distributions were significantly affected when increasing the cutting feed from 0.01 mm/rev to 0.08 mm/rev but only slightly changed with further increase to 0.15 mm/rev. The hoop SRS were somehow more sensitive to the changes of the cutting feed.

The cutting speed affects the residual stress profile in different ways, as seen in Figures 3-15 and 3-16. The compressive SRS in the hoop direction decreases with the increase of the cutting speed and the invers occurs for the axial compressive SRS. The highest level of SRS, MCS, and ACZ were recorded at the lowest cutting speed (54 m/min) in the hoop direction. Nevertheless, the highest values of MCS and ACZ were obtained at the highest cutting speed (202 m/min) in the axial direction. In general, the position of the MCS was deeper in the workpiece as the cutting speed increased. It can be stated that the residual state below the

machined surface (maximum compressive stress and area of the compressive zone) is only slightly affected by the cutting speed but is strongly influenced by the cutting feed. Figures 3-14 and 3-16 indicate that the ACZ in the hoop direction is higher than that measured in the axial direction. Besides, observing the trends of the ACZ, one can establish a proportionality relationship between the two directions (hoop and axial). In fact, during orthogonal cutting, a plane strain state is established in the cutting zone and the residual stresses measured in the hoop and axial directions can be considered as a principal stresses and proportional. This can explain this proportionality relationship (Liu et Barash, 1982).

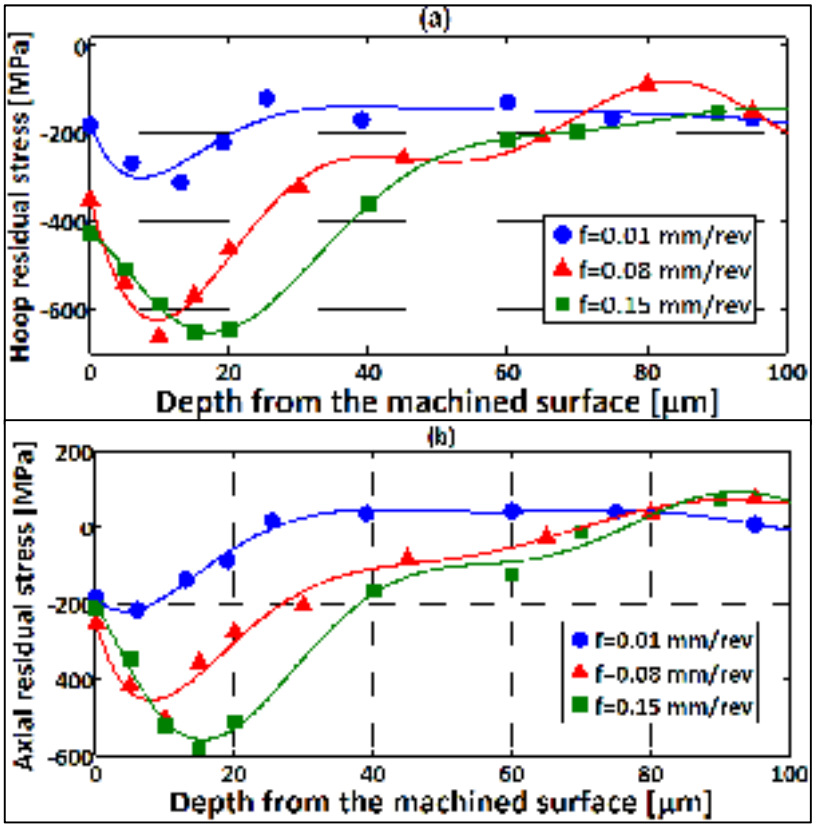

Figure 3-13 Effects of cutting feed on (a) hoop and (b) axial residual stresses for V=128 m/min and DOC=0.5 mm

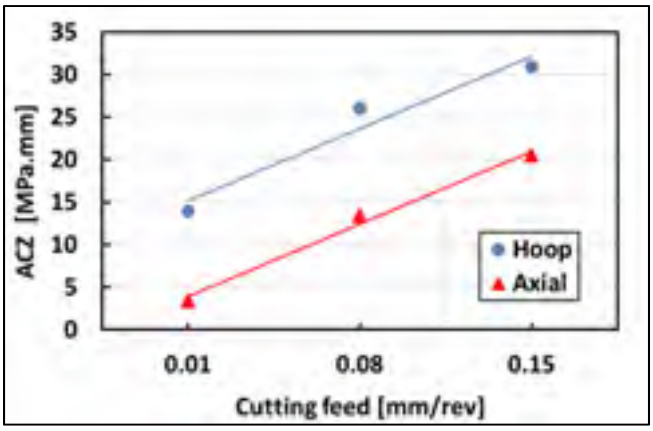

Figure 3-14 Effect of cutting feed on the ACZ for V=128 m/min and DOC=0.5 mm

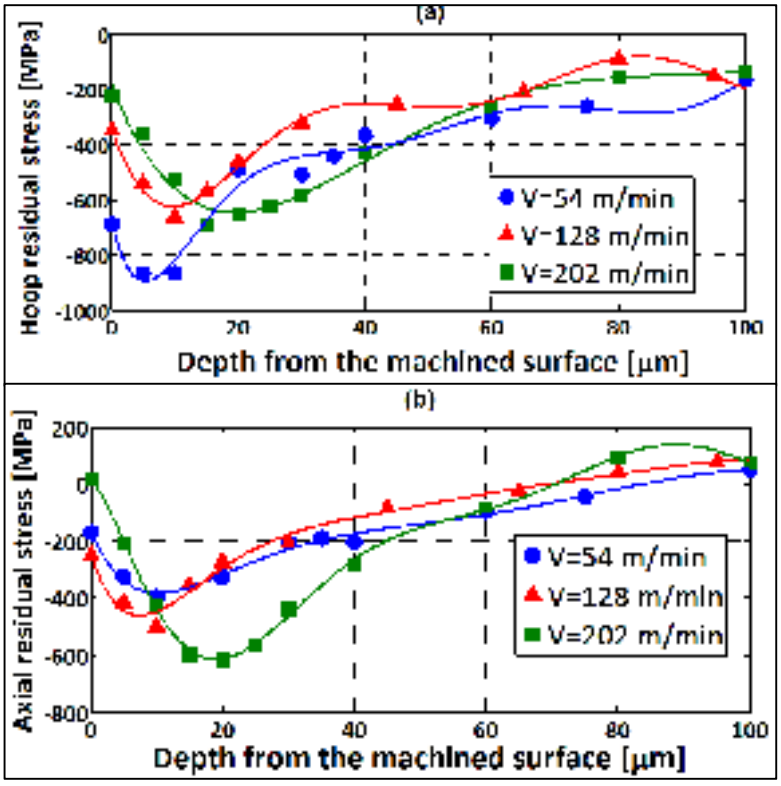

Figure 3-15 Effect of cutting speed on a) hoop and b) axial residual stresses for f=0.08 mm/rev and DOC= 0.5 mm

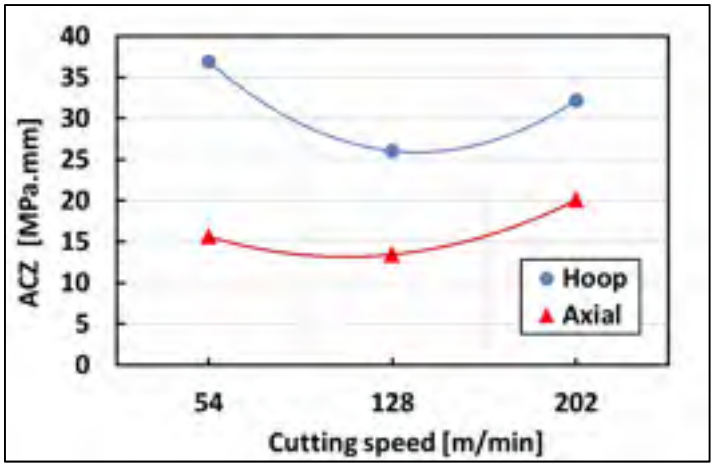

Figure 3-16 Effect of cutting speed on the ACZ
for V=0.08 mm/rev

3.3.5 Microstructure

The SEM images of the microstructures below the machined surfaces revealed the existence of a thin white layer (less than 2µm) and severe plastic deformation (Figures 3-17 and 3-18). The white layer was etching resistant and the SEM picture shows a featureless structure. The etching resistance of the turned white layer may be attributed to its nano-grains resulting from dynamic recovery and recrystallization (Guo et Sahni, 2004). It can be seen that the thicknesses of the white layer and deformed layer increase with the cutting feed and cutting speed (Figure 3-19).

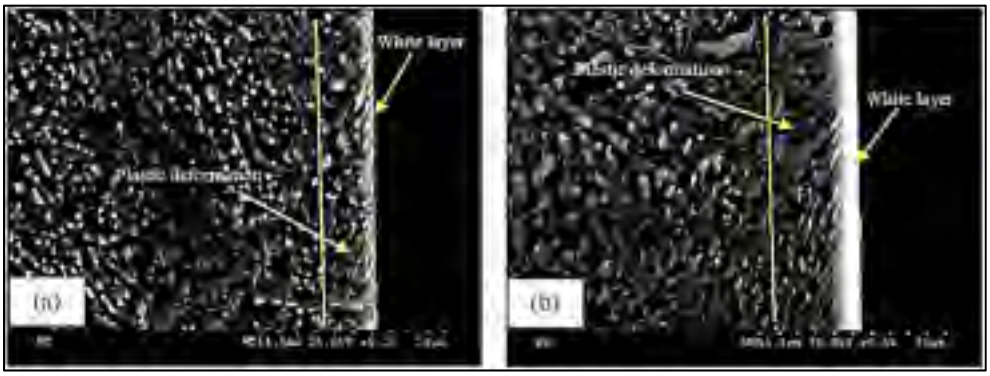

Figure 3-17 SEM images of the samples machined at cutting feed of
a) 0.01 mm/rev and b) 0.15 mm/rev, V=128 m/min, DOC=0.5 mm

Figure 3-18 SEM images of the samples machined at V= a) 56 m/min and b) 202 m/min, f=0.08 mm/rev, DOC=0.5 mm

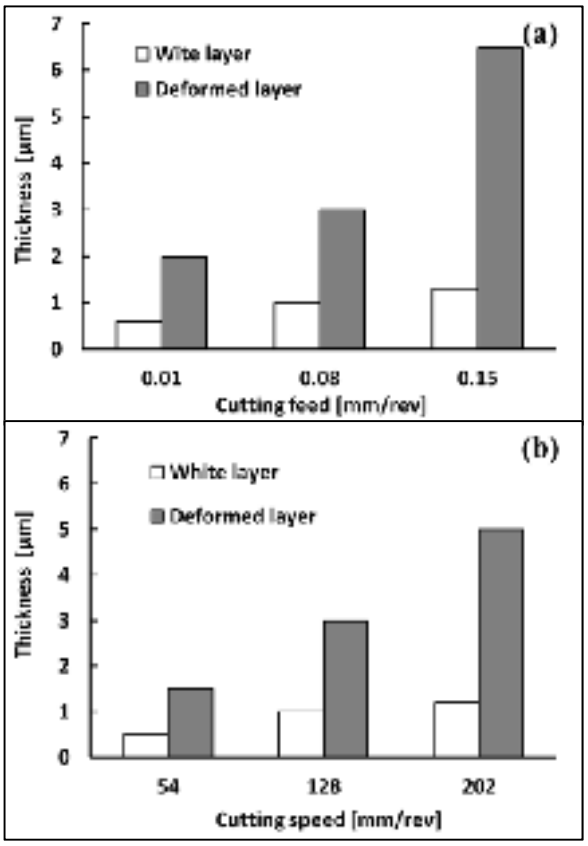

Figure 3-19 Effect of a) cutting feed and b) cutting speed on the thickness of the machining affected layer for DOC=0.5 mm

3.3.6 Microhardness

As the regions mainly affected by the cutting process are less than 100 µm, the assessment of the microhardness gradient was performed over 90 µm below the machined surface to document any possible tempering effect. To respect minimum indent spacing between two consecutive measurements (5µm), the indent line was inclined, forming a zigzag pattern as shown in Figure 3-20. The average results of three measurements for each depth was recorded and plotted in Figures 3-21 and 3-22. The load used for microhardness measurements was relatively low (25 gf) and significant variations in microhardness values from one sample to another can be found. These variations are similar to the order of variations observed in the induction treated regions before machining and are typical of the case hardness. The microhardness variations should then be analyzed for a given sample and cannot be compared. The microhardness profiles below the machined surfaces remain almost constant, except that obtained at the cutting feed of 0.15 mm/rev, as shown in Figure 3-21. It seems that in these severe cutting conditions, a possible tempering is taking place.

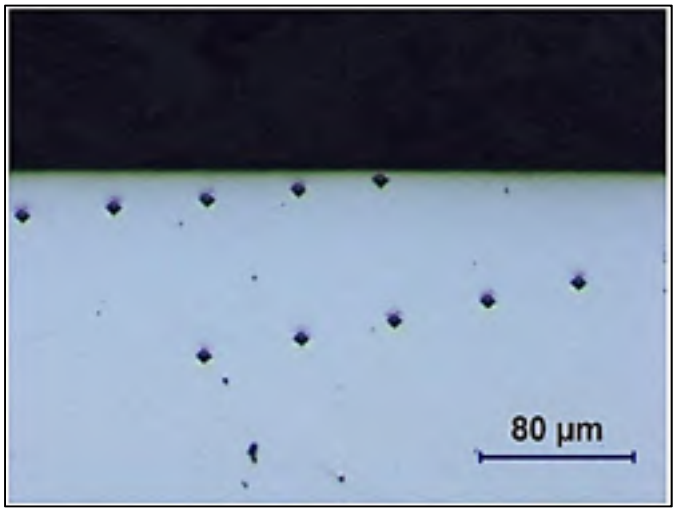

Figure 3-20 Microhardness measurements below the machined surface, for f=0.01 mm/rev, V=128 m/min, and DOC=0.5 mm

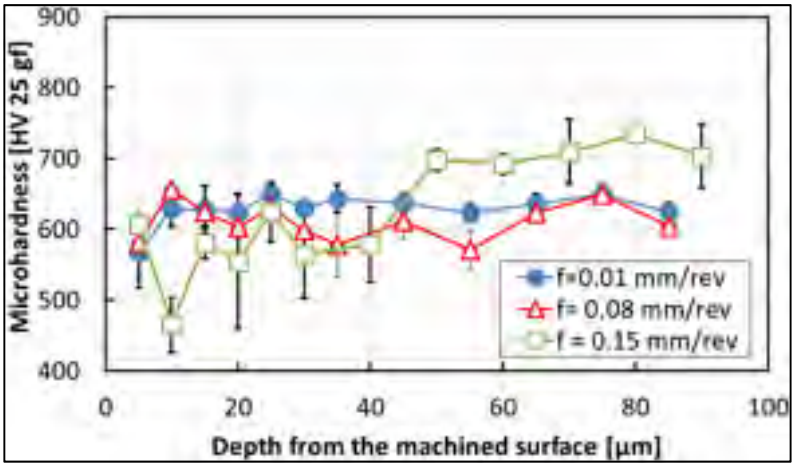

Figure 3-21 Effect of cutting feed on microhardness profiles for V=128 m/min and DOC=0.5 mm

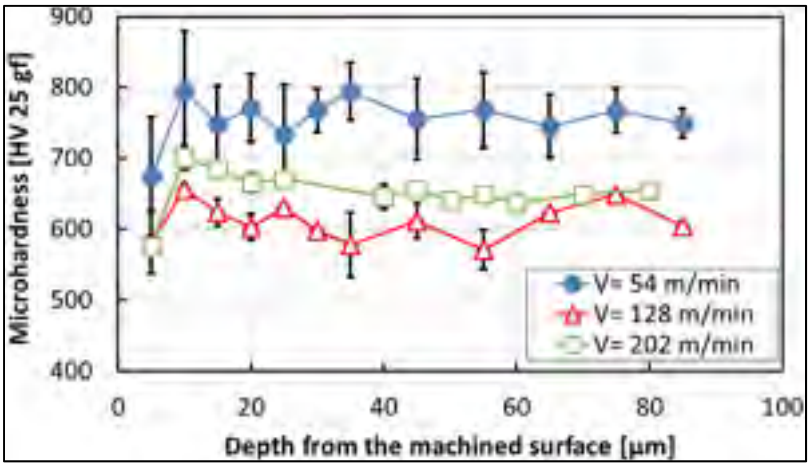

Figure 3-22 Effect of cutting speed on microhardness profiles for f=0.08 mm/rev and DOC=0.5 mm

3.4 Discussion

In an attempt to understand how the various surface attributes were affected by machining, the results relative to surface and subsurface alterations will be discussed based on the chip formation mechanisms, cutting forces, and cutting temperatures. The average temperatures of the machined surface and chip were calculated based on an analytical model proposed by Loewen and Shaw (Loewen et Shaw, 1954) and developed in APPENDIX I. Four attributes

of the machined surface integrity were analyzed successively: surface finish, residual stress distribution, microstructure and microhardness.

For surface finish assessment, the SEM analysis of the machined surfaces revealed different defect features. Chatter vibrations and micro-asperities on the cutting edge were the principle factors that deteriorate the surface quality of the machined surface. Figures 3-10 and 3-11 showed that an increase in cutting feed increases the chatter vibration, however, an increase in cutting speed decreases it. To understand these trends, an illustration of the chip formation process is presented in Figure 3-23. Machining at lower cutting feed (Figure 3.23a) induces low shearing angle (Figure 3-24) which leads in continuous chip formation (Figure 3.25a) and smooth surface finish with very few chatter marks. On the other hand, the machining at high cutting feed results in high shearing angles (Figure 3-24) and segmented chips (Figure 3-25b). The formation of segmented chips indicates that the cutting was taking place by brittle fracture rather than by shearing and this is a characteristic behavior when machining hard materials (Astakhov, Shvets et Osman, 1997a). Surface damages and chatter marks on the machined surface can actually be related to the amplitude of vibration rises due to the formation of these segmented chips (Taylor et al., 2013).

The surface defects variation with cutting conditions was correlated to the cutting temperature evolutions of the workpiece and the chip as calculated thanks to a modified analytical model (see details in APPENDIX I). This model proposed by Loewen and Shaw (1954), was modified to take into account the temperature rise due to the friction (rubbing) on the tool/workpiece interface (Equation (A.I-4) in APPENDIX I). Figure 3-26 shows that both the workpiece and chip temperatures increase with increasing in the cutting speed, which lead to the work material softening in the cutting zone. This makes the cutting easier, resulting in smoother machined surfaces with fewer chatter marks.

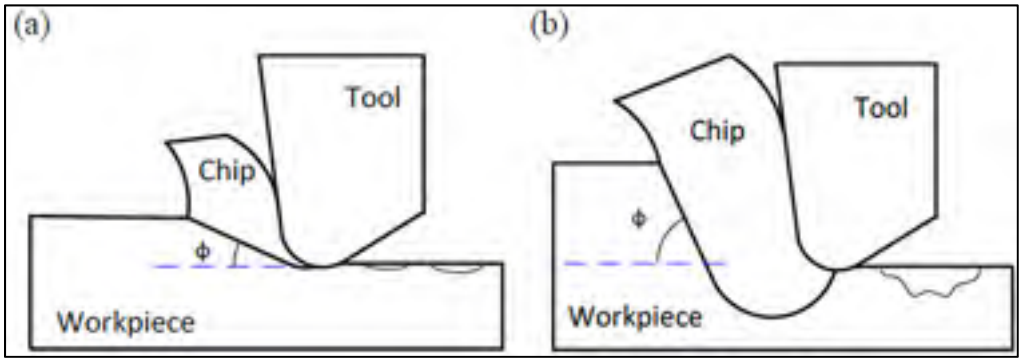

Figure 3-23 Illustration of chip formation and machined surface defects for (a) low and (b) high cutting feeds

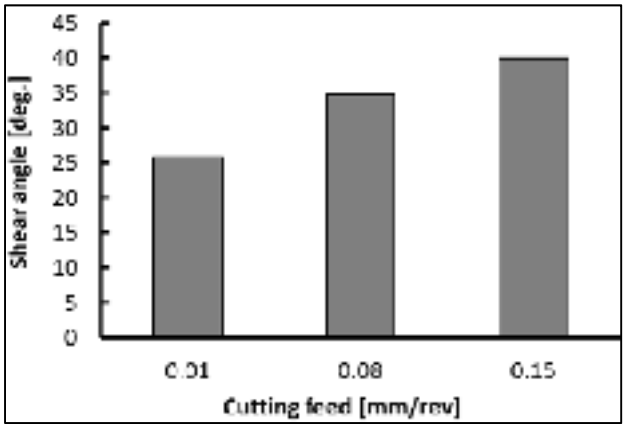

Figure 3-24 Effect of cutting feed on shear angle for V=128 m/min and DOC=0.5 mm

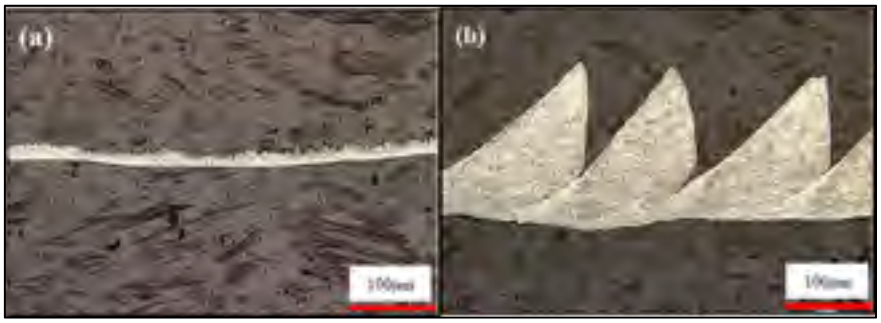

Figure 3-25 Chip structure at cutting feed of (a) 0.01 mm/rev and (b) 0.15 mm/rev, V=128 m/min and DOC=2 mm

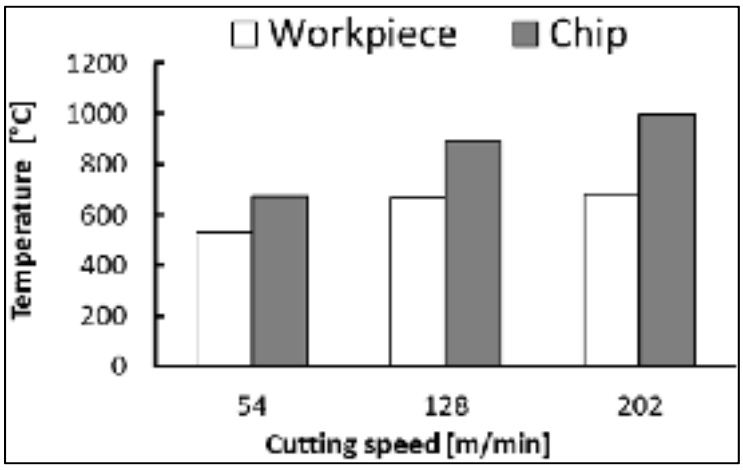

Figure 3-26 Effect of cutting speed on the workpiece and chip temperatures for f=0.08 mm/rev and DOC=0.5 mm

The residual stress state generated by the dry machining of induction hardened material was compressive. This can be attributed, principally, to the use of a negative rake angle (-5°) and the honed cutting edge (edge radius of about 25 µm) used for machining this fully hardened steel (Jomaa et al., 2011). It was found that the surface residual stress, the MCS below the machined surface, and the ACZ increase with the increase in cutting feed. Figure 3-27 displays the temperatures of the workpiece and the chip as a function of the cutting feed. As the latter increases, two opposing phenomena occur: the chip temperature increases and the workpiece temperature decrease. In fact, the fraction of the heat evacuated by the chip increases with the increase of the chip volume, leading to reduced workpiece temperature. Thus, the thermal contribution to residual stress formation decreases, leading to compressive residual stress on the machined surface. In addition, the increase of the cutting and thrust forces (Figure 3-28) when the cutting feed increases favour plastic deformation under the cutting tool, leading to even more tensile (plastic) deformation during the cutting process. This tensile deformation affects a greater depth of material below the machined surface and will result into more compressive stress in the deformed zone (Figures 3-13 and 3-14). This will result in the increase of the MCS and the ACZ when the cutting feed increases. As a plain strain state is established during the orthogonal cutting, the axial surface residual stress was found less sensitive to the cutting feed variations. This statement is confirmed by the low

amount/absence of burrs on the edge of the machined samples and the material side flow on the machined surfaces.

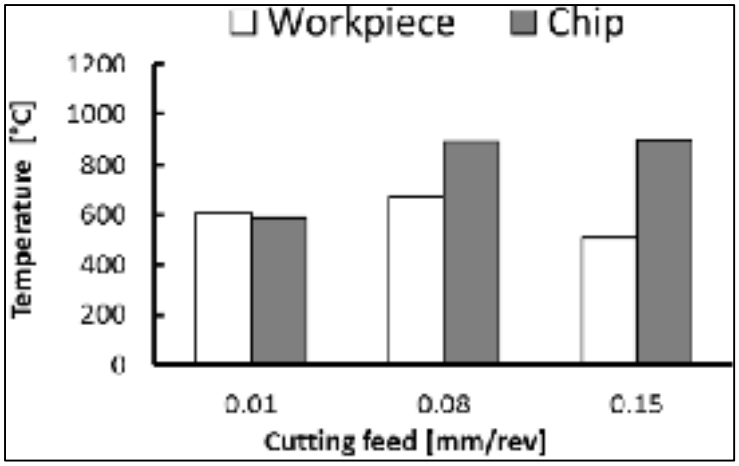

Figure 3-27 Effect of cutting feed on the workpiece and chip temperatures for V=128 m/min and DOC=0.5 mm

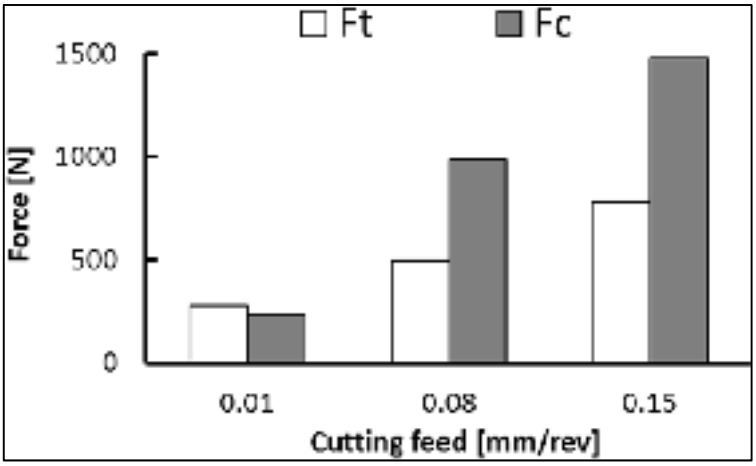

Figure 3-28 Effect of cutting feed on the main cutting force (*Fc*) and thrust force *(Ft*), for V=128 m/min and DOC=0.5 mm

When varying the cutting speed and feed, two opposing phenomena counteract to create the final residual stress state (Jacobson, Dahlman et Gunnberg, 2002). The first one, the mechanical one, comes from the increase of the strain rate and results in higher cutting forces, leading to a larger compressive stress (ACZ and MCS) below the machined surface

(Figure 3-15). The second one is a thermal effect which may result in excessive heat that can produce tensile residual stress below the surface. Moreover, when the cutting temperature reaches the phase transformation temperature of the material, a metallurgical effect will take place and compressive residual stress will be generated thanks to the volume expansion accompanying the phase transformation (Guo, Warren et Hashimoto, 2010). These opposing phenomena (mechanical, thermal, and metallurgical) counteract to create the final residual stress state. In the present work, the increase in the compressive residual stress with the cutting feed indicates that the mechanical (and eventually the metallurgical) effect is predominant versus the thermal one. The reverse occurs for the cutting speed as when the cutting speed increases, both the chip and workpiece temperatures increase leading to a slight decrease of the cutting force (Figures 3-26 and 3-29).

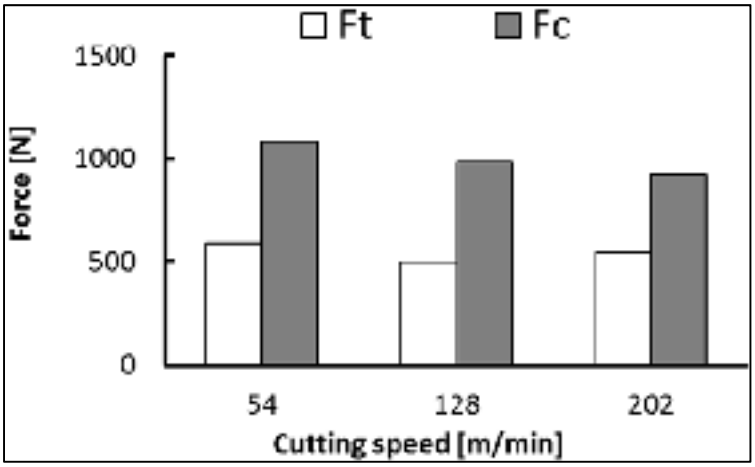

Figure 3-29 Effect of cutting speed on the main cutting force (*Fc*) and thrust force (*Ft*) for f=0.08 m/min and DOC=2 mm

In terms of microstructure, the thicknesses of white layer followed by a plastic deformed layer beneath the machined surfaces are sensitive to the variation of the cutting speed and feed (Figure 4-19). Research works (Guo, Warren et Hashimoto, 2010; Han et al., 2008; Kundrák et al., 2012; Shaw et Vyas, 1994; Umbrello, 2013) showed that the white layer formation during hard machining is caused, principally, by phase transformation. However, the workpiece surface temperature (Figures 4-26 and 4-27) were found to be below the phase

transformation temperature of the 4340 steel (800 °C for the typical heating rates reached during cutting operations). This result is in agreement with those obtained in previous works (Guo, Warren et Hashimoto, 2010; Han et al., 2008; Shaw et Vyas, 1994). In fact, stresses and strains induced in the machined-surface layer during hard turning is thought to play a role in causing phase transformation below the nominal phase transformation temperature (Chou et Song, 2005; Kundrák et al., 2012). Chou and Evans (2005) assumed 20% reduction of the phase transformation temperature due to mechanical working.

The residual stress measurements in the presence of white layer were the subject of debate within the scientific community. Warren and Guo, (2009) stated that in AISI 52100 steel (62 HRc) the white layer formed during machining was associated to a tensile residual stress state while Ramesh and Melkote (2008) have showed, thanks to a simulation model that additional compressive surface residual stresses will result from the white layer formation due to the volume expansion accompanying the phase transformation. As in the present work the penetration depth of the X-ray diffraction used during the measurements is thicker than the white layer (5 to 10 μm versus less than 2 μm), the measured residual stress on the top surface is the average of the penetration depth of the X-ray, which is a combination of a white layer and the plastic deformed layer. So the measured residual stresses at the surface cannot be considered as the residual stresses of the white layer only and no contribution can be made to this debate. Reversely, one do not need to involve the presence of white layers to explain the residual stress profiles measured in the present work as no specific trends are observed close to the surface.

Based on the obtained results, we can argue that machining induction hardened 4340 steel (58-60HRC) using a mixed ceramic insert under a cutting feed of 0.08mm/rev and cutting speed of 128m/min, can be a suitable machining conditions in terms of surface integrity (residual stresses and microstructure) and productivity (tool life). For the latter point, , Sahin (2009) has found that the tool life of the same cutting tool insert grade used in the present work decreases significantly when machining hardened bearing steel (AISI 52100 - 659HV) at cutting speed above 140m/min. Furthermore, other works (Dogra et al., 2010; Poulachon,

Moisan et Jawahir, 2001; Yallese et al., 2009) have showed that the optimal cutting speed for both, tool life and chip formation, is ranged between 100-130 m/min and they did not recommend further increase in cutting speed during hard machining.

In view of these findings, we can attested that dry machining of induction hardened 4340 steel using ceramic cutting tool may to be a suitable finishing process in terms of surface integrity and therefore, it can represent an alternative to grinding for the finishing of induction hardened components. This statement is approved by research works attesting that the grinding operation following the induction hardening operation deteriorates the surface stress state since grinding may induce tensile stresses (Grum, 2007; Grum, 2000; 2001). Recently, Guo et *al.* (2010) pointed out that samples produced by turning operations end up having superior fatigue life than to the ground ones. The residual stress profiles together with the morphology of the white layer induced by hard turning was found more favorable to longer service life compared to the ground one.

3.5 Conclusions

Orthogonal dry machining of induction hardened steel was conducted using mixed ceramic tool. The machined surfaces display different kind of surface defects (chatter marks, grooves, voids, material smearing). Increasing the cutting speed led to a reduction of surface defects; however, increasing in the cutting feed intensified the presence of chatter marks. A compressive residual stress state can be achieved after dry machining and the levels of these stresses were strongly affected by the cutting feed and cutting speed. A combination of a cutting feed of 0.08mm/rev and cutting speed of 128m/min was found to be a suitable machining condition in terms of surface integrity (residual stresses and microstructure). A thin white layer was formed for all machined surfaces. Dry machining using single point cutting tool can represent an alternative to grinding for finishing induction hardened 4340 components.

CHAPTER 4

AN HYBRID APPROACH BASED ON MACHINING AND DYNAMIC TESTS DATA FOR THE IDENTIFICATION OF MATERIALS CONSTITUTIVE EQUATION

Walid Jomaa, Victor Songmene, and Philippe Bocher

Article submitted, International Journal of Material Forming, 21st January, 2015

Abstract: This study attempts to provide a new methodology for identifying the coefficients of the Marusich's constitutive equation (MCE) which demonstrated a good capability for the simulation of the material behaviour in high speed machining. The proposed approach, which is based on an analytical inverse method together with dynamic tests, was applied to aluminums AA6061-T6 and AA7075-T651, and induction hardened AISI 4340 steel (60HRC). The response surface methodology (RSM) was also used in this approach. Two sets of material coefficients, for each tested work material, were determined using two different temperature models (Oxley and Loewen-Shaw). The obtained constitutive equations were validated using dynamic tests and finite element (FE) simulation of high speed machining. A sensitivity analysis revealed that the selected temperature model used in the analytical inverse method affects significantly the identified material constants and thereafter predicted dynamic response and machining modeling. In general, material constants obtained using Oxley temperature model was performed better than those obtained using Loewen-Shaw model for the tested conditions and work materials.

keywords: High speed machining, Material behaviour, Marusich's constitutive equation, Analytical inverse method, Finite elements modeling

4.1 Introduction

Over the few last decades, analytical and finite element modeling (FEM) of machining processes have received increasing attention. These techniques require accurate material constitutive equations in order to simulate the actual material behaviour during the process. Umbrello et al. (2007) showed that the material constants affect, significantly, the predicted cutting forces, chip formation, temperature, and residual stress distribution in finite element modelling of machining AISI 316L stainless steel. Thus, to succeed, two critical issues should be solved: first, the selection of the adequate constitutive equations for the material in use and, second, find the suitable constants. Many techniques had been used for the identification of constitutive equations applied to the FEM of machining process. These techniques include split Hopkinson pressure bar (SHPB) test (Lesuer, Kay et LeBlanc; 2001), Taylor test (Rule, 1997), and machining tests (Özel et Zeren, 2006; Tounsi et al., 2002). The former, also known as the "analytical inverse method", is considered a reliable technique since it can provide material constants at high strain rates and temperatures representing the actual material behaviour during machining (Li et al., 2011). Material constants are then obtained using a nonlinear regression solution. The disadvantage of this technique is its circular nature where machining tests are used for obtaining the flow stress data that are used for making machining prediction (Kristyanto, Mathew et Arsecularatne, 2002). The measured cutting forces and chip thickness are used to determine, analytically, the flow stress, strain, strain rates and temperatures in the primary shear zones. Various analytical models have been used for estimating the cutting temperature in the primary shear zone, however, large discrepancies have been observed in the results. As an illustration, the difference between the predicted primary shear zone temperatures in machining AISI 1045 steel was reported as high as 600°C (Özel et Zeren, 2006). On the other hand, the sensitivity of the FE modeling to the flow stress model, obtained with different methods (SHPB, Taylor test, Inverse method, etc.) was extensively studied (Fang, 2005; Umbrello, M'Saoubi et Outeiro, 2007). However, the effect of the cutting temperature model, used in the inverse method, on the material constants is still lacking.

In most of the cases, the metal cutting simulations were performed using the well regarded Johnson-Cooke (JC) material constitutive equation. Fang (2005) showed thanks to 18 different materials that the constitutive parameters may differ significantly even for the same type of material but with slight different chemical compositions or heat treatment conditions. Actually, the JC equation cannot always accurately describe the behaviour of all existed material (Abed et Makarem, 2012; Jaspers et Dautzenberg, 2002).

Marusich's constitutive equation (MCE) has shown encouraging results for modeling and simulating machining processes (Huang et Liang, 2003b; Ren et Altintas, 2000). However, its use was very limited since only a few material data were published in the open literature (AISI4340 in (Marusich et Ortiz, 1995), AA6061-T6 and AA7075-T6 in (Zaghbani et Songmene, 2009)). Accordingly, Zaghbani and Songmene (2009) determined the constants of MCE using an inverse optimization technique based on published J-C material models for aluminums 6061-T6 and 7075-T651. Some studies were done, based on the MCE, for FE modeling of machining using the commercial software Advantage^{TM}, but, due to data confidentiality, the material constants were not public shed. Basically, MCE has not been used or tested with other FEM packages (Sartkulvanich, Altan et Soehner, 2005).

The Marusich's constitutive equation is presented in as follow (Marusich et Ortiz, 1995):

$$\left(1+\frac{\dot{\varepsilon}_p}{\dot{\varepsilon}_0}\right)=\left(\frac{\sigma}{g(\varepsilon_p)}\right)^{m_1} \quad if\ \ \dot{\varepsilon}_p < \dot{\varepsilon}_t \tag{4.1a}$$

$$\left(1+\frac{\dot{\varepsilon}_p}{\dot{\varepsilon}_0}\right)\left(1+\frac{\dot{\varepsilon}_t}{\dot{\varepsilon}_0}\right)^{\frac{m_2}{m_1}-1}=\left(\frac{\sigma}{g(\varepsilon_p)}\right)^{m_2} \quad if\ \ \dot{\varepsilon}_p > \dot{\varepsilon}_t \tag{4.1b}$$

$$g(\varepsilon_p)=[1-\alpha_{NL}(T-T_0)]\sigma_0\left(1+\frac{\varepsilon_p}{\varepsilon_0}\right)^{1/n_{NL}} \tag{4.1c}$$

where σ is the equivalent Von-Mises stress, σ_0 is the yield stress, ε_p is the equivalent plastic stress, $\dot{\varepsilon}_p$ is the equivalent plastic strain rate, n_{NL} is the strain hardening exponent, m_1 and m_2 are low and high strain rate sensitivity exponents, α_{NL} is the thermal softening coefficient, and T is the current temperature.

In this context, this study aim to identify the MCE for some materials and verify its reliability for finite elements simulation of the high speed machining using Deform 2D™ software. The coefficients of the MCE for two Aluminum alloys (AA6061-T6 and AA7075-T6) and an induction hardened steel (AISI 4340- 60 HRC) were identified using a hybrid inverse method based on both dynamic and orthogonal machining tests. The response surface methodology was implemented to improve the accuracy of the inverse method by generating large sets of machining data. In order to highlight the influence of the temperature model on the material behaviour constants, two sets of material constants were determined for each material. The analytical temperature models developed by (Oxley et Hastings, 1977) and (Loewen et Shaw, 1954) were compared. A sensitivity analysis regarding the obtained material constants was carried out using FE simulation with Deform 2D™ software.

4.2 Experimentation

4.2.1 Work materials

Two aluminum alloys (6061-T6 and 7075-T651) and a hardened steel (AISI 4340) were selected as work material to be cut in order to cover a large range of material hardness and cutting behaviour. The 6061-T6 and 7075-T651 alloys are precipitation harden aluminums, the 6061-T6 is promising candidate for fabricating thermally stable, high strength and light weight nanostructured materials (Shankar et al., 2005) while the 7075-T651 is commonly used for the aerospace industry as structural materials (Ng et al., 2006). The AISI 4340 is a low-alloy steel with a good combination of strength, ductility, and toughness along with high hardenability. The as-received AISI 4340 was a normalized and tempered at 20-23 HRC.

After the induction hardening treatment, a finer martensitic microstructure was obtained along the case depth (2mm) with a typical hardness of 58-60 HRC. These work materials (AA7075-T651, AA6061-T6, and AISI 4340) are widely used for the manufacture of aerospace and automotive structural components.

The chemical compositions of the aluminum alloys (AA6061-T6 and AA7075-T651) and the hardened AISI 4340 steel are presented in Table 4-1 and 4-2, respectively.

Table 4-1 Nominal chemical composition (wt.%) of the tested aluminum alloys

Alloy	Si	Fe	Cu	Mn	Mg	Cr,	Zn	Ti	Al
AA6061-T6	0.6	0.20	0.28	0.10	1.0	0.20	0.22	0.12	balance
AA7075-T651	0.08	0.17	1.40	0.03	2.70	0.19	6.1	0.2	

Table 4-2 Nominal chemical composition (wt.%) of the steel AISI 4043

C	Mn	Cu	P	S	Si	Ni	Cr	Mo	Fe
0.4	0.7	0.1	0.004	0.001	0.27	1.76	0.76	0.24	Balance

4.2.2 Experimental methods

A series of orthogonal machining experiments were undertaken on MAZAK NEXUS 3-axis CNC machine without coolant. The aluminum alloys (AA6 061-T6, AA7075-T651) were machined using uncoated tungsten carbide insert (ISO code-TNMA120408) [Ref. K68]. Ceramic inserts with TiN coating (ISO code-TNGA 120408-E) [Ref. KY4400] were used for machining the hardened AISI 4340 steel. Inserts were mounted on right hand tool holders with a rake angle of -5°. The tested specimens were disc-shaped, with a 70 mm external diameter, a 19 mm internal diameter, and a 4.3 mm thickness. A "Kistler®" piezoelectric dynamometer (type 9255B) was used to acquire the cutting forces (tangential force, F_c, and feed force, F_f). An optical microscope, model Olympus GX51, was used to measure the chip thickness (t_c) and the chip/tool contact length (l_c). In this study, the cutting speed (V) and feed (f) were varied with respect to a proposed design of experiments (DOE). The DOE was used to develop empirical response models for the cutting forces, chip thickness, and chip/tool

contact length. In order to improve the optimization procedure used in the identification of the coefficient of the MCE, the proposed models were used for generating an extensive amount of data, 197 Trials for the two aluminums tested and 112 trials for the hardened AISI 4340 steel. These trials represent the combinations of different cutting speed and cutting feed selected in the applicability range of the response models. These data were used for computing physical machining data (flow stress, strain, strain rate, and temperature) which will be considered as inputs for the identification procedure of material constitutive equation presented in the following paragraphs. This DOE and also the identification procedure are detailed in the following sections.

4.2.3 Design of experiment (DOE)

One of the objectives of this work is to generate extensive experimental machining data (cutting forces, chip thickness and chip/tool contact length) that can be used to accurately identifying the material constants of the constitutive equation. For the purpose of minimizing the experimental work, a simple response surface methodology (RSM) with the central composite design (CCD) was used. A detailed description of this method is presented elsewhere (Montgomery, 2006). In this DOE, the cutting speed (V) and feed (f) were varied over five levels as shown in Table 4-3. According to the CCD, which is a second-order rotatable design with 2 independent variables, 10 experiments can be conducted with the combination of cutting feed and cutting speed (see details in Table 4-4). The width of cut (4.3 mm) and the rake angle (-5 deg.) were kept constant for all experiments. To have an assessment of pure error and model fitting error, the experimental Test#9 was duplicated (Test#10) (Montgomery, 2006). It should be noticed here that two additional tests (Tests#11 and 12 shown later in the Chapter) were carried out in order to validate the proposed models but they are not used for the determination of the MCE constants. The experimental results relative to 10 runs and corresponding with Table 4-4 are shown in Tables 4-5, 4-6, and 4-7 for AA6061-T6, AA7075-T651, and AISI4340, respectively. These results will be used in the next section to build the empirical models for cutting forces, chip thickness, and chip/tool contact length.

Table 4-3 Machining parameters and their levels

Levels	Aluminum alloys (AA6061-T6, AA7075-T6)		Hardened steel AISI 4340 (60 HRC)	
	f [mm/rev]	V [m/min]	f [mm/rev]	V [m/min]
-2	0.01	156	0.01	54
-1	0.08	300	0.03	75
0	0.15	650	0.08	128
+1	0.25	1000	0.13	180
+2	0.29	1144	0.15	202

Table 4-4 Experimental CCD matrix

Test	Aluminums (AA6061-T6, AA7075-T6)		Hardened steel AISI 4340	
	f [mm/rev]	V [m/min]	f [mm/rev]	V [m/min]
1	0.05	300	0.03	75
2	0.25	300	0.13	75
3	0.05	1000	0.03	180
4	0.25	1000	0.13	180
5	0.15	1144	0.08	202
6	0.15	156	0.08	54
7	0.01	650	0.01	128
8	0.29	650	0.15	128
9	0.15	650	0.08	128
10	0.15	650	0.08	128
11	0.03	650	0.03	128
12	0.05	650	0.05	128

Table 4-5 Experimental machining data for the AA6061-T6

Test	F_c [N]	F_f [N]	t_c [mm]	l_c [mm]
1	317	320	0.352	0.667
2	850	536	0.622	0.835
3	210	147	0.146	0.237
4	749	262	0.467	0.659
5	493	260	0.170	0.320
6	707	605	0.700	0.835
7	100	95	0.090	0.22
8	883	310	0.558	0.624
9	507	256	0.330	0.418
10	512	201	0.362	0.418

Table 4-6 Experimental machining data for the AA7075-T6

Test	F_c [N]	F_f[N]	t_c [mm]	l_c [mm]
1	271	168	0.130	0.428
2	901	323	0.217	0.426
3	234	108	0.105	0.113
4	707	171	0.196	0.312
5	514	148	0.180	0.218
6	680	362	0.334	0.409
7	77	66	0.035	0.061
8	829	233	0.188	0.343
9	556	189	0.254	0.249
10	558	153	0.241	0.237

Table 4-7 Experimental machining data for the AISI 4340

Test	F_c [N]	F_f[N]	t_c [mm]	l_c [mm]
1	582	551	0.025	0.113
2	1530	736	0.179	0.188
3	500	307	0.044	0.055
4	1271	709	0.138	0.220
5	919	543	0.110	0.118
6	1079	591	0.109	0.121
7	235	280	0.020	0.030
8	1478	779	0.166	0.189
9	981	498	0.106	0.117
10	1014	341	0.100	0.117

4.3 Response surface modeling (RSM)

According to the RSM proposed by Montgomery (2006), the machining responses for cutting forces, chip thickness, and chip tool contact length can be expressed as mathematical models. Usually when the response function is not known or non-linear, a second-order model is utilized. For the CCD with 2 factors (speed and feed), the general mathematical model has the following form (Montgomery, 2006):

$$y = b_0 + b_1 f + b_2 V + b_{11} f^2 + b_{12} fV + b_{22} V^2 \tag{4.2}$$

where y is the desired response and b_0, b_1,…, b_{22} are the regression coefficients to be determined for each response. f is the feed in mm/rev and V is the cutting speed.

In the present work, the second-order mathematical models are derived from the RSM and have been fitted, through Statgraphics software, to predict the main cutting force (F_c), the feed force (F_t), the chip thickness (t_c), and the chip/tool contact length (L_c):

For the aluminum AA6061-T6:

$$F_c = 336.9 + 3097.78f - 0.632511V - 1293.37f^2 + 0.0428571fV + 0.000341203V^2 \quad (4.3)$$

$$F_t = 577.013 + 1675.83f - 1.30897V - 1363.06f^2 - 0.721429fV + 0.000833055V^2 \quad (4.4)$$

$$t_c = 0.557541 + 1.53682f - 0.000972424V - 0.667063f^2 + 0.000364286fV + 4.00699\text{E}-7V^2 \quad (4.5)$$

$$L_c = 1.13598 - 0.286895f - 0.00207628V + 1.889f^2 + 0.00181429fV + 0.00000107568V^2 \quad (4.6)$$

For the aluminum AA7075-T651:

$$F_c = 103.351 + 5017.34f - 0.223933V - 5204.85f^2 - 1.13049fV + 0.000174558V^2 \quad (4.7)$$

$$F_t = 247.273 + 1404.29f - 0.506735V - 1360.49f^2 - 0.654682fV + 0.000324271V^2 \quad (4.8)$$

$$t_c = 0.0663864 + 2.723f - 0.0000906349V - 7.47843f^2 + 0.0000244286fV - 0.0000000542156V^2 \quad (4.9)$$

$$l_c = 0.599276 - 0.0502875f - 0.00100939V - 0.452349f^2 + 0.00143571fV + 0.000000418495V^2 \quad (4.10)$$

For the hardened steel AISI 4340:

$$F_c = 217.258 + 14745.0f - 1.14152V - 24122.0f^2 - 16.8309fV + 0.00443325V^2 \quad (4.11)$$

$$F_t = 1116.5 - 3433.65f - 9.99413V + 25205.7f^2 + 20.7222fV + 0.029457V^2 \quad (4.12)$$

$$t_c = -0.044343 + 2.27902f + 0.000213443V - 2.52739f^2 - 0.00573173fV + 0.000000767594V^2 \quad (4.13)$$

$$l_c = 0.182702 - 0.187779f - 0.00157438V + 1.58997f^2 + 0.00861311fV + 0.00000317537V^2 \quad (4.14)$$

The analysis of variance (ANOVA) was used to check the CCD model adequacy of the experimental design based response surface. These models were tested by the variance analyses (*P-test*) as shown in Tables 4-8, 4-9, and 4-10. It was found that the developed models are significant at 95% confidence interval as the *P-values* of all models were lower than 0.05. Table 4-11 presents coefficients of determination (R^2 and R^2_{adj}) values of the proposed models, which indicate a good correlation between the predicted and experimental machining data.

Confirmation tests were carried out to verify the mathematical models for the three tested materials. Corresponding set values (Table 4-4) and results are listed in Table 4-12. As it can be seen from this table, there is a good agreement between results obtained from models and experiments.

Table 4-8Analysis of variance for the aluminum AA6061-T6

Machining response	Sum of squares		Degrees of freedom		Mean square		*P-value*
	Regression	*residual*	*Regression*	*residual*	*Regression*	*residual*	
F_c	639298.	1813.3	5	4	127860.	453.326	0.0000
F_t	227624.	1805.4	5	4	45524.8	451.349	0.0003
t_c	0.36595	0.02082	5	4	0.07319	0.005205	0.0120
l_c	0.43271	0.00883	5	4	0.08654	0.00220	0.0017

Table 4-9 Analysis of variance for the aluminum AA7075-T6

Machining response	Sum of squares		Degrees of freedom		Mean square		*P-value*
	Regression	*residual*	*Regression*	*residual*	*Regression*	*residual*	
F_c	642189.0	141.092	5	4	128438.	35.273	0.0000
F_t	73068.6	1899.21	5	4	14613.7	474.804	0.0027
t_c	0.0644	0.00814	5	4	0.01289	0.002036	0.0490
l_c	0.13125	0.01610	5	4	0.02625	0.004026	0.0467

Table 4-10 Analysis of variance for the hardened steel AISI 4340 (60 HRC)

Machining response	Sum of squares		Degrees of freedom		Mean square		*P-value*
	Regression	*residual*	*Regression*	*residual*	*Regression*	*residual*	
F_c	1.58291E6	6335.78	5	4	316581.	1583.95	0.0001
F_t	269338.	20322.8	5	4	53867.5	5080.7	0.0200
t_c	0.0271024	0.00031	5	4	0.00542	0.000078	0.0006
l_c	0.0294763	0.00179	5	4	0.00589	0.000447	0.0135

Table 4-11 Coefficients of determination of the machining responses

Machining response	AA6061-T6		AA7075-T651		AISI 4340 (60HRC)	
	R^2	R^2_{adj}	R^2	R^2_{adj}	R^2	R^2_{adj}
F_c	99.7172	99.3636	99.978	99.9506	99.6013	99.103
F_t	99.2131	98.2295	97.4666	94.2999	92.9839	84.2138
t_c	94.6161	87.8862	88.7798	74.7546	98.8486	97.4094
l_c	97.9992	95.4982	89.07	75.4076	94.271	87.1098

Table 4-12 Results for the confirmation experiments

Material	Test	Fc [N]		F_f [N]		t_c [mm]		l_c [mm]	
		Exp.	*Pred.*	*Exp.*	*Pred.*	*Exp.*	*Pred.*	*Exp.*	*Pred.*
AA6061-T6	11	165	164	113	114	0.159	0.148	0.220	0.270
	12	221	218	131	133	0.180	0.179	0.280	0.288
AA7075-T651	11	177	157	95	83	0.111	0.082	0.113	0.146
	12	251	226	107	99	0.108	0.120	0.177	0.161
AISI 4340	11	557	505	335	319	0.061	0.040	0.067	0.063
	12	749	695	389	341	0.072	0.064	0.081	0.081

4.4 Identification of Marusich's constitutive equation (MCE)

The proposed method is a hybrid inverse approach which is based on the determination of the material constants in two steps. Figure 4-1 shows the flowchart of the identification procedures (2 steps).

The first step includes the determination of the material constants for low strain rate behaviour ($\dot{\varepsilon}_p < \dot{\varepsilon}_t$) (Equation 5.1(a)) at the reference temperature (T_0). The transition strain rate ($\dot{\varepsilon}_t$) was determined to be 10^4 sec^{-1} based on previous works on the strain rate sensitivity of the aluminum AA6061-T6 (Hoge, 1966; Manes et al., 2011), the aluminum AA7075-T6 (Lee et al., 2000; Rule et Jones, 1998), and the steel AISI 4340 (Lee et Lam, 1994). The Marusich's equation (Equation 4.1 (a)), at the reference temperature (T_0), becomes:

$$\sigma = \sigma_0 \left(1 + \frac{\varepsilon_p}{\varepsilon_0}\right)^{1/n_{NL}} \left(1 + \frac{\dot{\varepsilon}_p}{\dot{\varepsilon}_0}\right)^{1/m_1} \tag{4.15}$$

The reference strain ε_0 and strain rate $\dot{\varepsilon}_0$ were selected from the data ranges used in the identification procedure. The constants σ_0, n_{NL}, and m_1 can be identified thanks to least-squares method, from experimental results. Three different characterization techniques were used: dynamic tensile tests taken from (Zhu et al., 2011) for the aluminum AA6061-T6, radial collapse of thick-walled cylinder from (Yang, Zeng et Gao, 2008) for the aluminum

AA7075-T6, and compression spl it-Hopkinson bar technique (SHBT) from (Lee et Lam, 1996) for the steel AISI 4340.

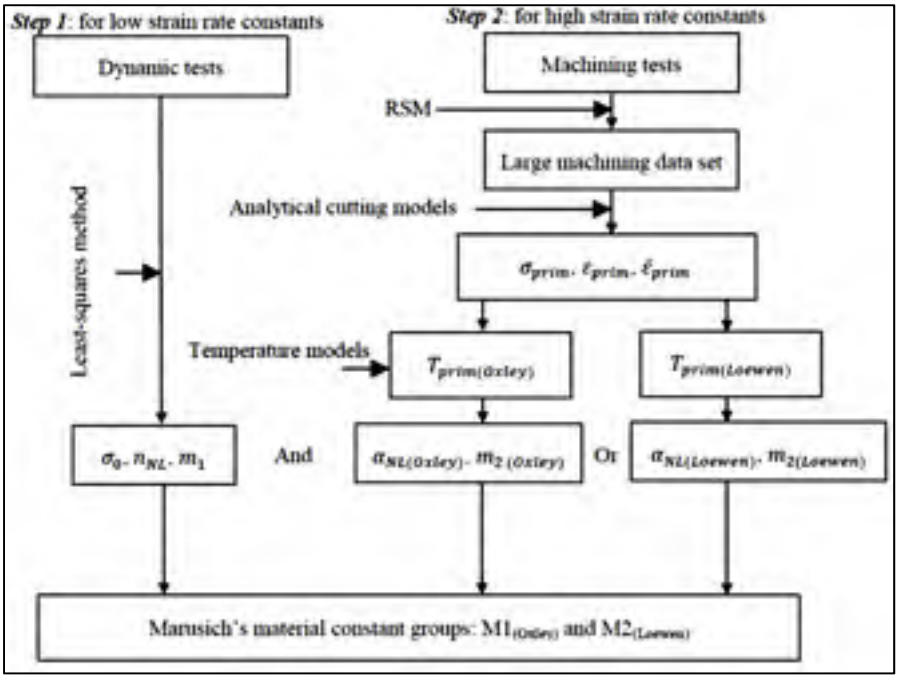

Figure 4-1 Flow chart of the identification procedure

In the second step, the remaining material constants (m_2, α_{NL}) (see Equation 4.1 (b)) will be determined using orthogonal machining tests (inverse method). The machining data including the strain (ε_{prim}), the strain rate $(\dot{\varepsilon}_{prim})$, the flow stress (σ_{prim}), and the average temperature (T_{prim}) on the primary shear zone, were generated from the machining tests. These data can be evaluated by the following relationships:

$$\varepsilon_{prim} = \frac{\cos\alpha}{2\sqrt{3}\sin\emptyset\cos(\emptyset-\alpha)} \tag{4.16}$$

$$\dot{\varepsilon}_{prim} = \frac{V\cos\alpha}{\sqrt{3}\cos(\emptyset-\alpha)\Delta Y_{prim}} \tag{4.17}$$

$$\sigma_{prim} = \sqrt{3}\frac{(F_c\cos\emptyset - F_t\sin\emptyset)\sin\emptyset}{\mathrm{w}f} \tag{4.18}$$

where $\emptyset$ is the shear angle and ΔY_{prim} is the thickness of the primary shear zone. In the present work, we have adopted the ΔY_{prim} developed by (Huang et Aifantis, 1997) to take into account the shear localization phenomenon which is observed in segmented chip formation during high speed machining:

$$\Delta Y_{prim} = \chi\frac{mf}{\beta(f,V)}\frac{\sin\emptyset}{\cos\alpha} \tag{4.19}$$

Here, χ is the Taylor-Quinney coefficient (equal to 1 in this work), m is a material strain rate sensitivity coefficient and $\beta(f,V)$ is the flow localization parameter as determined by the following relationship (Xie, Bayoumi et Zbib, 1995):

$$\beta(f,V) = -\frac{1}{m}\left[\frac{n}{\varepsilon_{prim}} + \frac{0.9a_w}{\rho_w C_w\left(1+1.328\sqrt{\frac{D_w\varepsilon_{prim}}{Vf}}\right)}\left(n+1-\frac{0.664\sqrt{\frac{D_w\varepsilon_{prim}}{Vf}}}{1+1.328\sqrt{\frac{D_w\varepsilon_{prim}}{Vf}}}\right)\right] \tag{4.20}$$

Material data such as the mass density ρ_w, the thermal conductivity K_w, the specific heat C_w, the strain-hardening coefficient n, and the thermal softening coefficient a_w, which can be determined from the stress-strain curves at different temperatures (Xie, Bayoumi et Zbib, 1995), are presented in Tables 4-13. The thermal diffusivity D_w can be calculated by using ρ_w, K_w, and C_w as:

$$D_w = \frac{K_w}{\rho_w C_w} \tag{4.21}$$

Table 4-13 Physical properties of the work materials

Property	AA6061-T6	AA7075-T651	AISI 43040
Density ρ_w (kg/m3)	2700	2810	7800
Thermal conductivity K_w (W/m°C)	167	130	43
Specific heat C_w (J/Kg °C)	896	960	600
Strain-hardening coefficient n	0.42	0.71	0.37
Thermal softening coefficient a_w (MPa/°C)	-0.675	-0.762	-0.001
Melting temperature (°C)	652	635	1520

Two machining temperature models were tested leading to two sets of material constants, referred to as models M1 and M2 for each tested work material. Models M1 and M2 were obtained based on the average temperature on the primary shear zone, T_{prim}, calculated using Oxley (1977) and Loewen and Shaw (Loewen et Shaw, 1954) models, respectively.

In Oxley model (Hastings, Mathew et Oxley, 1980), the average shear plane temperature T_{prim} is linked to the shear stress k_{AB} in the primary shear zone and can be determined from the following relationship:

$$T_{prim} = T_0 + \eta \left[\frac{1-\beta}{\rho_w C_w} \frac{k_{AB}\cos\alpha}{\sin\emptyset\cos(\emptyset-\alpha)}\right] \tag{4.22}$$

where η is a constant representing the amount of plastic work converted to heat (equal to 0.9 in this study) and β is the fraction of energy that enters into the workpiece (estimated to be 0.7).

In Loewen and Shaw model (1954), the T_{prim} was obtained using the moving heat source theory and is defined as:

$$T_{prim} = 0.754 \frac{(1-R_1) q_{shear} f\ csc(\emptyset)}{2 D_w \sqrt{L_1}} \tag{4.23}$$

where R_1 is the fraction of the heat dissipated into the chip and defined as (Loewen et Shaw, 1954):

$$R_1 = 0.754 \frac{1}{1 + 1.328\sqrt{\frac{D_w \gamma_{prim}}{Vf}}} \tag{4.24}$$

and q_{shear} is the heat intensity generated on the primary shear zone and defined as:.

$$q_{shear} = \frac{(F_c \cos \emptyset - F_t \sin \emptyset) V \cos\alpha}{\mathrm{w} t_c r \cos(\emptyset - \alpha) \csc \emptyset} \tag{4.25}$$

and L_1 the velocity-diffusivity factor relative to the primary shear zone.

$$L_1 = \frac{Vf\gamma_{prim}}{4D_w} \tag{4.26}$$

where r is the chip thickness ratio.

The remaining material constants m_2 and α_{NL} (see Equation 4.1b) can be determined by fitting the machining data using a least-squares approximation technique for the N runs:

$$(m_2, \alpha_{NL}) = \min\left(\sum_{i=1}^{N} \sqrt{\left[\sigma_{Exp}(i) - \sigma_{Model}(i)\right]^2}\right) \tag{4.27}$$

The material constants obtained in the step 1 and 2 are presented in Table 4-14 and 4-15, respectively. The calculated coefficient of determination R^2 showed a good fitting between experimental and optimized data. The aluminum AA6061-T6 has lower strain coefficient n_{NL} and comparable strain rate coefficient m_1 compared to AA7075-T651 alloy as shown in Table 4-15. The hardened AISI 4340 steel showed high strain rate coefficient compared to both tested aluminum alloys.

On the other hand, the material constants, obtained in step 2 using machining tests (Table 4-15), showed that the aluminum AA6061-T6 experienced high thermal softening coefficient α_{NL} and low strain rate coefficient m_2 compared to the AA7075-T651 alloys whatever the cutting temperature model used. The hardened AISI 4340 steel showed low thermal softening coefficient and high strain rate coefficient compared to the tested aluminum alloys.

The temperature models used in step 2 to determine the material constants inversely from the machining tests were found to significantly influence the material coefficients (Table 4-15). In fact, the thermal softening coefficients α_{NL}, obtained using Oxley model (Models M1), are higher than those obtained using the Loewen and Shaw model (Model M2) for all tested materials. The inverse is true for the strain rate coefficients m_2. It is worth noticing that cutting temperatures estimated using Oxley model were lower than those calculated using Loewen and Show model (Table 4-16). The thermal softening and the strain rate coefficients are the only parameters that varies between M1 and M2 material models. The only difference between the constitutive equations used for the material models validation was the thermal softening coefficient n_{NL} which was determined using machining tests. For the same flow stress levels, calculated using Equation 4.20, the cutting temperature on the primary shear zone calculated using Oxley's model (Equation 4.24) is higher than that calculated from Loewen and Shaw model (Equation 4.25) (Table 4-15) resulting in a lower thermal softening coefficient for M1material models compared to M2. Although the aluminums AA6061-T6 and AA7075-T651 were machined under the same cutting conditions, higher thermal softening coefficients were obtained in the case of the AA6061-T6 compared to AA7075-T651 for both M1 and M2 material models (see Table 4-15). This can be explained by the low thermal conductivity of the aluminum AA7075-T651 and high hardness compared to the AA6061-T6 (Table 4-16).

Table 4-14 Material constants, obtained in step 1, using dynamic tests

Material	$\sigma_0\ [MPa]$	m_1	n_{NL}	ε_0	$\dot{\varepsilon}_0\ [s^{-1}]$	R^2
6061-T6	278.46	4.34	3.32	0.1	200	0.97
7075-T651	529.02	2.63	11.23	0.025	2400	0.99
AISI 4340	874	23.23	3.40	0.1	1	0.98

Table 4-15 Material constants, obtained in step 2, using machining tests

Material	Model	m_2	α_{NL}	R^2
6061-T6	M1	150.72	0.00227	0.96
	M2	14.51	0.00359	0.98
7075-T651	M1	168.92	0.00174	0.95
	M2	72.05	0.00228	0.93
AISI 4340	M1	193.17	0.00075	0.95
	M2	150.02	0.00147	0.97

Table 4-16 Calculated temperature ranges used in the inverse method

Material	Model	Cutting temperature $[°C]$
6061-T6	M1	$102 \leq T \leq 362$
	M2	$85 \leq T \leq 216$
7075-T651	M1	$171 \leq T \leq 313$
	M2	$150 \leq T \leq 240$
AISI 4340	M1	$227 \leq T \leq 506$
	M2	$207 \leq T \leq 395$

4.5 Validation of M1 and M2 models using dynamic tests

In this section, the M1 and M2 material models will be verified using dynamic tests. This validation is motivated by the fact that a good accuracy can be obtained when measuring strain, strain rate, and temperature during dynamic tests. This validation was performed over a wide range of temperatures and strain rates from the literature. Experimental data from split Hopkinson pressure bar (SHPB) tests applied to 6061-T6 (Lee, Choi et Kim, 2011) and AISI 4340 steel (Lee et Yeh, 1997), and from radial collapse of thick-walled cylinder of 7075-T6 (Yang, Zeng et Gao, 2008) were used in this comparison.

Figures 4-2 to 4-4 present comparisons between predicted and experimental flow stresses for the AA6061-T6, AA7075-T651, and AISI 4340, respectively. Overall, the stress-strain curves at ambient temperature show a good accuracy between predictions and experiments for all tested materials and models. However, some discrepancies have been observed for

stress-strain curves obtained at elevated temperatures. The levels of these discrepancies were found to be depending on the tested material and material model. For the AA606-T6 alloy, the both material models (M1 and M2) underestimate the flow stress at elevated temperatures (Figure 4-2). For the AA7075-T651 alloy, the flow stress is accurately predicted, particularly, when M2 model was used (Figure 4-3b). For the hardened AISI 4340 steel, the M1 model performed better (Figure 4-4a) while a large discrepancy was obtained when M2 model was used to predict the flow stress at elevated temperatures (Figure 4-4b).

As shown in Figures 4-2 to 4-4, the flow stress is very sensitive to the increase of the temperature for all tested material. Overall, the M1material models predicted higher flow stresses at elevated temperature compared to those predicted using M2 Models. To explain these trends, it is worth recalling how the material constants involved in this validation were obtained for these material models. Since the dynamic tests used for the validation didn't exceed the critical strain rate $\dot{\varepsilon}_t$ (10^4 s^{-1}), only the constants n_{NL}, m_1, and α_{NL} are used in the constitutive equation. The constants n_{NL} and m_1 are the same for both models M1 and M2 (low strain rate range) as shown in Table 4-14. This result highlights the significant effect of the selected temperature model on the thermal softening coefficient and thereafter the predicted dynamic flow stress.

Since the thermal softening coefficients were determined using machining data, the cutting mechanisms have to be considered in understanding the results and trends explained above. The aluminum AA7075-T651 and also the hardened AISI 4340 steel exhibit a high tendency to shear localization during machining resulting in segmented chips while continuous chips were produced in the case of AA6061-T6. Shear localization together with low thermal conductivity of the aluminum AA7075-T651 and hardened AISI4340 steel make the prediction of temperature on the primary shear zone more accurate due to reduced heat lost on both the chip and workpiece during machining. This phenomenon can explain the good accuracy of the predicted flow stresses in the case of the AA7075-T651 and AISI4340.

In order to understand the effect of the material constants on the predicted machining data (cutting forces, temperature, chip thickness, etc.), the M1 and M2 material models will be verified using a finite element modeling of high speed machining.

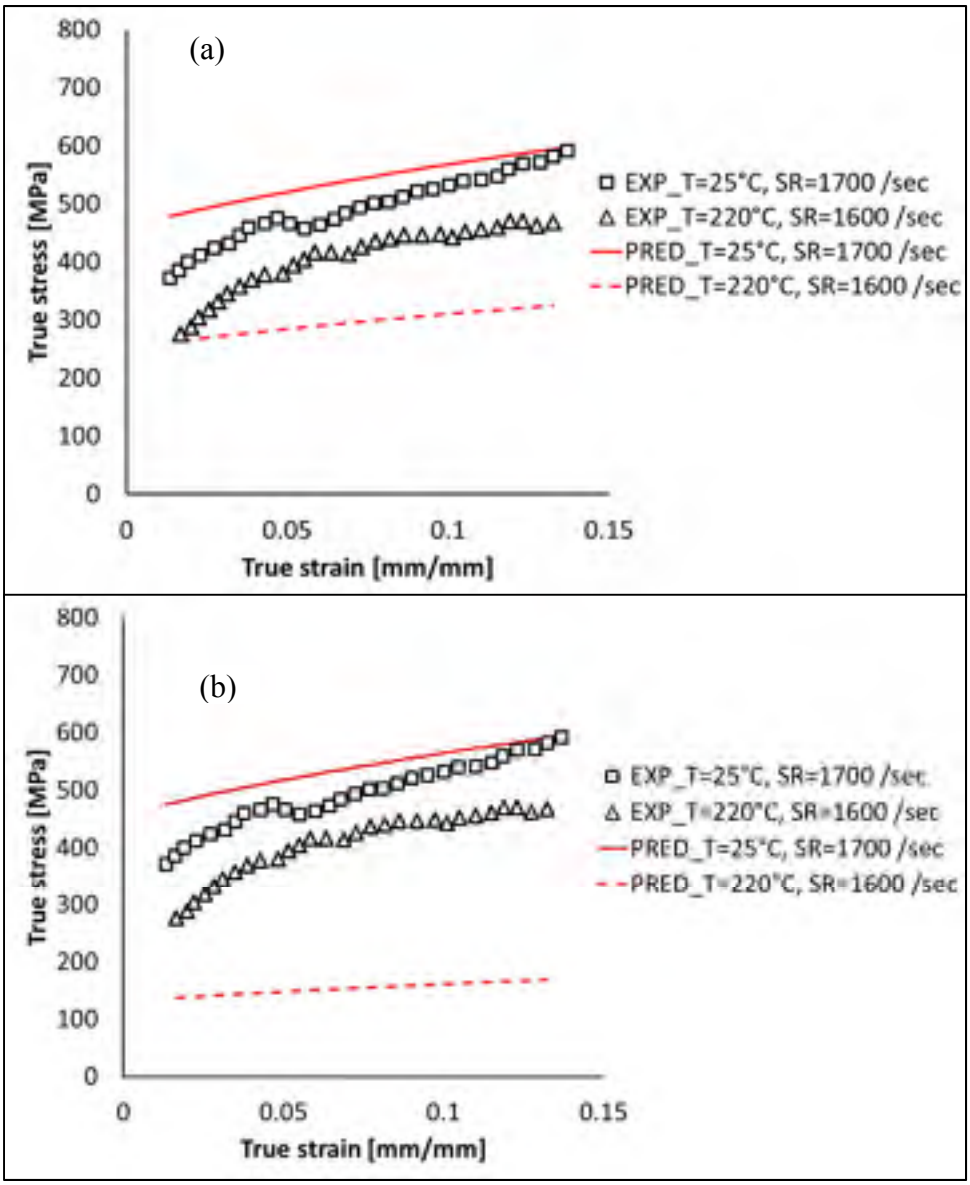

Figure 4-2 Comparison between predicted flow stress with a) model M1 and b) model M2 and experimental data for AA6061-T6 aluminum from (Lee, Choi et Kim, 2011)

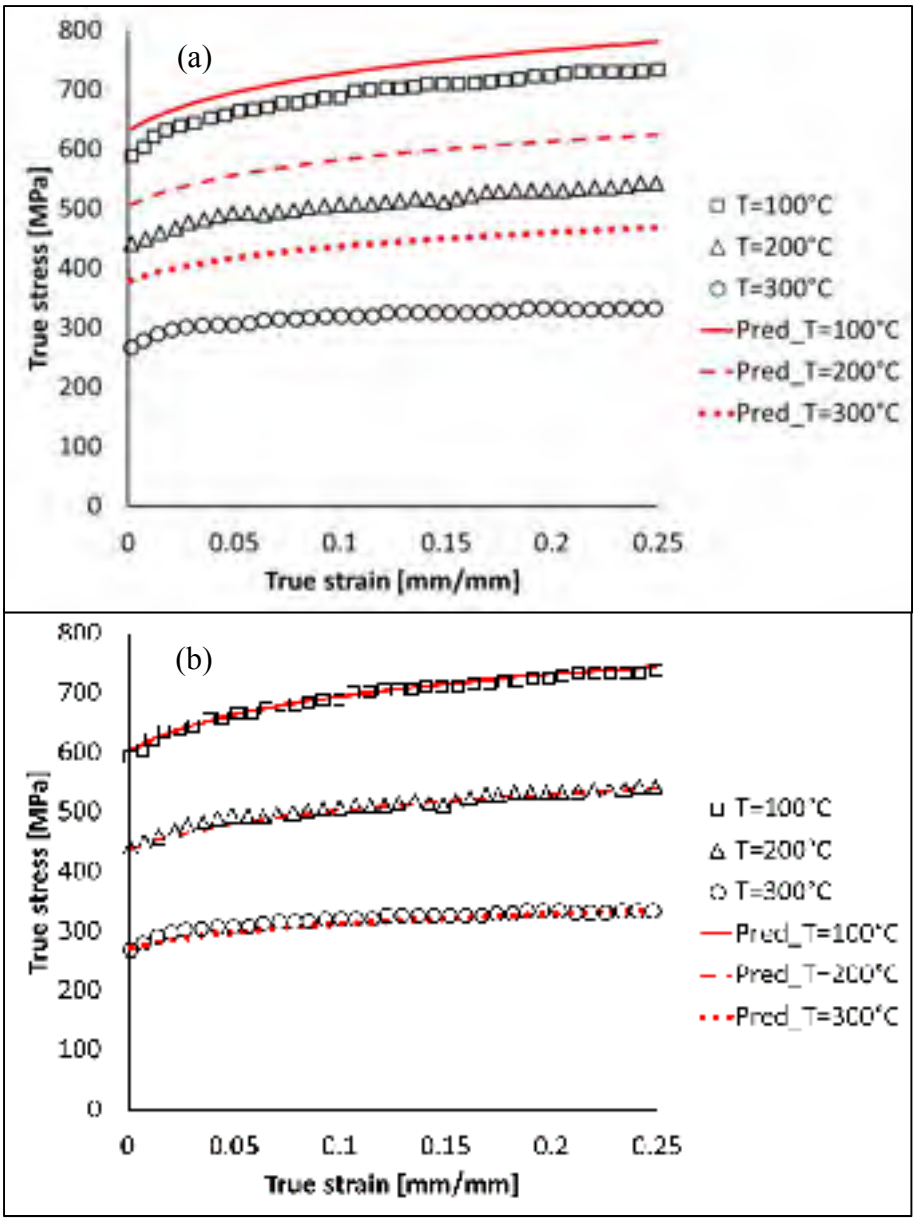

Figure 4-3 Comparison between predicted flow stress with a) model M1 and b) model M2 and experimental data for AA7075-T6 aluminum from (Li et Hou, 2013), strain rate=3100 s^{-1}

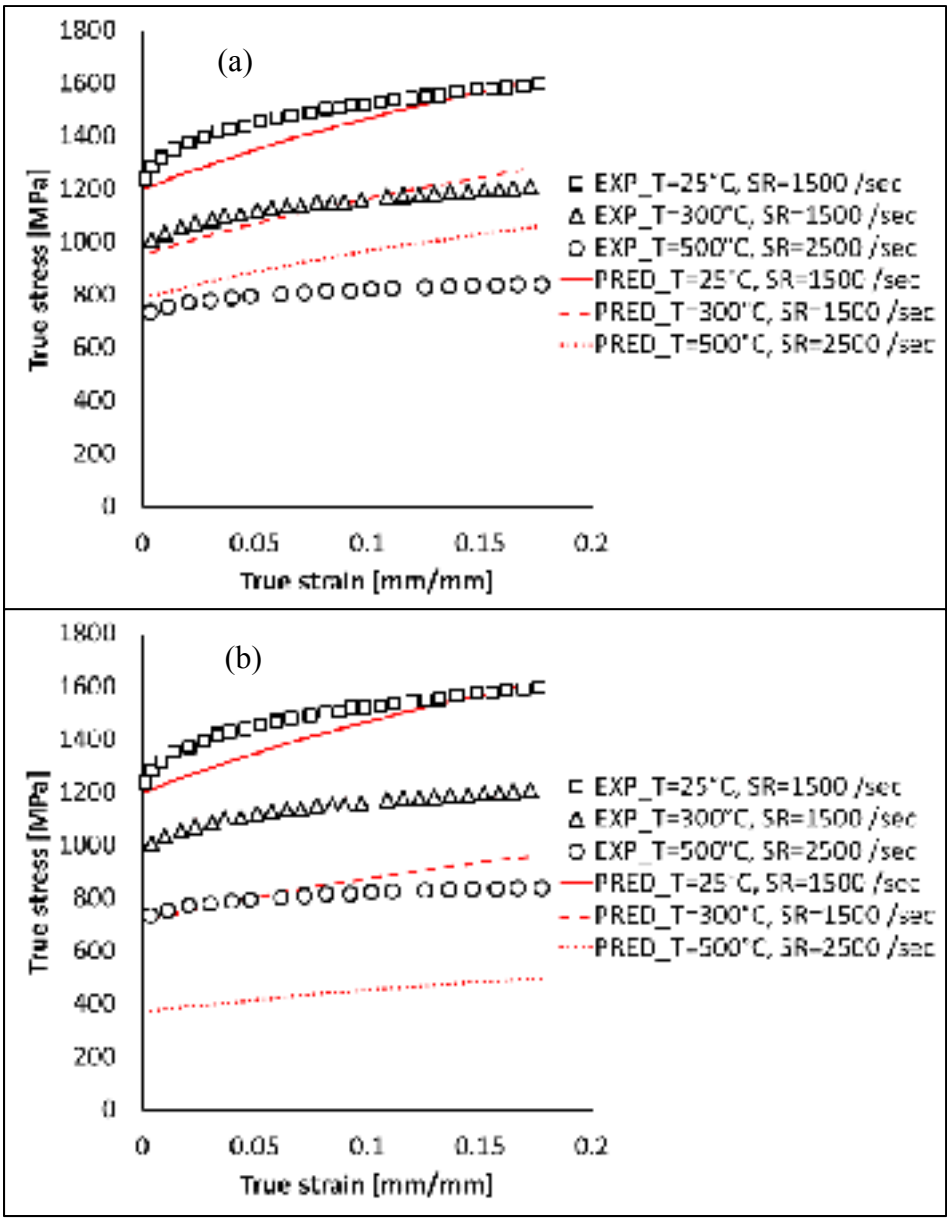

Figure 4-4 Comparison between predicted flow stress with a) model M1 and b) model M2 and experimental data for hardened AISI 4340 steel from (Lee et Yeh, 1997)

4.6 Finite element modeling

In this section, a sensitivity analysis of finite element models to M1 and M2 material models was developed. Finite element simulations of orthogonal machining were performed to verify the capability of the proposed flow stress models to predict the material behaviour high speed machining. The commercial FE software DEFORM-2D^{TM} version 10 was used for the simulation of the orthogonal cutting. A plan-strain coupled thermo-mechanical analysis was carried out. Work materials were modeled as elasto-plastic and cutting tool as a rigid. Since the MCE is not implemented in DEFORM-2D^{TM}, the flow stress data were represented by several tabulated data which depends on strain, strain rate and temperature. Workpiece and cutting tool were meshed with about 6000 and 1500 isoparametric quadrilateral elements, respectively. The friction on the chip/tool interface was modeled using a constant shear model with a constant frictional shear factor (m). A shear factor of 0.8 without any damage was selected for the aluminum AA6061-T6 since continuous chips were generated during machining even at the highest cutting speed (Test #5). On the other hand, Cockroft and Latham's criterion was employed to predict the effect of stresses on the chip segmentation during orthogonal cutting of the aluminum AA7075-T651 and the hardened AISI 4340 steel. In the present study, shear factors (m) and damage coefficients (D) were set to 1 and 35 MPa, and 0.8 and 50 MPa for aluminum AA7075-T651 and hardened AISI 4340 steel, respectively. The coefficient of heat transfer at the chip/tool interface was set to 10000 kW/m^{2}K for all work materials tested. The physical properties of the work materials and cutting tools were presented in Table 4-13 and 4-17, respectively.

Table 4-17 Properties of cutting tool materials

Property	WC-Co carbide (K68) (Yen et al., 2004)	Coated ceramic (KY4400) (Brito et al., 2009; El-Wardany, Mohammed et Elbestawi, 1996)	
		Mixed ceramic (Al2O3–TiC)	TiN coating
Density ρ_t (kg/m3)	11900	4260	4650
Thermal conductivity K_t (W/m°C)	86	24	21
Specific heat C_t (J/Kg °C)	334.01	700	645

4.6.1 Numerical validation and sensitivity analysis

The capability of the material models to predict machining parameters was performed based on the comparison between experimental data and FE predictions. Measured machining forces, chip morphology, and chip/tool contact length were used in this comparison. The FE simulations of machining were carried out at high cutting speed conditions (test #5 in Table 4-4) for each work material studied. It is worth recalling here that these cutting conditions were not used in the identification of the constitutive equations.

4.6.2 Prediction of machining forces

The predicted and experimental cutting and thrust forces were shown in Figure 4-5 and 4-6, respectively. For the AA6061-T6 alloy, the cutting force was accurately predicted by the both material models (error of 13.4 % for M1 and 9 % for M2) while the thrust force was underestimated, particularly, when the M2 material model was applied (error of 62.8 %). For the AA7075-T651 alloy, the cutting force was also well predicted with errors of 9.6 % and 11.5 % for M1 and M2 material models, respectively. For this alloy, the prediction of the thrust forces was more accurate (error of 8.8 % for M1 and 23 % for M2) compared to the AA6061-T6 alloy. For the hardened AISI 4340 steel, the M1 material model performed well while the M2 material models underestimate the predicted cutting and thrust forces with error of 27.9 % and 16.1 %, respectively.

On the other hand, one can observe that the predicted cutting and thrust forces, using the M1 material models, were higher than those predicted using the M2 material model. It is worth recalling here that M2 material models have resulted to low flow stresses, compared to M1material models (see Figures 4-2 to 4-4). This trend was attributed to the high thermal softening coefficients as shown in Table 4-14. Furthermore, the thrust forces were underestimated by the both tested material models except for the AISI 4340 steel when M1 model was applied. However, the ratio of the predicted thrust forces with the measured ones remains constant for both material Models tested (M1 and M2). These results suggested that

there is a general problem with correct prediction using the FEM as argued by Klocke *et al.* (2013).

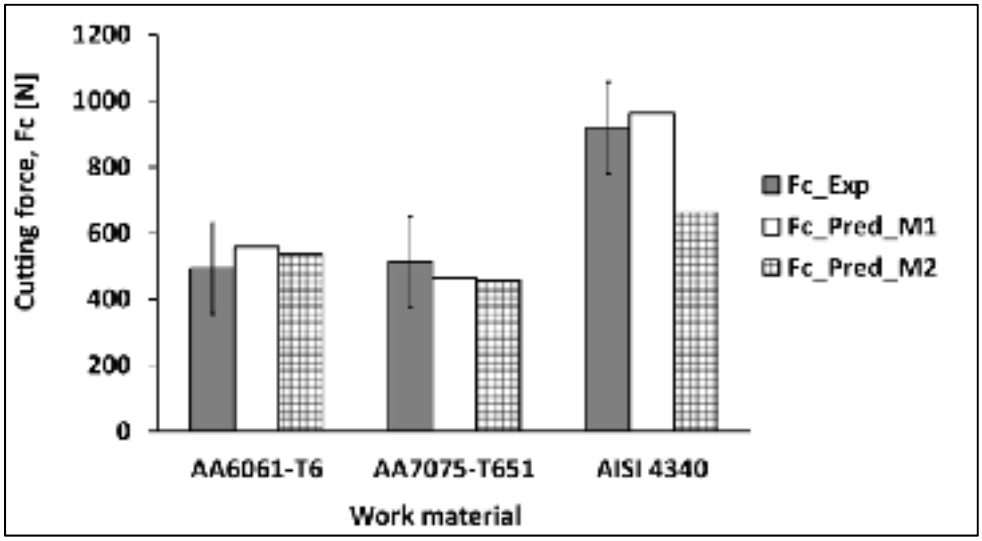

Figure 4-5 Comparison between predicted and measured cutting forces

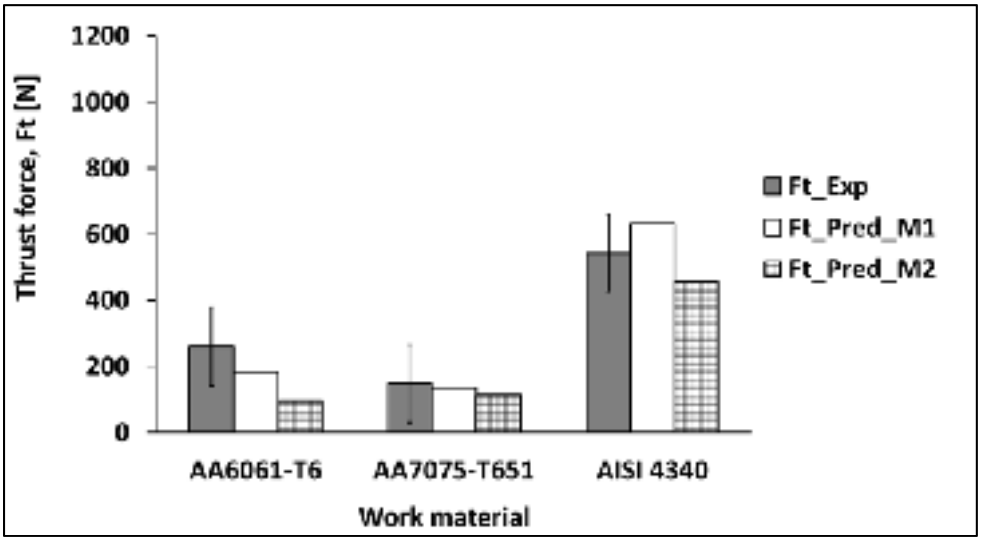

Figure 4-6 Comparison between predicted and measured thrust forces

4.6.3 Prediction of chip morphology and tool/chip contact length

One of the outputs of the FEM is the chip morphology. Figures 4-6 shows a comparison between the predicted chip geometries and experiments for the three tested materials (AA6061-T6, AA7075-T651, and AISI4340 steel). As no damage criterion was used for the AA6061-T6 alloy, a continuous chip was obtained while segmented ones can be predicted for the aluminum AA7075-T651 and the hardened AISI4340 steel. The M1 material Model gave reasonable agreement with the experimental data in terms of chip geometry. The M2 material model was not able to predict the chip segmentation in the case of the hardened AISI4340 steel (Figure 4-6c) instead of segmented one obtained in experiments. Overall, predicted chips exhibit lower chip up-curl radii compared to experimental ones regardless the material model used.

Figure 4-7 shows the comparison between predicted chip thicknesses and measured ones. The material model M2 performed better in predicting the chip thickness for the aluminum AA6061-T6 and the hardened AISI4340 steel although the material models M2 produce more realistic chip forms when compared to experimental ones.

Predicted chip/tool contact lengths were compared to the measured ones (Figure 4-8). The tested material models affected differently the predicted chip/tool contact lengths. The largest discrepancy was observed in the case of the aluminum AA6061-T6. The formation of the built-up edge and built-up layer during the machining of aluminum alloy, which were not considered in the FEM, could be the reason of the high discrepancies observed in predicting the chip thickness and the chip/tool contact length. Similar discrepancies were also reported in previous FEM studies using the software DEFORM-2D® together with the J-C constitutive equation (Bil, Kılıç et Tekkaya, 2004; Filice et al., 2007). The low chip up-curl radii of the predicted chips may be the origin of the lower predicted contact length. In addition, the experimental measurement technique (optical microscopy) may induce errors up to 50 % as suggested in (Bil, Kılıç et Tekkaya, 2004; Filice et al., 2007).

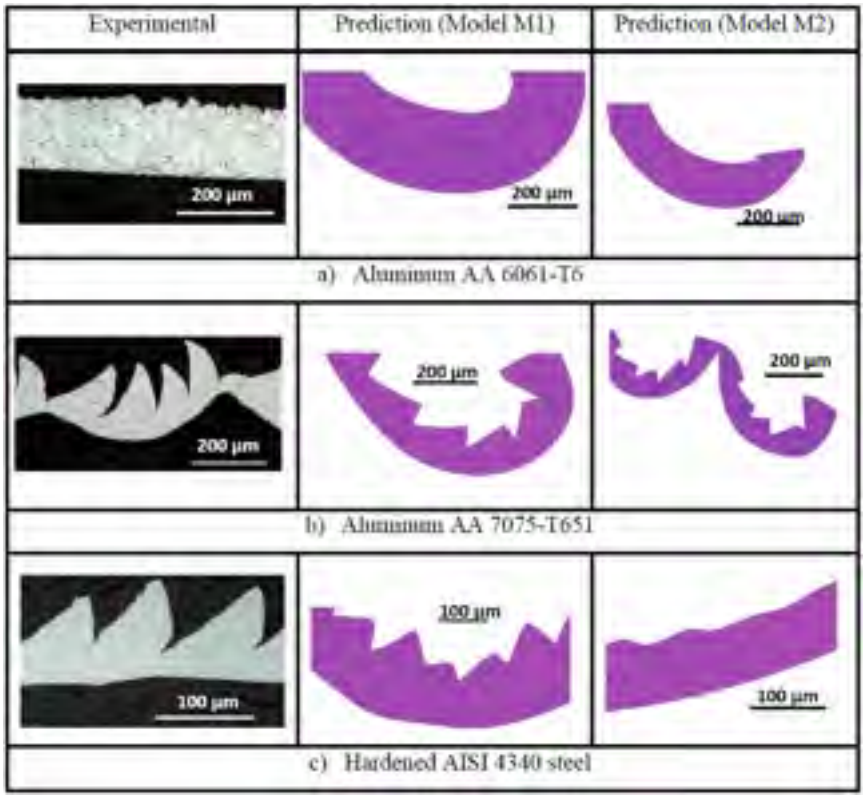

Figure 4-7 Comparison between predicted and measured chip geometry obtained using Model M1 and M2

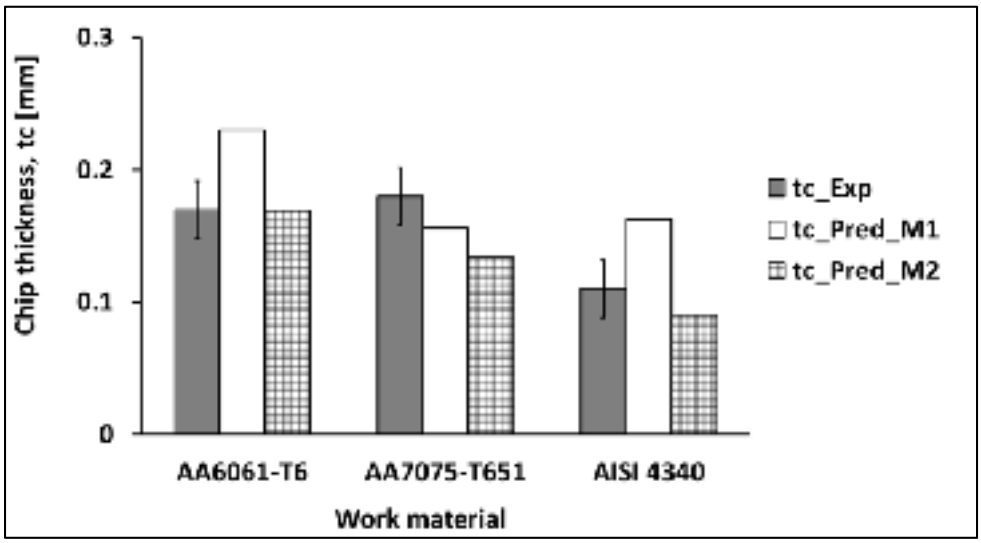

Figure 4-8 Comparison between predicted and measured chip thickness

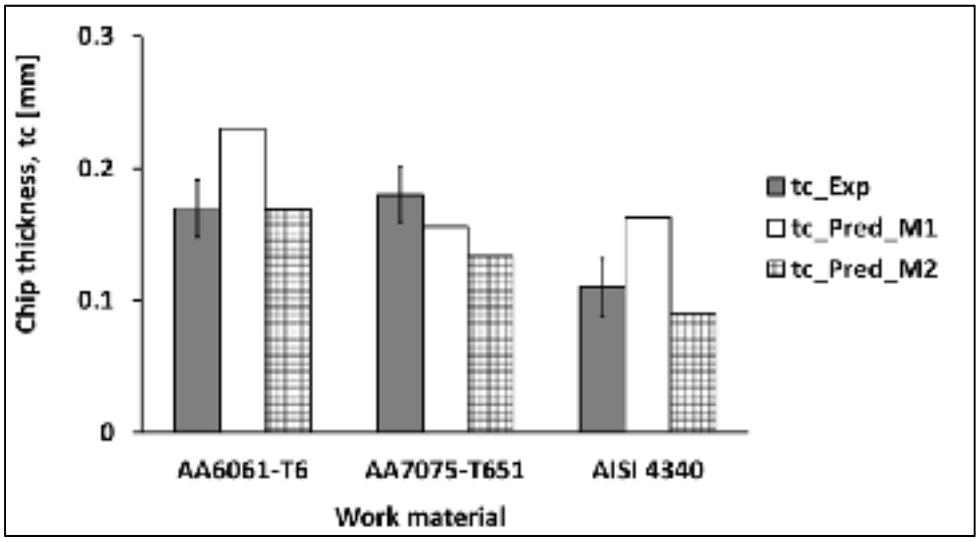

Figure 4-9 Comparison between predicted and measured chip/tool contact length

4.6.4 Prediction of cutting temperature distributions

The temperature distributions in the cutting zone for aluminums AA6061-T6, AA7075-T651, and hardened AISI4340 steel were shown in Figures 4-9 to 4-11, respectively. The maximum temperature was located at the tool/chip interface for all the material tested. The high speed machining of the aluminum AA6061-T6 leads to lower cutting temperature, for both material models, compared to the aluminum AA7075-T651. The lower thermal conductivity of the aluminum AA7075-T651 can be the reason of such trend.

Simulations performed using the material model M1 produces high cutting temperature compared the material models M2 resulting in a difference between the maximum temperatures of the chip/tool interface as high as 465 °C in the case of the hardened AISI 4340 steel (Figure 4-11). This is a very critical issue in FEM of machining, particularly, when residual stress prediction is considered.

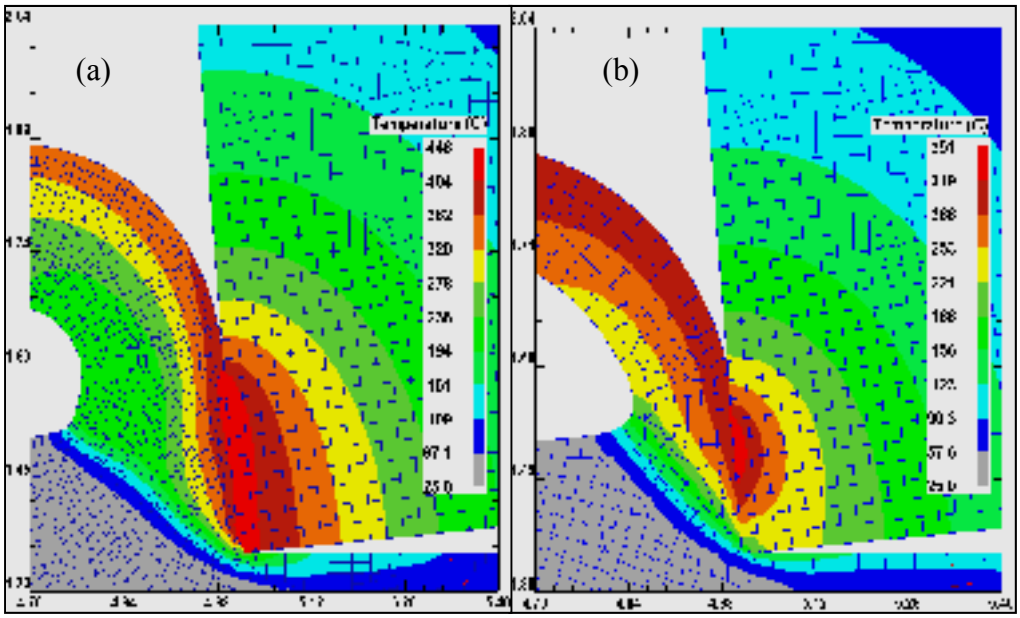

Figure 4-10 Temperature distribution obtained with a) Model 1 and b) Model M2 for the aluminum AA6061-T6

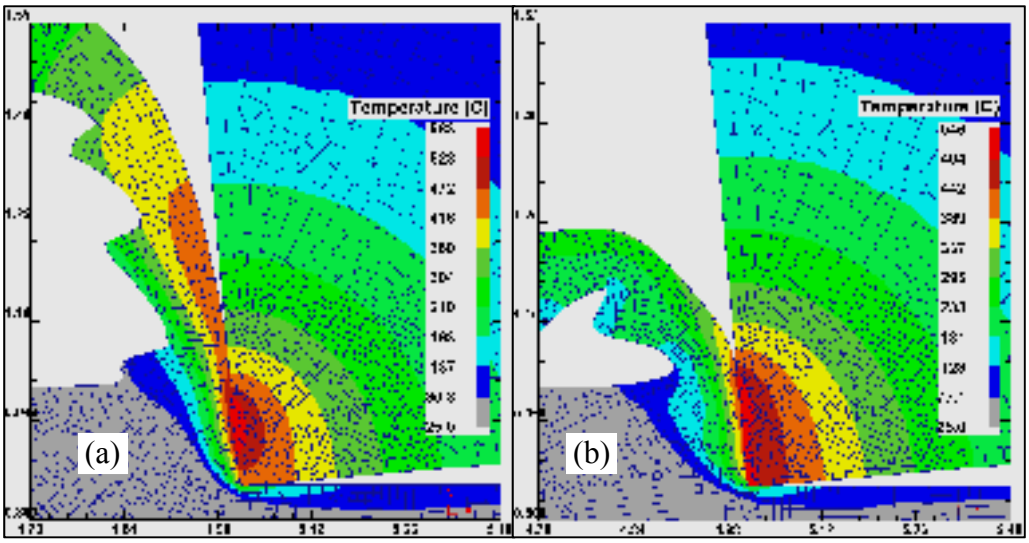

Figure 4-11 Temperature distribution obtained with a) Model 1 and b) Model M2 for the aluminum AA7075-T651

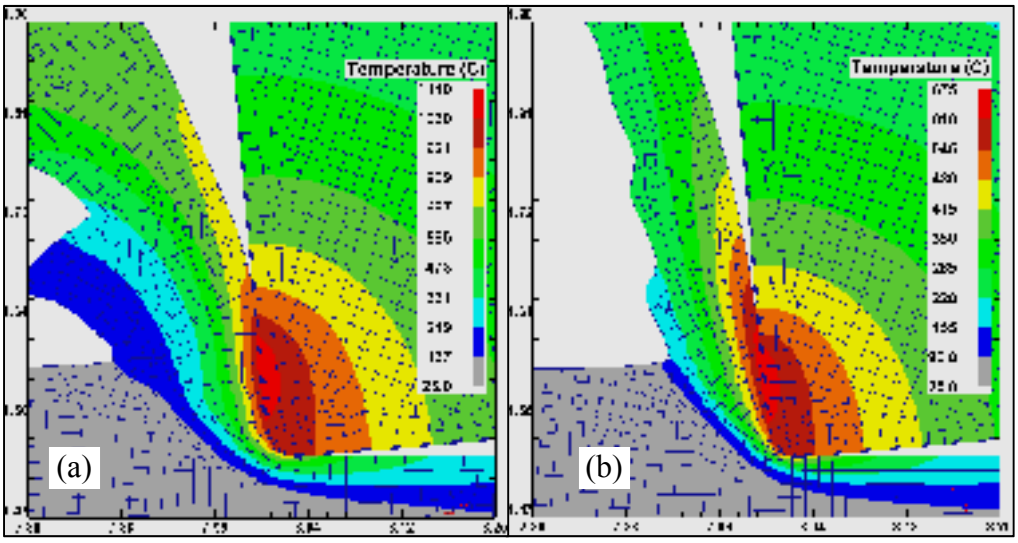

Figure 4-12 Temperature distribution obtained with a) Model 1 and b) Model M2 for the hardened AISI 4340 steel

4.7 Conclusions

This study presents a methodology to determine the coefficients of Marusich's constitutive equation for two aluminums alloys (AA6061-T6, AA7075-T651) and hardened AISI 4340 steel using an analytical inverse method combined with dynamic tests. RSM models were integrated within the inverse method in order to improve its accuracy. Two sets of material constants were determined, for each material, using two analytical temperature models (Oxley, Loewen and Shaw). Validation and sensitivity analysis of the proposed material models were performed using dynamic test results from published works and a finite element modeling of high speed orthogonal machining. The following conclusions can be drawn:

- The proposed identification procedure was successfully applied to determine material constants suitable for the prediction of dynamic response and FE simulation of high speed machining.

- Marusich's constitutive equation was successfully implemented in DEFORM-2D® software and a close agreement between the predicted and experimental results were obtained, particularly, for the cutting forces.

- The sensitivity analysis revealed that the selected temperature model used in the analytical inverse method affects significantly the identified material constants and thereafter predicted dynamic responses and machining modeling.

- Considering all predicted machining data, material constants obtained using Oxley temperature model was performed better for cutting forces

- The FE predicted cutting temperature was the parameter most sensitive to the material models and large discrepancy between the predicted results was obtained. This is a very critical issue in FEM of machining, particularly, when residual stress prediction is considered. Thus, the analytical temperature model should be carefully selected when used in the inverse methodology to identify material constants from machining tests.

In the next chapter, the Marusich's constitutive equation will be implemented in an analytical cutting forces model. The objective was to generalize the Oxley's theory to the high speed machining of aluminum alloys and hardened steels.

CHAPTER 5

ANALYTICAL CUTTING FORCES MODEL FOR HIGH SPEED MACHINING OF DUCTILE AND HARD METALS

Walid Jomaa, Victor Songmene, and Philippe Bocher

Article submitted, *Machining Science & Technology*: an International Journal, October 2014

Abstract: This paper aims to generalize the Oxley's machining theory (OMT) to the high speed machining of aluminum alloys and induction hardened steel using near-sharp and honed cutting edges, respectively. The Marusich constitutive equation (MCE) was used to model the behaviour of the aluminum alloys (AA6161-T6 and AA7075-T651) and the induction hardened AISI4340 steel (58-60 HRC). The predicted results were compared with experimental data from the present study and from the literature, covering a large range of cutting conditions (speed, feed, and rake angle). An encouraging good agreement has been found between predicted and measured cutting forces for all tested materials. The strain rate constants in the primary and secondary shear zone were found to be sensitive to the cutting conditions and their effects on the predicted data were discussed in detail.

Keywords: Machining, Predictive Modeling, Marusich's Constitutive equation, Oxley's predictive theory, aluminums, hardened steel

5.1 Introduction

In today's highly competitive machining industry, research's studies are focusing on the development of predictive models using analytical, empirical, and finite elements (FEM) in order to reduce parts cost. Although it provides precise results, FEM techniques are still time consuming and difficult to establish as large plastic deformations not only bring complications from the mathematical point of view, but also cause rapid solution degradation

due to element distortion (Vaz Jr et al., 2007). Empirical modeling needs extensive experimental works and therefore it is expensive and the applicability of the obtained results are limited to the tested condition domain. Finally, analytical modeling seems to be the optimal solution for machining process modeling since it can relate physical phenomena to technological process parameters with low computation time and few experimental data inputs. Oxley (1977) has developed a theory which is considered as the most fundamental approach in analytical modeling of the machining process based on the slip-line field theory. The main contribution of Oxley and co-workers was the development of a predictive machining theory by considering the effects of strain, strain-rate, and temperature on the flow stress of the work material. Only material properties, tool geometry and cutting conditions were needed to predict the cutting forces, chip thickness, average temperatures, and stresses in the deformation zones (Kopalinsky et Oxley, 1984). However, the simple material flow stress equation (power-law equation) used in OMT is only able to describe low carbon steels. Recently, Kristyanto et al (2002) have applied OMT to the turning of two aluminum alloys. However, some discrepancies, between predictions and experiments, were obtained for some cutting conditions due to lack of information about the flow stress properties at high strain rate and temperature encountered in machining. Moreover, Lee (Lee, 2011) argued that the power-law used in OMT is not suitable for hardened steels due to heat treating process. In the last decade, to overcome these shortcomings, some studies were carried out, to extend the applicability of OMT to a broader class of materials. Karpat and Özel (2006) developped a predictive thermal and anlytical modeling approch for orthogonal machining based on OMT and Johnson-Cooke (JC) constitutive equation. Their model was able to predict the temperature distribution on the tool, workpiece and chip during machining a carbon steel (AISI 1045) and aluminum alloys (Al6082-T6 and Al6061-T6). Lalwani et al (2009) extended the oxley's predictive analytical model for cutting forces by proposing an expression for the strain hardeneing exponent as function of JC equation constants. Their model was verified only in the case of carbon steels. Similarly, Lee (2011) has used the JC constititive equation to derive the material flow stress constant used in OMT and assumed a constant strain hardening exponent in the case of hard turning AISI 4140 steel (45 HRC). However, the propose analytical model overestimates the predicted thrust forces by about 20

% at low cutting speeds. Huang and Liang (2003b) developped an analytical cutting forces model based on OMT for orthogonal machining of AISI H13 steel at 52 HRC using CBN tools. This model takes into account for the tool thermal properties, however, the used JC equation was applicable for AISI H13 steel at 46 HRC. One can observes that these extensions of the OMT were mostly performed using the JC material model. However, Jaspers and Dautzenberg (2002) stated that the JC constitutive equation is not suitable for some materials. Moreover, Fang (2005) studied the sensitivity of the flow stress of 18 materials in machining and showed that the behaviour differs significantly from material to other and they cannot be described by only one equation. Even for the same type of material, chemical compositions and heat treatment conditions can also affect the constitutive behaviour.

As most of structural materials exhibit a transition, at a critical strain rate, from low to high strain rate sensitivity, Marusich and Ortiz (1995) proposed a simple constitutive equation (Equation 4.1 in Chapter 4) for this behaviour by assuming a stepwise variation of the rate sensitivity exponent (m) while maintaining continuity of stress. The Marusich's constitutive equation (MCE) was successfully validated in the FEM of high speed machining (HSM) AISI4340 steel (Marusich and Ortiz, 1995) and more recently in the cutting forces prediction during high speed end milling of aluminum alloys (Zaghbani and Songmene, 2009). It is worth noting that Zaghbani and Songmene (2009) have note used OMT in their approch.

Therefore, to generalize the Oxley machining theory for high speed machining of aluminum alloys and hardened steel, the work material flow stress were modeled using the MCE. The linear dependence between the flow stress and temperature in MCE (Equation 4.1c in Chapter 4), allow us to obtain a single solution for temperature without the need for the iterative loop used in the original formulation of OMT. The flow stress data, determined in Chapter 4 for the aluminums (AA6061-T6, AA7075-T651), and an induction hardened AISI4340steel (58-60 HRC) was used in the present Chapter.

5.2 Machining theory for orthogonal metal cutting

In the present study, an analytical model, based on OMT, was developed to predict the cutting forces for the orthogonal machining of two aluminum alloys and an induction hardened steel. The mean modifications of OMT as well as assumptions (geometrical and physical) are presented in the following sections.

5.2.1 Extension of the Oxley's predictive theory

Detailed information about the original formulation of OMT could be found in (Kopalinsky and Oxley, 1984). However, it is worthwhile to recall that the original formulation OMT is based on a power-law model (Equation 5.1) with material constants were assumed to be as function of a velocity-modified temperature parameter (Equation 5.2). The power-law model is given as:

$$\sigma = \sigma_1(T_{mod})\varepsilon^{n(T_{mod})} \tag{5.1}$$

where

$$T_{mod} = T\left[1 - \vartheta \log\left(\frac{\dot{\varepsilon}}{\dot{\varepsilon}_0}\right)\right] \tag{5.2}$$

where T is the temperature, $\dot{\varepsilon}$ is the strain rate, ϑ and $\dot{\varepsilon}_0$ are material constants, and σ_1 and n are polynomial equation function of T_{mod}. High order polynomials are used for greater accuracy and they can vary for different range of T_{mod}. However, only limited data using this concept were documented in the open literature, which significantly limits its uses.

Moreover, the original formulation of OMT was derived for cutting tool with sharp edge and for steady state continuous chip formation. On the other hand, the sharpness, which is a relative parameter that depends on the ratio of the uncut chip thickness to the tool cutting

edge radius, is of great importance when machining under finishing condition using honed tool edge (Outeiro, Dias et Jawahir, 2006). Therefore, the need for extending the OMT to the modeling of the high speed machining with near-sharp and honed cutting edge have motivated the present study and Marusich's constitutive equation was expected to be good candidate for modeling the material behaviour of the investigated materials (AA6061-T6, AA7075-T651, and hardened AISI 4340).

5.2.2 Assumptions and model geometry

Machining analytical modeling attempts to establish relationships between technological parameters (cutting feed, cutting speed, depth of cut, etc.) and state variables (strain, strain rate, temperatures, and stresses). Some assumptions should be considered in order to resolve the multi-physical problem as temperature, strain rates, and material behaviour are all related to each other.

As for the original formulation of OMT, the proposed model assumes a thin shear zone, chip equilibrium (Figure 5-1), and a uniform shear stress in the secondary deformation zone at the tool/chip interface (Kopalinsky and Oxley, 1984). The physical properties of the work material and the cutting tool are considered independent of the temperature in the present work. The proposed analytical model takes into account for the tool cutting edge radius. The machining using a large cutting edge radius contributes to additional ploughing forces (J.C. Outeiro, 2005). The ploughing forces are passive and do not participate in the cutting process, but affect the cutting force values; particularly, when low feeds are applied. In the present study, two cutting tool edges with relatively low finite radii (0.005 and 25µm) were chosen. Consequently, the ploughing force on the flank face of the tool was neglected and the resultant force R (Figure 5-1) is transmitted by both the shear plan AB and the tool/chip interface.

Based on previous works on machining using honed cutting edge (Outeiro et al., 2006), we assumed that the total undeformed chip thickness (t_u) can be divided into two parts: a part

representing the thickness of the layer that will be burnished by the round part of the edge δ_p (Astakhov, 2006) and the actual undeformed chip thickness (t_{au}) which is defined as:

$$t_{au} = t_u - \delta_p \tag{5.3}$$

The thickness of the layer to be burnished (δ_p) is estimated by (Astakhov, 2006):

$$\delta_p = r_e \left(1 - \frac{1}{\sqrt{1 + B_r^2}}\right) \tag{5.4}$$

where B_r is the Briks criterion calculated as (Astakhov, 2006):

$$B_r = \frac{\cos \alpha^*}{r_c - \sin \alpha^*} \tag{5.5}$$

r_c being the chip compression ratio determined by:

$$r_c = \frac{t_{au}}{t_c} = \frac{sin\emptyset}{cos(\emptyset - \alpha^*)} \tag{5.6}$$

where $\emptyset$ is the shear angle and α^* is the modified tool rake angle defined as (J.C. Outeiro, 2005):

$$\alpha^* = \begin{Bmatrix} arcsin\left(\frac{t_u}{r_e} - 1\right) \; if \; t_u < r_e.(1 + sin\alpha) \\ \alpha \quad if \quad t_u \geq r_e.(1 + sin\alpha) \end{Bmatrix} \tag{5.7}$$

where α is the normal rake angle.

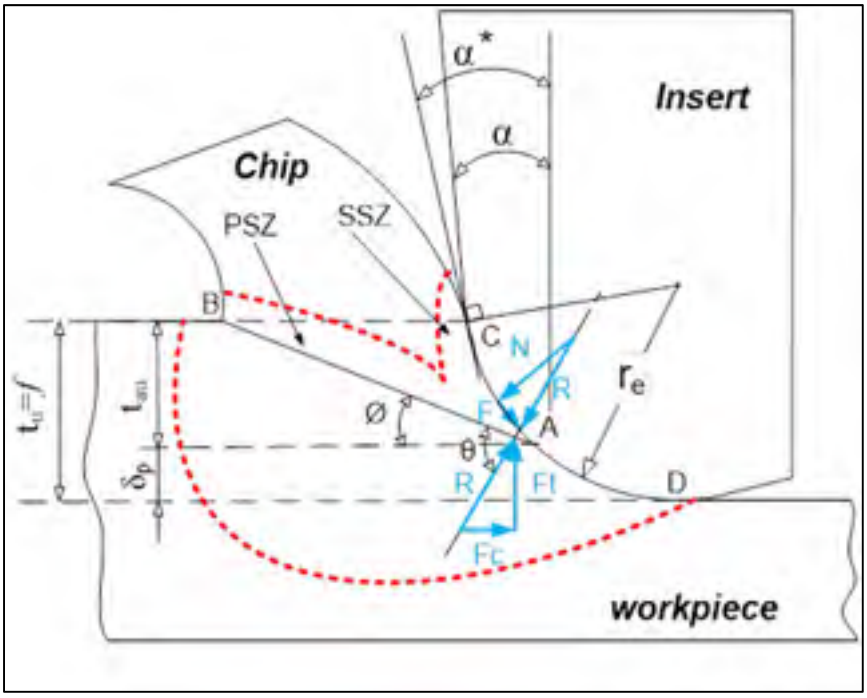

Figure 5-1 Geometric description of the chip formation model, PSZ is the primary shear zone, SSZ is the secondary shear zone

The parameters determined above were used for the calculations of the state variables such as strain, strain rate, stress, and temperatures. These state variables are needed for the estimation of the cutting forces (feed and cutting forces, friction and normal force, etc.). The Equations for the state variables which were determined in the primary and secondary shear zones are presented in the following paragraphs.

5.2.3 Calculation of state variables in the primary shear zone AB

In this section, the shear strain and strain rate, stresses, and temperatures are determined in the primary shear zone (Figure 5-1). The average shear strain (γ_{AB}) at AB, which because of the symmetry of the strain rate distribution in the vicinity of AB, is approximately half the total strain occurring in the shear zone and can be calculated as follows (Oxley and Hastings, 1977):

$$\gamma_{AB} = \frac{\cos \alpha^*}{2 \sin \emptyset \cos(\emptyset - \alpha^*)} \tag{5.8}$$

In order to measure the flow field and to evaluate the shear strain rate, Oxley and Hastings (1977) have used the quick-stop method and proposed a new slip-line field in the cutting zone. The slip-line field and the corresponding hodograph indicated that the strain rate in the primary shear zone increases with cutting speed and has a maximum value at the plan AB. Based on these experimental observations, Oxley proposed the empirical relation in Equation 5.9 for the average value of the shear strain rate ($\dot{\gamma}_{AB}$) along AB (Oxley and Hastings, 1977):

$$\dot{\gamma}_{AB} = C_0 \frac{V \cos\alpha^* \sin \emptyset}{t_{au} \cos(\emptyset - \alpha^*)} \tag{5.9}$$

where V is the cutting speed and C_0 is the strain rate constant defined as the ratio of the primary shear zone length l_{AB} to its thickness and will be estimated later.

The average shear plane temperature T_{AB} is linked to the shear stress k_{AB} in the primary shear zone and can be determined from the following relationship (Hastings, Mathew et Oxley, 1980):

$$T_{AB} = T_0 + \eta \left[\frac{1 - \beta}{\rho_w C_w} \frac{k_{AB} \cos\alpha^*}{\sin\emptyset \cos(\emptyset - \alpha^*)} \right] \tag{5.10}$$

where η is a constant representing the amount of plastic work converted to heat (equal to 0.9 in this study) and β is the fraction of energy that enters into the workpiece.

The determination of the shear stress in the primary shear zone using Marusich's constitutive equation combined with Oxley's theory was presented in APPENDIX II.

Substituting Equation 5.10 into Equations (A II-8) and (A II-9) (see APPENDIX II), gives the following expressions of the shear stress at AB:

$if\ \ \dot{\varepsilon}_{AB} < \dot{\varepsilon}_t$

$$k_{AB} = \frac{1}{\sqrt{3}}\left[1 - \alpha_{NL}\eta\frac{1-\beta}{\rho_w C_w}\frac{k_{AB}cos\alpha^*}{sin\emptyset cos(\emptyset - \alpha^*)}\right]\sigma_0\left(1+\frac{\varepsilon_{AB}}{\varepsilon_0}\right)^{\frac{1}{n_{NL}}}\left(1+\frac{\dot{\varepsilon}_{AB}}{\dot{\varepsilon}_0}\right)^{\frac{1}{m_1}} \tag{5.11}$$

$if\ \ \dot{\varepsilon}_{AB} > \dot{\varepsilon}_t$

$$k_{AB} = \frac{1}{\sqrt{3}}\left[1 - \alpha_{NL}\eta\frac{1-\beta}{\rho_w C_w}\frac{k_{AB}cos\alpha^*}{sin\emptyset cos(\emptyset - \alpha^*)}\right]\sigma_0\left(1+\frac{\varepsilon_{AB}}{\varepsilon_0}\right)^{\frac{1}{n_{NL}}}\left(1+\frac{\dot{\varepsilon}_{AB}}{\dot{\varepsilon}_0}\right)^{\frac{1}{m_2}}\left(1 + \frac{\dot{\varepsilon}_t}{\dot{\varepsilon}_0}\right)^{\frac{1}{m_1}-\frac{1}{m_2}} \tag{5.12}$$

Using the Von-Mises criterion, the equivalent stress, strain, and strain rate can be determined by the following relationships:

$$\sigma_{AB} = \sqrt{3}k_{AB};\ \varepsilon_{AB} = \frac{\gamma_{AB}}{\sqrt{3}};\ \dot{\varepsilon}_{AB} = \frac{\dot{\gamma}_{AB}}{\sqrt{3}} \tag{5.13}$$

Finally, the normal stress σ_N' at point A (Figure 5-1) can be found from the boundary condition of the slip-line. By considering the tool/chip interface as a direction of the maximum shear stress (Oxley and Hastings, 1977), the normal stress is therefore calculated by

$$\sigma_N' = k_{AB}\left[1 + 2(\frac{1}{4}\pi - \alpha^*) - \frac{2C_0\varepsilon_{AB}}{n_{NL}(\varepsilon_0 + \varepsilon_{AB})}\right] \tag{5.14}$$

The normal stress σ_N' is particularly useful to calculate the strain rate constant C_0.

5.2.4 Calculation of state variables along the tool/chip interface

To predict the shear angle ∅ and hence the cutting forces for a given set of cutting conditions, the strain, strain rate, and shear stress at the tool/chip interface are also needed. The average strain along the tool/chip interface (γ_{int}) is calculated from (Becze, 2002):

$$\gamma_{int} = \frac{l_c}{\delta t_c} \tag{5.15}$$

where δt_c is the average thickness of the secondary shear zone along the tool/chip interface (Figure 5-1) and l_c is its length.

By balancing the moment at point B, the tool-chip contact length l_c is computed in the present study as:

$$l_c = \frac{t_{au}\sin\theta}{\sin\emptyset\cos\lambda}\left[\frac{1+2\left(\frac{1}{4}\pi-\emptyset\right)}{3\left\{\left[1+2\left(\frac{1}{4}\pi-\emptyset\right)\right]-\frac{C_0\varepsilon_{AB}}{n_{NL}(\varepsilon_0+\varepsilon_{AB})}\right\}}+\frac{2}{3}\right] \tag{5.16}$$

where the angle θ is given as (see details in APPENDIX II):

$$tan\theta = 1+2(\frac{1}{4}\pi-\emptyset)-\frac{C_0\varepsilon_{AB}}{n_{NL}(\varepsilon_0+\varepsilon_{AB})} \tag{5.17}$$

The average strain rate along the tool/chip interface ($\dot{\gamma}_{int}$) is calculated from (Oxley and Hastings, 1977) as:

$$\dot{\gamma}_{int} = \frac{V\sin\emptyset}{\delta t_c cos(\emptyset-\alpha^*)} \tag{5.18}$$

The average temperature at the tool/chip interface (T_{int}) is then given as (Hastings et al., 1980):

$$T_{int} = T_0 + \left[\frac{1-\beta}{\rho_w C_w}\frac{k_{AB}cos\alpha^*}{sin\emptyset cos(\emptyset-\alpha^*)}\right] + \psi T_M \tag{5.19}$$

where T_M is the maximum temperature rise in the chip and the factor ψ is a constant (0.6 in this study). The maximum temperature rise is calculated based on Boothroyd's model as (Hastings et al., 1980):

$$Log\left(\frac{T_M}{T_C}\right) = 0.06 - 0.195\delta\left(\frac{R_T t_c}{l_c}\right)^{1/2} + 0.5\left(\frac{R_T t_c}{l_c}\right) \tag{5.20}$$

where T_C which is the average temperature in the chip as calculated by

$$T_C = \frac{k_{AB}sin\lambda}{\rho_w C_w \cos\theta cos(\emptyset-\alpha^*)} \tag{5.21}$$

given γ_{int}, $\dot{\gamma}_{int}$ and T_{int}, the shear flow stress k_{chip} along the tool/chip interface can be determined directly from the Marusich's constitutive Equation (A II-8) or (A II-9).

For a uniform stress distribution along the tool/chip interface, the normal stress can be expressed as (Oxley and Hastings, 1977):

$$\sigma_N = \frac{N}{l_c w} \tag{5.22}$$

and the shear stress at the tool/chip interface (τ_{int}) as:

$$\tau_{int} = \frac{F}{l_c w} \tag{5.23}$$

Once stresses and temperatures on the deformations zone (primary and secondary shear zone) are determined, the cutting force components F_c, F_t, F, and R (Figure 5-1) can be calculated by:

$$F_c = R\cos(\lambda - \alpha^*), F_t = R\sin(\lambda - \alpha^*) \tag{5.24}$$

$$F = Rsin\lambda, N = Rcos\lambda \tag{5.25}$$

$$R = \frac{k_{AB} t_u w}{sin\emptyset cos\theta} \tag{5.26}$$

$$\lambda = \alpha^* + \theta - \emptyset \tag{5.27}$$

where w is the width of cut, F and N are the tangential and normal forces at the tool/chip interface, respectively (Figure 5-1). λ is defined as the friction angle.

It is worthwhile to recall that the basis of the OMT (Oxley and Hastings, 1977) is to analyse the stresses along the primary shear zone (AB) and at the tool/chip interface as function of the shear angle $\emptyset$ and cutting conditions. The value of the shear angle $\emptyset$ is selected to ensure that the shear stress τ_{int}, calculated from the resultant force (R) across AB, equals the shear flow stress k_{chip} in the chip material at the interface. The strain rate constant C_0 is determined as part of the solution by imposing the condition σ_N=σ_N' and selecting the strain rate constant in the secondary shear zone δ so as to minimize the cutting force F_c (Equation 5-24). The flowchart of the general procedure used for cutting forces prediction is shown in Figure 5-2 for better clarification of the proposed algorithm.

5.2.5 Some issues in calculating the strain rate constant C_0 and δ

The strain rate constants C_0 and δ are fundamental parameters in OMT that are obtained as a solution of the iterative loop, however, authors have documented some discrepancies of the estimated strain rate constants among many previous works.

Shaw (1984) considered the primary shear zone thickness to be constant at 25 µm, which implies that C_0 can be considered constant for the studied material (plain carbon steel). Contrastingly, experimental results obtained by Kececioglu (1958) showed based on geometrical analysis of quick-stop micrograph that the primary shear zone thickness is one quarter of the chip thickness when SAE 1015 steel is machined in the range of cutting speed from 40 to 250 m/min. The constant C_0, is therefore, assumed to depend on the cutting conditions. Recently, by analysing published results for different materials (brass and steels), Tounsi *et al.* (2002) have concluded that the primary shear band thickness is approximately half of the uncut chip thickness. On the other hand, Kristyanto et *al*. (2002) have evaluated experimentally the strain rate constant δ in the secondary shear zone for two aluminum alloys and found it equal to 0.031.

On the other hand, Kopalinsky and Oxley (1984) have shown that the original formulation of Oxley's model was not able to converged for the high negative rake angle (-25°) condition. Their model has converged only by setting a constant strain rate coefficient C_0 and reducing the strain hardening coefficient by 35% from the calculated value to predict reasonable cutting forces. Özel and Zeren (2006), and more recently Lalwani *et al* (2009) have predicted cutting forces using modified versions of Oxley's machining theory. They have investigated the same reference data (0.38%C steel from (Oxley et Young, 1989)) and cutting conditions, but their results in terms of constants δ and C_0 were significantly different as can be seen in Table 5-1

Table 5-1 Constants δ and C_0 from literature for the steel 0.38%C
(*w=4 mm,* $\boldsymbol{\alpha}$*=-5°)*

Test#	V (m/min)	f (mm/rev)	(Özel and Zeren, 2006)		(Lalwani et al., 2009)	
			δ	C_0	δ	C_0
1	100	0.125	0.008	2.39	0.065	6
2	200	0.125	0.006	2.67	0.03	5.7
3	400	0.125	0.008	1.48	0.015	5.3
4	100	0.25	0.019	4.38	0.035	5.7
5	200	0.25	0.018	3.14	0.02	5.4
6	100	0.5	0.050	3.99	0.02	5.4

Based on the findings stated above, it is clear that the strain rate constants depend on the cutting conditions and/or the work materials and different sets of values may predict reasonable solutions. Therefore, the predicted values of these constants need to be validated and eventually adjusted to better fit the reality. The lack of experimental values for the strain rate constants makes such validation difficult.

In the present work the choice was made to keep the material constants, specifically the strain hardening coefficient (contrasting with Kopalinsky and Oxley approach (1984)). When large deviations between predictions and experiments were obtained, or when non-converged conditions were happening, an iterative procedure consisting of varying the strain rate constants $C_0$and/or δ was used to fit the measured cutting forces. If experimental data were available, they were used to set one of the constants. In particular, results from Kristyanto et *al*. (2002) were used to set the strain rate constant δ for both aluminum (AA7075-T651 and AA6061-T6). As no available data were found in the literature for the hardened AISI 4340 steel, the model was validated only using the experimental cutting forces as a criterion.

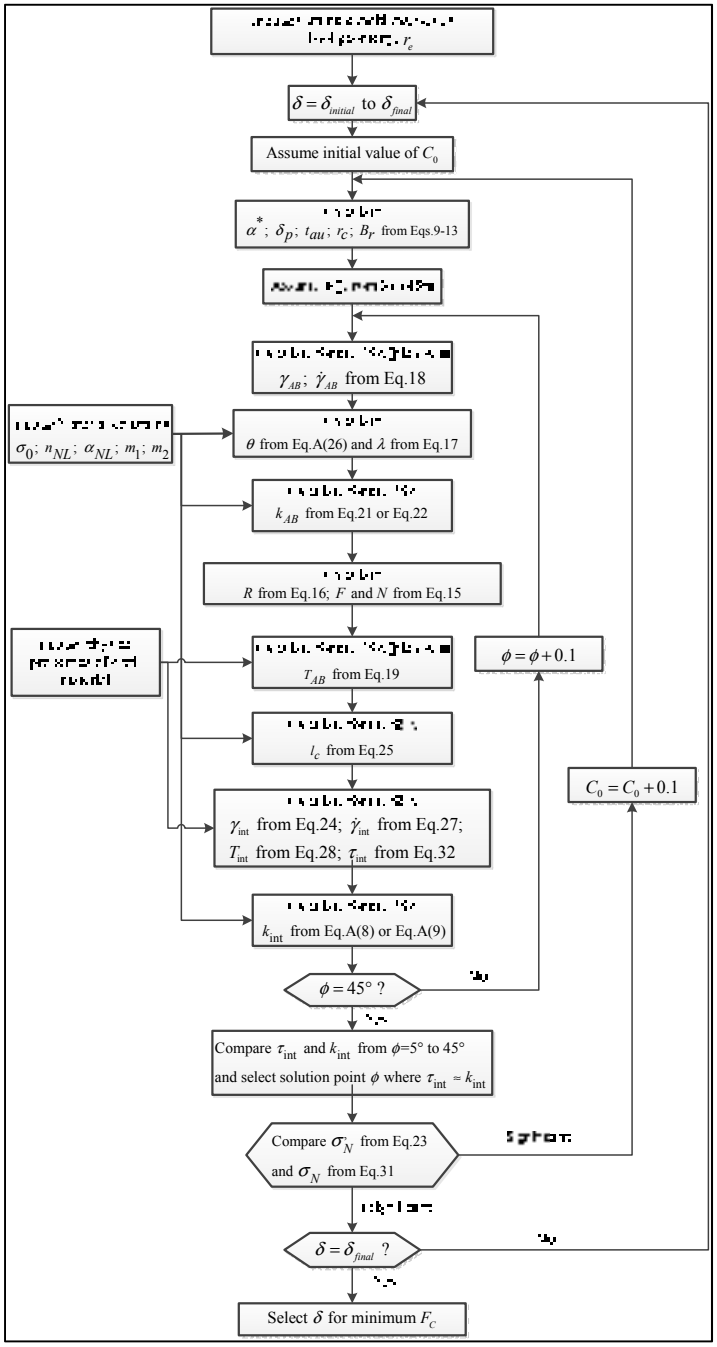

Figure 5-2 Flow chart of the extended Oxley machining theory adapted from (Kopalinsky and Oxley, 1984)

5.3 Model validation and discussion

To validate the above analytical model, the predicted machining data (cutting forces, chip thickness and chip/tool contact length) were compared to experimental ones. The work materials were two aluminums (AA6061-T6 and AA7075-T6) and hardened AISI 4340 (60HRC) steel. The physical properties of the work materials and those of the used cutting tools were taken from the literature and are listed in Table 5-2. A series of orthogonal machining experiments were carried out on a MAZAK 3-axis CNC machine without coolant. The aluminum alloys (AA7075-T651, AA6061-T6) were machined using uncoated tungsten carbide insert (ISO code-TNMA120408) [Ref. K68] with sharp edge radius (≈ 5µm). For machining the hardened AISI 4340 steel, ceramic inserts with TiN coating (ISO code-TNGA 120408-E) [Ref. KY4400] and with rounded edge radius (≈ 25µm) were used. In all cases the inserts were mounted on right hand tool holders with a rake angle of -5°. The tested workpieces were disc-shaped samples, with a 70 mm external diameter, a 19 mm internal diameter, and a 4.3 mm thickness. Table 6-3 details the 11 (eleven) cutting conditions used for the three tested materials. These cutting conditions were selected with respect to the tool manufacturer suggestions and based on an experimental design which is detailed in Chapter 4.

A Kistler® piezoelectric dynamometer (type 9255B) was used to acquire the cutting forces (tangential force, F_c, and feed force, F_f). An optical microscope, model Olympus GX51, was used to measure the chip thickness (t_c) and the chip/tool contact length (l_c). The flow stress data of the MCE for three tested work materials were deduced from machining and dynamic tests and they are listed in Table 5-4. The identification procedure is detailed in Chapter 4.

For the two aluminum alloys, the predictive model was then run for other cutting conditions to verify how close they are from published experimental data of orthogonal cutting machining. The results were published from (Guo, 2003) for the aluminum AA6061-T6 (Table 5-5) and included 16 different cutting conditions whereas and from (Sheikh-Ahmad et

Twomey, 2007) for the aluminum AA7075-T6 (Table 6-6) 10 cutting conditions were available.

Table 5-2 Thermal properties of work materials and cutting tools

Properties	Work material			Cutting insert	
	6061-T6	7075-T651	AISI 4340	Uncoated WC (K68) (Yen et al., 2004)	Mixed ceramic (KY4400) (Brito et al., 2009)
Density (kg/m3)	2700	2810	7800	15000	4650
Thermal conductivity (W/m°C)	167	130	43	46	21
Specific heat (J/Kg °C)	896	960	600	203	645
Melting temperature (°C)	652	635	1520	-	-

Table 5-3 Orthogonal Cutting conditions

Test#	Aluminums (6061-T6, 7075-T6)		Steel AISI 4340	
	f [mm/rev]	V [m/min]	f [mm/rev]	V [m/min]
1	0.05	300	0.03	75
2	0.25	300	0.13	75
3	0.05	1000	0.03	180
4	0.25	1000	0.13	180
5	0.15	1144	0.08	202
6	0.15	156	0.08	54
7	0.01	650	0.01	128
8	0.29	650	0.15	128
9	0.15	650	0.08	128
10	0.03	650	0.03	128
11	0.05	650	0.05	128

Table 5-4 Flow stress data of the Marusich's constitutive equations

Material	$\sigma_0\ [MPa]$	m_1	m_2	n_{NL}	α_{NL}	ε_0	$\dot{\varepsilon}_0\ [s^{-1}]$	$\dot{\varepsilon}_t [s^{-1}]$
6061-T6	278.46	4.34	150.72	3.32	0.002271	0.1	200	10^4
7075-T6	529.02	2.63	168.92	11.23	0.001746	0.025	2400	10^4
AISI 4340	874	23.23	193.17	3.40	0.000756	0.1	1	10^4

Table 5-5 Orthogonal machining data for the aluminum AA6061-T6, *w=1.7 mm, α=6°, diameter=50.8 mm, sharp carbide cutting tool* (Guo, 2003)

Test#	f [mm/rev]	V [m/min]	F_c[N]	F_t[N]	t_c[mm]
1	0.05	119	257	154	0.098
2	0.1	119	402	194	0.178
3	0.125	119	509	240	0.231
4	0.200	119	631	263	0.241
5	0.050	238	213	106	0.098
6	0.100	238	364	147	0.178
7	0.200	238	603	202	0.366
8	0.050	475	209	97	0.096
9	0.100	712	349	119	0.151
10	0.200	712	507	129	0.305

Table 5-6 Orthogonal machining data for the aluminum AA7075-T6, *w=3.81 mm, α=0°, diameter=76 mm, sharp carbide cutting tool* (Sheikh-Ahmad and Twomey, 2007)

Test#	f [mm/rev]	V [m/min]	F_c[N]	F_t[N]	t_c[mm]
1	0.066	77	225	109	0.428
2	0.066	123	182	91	0.336
3	0.066	154	182	86	0.354
4	0.066	193	150	69	0.294
5	0.086	77	210	106	0.520
6	0.086	123	176	88	0.492
7	0.086	154	164	76	0.434
8	0.086	193	144	68	0.412
9	0.107	77	211	112	0.600
10	0.107	123	203	99	0.550
11	0.107	154	209	94	0.470
12	0.107	193	166	76	0.458
13	0.122	77	264	129	0.746
14	0.122	123	211	96	0.550
15	0.122	154	202	88	0.500
16	0.122	193	197	86	0.518

5.3.1 Aluminum AA6061-T6

Figure 5-3 and Figure 5-4 show a comparison between the predicted and measured forces as calculated by the model for the 11 cutting conditions presented in Table 5-3. Preliminary simulations showed that the analytical model underestimate, sometime significantly, the cutting forces when the fully predictive procedure was applied to lower cutting speed and/or feed (i.e. Tests #1, #3, #6, #7, #11, and #12). Thus for these tests, the constant δ was selected equal to 0.031 based on experimental findings of Kristyanto et *al*. (2002), while the constants C_0 was obtained iteratively for best agreement between experimental and predicted cutting force, F_c. The predicted forces matched very well the experimental trends as shown in Figures 5-3 and 5-4. Both calculated and measured cutting and feed forces, increase with the cutting feed and decreases with the cutting speed. Good agreements between the predicted and experimental values were observed except for some cutting conditions for which large errors were found about 25% and 120% for cutting and feed forces, respectively. On the other hand, the predicted chip thickness (t_c), as well as the chip/tool contact length (l_c), were under estimated by the predictive Model (Table 5-7).

Figures 5-5 to 5-7 show the comparison between predicted forces and chip thicknesses with the sixteen experimental data from (Guo, 2003). Although the analytical model has converged for all cutting conditions, very high discrepancies were obtained between predictions and experiments. It was decided for this set of experiments to imposed the value of δ equal to 0.031 from (Kristyanto et al., 2002) and the constant C_0 was obtained iteratively for the best agreement with the experimental results (cutting forces). By comparing Figures 5-5 and 5-6 with Figures 5-3 and 5-4 one can see that the cutting and feed force values in (Guo, 2003) were significantly lower than those obtained in the present work. In fact, a lower width of cut (w=1.7 mm) was used in the experiment from (Guo, 2003) which is about 2.5 less than in the present work (w=4.3 mm). For this set of data too, a good agreement is observed between predicted and experimental measured forces. The average errors between calculated and measured values were equal to 2.4% and 7.7 % for cutting and feed forces,

respectively (Figure 5-5 and 5-6). However, the predicted chip thickness is systematically underestimated (Figure 5-7).

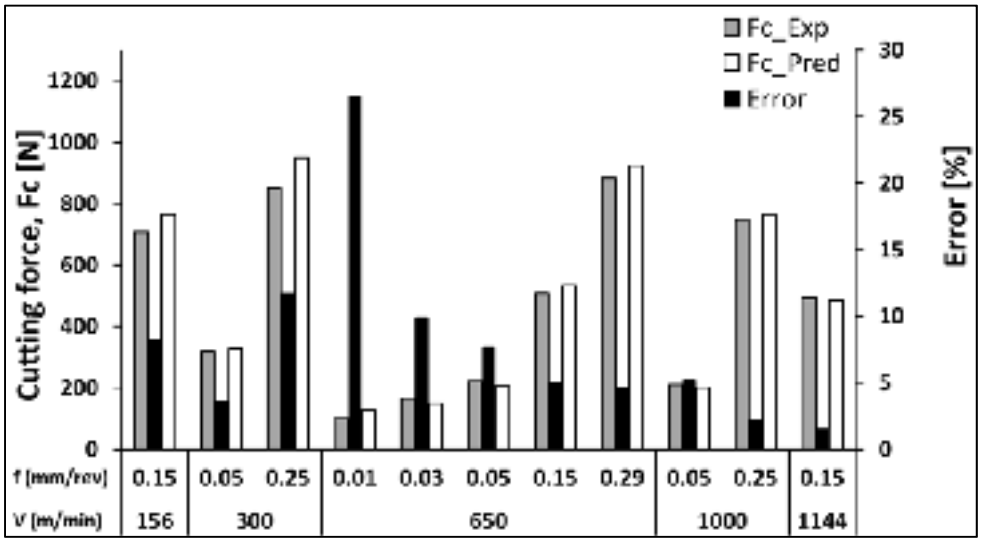

Figure 5-3 Comparison of predicted cutting force with the experimental data for AA6061-T6 alloy, *w=4.3 mm, α=-5°*

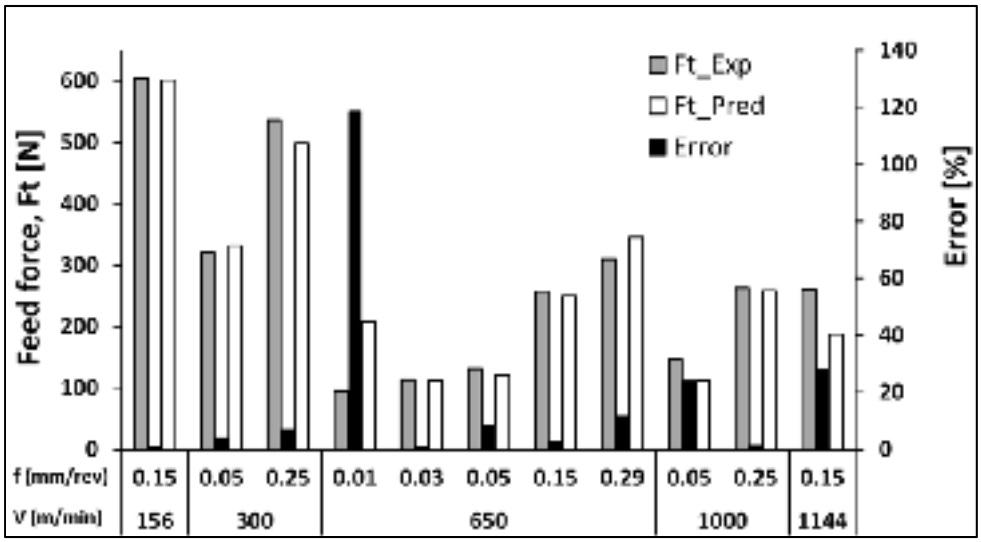

Figure 5-4 Comparison of predicted feed force with the experimental data for AA6061-T6 alloy, *w=4.3 mm, α=-5°*

Table 5-7 Experimental and predicted machining data for AA6061-T6, *w=4.3 mm,* α*=-5°*

Test#	C_0	δ	t_c [mm]			l_c [mm]		
			Exp.	Pred.	Error [%]	Exp.	Pred.	Error [%]
1	1.0	0.031*	0.352	0.180	49	0.667	0.231	65
2	2.1	0.020	0.622	0.562	10	0.835	0.614	27
3	1.3	0.031*	0.146	0.105	28	0.237	0.116	51
4	1.9	0.020	0.467	0.431	8	0.659	0.451	32
5	1.9	0.030	0.170	0.274	61	0.320	0.289	10
6	1.0	0.031*	0.700	0.400	43	0.835	0.472	43
7	0.1	0.031*	0.090	0.073	19	0.220	0.116	47
8	1.9	0.030	0.558	0.523	6	0.624	0.550	12
9	2.0	0.030	0.330	0.309	6	0.418	0.332	21
10	1.0	0.031*	0.159	0.068	57	0.220	0.079	64
11	0.1	0.031*	0.180	0.092	49	0.280	0.102	64

* Imposed experimental value from Kristyanto et al. (2002)

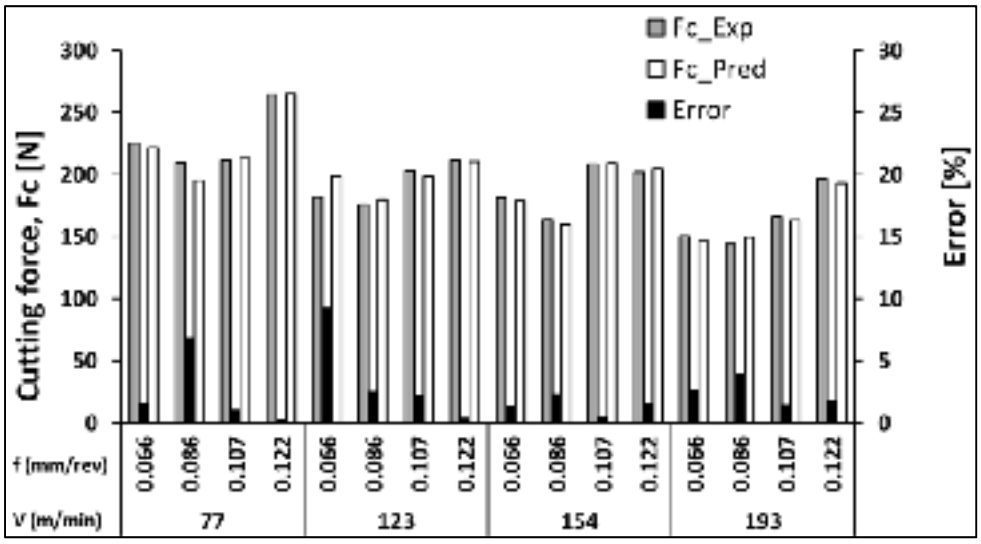

Figure 5-5 Comparison of predicted cutting forces with experimental data for AA6061-T6 from, *w=1.7 mm,* α*=6°* (Guo, 2003)

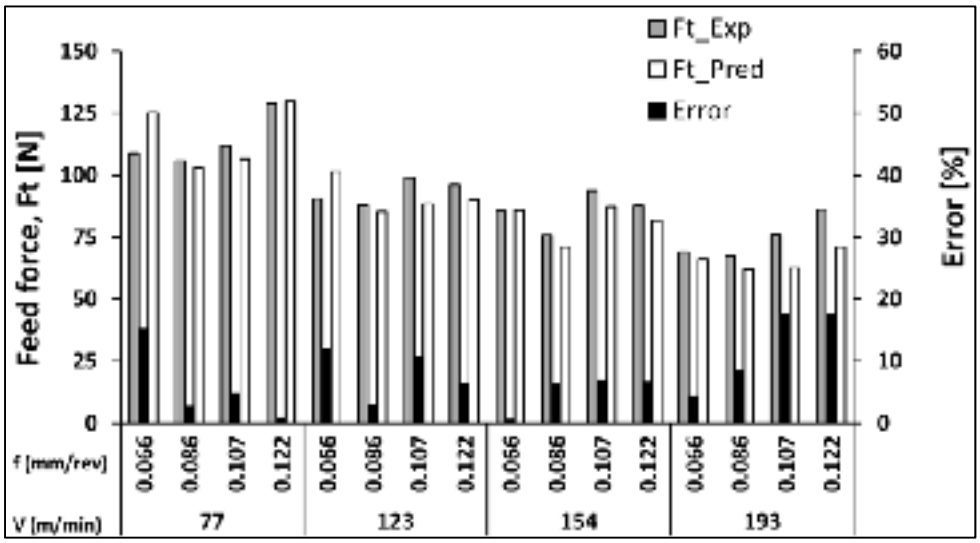

Figure 5-6 Comparison of predicted feed forces with experimental data for AA6061-T6 from (Guo, 2003), w=1.7 mm, α=6°

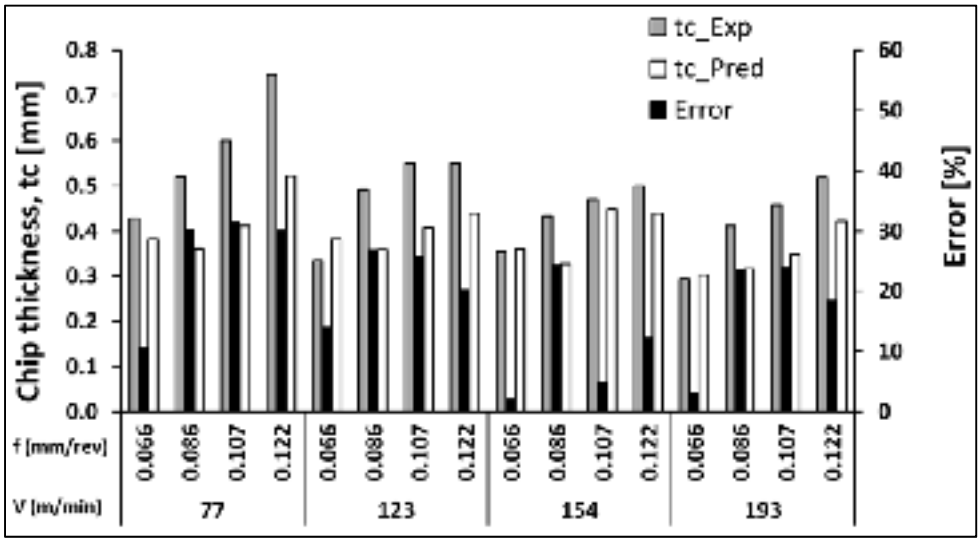

Figure 5-7 Comparison of the predicted chip thickness with the experimental data for AA6061-T6 from (Guo, 2003), *w=1.7 mm, α=6°*

5.3.2 Aluminum AA7075-T651

For the aluminum AA7075-T651, Figures 5-8 and 5-9 compare the predicted cutting and feed forces to experiment results for the machining conditions described in Table 5-3. For the predicted forces, the strain-rate constants C_0 and δ were obtained as part of the solution using the analytical model except those under lower cutting speed and/or cutting feed (Tests #1, #2, #6, #7, #11, and #12,). Again, for these tests the predicted forces were too large and the constants δ had to be imposed (0.031) based on experimental findings of Kristyano et *al*. (2002). The constant C_0 was then obtained iteratively for each cutting condition for best agreement between experimental and predicted cutting forces. In these conditions, the analytical model predicts accurately the cutting and feed forces trends. The average errors values are relatively low (11.3%) for the calculated cutting force (Figure 5-8). However, large discrepancies were observed for the feed force and errors higher than 50 % were obtained in some specific cutting conditions (Figure 5-9). Furthermore, Table 5-8 shows significant discrepancies between predicted and measured chip thickness and chip/tool contact lengths for some cutting conditions. This matter will be discussed below.

For the ten experimental data from (Sheikh-Ahmad and Twomey, 2007) (see Table 5-6), the comparison between predicted forces and chip thicknesses are displayed in Figures 5-10 to 5-12. The strain-rate constants C_0 and δ were obtained from the modified Oxley's machining theory presented here only for Tests #9 and #10 (high cutting speed 712 m/min conditions) as only these test conditions gave acceptable agreements between predicted and experimental cutting force values. A good agreement between predicted and measured chip thickness with errors less than 10% was obtained when the fully predictive procedure was applied (Tests #9 and #10 in Figure 5-12). The highest errors were obtained at low cutting speed conditions.

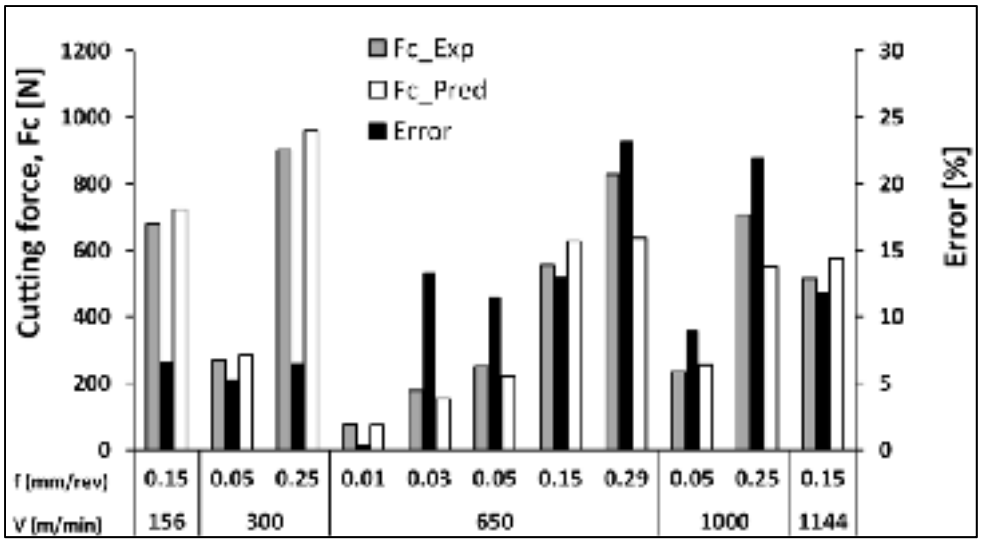

Figure 5-8 Comparison of predicted cutting force with the experimental data for AA7075-T651 alloy, *w=4.3 mm, α=-5°*

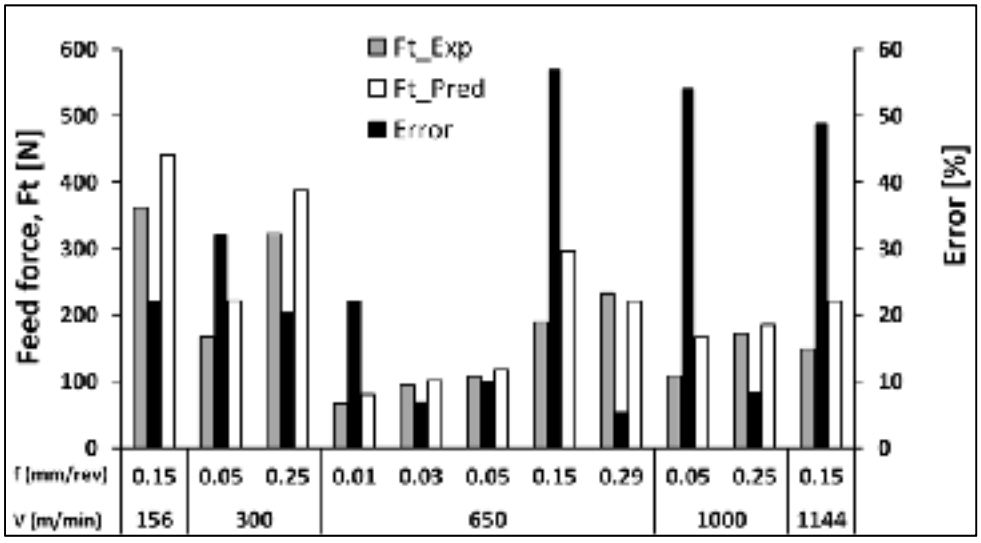

Figure 5-9 Comparison of predicted feed force with the experimental data for AA7075-T651 alloy, w=4.3 mm, α=-5°

Table 5-8 Experimental and predicted machining data for AA7075-T651

Test#	C_0	δ	t_c [mm]			l_c [mm]		
			Exp.	Pred.	Error [%]	Exp.	Pred.	Error [%]
1	0.10	0.031*	0.130	0.115	11	0.428	0.134	69
2	0.18	0.031*	0.217	0.366	68	0.426	0.396	7
3	7.00	0.030	0.105	0.138	31	0.113	0.157	39
4	6.20	0.060	0.196	0.268	37	0.312	0.268	14
5	6.20	0.010	0.180	0.281	56	0.218	0.296	36
6	0.19	0.031*	0.334	0.281	16	0.409	0.315	16
7	0.10	0.031*	0.035	0.032	9	0.061	0.041	33
8	6.20	0.040	0.188	0.308	64	0.343	0.308	10
9	6.20	0.010	0.254	0.313	23	0.249	0.337	35
10	0.10	0.031*	0.111	0.060	46	0.113	0.068	40
11	0.10	0.031*	0.108	0.085	21	0.177	0.094	47

* Imposed experimental value from Kristyanto et al. (2002)

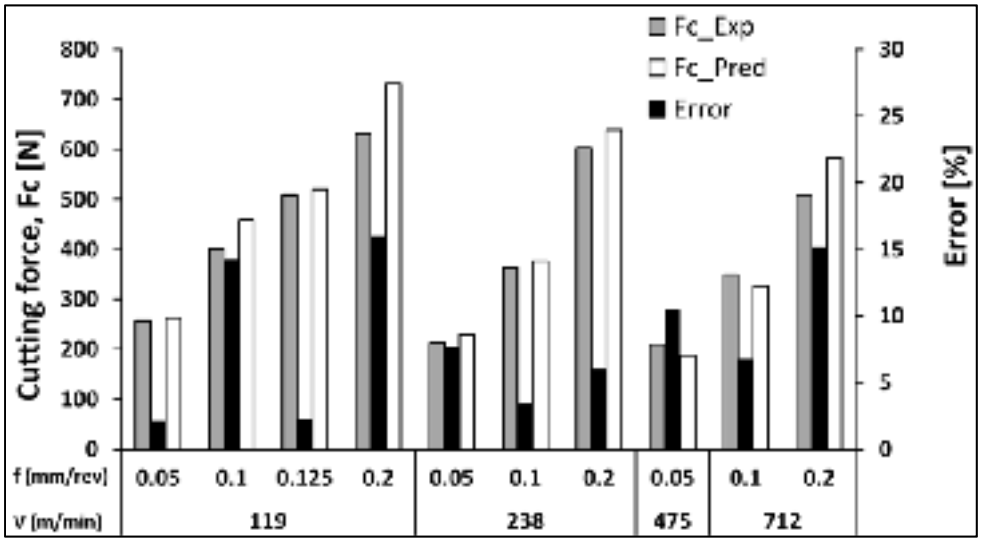

Figure 5-10 Comparison of predicted cutting forces with experimental data for AA7075-T651 from (Sheikh-Ahmad and Twomey, 2007), *w=3.81 mm,* $\boldsymbol{\alpha}$*=0°*

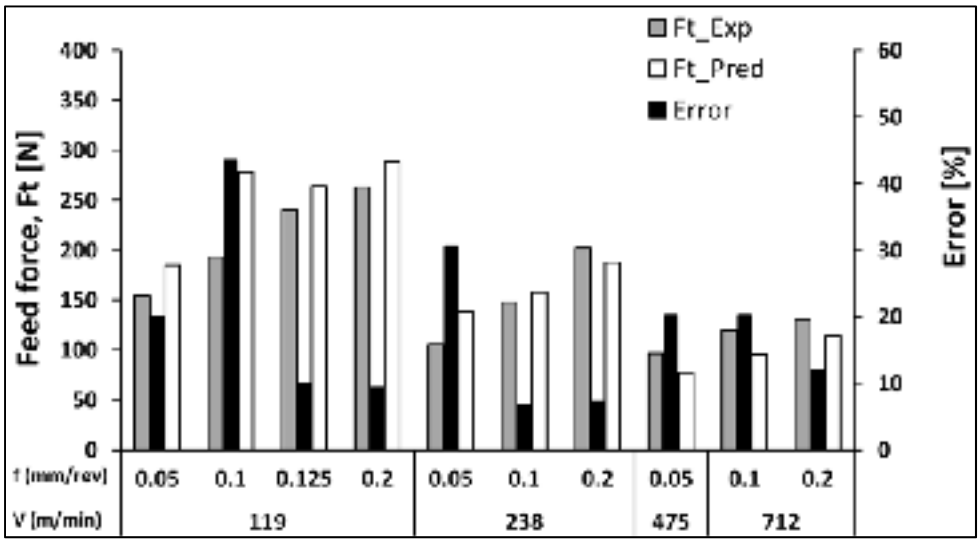

Figure 5-11 Comparison of predicted feed forces with experimental data for AA7075-T651 from (Sheikh-Ahmad and Twomey, 2007), *w=3.81 mm,* $\boldsymbol{\alpha}$*=0°*

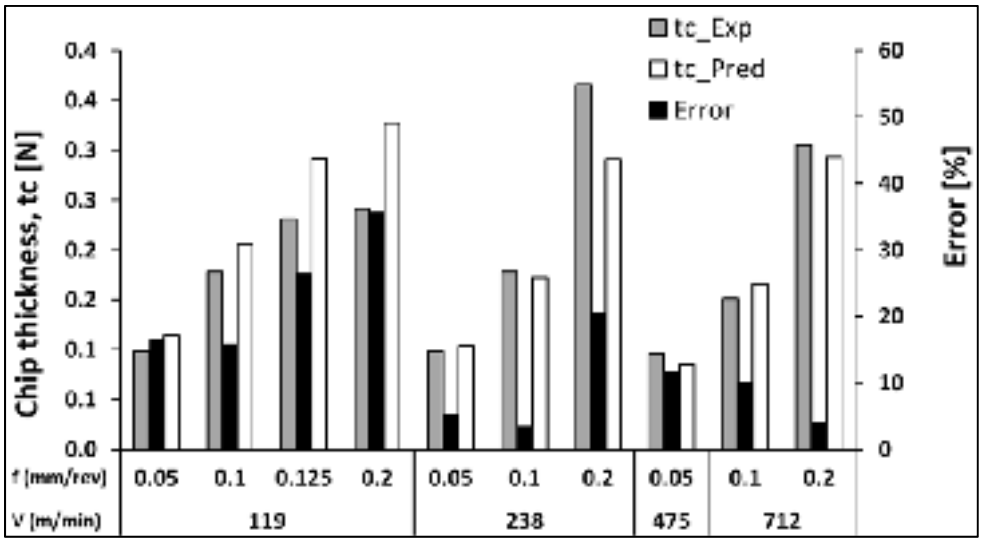

Figure 5-12 Comparison of the predicted chip thickness with the experimental data for AA7075-T651 from (Sheikh-Ahmad and Twomey, 2007), *w=3.81 mm,* $\boldsymbol{\alpha}$*=0°*

5.3.3 Hardened steel AISI 4340

The predicted and measured forces, obtained when machining the hardened AISI4340 steel (58-60 HRC) were much high then for the aluminum alloys and they are presented in Figures 6-13 and 6-14. For the predicted forces, the strain-rate constants C_0 and δ were calculated as part of the solution only for Tests #3, #4, #5, and #8 (Table 5-3). The predictive model catches accurately the general trends and a good agreement between predicted and experimental measured forces was observed. The errors recorded between experimental and predicted values are quite lower and are around of 5% and 10% for the cutting and feed force, respectively, except for some cutting conditions, i.e., Tests #1, #2, #6, #7, #9, #10 and #11. Again, as for the aluminum alloys, they represent the low cutting feed and/or low cutting speed conditions. As no experimental datum was available for the constant δ, both constants, δ, and C_0 were obtained iteratively for best agreement between experimental and predicted cutting force. The predicted chip thickness (t_c) as well as the chip/tool contact length (l_c), were overestimated by the predictive model as shown in Table 5-9.

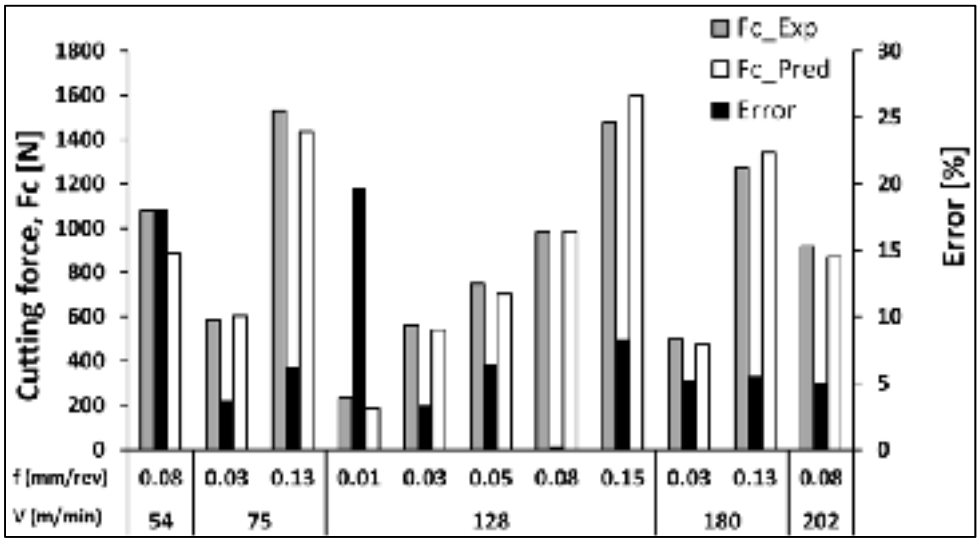

Figure 5-13 Comparison of predicted cutting force with the experimental data for hardened AISI 4340 steel, w=4.3 mm, α=-5°

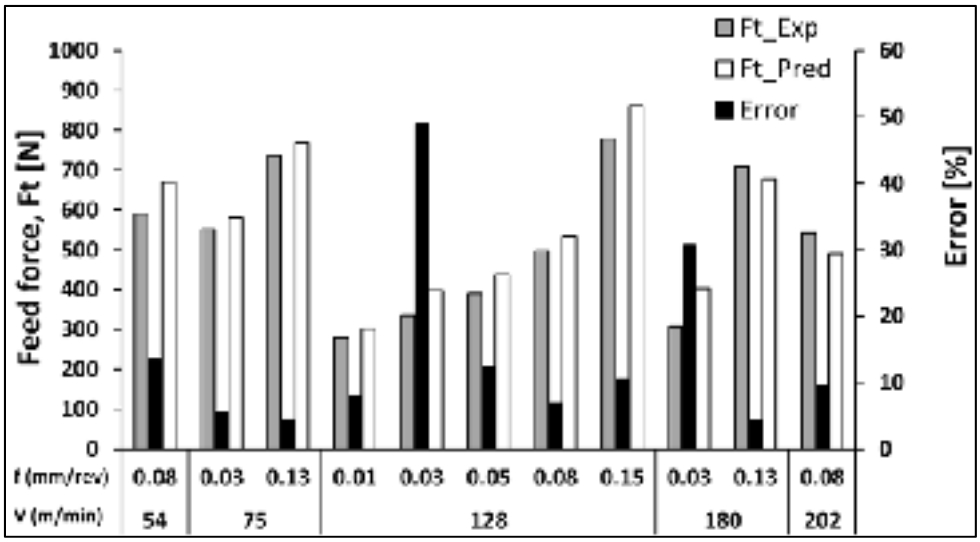

Figure 5-14 Comparison of predicted feed force with the experimental data for hardened AISI 4340 steel, w=4.3 mm, α=-5°

Table 5-9 Experimental and predicted machining data for hardened 4340 steel (60 HRC)

Test#	C_0	δ	t_c [mm]		l_c [mm]	
			Exp.	Pred.	Exp.	Pred.
1	10.0	0.100	0.025	0.256	0.113	0.134
2	8.2	0.005	0.179	0.593	0.188	0.299
3	2.7	0.100*	0.044	0.119	0.055	0.143
4	2.6	0.100*	0.138	0.309	0.220	0.332
5	2.6	0.100*	0.110	0.205	0.118	0.223
6	8.7	0.020	0.109	0.347	0.121	0.222
7	12.8	0.150	0.020	0.050	0.030	0.146
8	2.6	0.100*	0.166	0.372	0.189	0.404
9	8.5	0.050	0.106	0.436	0.117	0.311
10	9.5	0.005	0.061	0.244	0.067	0.148
11	8.9	0.020	0.072	0.310	0.081	0.208

* Calculated as part of the solution

5.4 Discussion

The Oxley machining model using Marusich's constitutive equation for material behaviour description was successfully generalized to aluminum alloys (AA7075-T651 and AA6061-T6) and induction hardened AISI4340 steel (58-60 HRC). The preliminary simulations of the orthogonal cutting showed that, although the proposed analytical model had converged, large discrepancies between measured and predicted forces (cutting and feed forces) were observed at low speed and/or feed conditions. Thus, two prediction procedures were applied depending on the cutting conditions. The first one is a fully predictive method which was applied for high cutting speed and/or feed conditions: the strain rate constants (C_0 and δ) were calculated as part of the solution of the analytical model. The second one is an iterative method which was applied to low cutting speeds and/or feeds conditions: the strain rate constant δ was set to a reported experimental value and the C_0 constants were determined iteratively for the best agreement between experimental and predicted cutting force. If no experimental data were available, both, C_0 and δ constants were determined iteratively to fit the measured cutting force. For simplicity, the results obtained at high and low cutting speeds and/or feeds will be discussed separately. In the present work, low cutting speeds and feeds for the tested aluminum alloys were found for less than 300 m/min and 0.25 mm/rev, respectively. On the other hand, the cutting speed of 128 m/min and the feed of 0.08 mm/rev were found to be the limits separating the high and low speed and feed ranges, respectively, for the hardened AISI 4340 steel.

5.4.1 Cutting force prediction

Overall, the cutting forces were accurately predicted but the feed forces were underestimated when prediction was carried out for high cutting speed and/or feeds condition. This trend was reported by many previous works on both analytical (Li et al., 2011) and finite element modeling of machining process (Klocke et al., 2013). These deviations of the feed force could be related to the assumption that the ploughing forces can be neglected as discussed

earlier leading to greater discrepancies between the predicted and measured feed forces (Li et al., 2011). In fact, the projection of such a force in the feed direction is greater than that in the cutting direction, which could result in greater discrepancies between the predicted and measured feed force as stated by Li et *al.* (2011). The ploughing force can be particularly significant when machining at lower cutting feed (Li et al., 2011) given a possible explanation for the large discrepancies between predictions and experiments observed for these cutting conditions. Moreover, the adopted friction model (Coulomb) which takes account for the sliding effect ignores the existence of sticking between the chip and tool face could be another reason for the trend discussed.

On the other hand, the predictive model overestimates the feed force for some low cutting speed and/or feed conditions, when the iterative method was applied, even if the ploughing force has not been taken into consideration. It is worthwhile to recall that for this method, the condition σ_N=σ'_N (Equations 5.14 and 5.22) was not respected when calculating the strain rate constants C_0 as large discrepancies were obtained when the fully predictive procedure was applied. However, this induces systematically a deviation on the resultant force direction (θ) (Equation 5.17) which affects directly the feed force values.

The discrepancies between predictions and experiments at low cutting speed conditions have been documented in several previous works on Aluminum alloys (Kristyanto et al., 2002), AISI 4140 steel (Lee, 2011), and AISI 316L stainless steel (Li et al., 2011), showing that this trend seems to be independent of the machined materials and is most likely related to the analytical machining model assumptions and/or the material model. The material models used in these works were the Power-law in (Kristyanto et al., 2002) and the Johnson-Cooke equation in (Lee, 2011) and (Li et al., 2011). For instance, the predicted cutting force values were 20% higher than experiments when machining AISI 4140 steel at cutting speeds ranging between 50 -100 m/min in (Lee, 2011).

5.4.2 Chip thickness and contact length

The predicted chip thicknesses and contact length trends were consistent with the experimental values (Figures 5-7 and 5-12, Tables 5-7 to 5-9) even if large variations were observed for some conditions. It is worth noticing that the experimental optical method used for the chip thickness and chip/tool contact length measurements may induce significant errors as reported in (Filice et al., 2007) and the calculated values can be a good source of information to better understand the material behaviour during high speed machining.

The predicted chip thickness was, in general, underestimated for the aluminum AA6061-T6. The high ductility of this alloy, compared to the aluminum AA7075-T651, produces continuous chips that tend to adhere to the rake face of the tool. Build-up edge on the tool can form which can dramatically changes the cutting conditions. This was not considered in the proposed predictive model and it will have the effect of underestimating the actual chip thickness and/or the tool/chip contact length.

On the other hand, the deviations of the predicted chip thickness and tool/chip contact length values were found to vary with cutting conditions for the aluminum AA7075-T651, while an overestimation of these parameters were found for the hardened AISI 4340 steel. The low ductility of these alloys induces the formation of segmented chips which can affect chip thickness and chip/tool contact length. This mechanism of segmentation was not yet incorporated in the present version of the proposed predictive model.

5.4.3 Effects on C_0 and δ values

The various prediction procedures used in this study resulted in different values of the strain rate constants C_0 and δ. Hence, it is worthwhile investigating how the choice of these parameters affects the predicted values for the cutting conditions and work materials studied in the present paper.

The strain rate constants C_0 values obtained from the Oxley machining theory as a part of solution for high cutting speed and/or feed were ranging between 1.9 and 2.1; and between 6.2 and 7 for aluminums AA6061-T6 (Table 5-7) and AA7075-T651 (Table 5-8), respectively. For the test simulated by the iterative method (low cutting speed and/or feed tests), the strain rate constants C_0 values were ranging between 0.1 - 1.3, and between 0.1 - 0.19 for the aluminums AA6061-T6 and AA7075-T651, respectively.

On the other hand, the strain rate constants δ obtained for high cutting speeds and/or feeds were ranging between 0.02 - 0.03 and between 0.01 - 0.06 for the aluminums AA6061-T6 and AA7075-T651, respectively. These values are similar to the experimental value (0.031) obtained for aluminum alloys (Kristyanto et al., 2002) that was set for the low cutting speeds and feeds. This confirms that the adopted constitutive equation and the proposed predictive model are capable to estimate properly the experimental machining data values.

Surprisingly, the strain rate constants C_0 values, obtained when predicting machining data for AA7075-T651 from Sheikh-Ahmad and Twomey (2007) (see Table 5-6) at high cutting speeds and/or feeds, are lower than those predicted for machining tests performed in the present work (Table 5-3). They were found to be ranged between 3-3.7. We recall here that for AA60621-T6 from (Guo, 2003) neither high cutting speeds nor high feed rates were used.

For low cutting speed and/or feed conditions, the strain rate constants C_0 were ranging between 0.1 - 1.2 and 8.2 - 10 for AA7075-T651 from (Sheikh-Ahmad and Twomey, 2007) and for AA60621-T6 from (Guo, 2003) (Table 6-5), respectively.

The rake angles used to obtain machining data from the literature were different from that used in the present work: +6 degree for the machining tests done on AA6061-T6 from (Guo, 2003) (Table 5-5) and 0 degree for AA7075-T651 from (Sheikh-Ahmad and Twomey, 2007), compared to -5 degree used in the present machining tests (Table 5-3). The rake angles can significantly influence the shear zone thickness (Kececioglu, 1958), which can explain the difference of the strain rate constant C_0 values obtained for the machining tests performed in

the present work and those from the literature. This result may illustrate the high sensitivity of the proposed model to the actual cutting conditions. It is well known that the strain rate in the primary shear zone depends significantly on the rake angle (Equation 5-7); thus, the sensitivity of the proposed model to the rake angle could indirectly be a consequence of the sensitivity of the Marusich's constitutive equation to strain.

Although the observed discrepancies, the general trend of the obtained results in terms of C_0 showed that this value do not significantly vary for the aluminums AA6061-T6 and AA7075-T651 at low cutting speeds and/or cutting feed. This shows that these alloys are not sensitive to strain rate as the strain rate $\dot{\gamma}_{AB}$ in the primary shear zone is directly proportional to C_0 (Eq.9). These results are in agreement with those found by Kristyanto et *al.* (2002) in the case of turning for aluminum alloys. On the other hand, the calculated C_0 at high cutting speed and /or feed were found to be 3 to 4 times those calculated at low cutting speed and/or feed conditions, showing that the hardened AISI 4340 steel is less sensitive to the strain rate at low cutting speed and/or feed.

In order to better understand the sensitivity of the proposed model to the strain rate constants, the variations of the cutting force with regard to the possible variation of the strain rate constants C_0 and δ were documented. In this case study, we will focus on the low cutting speed conditions for which the strain rate constants δ was fixed at the experimental value 0.031from (Kristyanto et al., 2002) and the constants C_0 were obtained iteratively for the best agreement between the calculated and measured cutting forces. The cutting conditions relative to Test#6 for the aluminum AA7075-T651 in the present experimental campaign (Table 5-3) was selected as an example of this case study. First, we calculated the cutting forces for δ equal to 0.031 (Figure 5-15). Second, we calculated the cutting forces over a range of possible strain rate δ at a fixed C_0 (C_0 resulting for the best agreement between calculated and measured cutting force) (Figure 5-16).

Figure 5-15 shows that the calculated forces vary only slightly in the tested range of the strain rate constants C_0 and the lowest error between calculated and measured forces was

found at C_0 equal to 0.19. The variations (around +20 N) are actually in the range of the discrepancy between the proposed (724 N) and measured (680N) ones; the proposed value from the model being the one that minimize the latter discrepancy, however, other values of C_0 could lead to acceptable values of the cutting force.

The sensitivity of the cutting force to the variation of the strain rate constant δ at C_0 equal to 0.19 is shown in Figure 6-16. Again, the variation of the calculated cutting force is relatively low and it is negligible from δ value around 0.03 which is in agreement with the experimental value (0.031) adopted from Kristyanto et al.(2002).

The sensitivity analysis illustrate that the proposed iterative methodology used for low cutting speed and/or feed conditions leads to consistent results in terms of both cutting forces and strain rate constants. Nevertheless, a comprehensive study should be carried out in order to estimate accurately the thicknesses of the primary and secondary shear zones and how these thicknesses are actually affected by the cutting conditions. This would provide a reliable validation of the Oxley's machining theory using Marusich's constitutive equation for large range of cutting conditions and materials.

It is well known that state variables such as local strains, strain rates, and temperatures depend significantly on the material properties. Thus, it is worthwhile to discuss the observed trends of predicted data from the material constitutive equation point of view. In the present study, the analytical model systematically underestimates the cutting forces when the fully predictive approach was applied to low cutting speed and /or feed. In fact, the stepwise variation of the strain rate sensitivity coefficients in Marusich's equation for low and high strain rates (as displayed in Table 5-4) can explain such underestimations. For lower strain rates ($\dot{\varepsilon}_p < 10^4$) the strain rate sensitivity coefficient was determined using dynamic tests which are far from representing the actual behaviour of the work material during machining (Fang, 2005). This may underestimate the actual value of this parameter and result in a lower cutting force.

On the other hand, for typical strain rates encountered in high speed machining ($\dot{\varepsilon}_p > 10^4$), the strain rate sensitivity coefficient of Marusich's equation (Equation 5.1b) was determined using machining tests in Chapter 4, leading to a better estimation of the calculated flow stress. In these conditions, the proposed model was able to predict accurately the cutting forces and realistic strain rate constants δ at C_0 were obtained as part of the solutions.

Moreover, the implementations the cutting edge radius make the proposed model capable of predicting cutting forces over a wide range of high speed machining conditions using near-sharp and honed edge tools.

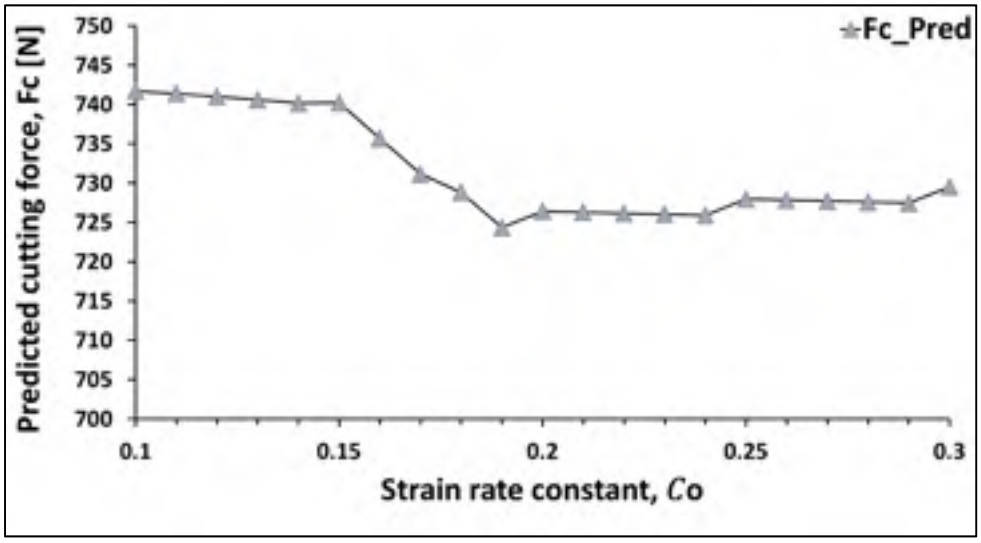

Figure 5-15 Sensitivity of the predicted cutting force to the strain rate constant C_0 for Tests#6 (AA7075-T651) and δ =0.031

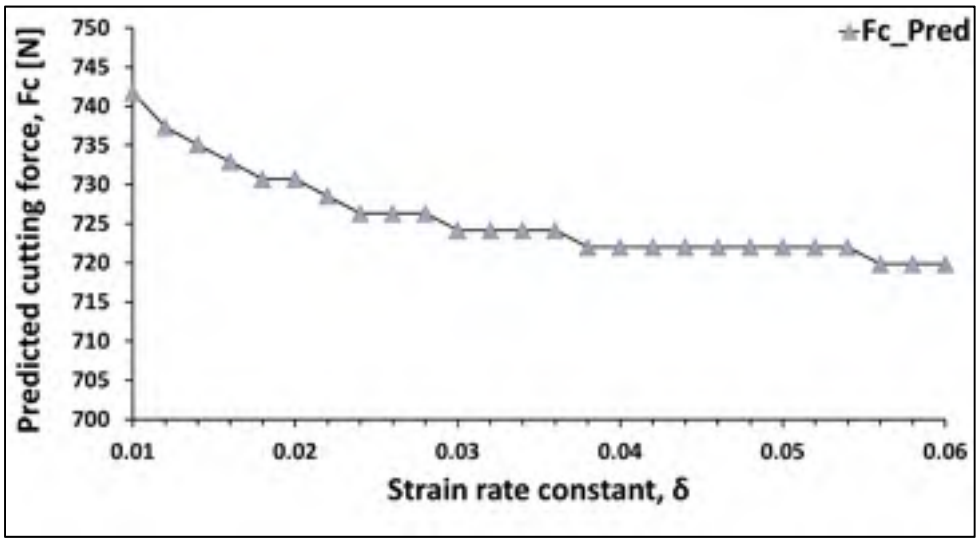

Figure 5-16 Sensitivity of the predicted cutting force to the strain rate constant δ for Tests#6 (AA7075-T651) and C_0=0.19

5.5 Conclusions

In this paper, Oxley machining theory was generalized for high speed machining using near-sharp and honed cutting tool edges. The concept of "variable rake angle" was used in the proposed modelling. The material tested were aluminums AA6061-T6 and AA7075-T651 and induction hardened AISI4340 steel (60 HRC). Marusich's constitutive equation was used to describe material behaviour and the proposed model was able to converge and predicted well the cutting forces, especially at high cutting speeds. However, for low cutting speed cutting conditions, specific prediction procedure was applied to reduce the discrepancy between prediction and measured cutting forces by imposing a strain rate constant from literature. The obtained predicted results attested that the behaviour, of materials with so different mechanical characteristics (ductility, hardness) in high speed machining were successfully described using the Marusich's constitutive equation. The primary strain rate constants C_0 were found to be sensitive to the cutting conditions in agreement with the literature. Furthermore, a sensitivity analysis showed that the predicted results are in good agreement with experiments in terms of the strain rate constants obtained in the machining of aluminum alloys. On the other hand, some discrepancies were obtained in the predicted chip thickness and chip/tool contact length. This was attributed to physical phenomena such as

built-up edge formation and/or segmented chip formations during machining which were not considered in the proposed model. Further investigation should be addressed to the applied friction model in order to improve the predicted data. Extensive experimental data of primary and secondary shear zone thicknesses are needed to validate further the Oxley's approach.

CONCLUSIONS

The current research work addressed a comprehensive investigation on materials behaviour in high speed machining of some high strength aluminum alloys (AA6061-T6, AA7075-T651) and induction hardened AISI 4340 steel used in structural aeronautic components. This investigation involved the characterization of the surface integrity of the machined surfaces and chip formation during machining. For the experimental investigation, the focus was on the establishment of relationships among the surface integrity characteristics (surface finish, residual stress, microhardness, and microstructure), technological parameters (cutting speed and feed rate), and machining data (cutting forces, cutting temperatures, chip thickness, etc.). The machining tests were carried out under orthogonal cutting conditions with varied cutting speeds and feed rates. The cutting conditions were selected to cover a wide range of cutting speed and ratio of the uncut chip thickness to the tool cutting edge radius.

Observing the experimental results, it was argued that the surface integrity characteristics can be related directly to the machining data such as cutting forces, shear and friction angles, and cutting temperature. The prediction of such quantities is of great importance and could help in understanding the mechanisms of surface alterations over a wide range of machining conditions.

The prediction of surface integrity characteristics of machined surfaces can be achieved only through the prediction of cutting forces and temperature during the chip formation. Since advanced machining modeling using analytical and finite elements methods requires a suitable constitutive equation, we proposed, firstly, a methodology for the identification of a selected constitutive equation (Marusich's equation). The coefficients of this equation were determined using a hybrid method which is based on orthogonal machining tests and dynamic tests. The obtained material models were successfully validated and implemented in finite element simulations of the orthogonal machining of aluminums (AA6061-T6 and AA7075-T651) and an induction hardened AISI 4340 steel using Deform 2D software.

Secondly, the developed material models were used to generalize Oxley's machining theory to the high speed machining of aluminum alloys and hardened steels through an analytical predictive modelling of cutting forces. The proposed model is fully predictive and needs only cutting conditions (speed, feed and depth of cut), work material properties, and cutting tool geometry (rake angle and edge radius) as inputs. Cemented carbide (WC) inserts and mixed ceramic inserts were used in the machining of the aluminum alloys (AA6061-T6 and AA7075-T651) and the induction hardened 4340 steel, respectively. All the machining experiments were carried out in dry condition. We selected these materials in an attempt to provide a comprehensive study for the machining of metals with different behaviours (ductile and hard material). Chapters 3 and 4 were devoted to a comprehensive experimental investigation on the effect of cutting conditions on the chip formation and surface integrity in high speed machining of aluminum alloys and hardened steel, respectively. In chapter 5, we proposed a methodology to identify the Marusich's constitutive equation for the tested materials in order to predict the material behaviour under high speed machining conditions. Finally, the obtained material model in chapter 5, were implemented in a predictive analytical model for cutting forces and temperature. The proposed predictive analytical model is an extension of Oxley's machining theory to the high speed machining of ductile and hardened materials.

In sight of the obtained results, the main conclusions may be drawn as:

i) Surface integrity characteristics in dry high speed machining of high strength aluminum alloys

The orthogonal cutting configuration was used for the first time to highlights the tool/workpiece interaction and its effects on surface finish and residual stress state in machining aluminum AA7075-T651. Based on the experimental results, we demonstrated that the formation of built-up edge (BUE) was intensified by an increase in the cutting feed; however, an increase in the cutting speed reduced it and promoted the formation of the built-up layer (BUL) on the rake face. SEM and EDS analyses showed that the primary origin of

surface damage was the interaction between the tool edge and the iron-rich intermetallic phases present within the work material matrix. By controlling the cutting speed and feed, it is possible to generate a benchmark residual stress state and good surface finish which can improve the in-service life of structural parts made of aluminum alloys.

ii) Hard Machining of Induction Hardened AISI 4340 Steel (58-60 HRC)

Excessive induction hardening treatment was found to result in deep hardened layers with related low compressive residual stress which may affect the performance of the induction heat treated parts. However, a judicious selection of the finishing process that eventually follows the surface treatment may overcome this inconvenient. To illustrate this, dry orthogonal machining of induction hardened AISI 4340 steel (58-60 HRC) using mixed ceramic inserts, was performed in this work. The machining of induction hardened 4340 steel (60HRC) at lower cutting feed induces low shearing angles leading to continuous chip formation and smooth surface finish with very few chatter marks. On the other hand, the machining at high cutting feed results in high shearing angles and segmented chips. The formation of segmented chips indicated that the cutting was taking place by brittle fracture rather than by shearing and this is a characteristic behaviour when machining hard materials. Surface damages and chatter marks on the machined surface can actually be related to the amplitude of vibration rises due to the formation of these segmented chips. High compressive residual stress levels at and below the machined surface were produced. The residual stress distribution is strongly affected by the cutting feed and the cutting speed. The surface residual stress tends to become tensile when the cutting speed is increased. On the other hand, an increase in cutting feed accentuates surface damage whilst it increases compressive surface residual stress. Microstructural analysis shows the formation of a thin white layer less than 2μm under a workpiece surface temperature below the phase transformation temperature of the 4340 steel (800 °C for the typical heating rates reached during cutting operations). This result is in agreement with those obtained in previous works. The hard machining using mixed ceramic tools improves the surface condition of induction hardened components which can improve their performance and fatigue life.

iii) Prediction of the Material Behaviour in High Speed Metal Cutting Process

A methodology for identifying the coefficients of Marusich's constitutive equation (MCE), which demonstrated a good capability for the simulation of the material behaviour in high speed machining, has been developed. The proposed approach, which is based on an analytical inverse method together with dynamic tests, was applied to aluminums AA6061-T6 and AA7075-T651, and induction hardened AISI 4340 steel (60HRC). The response surface methodology (RSM) was also used in this approach. Two sets of material coefficients, for each work material, were determined using two different temperature models (Oxley and Loewen-Shaw). The obtained constitutive equations were validated using dynamic tests and finite element (FE) simulation of high speed machining. A sensitivity analysis revealed that the selected temperature model used in the analytical inverse method affects significantly the identified material constants and thereafter predicted dynamic response and machining modeling. In general, material constants obtained using Oxley temperature model was performed better than those obtained using Loewen-Shaw model for the tested conditions and work materials.

iv) Predictive analytical modeling for high speed machining of ductile and hard materials

Oxley's machining theory, which is considered as the most fundamental approach in analytical modeling of the machining process, was generalized to the high speed machining of aluminum alloys and hardened steel using Marusich constitutive equation. The proposed model was successfully used in predicting cutting forces in machining with near-sharp and honed cutting edges and an encouraging good agreement has been found between prediction and experiments.

SUBSTANTIAL CONTRIBUTIONS

The main contributions achieved in the present study can be summarized as:

- The identification of two mechanisms controlling the surface damage during machining of AA7075-T651: interactions between hard intermetallic and build-up-edge on the cutting tool.

- The highlights of the machining conditions leading to brittle fracture in machining hardened 4340 steel;

- The establishment of a relationship between the chip formation, the white layer formation, and the residual stress when machining induction hardened 4340 steel;

- The development of a new procedure based on machining and dynamic tests data for the identification of Marusich's constitutive equation. This is very important for finite element modeling of high speed machining of aluminum alloys and hardened steels;

- The emphasis of the importance of the cutting temperature model selection when material coefficients are determined inversely from machining tests (inverse method);

- The generalization of Oxley machining theory to the high speed machining of aluminum alloys and hardened steel using of Marusich's constitutive equations, honed cutting edges and variable rake angle.

RECOMENDATIONS

In the present work, some of the obtained results can be further improved by using additional instruments and characterization techniques.

For the experimental part, we recommend the following methods:

- XRD texture analysis and nano-indentation measurements to evaluate, precisely, the work harden/softened layer after high speed machining.
- The Measurement of residual austenite to confirm the phase transformation accompanied with the white layer formation during hard machining.
- Quick-stop tests to demonstrate the effect of the intermetallic particles on the cutting mechanisms during machining high strength aluminum alloys.

For the theoretical part, we propose the following points:

- For the identification of material constants, we suggested to use analytical models adapted for segmented chip formation for the calculation of machining data (flow stress, strain, strain rate, and temperature).
- The friction model should be revised to improve the actual predictive model for cutting forces.
- Take account for ploughing forces.

Considering the cutting condition ranges used in this study, it is worth noticed that the experimental results and the proposed predictive modelling in the present work can be extended to investigate 3D machining (turning, milling, and drilling) and also micro-machining processes.

APPENDIX I

CUTTING TEMPERATURE MODEL FOR HARD MACHINING OF AISI 4340 STEEL USING HONED CUTTING EDGE TOOL

Three sources of heat generation were depicted in the cutting zone during machining: the primary shear zone, PSZ (Zone I), the secondary shear zone, SSZ (zone II) and the tertiary shear zone, TSZ (zone III) as shown in Fig. A.1. Hence, the workpiece temperature and the chip temperature are the results of the interaction between these heating sources (Huang et Liang, 2003a). The physical properties of the work material and the tool insert used in the experiments are summarised in Table A.1.

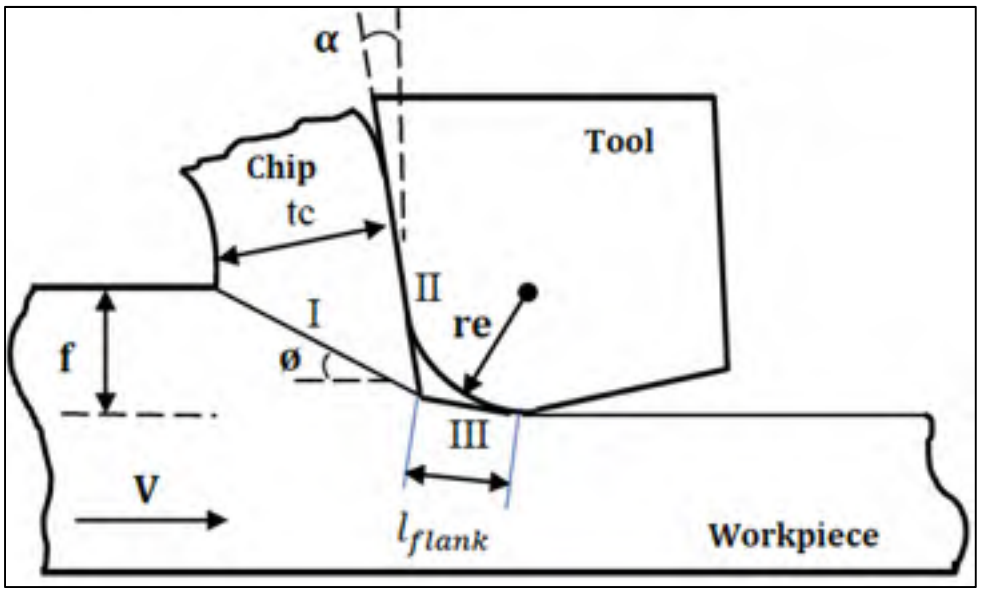

Fig. A.1 Geometry of the cutting zone

Table A.1 Properties of the work material and tool insert

Material	Workpiece AISI 4340 (Feng et Bassim, 1999)	Tool insert Mixed ceramic (Al2O3/TiCN) (Brito et al., 2009)
ρ (Kg/m3)	7830	4650
K (W/m°C)	54	21
Cp(J/kg°C)	465	645

a) Chip temperature, T_{chip}

The temperature rise on the chip can be written as (Huang et Liang, 2003a):

$$T_{chip} = T_{prim} + T_{int} + T_0 \quad \text{(A I-1)}$$

where T_{AB} and T_{int} were given in (Loewen et Shaw, 1954) as:

$$T_{prim} = 0.754 \frac{(1 - R_1) q_{shear} f \csc(\emptyset)}{2 D_w \sqrt{L_1}} \quad \text{(A I-2)}$$

and

$$T_{int} = 0.377 \frac{R_2 q_{int} lc}{K_w \sqrt{L_2}} \quad \text{(A I-3)}$$

b) Workpiece temperature, $T_{workpiece}$

The temperature rise on the machined surface can be written as (Huang et Liang, 2003a):

$$T_{workpiece} = T_{AB} + T_{rubbing} + T_0 \quad \text{(A I-4)}$$

The Temperature rise on the machined surface due to rubbing, $T_{rubbing}$, will be estimated here based on moving rectangular heat source (tool) of uniform strength moving over a semi-infinite body (workpiece). The $T_{rubbing}$ is determined as:

$$T_{rubbing} = (1 - R)\frac{q_{rubbing} l_{flank} A}{D_w} \quad \text{(A I-5)}$$

where

$$q_{rubbing} = \frac{F_r V}{w l_{flank}} \quad \text{(A I-6)}$$

is the heat intensity of rubbing heat source along the tool/workpiece interface (Huang et Liang, 2003a). The rubbing force,F_r, is computed based on the slip-line field method as proposed by Waldorf et al. (Waldorf, 2006):

$$F_r = \tau_{ter} w r_e \tan\left(\frac{\pi}{4} + \frac{\alpha}{2}\right) \quad \text{(A I-7)}$$

Waldorf et al (Waldorf, DeVor et Kapoor, 1999) showed the evidence of a stable build-up edge formation in machining with negative-rake machining. According to Waldorf et al. (Waldorf, DeVor et Kapoor, 1998), the length of the lower interface between the tool (build-up region) and the work l_{flank} (Figure 29), is defined as:

$$l_{flank} = r_e \tan\left(\frac{\pi}{4} + \frac{\alpha}{2}\right) \quad \text{(A I-8)}$$

and

$$K_{ter} = m K_{AB} \quad \text{(A I-9)}$$

Where K_{AB} is the material shear flow stress which is assumed equal to the shear stress developed on the primary shear zone (Waldorf, DeVor et Kapoor, 1999):

$$K_{AB} = \frac{F_c \cos \emptyset - F_t \sin \emptyset}{wf} \sin \emptyset \quad \text{(A I-10)}$$

APPENDIX II

EXTENSION OF THE OXLEY'S MACHINING THEORY USING THE MARUSICH'S CONSTITUTIVE EQUATION

In this section, we presents the extension of Oxley's machining theory to the machining of aluminum alloys and hardened steel using the Marusich's constitutive equation. The stresses in the primary shear zone were analysed and a modified equation for the resultant force direction (θ) was developed.

In the slip-line field analysis, Oxley and Hastings (Oxley and Hastings, 1977) showed that the plan AB as shown in Figure 6-1 is considered as an α-slip-line and the variation of the hydrostatic stress (p) along it is given by:

$$\frac{\partial p}{\partial s_1} + 2k\frac{\partial \Psi}{\partial s_1} - \frac{\partial k}{\partial s_2} = 0 \qquad \text{(A II-1)}$$

where s_1 and s_2 are distances measured along and normal to the slip-lines, respectively, k is the shear flow stress of the work material, and Ψ is the anticlockwise angular rotation of the I slip-line from a fixed reference axis. From the stress distributions along AB, θ can be calculated as (Oxley and Hastings, 1977):

$$tan\theta = \frac{p_A + p_B}{2k_{AB}} \qquad \text{(A II-2)}$$

where p_A and p_B are the hydrostatic stress at A and B. p_A can be estimated as (Oxley and Hastings, 1977):

$$p_A = k_{AB}\left[1 + 2\left(\frac{1}{4}\pi - \emptyset\right)\right] \qquad \text{(A II-3)}$$

On the other hand, p_B can be calculated from the change of the stress along AB from the stress equilibrium equation (Oxley and Hastings, 1977):

$$p_A - p_B = l_{AB}\frac{dk_{AB}}{ds_2} \tag{A II-4}$$

By neglecting any strain rate and temperature gradients on AB, the term $\frac{dk_{AB}}{ds_2}$ can be written as:

$$\frac{dk_{AB}}{ds_2} = \frac{dk_{AB}}{d\gamma_{AB}}\frac{d\gamma_{AB}}{dt}\frac{dt}{ds_2} \tag{A II-5}$$

where $\frac{d\gamma_{AB}}{dt}$ is calculated as:

$$\frac{d\gamma_{AB}}{dt} = C_0\frac{Vcos\alpha}{l_{AB}cos(\emptyset - \alpha)} \tag{A II-6}$$

and

$$\frac{dt}{ds_2} = \frac{1}{Vsin\alpha} \tag{A II-7}$$

Based on the Marusich constitutive equation (Equation 6.1) and the Von-Mises criterion, the shear stress on AB, k_{AB}, is given as:

$$k_{AB} = \frac{1}{\sqrt{3}}[1 - \alpha_{NL}(T_{AB} - T_0)]\sigma_0\left(1 + \frac{\varepsilon_{AB}}{\varepsilon_0}\right)^{\frac{1}{n_{NL}}}\left(1 + \frac{\dot{\varepsilon}_{AB}}{\dot{\varepsilon}_0}\right)^{\frac{1}{m_1}} \tag{A II-8}$$
$$if\ \ \dot{\varepsilon}_{AB} < \dot{\varepsilon}_t$$

$$k_{AB} = \frac{1}{\sqrt{3}}[1 - \alpha_{NL}(T_{AB} - T_0)]\sigma_0\left(1 + \frac{\varepsilon_{AB}}{\varepsilon_0}\right)^{\frac{1}{n_{NL}}}\left(1 + \frac{\dot{\varepsilon}_{AB}}{\dot{\varepsilon}_0}\right)^{\frac{1}{m_2}}\left(1 + \frac{\dot{\varepsilon}_t}{\dot{\varepsilon}_0}\right)^{\frac{1}{m_1}-\frac{1}{m_2}} \tag{A II-9}$$
$$if\ \ \dot{\varepsilon}_{AB} > \dot{\varepsilon}_t$$

so, the derivation of Equations A II-8 and A II-9 regarding γ_{AB} led to:

$$\frac{dk_{AB}}{d\gamma_{AB}} = \frac{\sigma_{AB}}{3n_{NL}(\varepsilon_0 + \varepsilon_{AB})} \tag{A II-10}$$

and, therefore

$$\frac{dk_{AB}}{ds_2} = \frac{2C_0 k_{AB}\varepsilon_{AB}}{n_{NL}(\varepsilon_0 + \varepsilon_{AB})l_{AB}} \tag{A II-11}$$

substituting Equations A II-3 and A-II-11 into Equation A II-4 we have

$$p_B = k_{AB}\left[1 + 2\left(\frac{1}{4}\pi - \emptyset\right)\right] - \frac{2C_0 k_{AB}\varepsilon_{AB}}{n_{NL}(\varepsilon_0 + \varepsilon_{AB})} \tag{A II-12}$$

substituting Equations A II-3 and A II-12 into Equation A II-2 yield to

$$tan\theta = 1 + 2\left(\frac{1}{4}\pi - \emptyset\right) - \frac{C_0\varepsilon_{AB}}{n_{NL}(\varepsilon_0 + \varepsilon_{AB})} \tag{A II-13}$$

LIST OF REFERENCES

Abdullah, A. 1996. « Machining of aluminium based metal matrix composite (MMC) ». PhD, University of Warwick.

Abed, F., and Fadi M. 2012. « Comparisons of Constitutive Models for Steel Over a Wide Range of Temperatures and Strain Rates ». *Journal of Engineering Materials and Technology,* vol. 134, n° 2, p. 021001-021001.

Abou-El-Hossein, K., Neethling, J., and Olufayo, O. 2013. « Ultra-High Precision Machining of Modified High Strength Aluminium for Optical Mould Inserts ». In *International Conference on Competitive Manufacturing (COMA'2013)*. (Stellenbosch University, January 30, 2013 – February 1, 2013).

Abrão, Alexandre M., and Aspinwall, D.K.. 1996. « The surface integrity of turned and ground hardened bearing steel ». *Wear,* vol. 196, n° 1–2, p. 279-284.

Adibi, S., Amir H, Vis Madhavan, and Behnam B. 2003. « Extension of Oxley's analysis of machining to use different material models ». *transactions-american society of mechanical engineers journal of manufacturing science and engineering,* vol. 125, n° 4, p. 656-666.

Ammula, S.C., and Y.B. Guo. 2005. « Surface Integrity of Al 7050-T7451 and Al 6061-T651 Induced by High Speed Milling ». In. SAE Technical Paper, No.2005-01-3346.

Astakhov, V. P. 2006. *Tribology of Metal Cutting, Volume 52*. Elsevier.

Astakhov, V. P., S. V. Shvets and M. O. M. Osman. 1997a. « Chip structure classification based on mechanics of its formation ». *Journal of Materials Processing Technology,* vol. 71, n° 2, p. 247-257.

Astakhov, VP, SV Shvets and MOM Osman. 1997b. « Chip structure classification based on mechanics of its formation ». *Journal of Materials Processing Technology,* vol. 71, n° 2, p. 247-257.

Bailey, J. A., and Jeelani, S. 1976. « Determination of subsurface plastic strain in machining using an embossed grid ». *Wear,* vol. 36, n° 2, p. 199-206.

Bailey, John A. 1977. « Surface damage during machining of annealed 18% nickel maraging steel Part 1 — Unlubricated conditions ». *Wear,* vol. 42, n° 2, p. 277-296.

Bandyopadhyay, B. P. 1984a. « Mechanism of formation of built-up edge ». *Precision Engineering,* vol. 6, n° 3, p. 148-151.

Bandyopadhyay, BP. 1984b. « Mechanism of formation of built-up edge ». *Precision Engineering,* vol. 6, n° 3, p. 148-151.

Barry, J, and G Byrne. 2002a. « TEM study on the surface white layer in two turned hardened steels ». *Materials Science and Engineering: A,* vol. 325, n° 1, p. 356-364.

Barry, J., and G. Byrne. 2002b. « TEM study on the surface white layer in two turned hardened steels ». *Materials Science and Engineering: A,* vol. 325, n° 1–2, p. 356-364.

Barry, John, and Gerald Byrne. 2002c. « The mechanisms of chip formation in machining hardened steels ». *Journal of Manufacturing Science and Engineering,* vol. 124, n° 3, p. 528-535.

Barter, SA, PK Sharp, G Holden and G Clark. 2002. « Initiation and early growth of fatigue cracks in an aerospace aluminium alloy ». *Fatigue & Fracture of Engineering Materials & Structures,* vol. 25, n° 2, p. 111-125.

Becze, C. E. 2002. « A chip formation based analytic force model for oblique cutting ». *International journal of machine tools & manufacture,* vol. 42, n° 4, p. 529-538.

Bil, H., Kılıç, S., and Tekkaya A.E. 2004. « A comparison of orthogonal cutting data from experiments with three different finite element models ». *International Journal of Machine Tools and Manufacture,* vol. 44, n° 9, p. 933-944.

Boothroyd, Geoffrey. 1988. *Fundamentals of metal machining and machine tools*, 28. CRC Press.

Brinksmeier, E., J. T. Cammett, W. König, P. Leskovar, J. Peters and H. K. Tönshoff. 1982. « Residual Stresses — Measurement and Causes in Machining Processes ». *CIRP Annals - Manufacturing Technology,* vol. 31, n° 2, p. 491-510.

Brito, R.F, De Carvalho, S.R., Silva, S.M. and Ferreira, J.R. 2009. « Thermal analysis in coated cutting tools ». *International Communications in Heat and Mass Transfer,* vol. 36, n° 4, p. 314-321.

Cai, X.J., Ming, W.W. and Chen, M. 2012a. « Surface integrity analysis on high speed end milling of 7075 aluminium alloy ». *Advanced Materials Reaserch,* vol. 426, p. 321-324.

Cai, X.J., Ming, W.W. and Chen, M. 2012b. « Surface Integrity Analysis on High Speed End Milling of 7075 Aluminum Alloy ». *Advanced Materials Research,* vol. 426, p. 321-324.

Campbell, CE, Bendersky, L.A., Boettinger, W.J., and Ivester, R. 2006. « Microstructural characterization of Al-7075-T651 chips and work pieces produced by high-speed machining ». *Materials Science and Engineering: A,* vol. 430, n° 1, p. 15-26.

Capello, E. 2005. « Residual stresses in turning: Part I: Influence of process parameters ». *Journal of Materials Processing Technology,* vol. 160, n° 2, p. 221-228.

Carrilero, M. S., Bienvenido, R., Sánchez, J.M., Álvarez M., González A., and Marcos, M. 2002. « A SEM and EDS insight into the BUL and BUE differences in the turning processes of AA2024 Al–Cu alloy ». *International Journal of Machine Tools and Manufacture,* vol. 42, n° 2, p. 215-220.

Chandrasekaran, H., and M'Saoubi, R. 2006. « Improved machinability in hard milling and strategies for steel development ». *Cirp Annals-Manufacturing Technology,* vol. 55, n° 1, p. 93-96.

Chaussumier, M., Mabru, C., Shahzad, M., Chieragatti, R. and Rezai-Aria F. 2013. « A predictive fatigue life model for anodized 7050 aluminium alloy ». *International Journal of Fatigue,* vol. 48, p. 205-213.

Chou, Y.K. 2002. « Surface hardening of AISI 4340 steel by machining: a preliminary investigation ». *Journal of materials processing technology,* vol. 124, n° 1, p. 171-177.

Chou, Y.K., and Song, H.. 2005. « Thermal modeling for white layer predictions in finish hard turning ». *International Journal of Machine Tools and Manufacture,* vol. 45, n° 4, p. 481-495.

Çiçek, A., Kara, F., Kivak, T. andt Ekici E. 2013. « Evaluation of machinability of hardened and cryo-treated AISI H13 hot work tool steel with ceramic inserts ». *International Journal of Refractory Metals and Hard Materials,* vol. 41, n° 0, p. 461-469.

Dahlman, P., Gunnberg, F. and Jacobson, M. 2004. « The influence of rake angle, cutting feed and cutting depth on residual stresses in hard turning ». *Journal of Materials Processing Technology,* vol. 147, n° 2, p. 181-184.

Davim, J.P., 2010. *Surface Integrity in Machining*. Springer Verlag.

Denkena, B., Boehnke, D., and De Léon, L. 2008. « Machining induced residual stress in structural aluminum parts ». *Production Engineering,* vol. 2, n° 3, p. 247-253.

Dhar, N. R., Kamruzzaman M., and Ahmed, M. 2006. « Effect of minimum quantity lubrication (MQL) on tool wear and surface roughness in turning AISI-4340 steel ». *Journal of Materials Processing Technology,* vol. 172, n° 2, p. 299-304.

Dogra, M., Sharma, V.S., and Dureja, J. 2011. « Effect of tool geometry variation on finish turning–A Review ». *Journal of Engineering Science and Technology Review,* vol. 4, n° 1, p. 1-13.

Dogra, M., Sharma, V.S., Narinder, A.S., and Dureja, J.S. 2010. « Tool wear, chip formation and workpiece surface issues in CBN hard turning: A review ». *International Journal of Precision Engineering and Manufacturing,* vol. 11, n° 2, p. 341-358.

El-Wardany, T.I., Mohammed, E.and Elbestawi, M.A. 1996. « Cutting temperature of ceramic tools in high speed machining of difficult-to-cut materials ». *International Journal of Machine Tools and Manufacture,* vol. 36, n° 5, p. 611-634.

Elkhabeery, M. M., and Bailey, J.A. 1984. « Surface Integrity in Machining Solution-Treated and Aged 2024-Aluminum Alloy, Using Natural and Controlled Contact Length Tools. Part I—Unlubricated Conditions ». *Journal of Engineering Materials and Technology,* vol. 106, n° 2, p. 152-160.

Ezugwu, E.O., Wang, Z.M., and Okeke, C.I. 1999. « Tool life and surface integrity when machining Inconel 718 with PVD- and CVD-coated tools ». *Tribology Transactions,* vol. 42, n° Compendex, p. 353-360.

Fang, N. 2005. « A new Quantitative sensitivity analysis of the flow stress of 18 engineering materials in machining ». *Journal of engineering materials and technology,* vol. 127, n° 2, p. 192-196.

Feng, H., and Bassim, M.N. 1999. « Finite element modeling of the formation of adiabatic shear bands in AISI 4340 steel ». *Materials Science and Engineering: A,* vol. 266, n° 1–2, p. 255-260.

Field, M., and Kahles, J.F. 1964. « the surface integrity of machined and ground high strength steels ». *DMIC Report,* vol. 2010, n° 54-77, p. 54-60.

Filice, L, Micari, F., Rizzuti, S. and Umbrello, D. 2007. « A critical analysis on the friction modelling in orthogonal machining ». *International Journal of Machine Tools and Manufacture,* vol. 47, n° 3, p. 709-714.

Gadelmawla, E.S., Koura, M.M., Maksoud, T.M.A., Elewa, I.M., and Soliman, H.H. 2002. « Roughness parameters ». *Journal of Materials Processing Technology,* vol. 123, n° 1, p. 133-145.

Gaitonde, V.N., Karnik, S.R., Figueira, L. and Davim, J.P. 2009. « Machinability investigations in hard turning of AISI D2 cold work tool steel with conventional and wiper ceramic inserts ». *International Journal of Refractory Metals and Hard Materials,* vol. 27, n° 4, p. 754-763.

Gangopadhyay, S., Acharya, R., Chattopadhyay, A.K. and Sargade, V.G. 2010. « Effect of cutting speed and surface chemistry of cutting tools on the formation of BUL or BUE and surface quality of the generated surface in dry turning of AA6005 aluminium alloy ». *Machining Science and Technology,* vol. 14, n° 2, p. 208-223.

Gómez-Parra, A., Álvarez-Alcón, M., Salguero, J., Batista, M. and Marcos, M. 2013. « Analysis of the evolution of the Built-Up Edge and Built-Up Layer formation mechanisms in the dry turning of aeronautical aluminium alloys ». *Wear,* vol. 302, n° 1–2, p. 1209-1218.

Griffiths, B. 2001. *Manufacturing surface technology: surface integrity and functional performance*. Elsevier.

Grum, J. 2007. « Influence of various induction-heating and grinding conditions on residual stress profiles ». *International journal of microstructure and materials properties,* vol. 2, n° n 3-4, p. 301-325.

Grum, J. 2000. « Measuring and Analysis of Residual Stresses After Induction Hardening and Grinding ». *, Materials Science Forum,* vol. 453, p. 347-349.

Grum, J. 2001. « A review of the influence of grinding conditions on resulting residual stresses after induction surface hardening and grinding ». *Journal of Materials Processing Technology,* vol. 114, n° 3, p. 212-226.

Grzesik, W. 2009. « Wear development on wiper Al2O3–TiC mixed ceramic tools in hard machining of high strength steel ». *Wear,* vol. 266, n° 9–10, p. 1021-1028.

Grzesik, W., and Wanat, T. 2005. « Comparative assessment of surface roughness produced by hard machining with mixed ceramic tools including 2D and 3D analysis ». *Journal of Materials Processing Technology,* vol. 169, n° 3, p. 364-371.

Grzesik, W., et T. Wanat. 2006. « Surface finish generated in hard turning of quenched alloy steel parts using conventional and wiper ceramic inserts ». *International Journal of Machine Tools and Manufacture,* vol. 46, n° 15, p. 1988-1995.

Grzesik, W. 2008. *Advanced machining processes of metallic materials: theory, modelling and applications*. Elsevier.

Guo, Y. B., et Sahni, J. 2004. « A comparative study of hard turned and cylindrically ground white layers ». *International Journal of Machine Tools and Manufacture,* vol. 44, n° 2–3, p. 135-145.

Guo, Y.B., Warren, A.W. and Hashimoto, F. 2010. « The basic relationships between residual stress, white layer, and fatigue life of hard turned and ground surfaces in rolling contact ». *CIRP Journal of Manufacturing Science and Technology,* vol. 2, n° 2, p. 129-134.

Guo, YB. 2003. « An integral method to determine the mechanical behavior of materials in metal cutting ». *Journal of materials processing technology,* vol. 142, n° 1, p. 72-81.

Han, S., Melkote, S.N., Haluska, M.S. and T.R. Watkins. 2008. « White layer formation due to phase transformation in orthogonal machining of AISI 1045 annealed steel ». *Materials Science and Engineering: A,* vol. 488, n° 1, p. 195-204.

Handbook, ASM. 2005. « Volume 9 ». *Metallography and Microstructures,* vol. 12.

Hashimoto, F., Guo, Y.B. and Warren, A.W. 2006. « Surface Integrity Difference between Hard Turned and Ground Surfaces and Its Impact on Fatigue Life ». *CIRP Annals - Manufacturing Technology,* vol. 55, n° 1, p. 81-84.

Hastings, W.F, Mathew, P. and. Oxley, P.L.B. 1980. « A machining theory for predicting chip geometry, cutting forces etc. from work material properties and cutting conditions ». *Proceedings of the Royal Society of London. A. Mathematical and Physical Sciences,* vol. 371, n° 1747, p. 569-587.

Hoge, K.G. 1966. « Influence of strain rate on mechanical properties of 6061-T6 aluminum under uniaxial and biaxial states of stress ». *Experimental Mechanics,* vol. 6, n° 4, p. 204-211.

Hua, J., Shivpuri, R.,. Cheng, X., Bedekar, V., Matsumoto, Y., Hashimoto, F., and Watkins, T.R. 2005. « Effect of feed rate, workpiece hardness and cutting edge on subsurface residual stress in the hard turning of bearing steel using chamfer+hone cutting edge geometry ». *Materials Science and Engineering: A,* vol. 394, n° 1–2, p. 238-248.

Huang, J., and Aifantis, E.C. 1997. « A note on the problem of shear localization during chip formation in orthogonal machining ». *Journal of Materials Engineering and Performance,* vol. 6, n° 1, p. 25-26.

Huang, Y., and Liang, S.Y.. 2003a. « Modelling of the cutting temperature distribution under the tool flank wear effect ». *Proceedings of the Institution of Mechanical Engineers, Part C: Journal of Mechanical Engineering Science,* vol. 217, n° 11, p. 1195-1208.

Huang, Y., Chou, Y.K. and Liang, S.Y. 2007. « CBN tool wear in hard turning: a survey on research progresses ». *The International Journal of Advanced Manufacturing Technology,* vol. 35, n° 5-6, p. 443-453.

Huang, Y., and Liang, S.Y. 2003b. « Cutting forces modeling considering the effect of tool thermal property—application to CBN hard turning ». *International journal of machine tools and manufacture,* vol. 43, n° 3, p. 307-315.

Iwata, K., and.Ueda, K. 1980. « Fundamental analysis of the mechanism of built-up edge formation based on direct scanning electron microscope observation ». *Wear,* vol. 60, n° 2, p. 329-337.

Jacobson, M., Dahlman, P. and Gunnberg, F. 2002. « Cutting speed influence on surface integrity of hard turned bainite steel ». *Journal of Materials Processing Technology,* vol. 128, n° 1–3, p. 318-323.

Jaspers, SPFC, and Dautzenberg, J.H.. 2002. « Material behaviour in conditions similar to metal cutting: flow stress in the primary shear zone ». *Journal of Materials Processing Technology,* vol. 122, n° 2, p. 322-330.

Jeelani, S., Biswas, S.and Natarajan, R. 1986. « Effect of cutting speed and tool rake angle on residual stress distribution in machining 2024-T351 aluminium alloy—unlubricated conditions ». *Journal of materials science,* vol. 21, n° 8, p. 2705-2710.

Jin, D., and Liu, Z. 2013. « Damage of the machined surface and subsurface in orthogonal milling of FGH95 superalloy ». *The International Journal of Advanced Manufacturing Technology*, p. 1-9.

Jomaa, W. , Ben Fredj, N., Zaghbani, I., and Songmene, V. 2011. « Non-Conventional Turining of Hardened AISI D2 Tool Steel ». *International Journal of Advances in Machining and Forming Operations,* vol. Vol.3 n° No.2, p. 93-126.

Karpat, Y., and Özel, T. 2006. « Predictive analytical and thermal modeling of orthogonal cutting process—part I: predictions of tool forces, stresses, and temperature distributions ». *Journal of manufacturing science and engineering,* vol. 128, n° 2, p. 435-444.

Karpat, Y., and Özel, T. 2007. « 3-D FEA of hard turning: investigation of PCBN cutting tool micro-geometry effects ». *Transactions of NAMRI/SME,* vol. 35, p. 9-16.

Kececioglu, D. 1958. « Shear-strain rate in metal cutting and its effects on shear-flow stress ». *Trans. ASME,* vol. 80, n° 1, p. 158-165.

Kirman, I. 1971. « The relation between microstructure and toughness in 7075 aluminum alloy ». *Metallurgical Transactions,* vol. 2, n° 7, p. 1761-1770.

Klocke, F., Lung, D., Buchkremer, S., and Jawahir, I. S. (2013). « From Orthogonal Cutting Experiments towards Easy-to-Implement and Accurate Flow Stress Data ». *Materials and Manufacturing Processes*, 28(11), 1222-1227.

Komanduri, R., Schroeder, T. Hazra, J. von Turkovich B.F., and Flom, D.G. 1982. « On the Catastrophic Shear Instability in High-Speed Machining of an AISI 4340 Steel ». *Journal of Manufacturing Science and Engineering,* vol. 104, n° 2, p. 121-131.

König, W., Berktold, A. and Koch, K.F. 1993. « Turning versus Grinding – A Comparison of Surface Integrity Aspects and Attainable Accuracies ». *CIRP Annals - Manufacturing Technology,* vol. 42, n° 1, p. 39-43.

Kopalinsky, E.M., and Oxley, P.L.B.. 1984. « An Investigation of the Influence of Feed and Rake Angle on the Ratio of Feed Force to Cutting Force when Machining with Negative Rake Angle Tools ». *CIRP Annals - Manufacturing Technology,* vol. 33, n° 1, p. 43-46.

Kristyanto, B, Mathew, P. and Arsecularatne, J.A. 2002. « Development of a variable flow stress machining theory for aluminium alloys ». *Machining science and technology,* vol. 6, n° 3, p. 365-378.

Kundrák, J., Gácsi, Z., Gyáni, K., Bana V., and Tomolya G. 2012. « X-ray diffraction investigation of white layer development in hard-turned surfaces ». *The International Journal of Advanced Manufacturing Technology,* vol. 62, n° 5-8, p. 457-469.

Kuttolamadom, M., Hamzehlouia, S. et Mears, L. 2010. « Effect of Machining Feed on Surface Roughness in Cutting 6061 Aluminum ». *SAE International Journal of Materials & Manufacturing,* vol. 3, n° 1, p. 108-119.

Lalwani, D. I., Mehta N.K., and Jain, P.K. 2008. « Experimental investigations of cutting parameters influence on cutting forces and surface roughness in finish hard turning of MDN250 steel ». *Journal of Materials Processing Technology,* vol. 206, n° 1–3, p. 167-179.

Lalwani, DI, Mehta, N.K. and Jain, P.K. 2009. « Extension of Oxley's predictive machining theory for Johnson and Cook flow stress model ». *Journal of Materials Processing Technology,* vol. 209, n° 12, p. 5305-5312.

Lee, O., Choi, H. and Kim, H. 2011. « High-temperature dynamic deformation of aluminum alloys using SHPB ». *Journal of Mechanical Science and Technology,* vol. 25, n° 1, p. 143-148.

Lee, T.H. 2011. « Development of a theoretical model to predict cutting forces for hard machining ». *International Journal of Precision Engineering and Manufacturing,* vol. 12, n° 5, p. 775-782.

Lee, W.S., and Lam, H.F.. 1996. « The deformation behaviour and microstructure evolution of high-strength alloy steel at high rate of strain ». *Journal of materials processing technology,* vol. 57, n° 3, p. 233-240.

Lee, W.S., Sue, W.C., Lin C.F. and Wu, C.J. 2000. « The strain rate and temperature dependence of the dynamic impact properties of 7075 aluminum alloy ». *Journal of Materials Processing Technology,* vol. 100, n° 1, p. 116-122.

Lee, W.S., and Yeh, G.W. 1997. « The plastic deformation behaviour of AISI 4340 alloy steel subjected to high temperature and high strain rate loading conditions ». *Journal of Materials Processing Technology,* vol. 71, n° 2, p. 224-234.

Lee, W.S., and Lam, H.F. 1994. « Mechanical response and dislocation substructure of high strength Ni-Cr-Mo steel subjected to impact loading ». *Le Journal de Physique IV,* vol. 4, n° C8, p. C8-307-C8-312.

Lesuer, D.R,. Kay G.J, and LeBlanc, M.M. 2001. « Modeling large-strain, high rate deformation in metals ». In *Modelling the Performance of Engineering Structural Materials II. Proceedings of a Symposium, DR Lesuer and TS Srivatsan, eds., TMS, Warrendale, PA*. p. 75-86.

Li, B., Wang, X., Hu, Y. and Li, C. 2011. « Analytical prediction of cutting forces in orthogonal cutting using unequal division shear-zone model ». *The International Journal of Advanced Manufacturing Technology,* vol. 54, n° 5-8, p. 431-443.

Li, S., and Hou, B. 2013. « Material Behavior Modeling in Machining Simulation of 7075-T651 Aluminum Alloy ». *Journal of Engineering Materials and Technology,* vol. 136, n° 1, p. 011001-011001.

Liu, C. R., and Barash, M.M. 1976. « The Mechanical State of the Sublayer of a Surface Generated by Chip-Removal Process—Part 1: Cutting With a Sharp Tool ». *Journal of Manufacturing Science and Engineering,* vol. 98, n° 4, p. 1192-1199.

Liu, C. R., and Barash, M.M. 1982. « Variables Governing Patterns of Mechanical Residual Stress in a Machined Surface ». *Journal of Engineering for Industry,* vol. 104, n° 3. P. 257-264

Liu, M., Takagi, J. and Tsukuda, A. 2004. « Effect of tool nose radius and tool wear on residual stress distribution in hard turning of bearing steel ». *Journal of Materials Processing Technology,* vol. 150, n° 3, p. 234-241.

Liu, X. L., Wen, D.H., Li, Z.J., Xiao, L. and Yan, F.G.. 2002. « Experimental study on hard turning hardened GCr15 steel with PCBN tool ». *Journal of Materials Processing Technology,* vol. 129, n° 1–3, p. 217-221.

Liyao, G., Minjie, W. and Chunzheng, D. 2013. « On adiabatic shear localized fracture during serrated chip evolution in high speed machining of hardened AISI 1045 steel ». *International Journal of Mechanical Sciences,* vol. 75, p. 288-298.

Loewen, E.G., and Shaw, M.C.. 1954. « On the analysis of cutting tool temperature ». *Trans. ASME* vol. 76 no. 2, p. 217-223.

Long, Y., and Huang, Y. 2005. « Force modeling under dead metal zone effect in orthogonal cutting with chamfered tools ». *Transactions of NAMRI/SME,* vol. 33, p. 573-580.

M'Saoubi, R., Outeiro, J.C., Chandrasekaran, H., and Dillon J.O.W.. 2008. « A review of surface integrity in machining and its impact on functional performance and life of machined products ». *International Journal of Sustainable Manufacturing,* vol. 1, n° 1, p. 203-236.

M'saoubi, R., Outeiro, J.C., Changeux, B., Lebrun, J.L. and Morao Dias, A. 1999. « Residual stress analysis in orthogonal machining of standard and resulfurized AISI 316L steels ». *Journal of Materials Processing Technology,* vol. 96, n° 1-3, p. 225-233.

MacGregor, C.W., and Fisher, J.C. 1946. « A velocity-modified temperature for the plastic flow of metals ». *Journal of applied mechanics-transactions of the ASME,* vol. 13, n° 1, p. A11-A16.

Manes, A, Peroni, L., Scapin, M., and Giglio, M. 2011. « Analysis of strain rate behavior of an Al 6061 T6 alloy ». *Procedia Engineering,* vol. 10, p. 3477-3482.

Marusich, T.D., and Ortiz, M. 1995. « Modelling and simulation of high-speed machining ». *International Journal for Numerical Methods in Engineering,* vol. 38, n° 21, p. 3675-3694.

Montgomery, D. C. 2006. *Design and Analysis of Experiments*. John Wiley & Sons.

Mustafa, A., and Tanju, K. 2011. « Investigation of the machinability of the Al 7075 alloy using DLC coated cutting tools ». *Scientific Research and Essays,* vol. 6, n° 1, p. 44-51.

Ng, C.K., Melkote, S.N., Rahman, M. and Kumar, A.S. 2006. « Experimental study of micro- and nano-scale cutting of aluminum 7075-T6 ». *International Journal of Machine Tools and Manufacture,* vol. 46, n° 9, p. 929-936.

Novovic, D., Dewes, R.C., Aspinwall, D.K., Voice, W., and Bowen, P. 2004. « The effect of machined topography and integrity on fatigue life ». *International Journal of Machine Tools and Manufacture,* vol. 44, n° 2-3, p. 125-134.

Oishi, K. 1996. « Mirror cutting of aluminum with sapphire tool ». *Journal of Materials Processing Technology,* vol. 62, n° 4, p. 331-334.

Ojolo, S.J., Damisa, O., and Iyekolo, O. 2011. « Investigation into the effects of solid lubricant on the surface characteristique of some metals during orthogonal machining ». *Journal of Engineering, Design and Technology,* vol. 9, n° 2, p. 130-142.

Outeiro, J.C., Umbrello, D. and M'Saoubi, R. 2006. « Experimental and numerical modelling of the residual stresses induced in orthogonal cutting of AISI 316L steel ». *International Journal of Machine Tools and Manufacture,* vol. 46, n° 14, p. 1786-1794.

Outeiro, J.C., Dias, A.M., and Jawahir, I.S. 2006. « On the effects of residual stresses induced by coated and uncoated cutting tools with finite edge radii in turning operations ». *CIRP Annals-Manufacturing Technology,* vol. 55, n° 1, p. 111-116.

Oxley, P.L. B., and Young, H.T.. 1989. « The mechanics of machining: an analytical approach to assessing machinability ». *Ellis Horwood Publisher*, p. 136-182.

Oxley, P.L.B., and Hastings, W.F.. 1977. « Predicting the strain rate in the zone of intense shear in which the chip is formed in machining from the dynamic flow stress properties of the work material and the cutting conditions ». *Proceedings of the Royal Society of London. A. Mathematical and Physical Sciences,* vol. 356, n° 1686, p. 395-410.

Özel, T. 2003. « Modeling of hard part machining: effect of insert edge preparation in CBN cutting tools ». *Journal of Materials Processing Technology,* vol. 141, n° 2, p. 284-293.

Özel, T., and Zeren, E. 2004. « Determination of work material flow stress and friction for FEA of machining using orthogonal cutting tests ». *Journal of Materials Processing Technology,* vol. 153, p. 1019-1025.

Özel, T., and Zeren, E. 2006. « A methodology to determine work material flow stress and tool-chip interfacial friction properties by using analysis of machining ». *Journal of manufacturing science and Engineering,* vol. 128, n° 1, p. 119-129.

Pawade, R.S., Joshi, S.S. and Brahmankar, P.K. 2008. « Effect of machining parameters and cutting edge geometry on surface integrity of high-speed turned Inconel 718 ». *International Journal of Machine Tools and Manufacture,* vol. 48, n° 1, p. 15-28.

Poulachon, G., Albert, A. Schluraff, M., and Jawahir, I.S. 2005. « An experimental investigation of work material microstructure effects on white layer formation in PCBN hard turning ». *International Journal of Machine Tools and Manufacture,* vol. 45, n° 2, p. 211-218.

Poulachon, G., Moisan, A. and Jawahir, I.S.. 2001. « Tool-wear mechanisms in hard turning with polycrystalline cubic boron nitride tools ». *Wear,* vol. 250, n° 1, p. 576-586.

Ramesh, A., Thiele, J.D., and Melkote, S.N. 1999. « Residual stress and sub-surface flow in finish hard turned AISI 4340 and 52100 steels: a comparative study ». *Manufacturing Science and Engineering MED,* vol. 10, p. 831-837.

Ramesh, A., and Melkote, S.N. 2008. « Modeling of white layer formation under thermally dominant conditions in orthogonal machining of hardened AISI 52100 steel ». *International Journal of Machine Tools and Manufacture,* vol. 48, n° 3, p. 402-414.

Rao, B., and Shin, Y.C. 2001. « Analysis on high-speed face-milling of 7075-T6 aluminum using carbide and diamond cutters ». *International Journal of Machine Tools and Manufacture,* vol. 41, n° 12, p. 1763-1781.

Rech, J., and Moisan, A.. 2003. « Surface integrity in finish hard turning of case-hardened steels ». *International Journal of Machine Tools and Manufacture,* vol. 43, n° 5, p. 543-550.

Ren, H., and Altintas, Y.. 2000. « Mechanics of machining with chamfered tools ». *Journal of manufacturing science and engineering,* vol. 122, n° 4, p. 650-659.

Roy, P., Sarangi, S.K., Ghosh, A., and Chattopadhyay, A.K. 2009. « Machinability study of pure aluminium and Al–12% Si alloys against uncoated and coated carbide inserts ». *International Journal of Refractory Metals and Hard Materials,* vol. 27, n° 3, p. 535-544.

Rule, W.K., and Jones, S.E. 1998. « A revised form for the Johnson–Cook strength Model ». *International Journal of Impact Engineering,* vol. 21, n° 8, p. 609-624.

Rule, W.K. 1997. « A numerical scheme for extracting strength model coefficients from Taylor test data ». *International Journal of Impact Engineering,* vol. 19, n° 9, p. 797-810.

Sahin, Y. 2009. « Comparison of tool life between ceramic and cubic boron nitride (CBN) cutting tools when machining hardened steels ». *Journal of materials processing technology,* vol. 209, n° 7, p. 3478-3489.

Sánchez, J. M., Rubio, E., Álvarez, M., Sebastián, M.A., and Marcos, M. 2005. « Microstructural characterisation of material adhered over cutting tool in the dry machining of aerospace aluminium alloys ». *Journal of Materials Processing Technology,* vol. 164–165, n° 0, p. 911-918.

Sartkulvanich, P., Altan, T., and Soehner, J. 2005. « Flow stress data for finite element simulation in metal cutting: A progress report on madams ». *Machining science and technology,* vol. 9, n° 2, p. 271-288.

Sasimurugan, T., and Palanikumar, K. 2011. « Analysis of the Machining Characteristics on Surface Roughness of a Hybrid Aluminium Metal Matrix Composite (Al6061-SiC-Al2O3) ». *Journal of Minerals & Materials Characterization & Engineering,* vol. 10, n° 13, p. 1213-1224.

Savaria, V., Bridier, F., and Bocher, P. (2012). « Computational quantification and correction of the errors induced by layer removal for subsurface residual stress measurements ». *International Journal of Mechanical Sciences*, 64(1), 184-195.

Shankar, M. R., Chandrasekar, S., Compton, W. D., and King, A. H. (2005). « Characteristics of aluminum 6061-T6 deformed to large plastic strains by machining ». *Materials Science and Engineering: A*, 410, 364-368.

Shaw, M. C., and Vyas, A. (1994). « Heat-affected zones in grinding steel ». *CIRP Annals-Manufacturing Technology*, 43(1), 279-282.

Shaw, M.C. 1984. *Metal Cutting Principles*. New York: Oxford University Press.

Sheikh-Ahmad, J., and Twomey, J. (2007). « ANN constitutive model for high strain-rate deformation of Al 7075-T6 ». *Journal of materials processing technology*, 186(1), 339-345.

Sugimura, J., Watanabe, T., and Yamamoto, Y. (1994). « Effects of surface roughness pattern on the running-in process of rolling/sliding contacts ». *Tribology Series*, 27, 125-137.

Suraratchai, M., Limido, J., Mabru, C., and Chieragatti, R. (2008). « Modelling the influence of machined surface roughness on the fatigue life of aluminium alloy ». *International Journal of fatigue*, 30(12), 2119-2126.

Sutherland, J. W., Kulur, V. N., King, N. C., and Von Turkovich, B. F. (2000). « An experimental investigation of air quality in wet and dry turning ». *CIRP Annals-Manufacturing Technology*, 49(1), 61-64.

Taylor, C. M., Turner, S., Papatheou, E., and Sims, N. D. (2013). « Modelling of segmentation-driven vibration in machining ». *The International Journal of Advanced Manufacturing Technology*, 66(1-4), 207-219.

Thiele, J. D., Melkote, S. N., Peascoe, R. A., and Watkins, T. R. (2000). « Effect of cutting-edge geometry and workpiece hardness on surface residual stresses in finish hard turning of AISI 52100 steel ». *Journal of Manufacturing Science and Engineering*, 122(4), 642-649.

Thiele, J. D., and N Melkote, S. (1999). « Effect of cutting edge geometry and workpiece hardness on surface generation in the finish hard turning of AISI 52100 steel ». *Journal of Materials Processing Technology*, 94(2), 216-226.

Tounsi, N., Vincenti, J., Otho, A., and Elbestawi, M. A. (2002). « From the basic mechanics of orthogonal metal cutting toward the identification of the constitutive equation ». *International Journal of Machine Tools and Manufacture*, 42(12), 1373-1383.

Ucun, İ., and Aslantas, K. (2011). « Numerical simulation of orthogonal machining process using multilayer and single-layer coated tools ». *The International Journal of Advanced Manufacturing Technology*, 54(9-12), 899-910.

Ulutan, D., and Ozel, T. 2011. « Machining induced surface integrity in titanium and nickel alloys: A review ». *International Journal of Machine Tools and Manufacture,* vol. 51, p. 250-280.

Umbrello, D. 2013. « Analysis of the white layers formed during machining of hardened AISI 52100 steel under dry and cryogenic cooling conditions ». *The International Journal of Advanced Manufacturing Technology,* vol. 64, n° 5-8, p. 633-642.

Umbrello, D., M'Saoubi, R. and Outeiro, J. C. 2007. « The influence of Johnson–Cook material constants on finite element simulation of machining of AISI 316L steel ». *International Journal of Machine Tools and Manufacture,* vol. 47, n° 3–4, p. 462-470.

Vamsi Krishna, P., Srikant, R. R., and Nageswara Rao, D. (2010). « Experimental investigation on the performance of nanoboric acid suspensions in SAE-40 and coconut oil during turning of AISI 1040 steel ». *International Journal of Machine Tools and Manufacture*, 50(10), 911-916.

Vaz Jr, M., Owen, D. R. J., Kalhori, V., Lundblad, M., and Lindgren, L. E. (2007). « Modelling and simulation of machining processes ». *Archives of computational methods in engineering*, 14(2), 173-204.

Vernaza-Peña, K.M., Mason, J.J., and Ovaert, T. 2003. « Temperature Generation in Cutting of Aluminum at Low and Negative Rake Angles ». In *SEM Annual Conference & Exposition on Experimental and Applied Mechanics*. p. 7.

Vyas, A, and Shaw, M.C. 1999. « Mechanics of saw-tooth chip formation in metal cutting ». *Journal of Manufacturing Science and Engineering,* vol. 121, n° 2, p. 163-172.

Waldorf, D.J., DeVor, R.E., and Kapoor, S.G. 1998. « A Slip-Line Field for Ploughing During Orthogonal Cutting ». *Journal of manufacturing science and engineering,* vol. 120, n° 4, p. 693-699.

Waldorf, D.J. 2006. « A simplified model for ploughing forces in turning ». *Journal of manufacturing processes,* vol. 8, n° 2, p. 76-82.

Waldorf, D.J., DeVor, R.E. and Kapoor, S.G. 1999. « An evaluation of ploughing models for orthogonal machining ». *Journal of manufacturing science and engineering,* vol. 121, n° 4, p. 550.

Warren, AW, andt Guo, Y.B. 2009. « Characteristics of residual stress profiles in hard turned versus ground surfaces with and without a white layer ». *Journal of manufacturing science and engineering,* vol. 131, n° 4:041004.

Withers, P.J., and Bhadeshia, H. 2001. « Residual stress. Part 1–measurement techniques ». *Materials science and Technology,* vol. 17, n° 4, p. 355-365.

Withers, P. J., Turski, M., Edwards, L., Bouchard, P. J., and Buttle, D. J. (2008). « Recent advances in residual stress measurement ». *International Journal of Pressure Vessels and Piping*, 85(3), 118-127.

Xie, JQ, Bayoumi, A.E., and Zbib, H.M. 1995. « Analytical and experimental study of shear localization in chip formation in orthogonal machining ». *Journal of materials engineering and performance,* vol. 4, n° 1, p. 32-39.

Yallese, M. A., Chaoui, K., Zeghib, N., Boulanouar, L., and Rigal, J. F. (2009). « Hard machining of hardened bearing steel using cubic boron nitride tool ». *Journal of Materials Processing Technology*, 209(2), p. 1092-1104.

Yang, Y., Zeng, Y., and Gao, Z.W. 2008. « Numerical and experimental studies of self-organization of shear bands in 7075 aluminium alloy ». *Materials Science and Engineering: A,* vol. 496, n° 1, p. 291-302.

Yen, Y-C, Jain, A., Chigurupati, P., Wu, W.-T., and Altan, T. 2004. « Computer simulation of orthogonal cutting using a tool with multiple coatings ». *Machining science and technology,* vol. 8, n° 2, p. 305-326.

Yen, Y. C., Jain, A., and Altan, T. (2004).« A finite element analysis of orthogonal machining using different tool edge geometries ». *Journal of Materials Processing Technology*, 146(1), p. 72-81.

Youssef, H.A., and El-Hofy, H. 2008a. « *Machining technology: machine tools and operations* ». CRC Press.

Youssef, H. A., and El-Hofy, H. 2008b. « Accuracy and Surface Integrity Realized by Machining Processes ». In *Machining Technology*. p. 575-602. CRC Press.

Zaghbani, I., and Victor, S. 2009. « A force-temperature model including a constitutive law for Dry High Speed Milling of aluminium alloys ». *Journal of Materials Processing Technology,* vol. 209, n^{o} 5, p. 2532-2544.

Zhou, J. M., Walter, H., Andersson, M., and Stahl, J. E. 2003. « Effect of chamfer angle on wear of PCBN cutting tool ». *International Journal of Machine Tools and Manufacture,* vol. 43, n^{o} 3, p. 301-305.

Zhu, D., B. Mobasher, Rajan, S.D., and Peralta, P. 2011. « Characterization of dynamic tensile testing using aluminum alloy 6061-T6 at intermediate strain rates ». *Journal of Engineering Mechanics,* vol. 137, n^{o} 10, p. 669-679.